TOBIAS CONRADT

Challenges of regional hydrological modelling in the Elbe River basin

Investigations about model fidelity on sub-catchment level

CHALLENGES OF REGIONAL HYDROLOGICAL MODELLING IN THE ELBE RIVER BASIN

Investigations about model fidelity on sub-catchment level

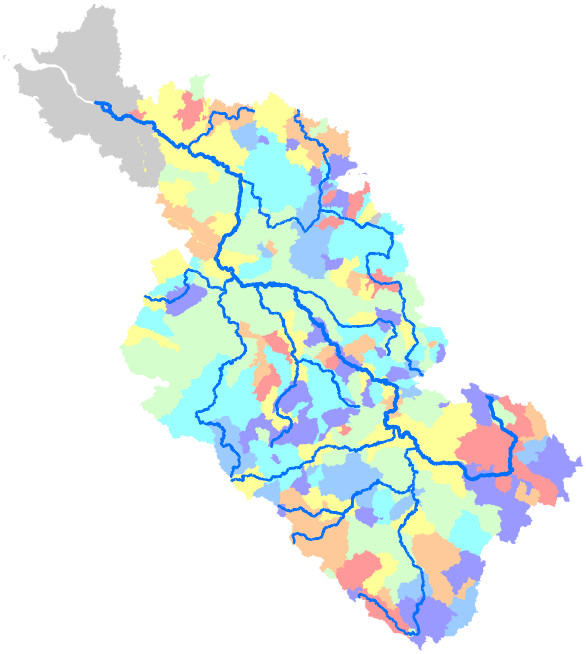

KUMULATIVE DISSERTATION

zur Erlangung des akademischen Grades
»doctor rerum naturalium« (Dr. rer. nat.)
in der Wissenschaftsdisziplin Geoökologie / Hydrologie

eingereicht an der
Mathematisch-Naturwissenschaftlichen Fakultät
der Universität Potsdam

von

TOBIAS CONRADT

Januar 2013

Published online at the
Institutional Repository of the University of Potsdam:
URL http://opus.kobv.de/ubp/volltexte/2013/6524/
URN urn:nbn:de:kobv:517-opus-65245
http://nbn-resolving.de/urn:nbn:de:kobv:517-opus-65245

Tobias Conradt: *Challenges of regional hydrological modelling in the Elbe River basin*. PhD Thesis. University of Potsdam, Germany.

Submitted: 9th January 2013
Defended: 6th May 2013
Published: May 2013

Referees:
Prof. Dr. Axel Bronstert — University of Potsdam, Germany
Prof. Dr. Stefan Uhlenbrook — UNESCO-IHE Delft, The Netherlands
Prof. Dr.-Ing. Uwe Haberlandt — University of Hanover, Germany

Dedicated to all R-tists and TEXnicians.

ABSTRACT

Within a research project about future sustainable water management options in the Elbe River basin, quasi-natural discharge scenarios had to be provided. The semi-distributed eco-hydrological model SWIM was utilised for this task. According to scenario simulations driven by the stochastical climate model STAR, the region would get distinctly drier. However, this thesis focuses on the challenge of meeting the requirement of high model fidelity even for smaller sub-basins. Usually, the quality of the simulations is lower at inner points than at the outlet.

Four research paper chapters and the discussion chapter deal with the reasons for local model deviations and the problem of optimal spatial calibration. Besides other assessments, the Markov Chain Monte Carlo method is applied to show whether evapotranspiration or precipitation should be corrected to minimise runoff deviations, principal component analysis is used in an unusual way to evaluate local precipitation alterations by land cover changes, and remotely sensed surface temperatures allow for an independent view on the evapotranspiration landscape.

The overall insight is that spatially explicit hydrological modelling of such a large river basin requires a lot of local knowledge. It probably needs more time to obtain such knowledge as is usually provided for hydrological modelling studies.

ZUSAMMENFASSUNG

Innerhalb eines Forschungsprojekts zu zukünftigen nachhaltigen Optionen der Wasserwirtschaft im Elbe-Einzugsgebiet mußten quasinatürliche Abflußszenarien bereitgestellt werden. Zu diesem Zweck wurde das räumlich diskretisierte ökohydrologische Modell SWIM eingesetzt. Nach den von dem stochastischen Klimamodell STAR angetriebenen Szenariosimulationen würde die Region deutlich trockener werden. Allerdings ist das Hauptthema dieser Dissertation die Herausforderung, die Ansprüche an hohe Modelltreue auch für kleinere Teileinzugsgebiete zu erfüllen. Normalerweise ist die Qualität der Simulationen für innere Punkte geringer als am Gebietsauslaß.

Vier Fachartikel-Kapitel und das Diskussionskapitel beschäftigen sich mit den Gründen für lokale Modellabweichungen und dem Problem optimaler räumlicher Kalibrierung. Unter anderem wird die Markovketten-Monte-Carlo-Methode angewendet, um zu zeigen, ob Verdunstung oder Niederschlag korrigiert werden sollte, um Abweichungen des Abflusses zu minimieren, die Hauptkomponentenanalyse wird auf eine unübliche Weise benutzt, um lokale Niederschlagsänderungen aufgrund

von Landnutzungsänderungen zu untersuchen, und fernerkundete Oberflächentemperaturen erlauben eine unabhängige Sicht auf die Verdunstungslandschaft.

Die grundlegende Erkenntnis ist, daß die räumlich explizite hydrologische Modellierung eines so großen Flußeinzugsgebiets eine Menge Vor-Ort-Wissen erfordert. Wahrscheinlich wird mehr Zeit benötigt, solches Wissen zu erwerben, als üblicherweise für hydrologische Modellstudien zur Verfügung steht.

ACKNOWLEDGEMENTS

This work would not have been published without the help of my supervisors, many colleagues, some hundred persons I never met, and those who are most important.

Big thanks to Axel Bronstert, Fred F. Hattermann, and Frank Wechsung for many helpful hints and subtle pressure (which was sometimes needed to see beyond the everyday project workload); lots of thanks to all present and former colleagues from Telegraph Hill and the Pappel for great support, especially Hagen Koch, Peggy Gräfe, Valentina Krysanova, Martin Gutsch, Joachim Post, Cornelia Hesse, Karl-Erich Lindenschmidt, Silke Schmidt, Stefan Liersch, our former librarian Bärbel Uffrecht, and the D&C team; and special thanks to everyone at GLOWA-Elbe!

The persons I never met but who contributed a lot are the free software community. Thank you for Linux, LaTeX, R, GRASS-GIS, GMT, and all the other friends.

Finally, the three most important persons shall be acknowledged: Jan Behrens, not only for sharing general problems with PhD-theses, my father Kurt Conradt for always hosting us with too much food, and last but not least my wife Dorothée for her unbroken love in a challenging time of our lives.

CONTENTS

LIST OF FIGURES

LIST OF TABLES

1

INTRODUCTION

This thesis developed within the framework of the German GLOWA-Elbe project (see Section 1.1 below for details). I joined the project at the beginning of its second phase in 2005 when distributed hydrological modelling of almost the entire Elbe River basin was required. The commission was to produce scenario output of sub-basin water fluxes for quality, management, and socio-economic analyses by an appropriate setup of SWIM, a hydrotope-based semi-distributed eco-hydrological model.

In the course of applying SWIM as described in Chapter 2, it became clear what was meant by the GLOWA approach of new integrative and interdisciplinary research "networked at an adequate level of abstraction" (Rieland 2004): About 25 years of spatially distributed hydrological modelling produced lots of studies mainly evaluating the simulated hydrograph at the outlet of the respective model domain, whereas in our project it was essential to get realistic results for hundreds of sub-catchments. Hence, two major obstacles had to be overcome.

The first one reflects a general pattern which may be adopted as natural law for distributed modelling: *The quality of results decreases when the output resolution increases.* This holds both for spatial and for temporal discretisations. In our case, the simulated discharges for many of the sub-basins turned out to be too low or too high and often suffered from biased distributions, while the hydrographs for bigger contributors looked quite well and nearly perfect for the main outlet. This is illustrated in Section 1.4.2 below and by Figure 41 on Page 94.

The second problem emerges from area-specific, regional environmental change impacts which are now common to most larger river basins of the world. The currently most important impacts to the Elbe River basin happen in the open-cast mining landscapes near Leipzig, in Lusatia, and in northern Bohemia. During the 1980s, when lignite mining activities peaked, ground water extractions to the Spree River (i. e. from Lusatia alone) reached a constant rate of more than 30 $m^3 s^{-1}$. The total water deficit accumulated to about $13 \cdot 10^9$ m^3 (Grünewald 2001).

After Germany's reunification the tide has turned: lignite mining is still going on, but most of the sites are being flooded to become a landscape of lakes; new water surfaces of 146 km^2 in Lusatia and 262 km^2 in the entire German part of the Elbe basin are planned, cf. Section 4.2. This notably decreases the remaining discharge of the Spree river, the local evaporation increases, and the new land-lake pattern may alter the local climate. Such effects are not covered by any standard model and require customised solutions.

In dealing with the two problems concerning the "adequate level of abstraction" the motivation for this thesis cristallised into the following questions. These were also starting points to the research papers in the following chapters.

- How can we cope with the uncertainty principle of distributed modelling when distributed outputs of high resolution *and* quality are required? (The fundamental question of this thesis – more or less addressed by all chapters)
- Do the post-mining landscapes influence the local climate and thus hydrology, in addition to their direct impact? How is it possible to quantify respective effects by standard precipitation measurements of the German Weather Service (DWD)? (Chapter 4)
- How can ready-available, remotely sensed data be utilised for spatially differentiated model calibration? How can the spatio-temporal information of daily satellite images be implemented efficiently? (Chapter 5)

An underlying leitmotiv of all these questions is the intention to provide future research with methods and ideas for a better integration of regional environmental characteristics into hydrological modelling.

1.1 THE PROJECT FRAMEWORK

In December 1998, the German Federal Ministry of Education and Research (Bundesministerium für Bildung und Forschung, BMBF) launched the research programme GLOWA – Globaler Wandel des Wasserkreislaufs / Global Change and the Hydrological Cycle – by public announcement. The programme aimed at developing strategies for a sustainable water management on the regional scale regarding global environmental change and socio-economic boundary conditions. As already mentioned, new integrative and interdisciplinary research approaches interlinking the scales were required, as impacts and consequences of global change take place locally (Rieland 2004, Schönlau & van der Veen 2005).

GLOWA consisted of five case studies in larger river basins (each about 100 000 km²) located in Europe, Africa, and Southwestern Asia, of which the Elbe River basin in Central Europe was the northernmost. The respective 'GLOWA-Elbe' project had been started in May 2000 and was furthered until 2010. It was structured into three major phases.

The first phase focused on hot spots in the German part of the Elbe basin, but the regional scope of the project was expanded to the entire basin in the second phase which started in 2004 (Cramer et al. 2005). The research was organised along the course of scenario data in a cluster of models, starting from the regionalisation of global climate change

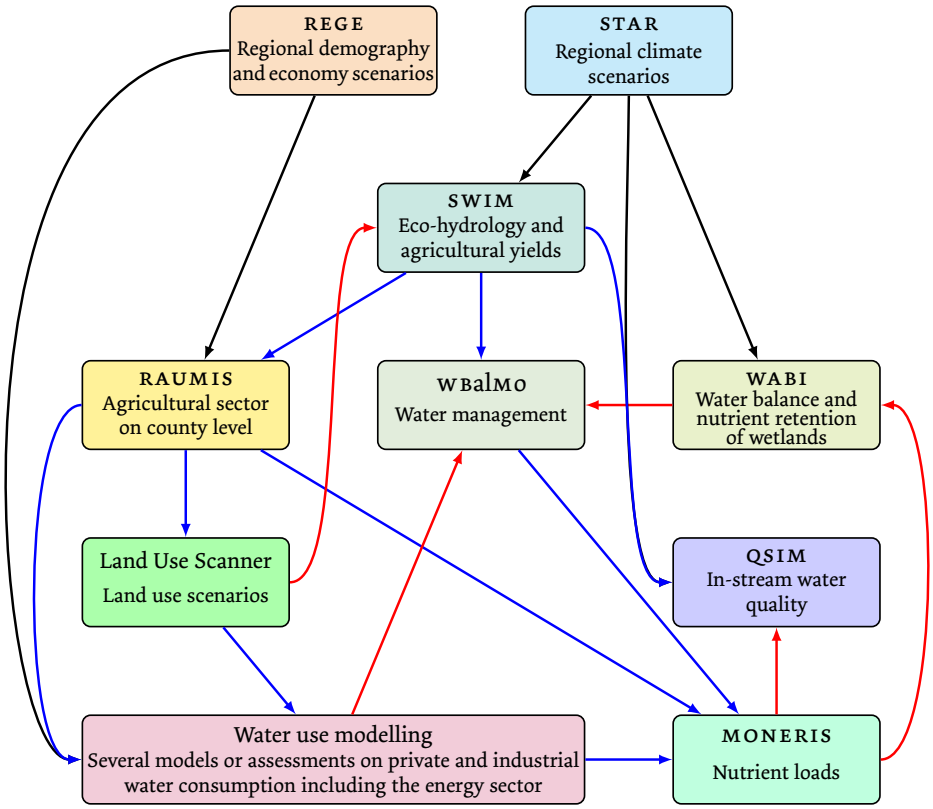

Figure 1: Model interconnections in the GLOWA-Elbe project. Driven by scenario data of REGE and STAR (black arrows), the output of SWIM affected more or less all subsequent models, their data exchange (coloured arrows: down- and right-pointing in blue, up- and left-pointing in red), and hence most scenario results.

and finally delivering multiple spatio-temporal impact projections, e. g. for in-stream ecology (Quiel et al. 2011) or sector-specific economical cost-benefit analyses (Grossmann et al. 2013). Our eco-hydrological model SWIM played a pivotal role in this model cluster by projecting the primary hydrological consequences of the climate and land use scenarios; this is illustrated in Figure 1.

As the following chapters show, the goal of a credible scenario simulation was hard to achieve for many sub-regions. Therefore the respective research on the eco-hydrological modelling of the Elbe River basin went on during the third project phase (2008–2010) which was primarily aimed at delivering the database and modelling framework in form of a toolbox to interested users and institutions (Kaden et al. 2010).

The output of SWIM was important for many of the results produced and communicated by the GLOWA-Elbe project, and many similar multi-model projects in the framework of today's integrated water resource management (IWRM; GWP-TAC 2000, GWP-INBO 2009) rely on spatially distributed hydrological modelling which is then usually confronted by similar problems. Hence it seems rather meaningful to

research into the scale-dependent uncertainties and error sources of this methodology.

1.2 THE ELBE RIVER BASIN

Due to the cumulative composition of this thesis two introductions on the research area, the Elbe River basin, are given in respective sections of the scientific papers that make up the following chapters: The Introduction of Chapter 2 on page 26 focuses mainly on the water balance of the area, but contains in Figure 15 a nice general map. A more detailed description of the different landscapes is given in the likewise named Section 'The Elbe River basin' of Chapter 5 on page 97.

To avoid unneccessary redundancy the already partially overlapping contents of these sections will not be repeated here once more, but as their Figs. 15, 42a, and 42b contain only physical and land use maps, the soil landscape shall be presented here in Figure 2 together with the wetland map in Figure 3 as both maps were used for modelling.

The north-east of the Elbe River basin is dominated by glacial sands with limited retention capacity for water and nutrients. Therefore, peat soils have been accumulated onto these sands in the wetlands of the lowland regions. Sandy soils can also be found along the mountain crests, but as they are autochthonous residues from rock weathering they are typically loamy and contain lots of stones.

In a wide swath from the Magdeburg Börde (the region west and south of Magdeburg) to the Czech Elbe Lowland, only discontinued by the Ore Mountains, silty loess soils dominate. These soils are agriculturally most productive, because loess has excellent water and high nutrient storage capacities, and these soils are easily penetrable for plant roots.

The south of the basin is dominated by loamy and partially stony soils produced from local rock weathering. They may also be rather fertile, but are often hard to work. Places with limestone underground are covered with clay soils as weathering product.

Along the river courses the soils are made up from fluviatile deposits. These are regularly more or less loamy sands; directly in the riparian zone they are often covered by riparian loam. The composition of the fluviatile deposits varies according to the local source material.

FURTHER READING For an extensive description about the Elbe River basin the reader is advised to consult the Elbe-Atlas (Wechsung et al. 2011) that has also been published in the framework of the GLOWA-Elbe project. There are also large-scale visualisations of the maps and scenarios which either served as basis for the eco-hydrological modelling or are made up from selected simulation results.

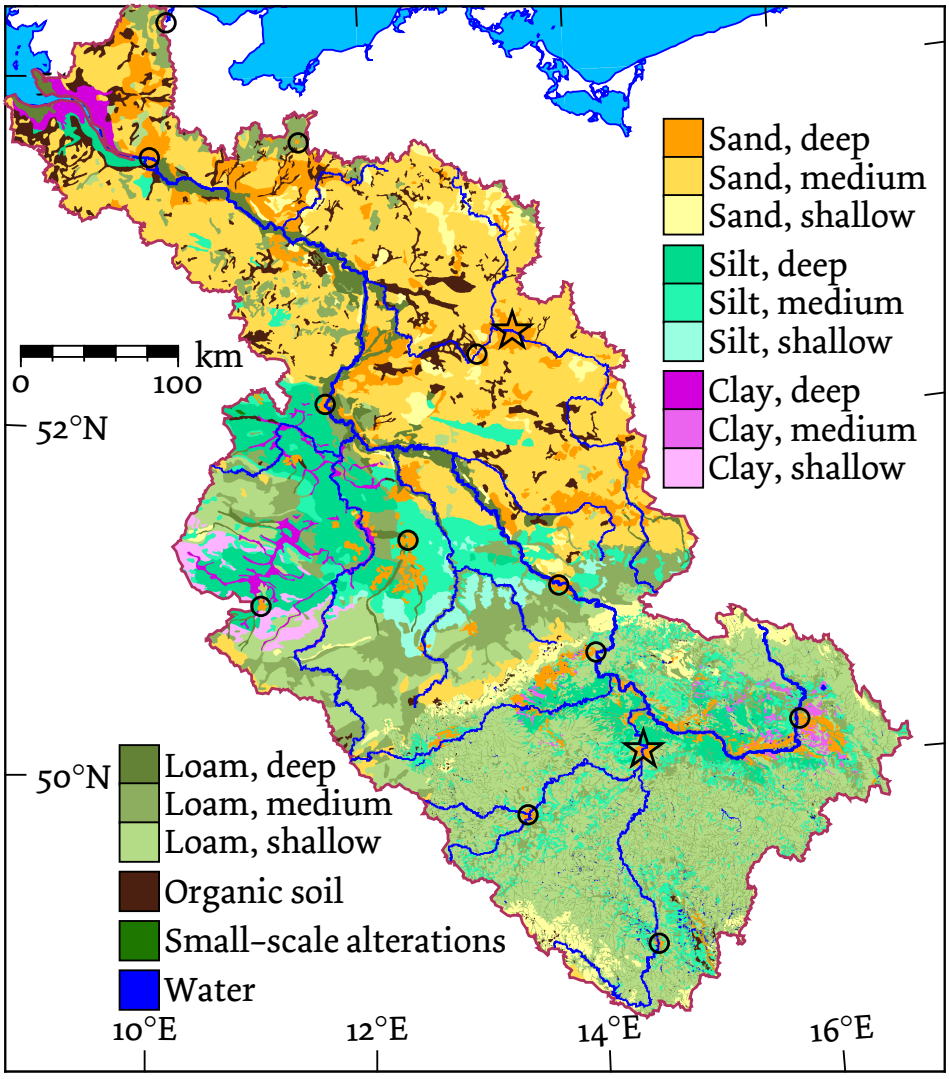

Figure 2: Topsoil textures in the Elbe river basin. It is the texture view of the soil map that served as basis for the SWIM simulations. This map was made by joining of the German general soil map BÜK 1000 and a Czech soil map; cf. Section 2.2.2 on page 29.

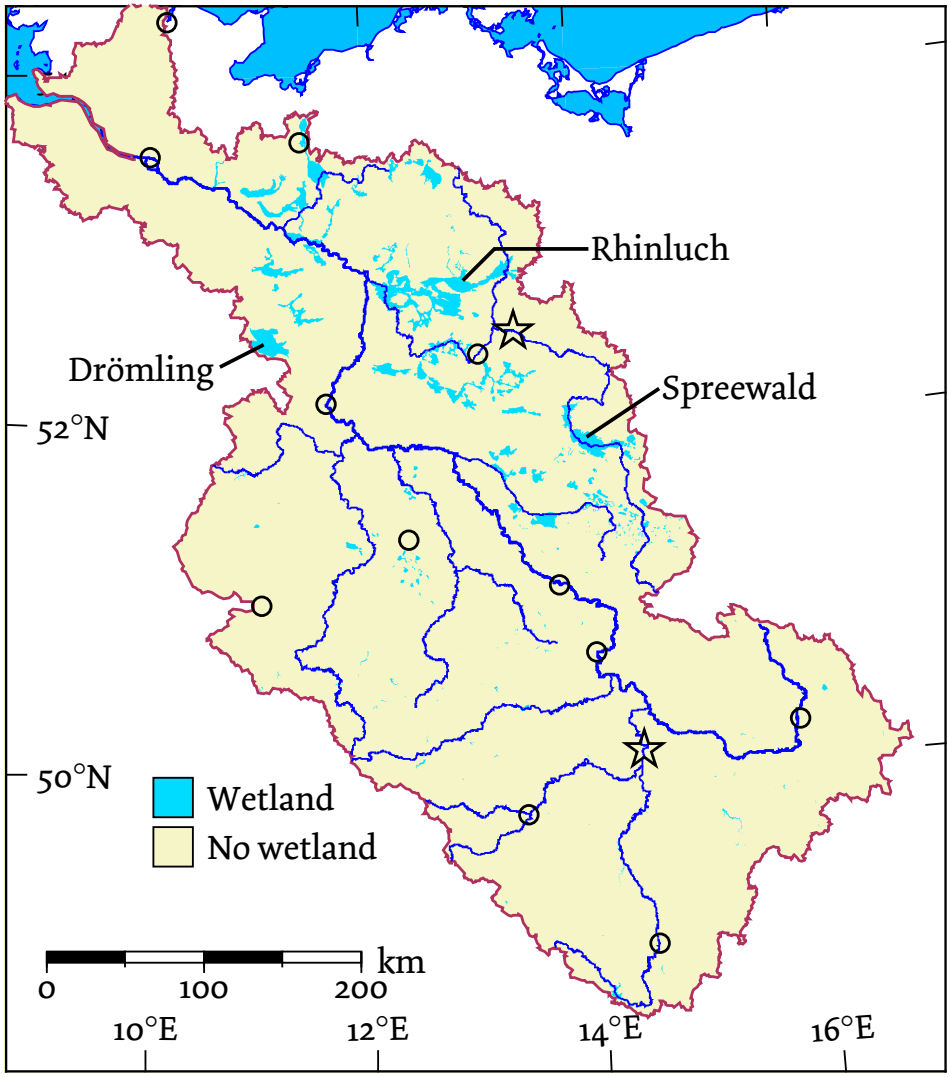

Figure 3: Wetlands in the Elbe river basin. This was one of the basis maps for hydrotope delineation, cf. Section 1.4.1. The vegetation in wetlands is assumed to have access to ground water independent from soil water status. This increases evapotranspiration during the summer season and reduces water discharge from wetland areas accordingly.

1.3 SEMI-DISTRIBUTED ECO-HYDROLOGICAL MODELLING

Spatially distributed hydrological models are not new. The concept of a 'gridded multi-layer landscape' where water fluxes between the cells are numerically discretised from physically based process equations was first realised by Bernard in 1937, but computational requirements could only be matched by graphical approximations then, and the example which included a land use change assessment was forgotten for long (Hjelmfelt & Amerman 1980).

The idea was resurrected in the late 1960s (Freeze & Harlan 1969), and only lack of powerful computer systems seems to have delayed implementation. First realisations came up in the late 1970s (e. g. Gupta & Solomon 1977a,b, Solomon & Gupta 1977), and the 1980s saw the deployment of the SHE (Abbott et al. 1986a,b), which formed the basis for the well known successors SHETRAN and MIKE SHE.

The major disadvantage of these fully distributed models is the high computational burden. Refsgaard et al. (2010) note that the development of the SHE may have started a decade too early, because the machines that were available in the beginning of the 1980s were just powerful enough to simulate a few days on some dozens of raster cells during one night of computing.

Although computationally less demanding, the idea of coupling several lumped single-catchment models for sub-catchments or hydrologically homogeneous units of a larger basin to obtain a so-called semi-distributed model gained ground just about the same time – the beginning availability of micro-computers seems to have paved the way for spatial hydrological modelling in principle.

Under the first of many exponents are the widely known TOPMODEL of Beven & Kirkby (1979) and the 'Precipitation-Runoff Modeling System' (PRMS; Leavesley et al. 1983). Lindström et al. (1997) report that the HBV model gradually developed into semi-distributed shape; its lumped conceptual roots for single catchments date back to the early 1970s (Bergström & Forsman 1973). All these semi-distributed models are still maintained and used by numerous projects. This holds also more or less for SWRRB (Williams et al. 1985), which lives on in the codes of SWAT (Arnold et al. 1993) and the model that has been used for the research presented here – SWIM (Krysanova et al. 1998, 2000).

Semi-distributed models have been criticised to be less physically based compared to fully-distributed (i. e. gridded) models, and therefore not capable of modelling pollution pathways or the effects of deforestation (cf. Jensen & Mantoglou 1992). Abbott et al. (1986a) argued:

> "Because of their inherent structure these models also make very little use of contour, soil and vegetation maps, or of the increasing body of information in such areas as soil physics and plant physiology. Similarly, much historical information frequently consulted during project planning, for

> example crop yields over specific periods, survival patterns of particular types of vegetation and characteristic events occurring during floods and droughts, is not used directly."

This may have been correct at the time of the writing, but the approach of hydrological response units (HRUs) or hydrotopes – spatial simulation units of relatively homogeneous hydrological properties – has been implemented by most semi-distributed models today, and these hydrotopes are indeed derived from elevation, soil, and vegetation maps. Regarding vegetation and crop yields the critic seems also to be outdated as both are integral parts of eco-hydrological semi-distributed models like SWIM.

On the contrary, fully-distributed hydrological models have been heavily criticised, because they did not come up to the expectations. Beven (1989) spearheaded the attacks. He argued that physically-based distributed models can only *in principle* overcome the deficiencies of (semi-distributed) lumped parameter models, because they are still an extreme simplification of reality: Their descriptive equations would imply homogeneous *model* catchments while existing sub-grid heterogeneity could not be considered correctly even by lumped or effective parameters due to nonlinear processes. These models would be wildly overparameterised, Beven continues; comparison of model outputs and available data could not validate the purported simulation of the internal responses of a catchment. Last but not least, many parameter values could not be determined from the available measurements or physical reasoning; calibration is always needed.

There have been a few inter-model comparisons between representatives of the different spatial discretisations during the following decades, but these studies do not show that a certain type of model is principally superior with respect to simulation fidelity:

Refsgaard (1996) found a lumped conceptual model for an African catchment (with limited data availability) more accurate than a physically based distributed one while El-Nasr et al. (2005) who compared the discharge simulations of the fully distributed MIKE SHE to those of the semi-distributed SWAT for the Belgian Jeker catchment found that the fully distributed model appeared to be slightly better. To give a final example, Yang et al. (2000) yielded results of comparable quality from the fully distributed MIKE SHE and two semi-distributed lumped parameter models, TOPMODEL and GB, for the Seki River in Japan.

But it might be worthwhile to look not on simulation quality alone. In the final example, MIKE SHE needed 72 hours for the one-year run, while the other two models were content with 12 and 2 minutes of computation time, respectively. And the Jeker catchment used by El-Nasr et al. (2005) has an area of only 465 km² – it seems unlikely that the fully distributed approach would be feasible for larger catchments despite the advances in computer technology.

Further development of the SHE included a method for scanning the model grid and identifying groups of identical soil column conditions. This allowed Richards' equation to be solved for much fewer representative soil columns. Refsgaard et al. (2010) who report this write literally: "This is similar to the principles behind 'hydrological response units' commonly used in semi-distributed models."

Hence it is clear that the idea of physically based hydrological modelling by determining water fluxes between small, homogeneous grid elements in a fully distributed manner remains only a theoretical alternative to less physical, semi-distributed approaches when simulations for larger river basins are required. Woolhiser (1996) put it a bit defeatist by concluding that physically based models may be used for small watersheds while for intermediate and large watersheds simpler models would give equally bad answers at a lower cost. But if space-related results are desired, there is also no single-catchment model alternative to semi-distributed modelling.

1.4 APPLICATION OF SWIM IN THE ELBE RIVER BASIN

1.4.1 *Spatial model set-up*

Here the construction of SWIM's hydrotope structure is shown in detail by large-scale cut-outs of the underlying thematic maps. This is not only for visualising the concept of semi-distributedness by practical example, but it also gives a spatial impression of the input data that was used for the model set-up presented and used in the following chapters.

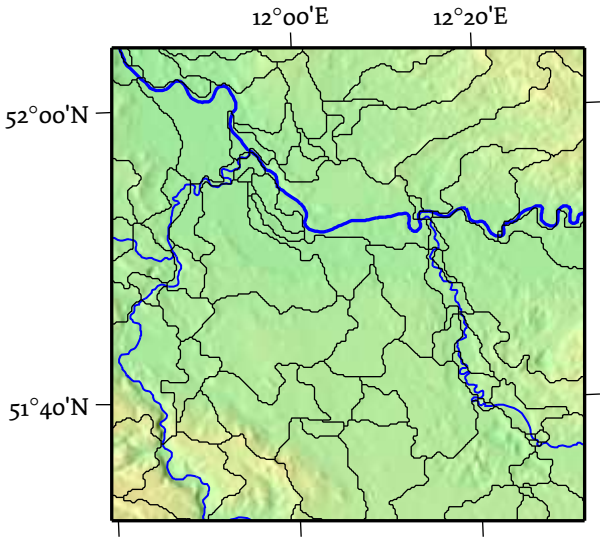

Figure 4: Sub-basin structure at Dessau. The map (scale approx. 1 : 1 000 000) covers 3600 km², about 2·7 % of the model domain; each edge measures 60 km.

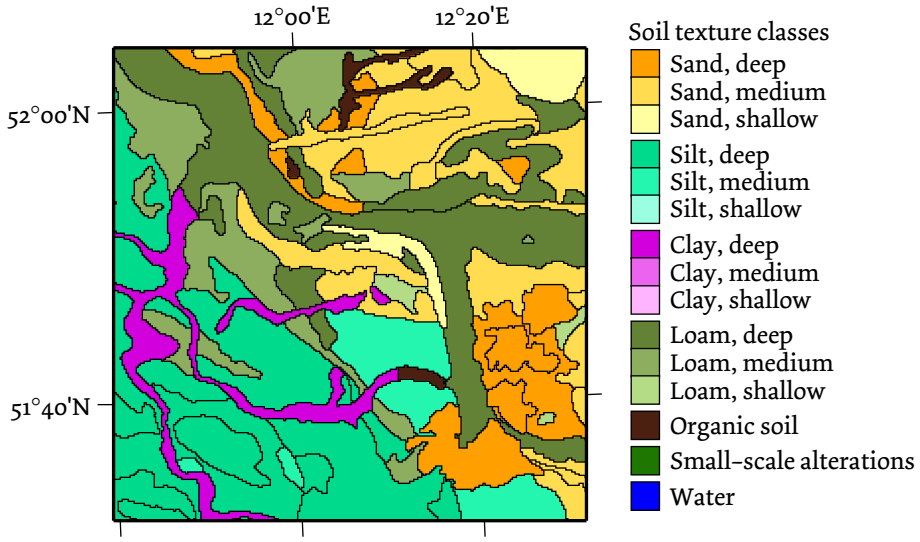

Figure 5: Soil textures at Dessau. This part of the map is based on the BÜK 1000. Map location, scale, and coverage are identical to Fig. 4.

We start with the sub-basin map. The cut-out shown in Figure 4 is located at the central part of the Elbe River and includes the inflows of Mulde and Saale. The shaded background visualisation of the rather level lowland relief does not easily suggest the sub-basin structure. It is indeed not derived from elevation data but imported from a quasi-official sub-basin delineation map of Germany (cf. Section 2.2.2 on Page 29).

One of the most interesting things to be observed in this map may be the wide range of sub-basin areas. Of all the 2278 sub-basins, the smallest 10 % are smaller than 4·18 km² while the largest 10 % are larger than 152·56 km². Many very small sub-basins are unavoidable at the interstices between subsequent inflows of river branches, but it is an open question whether this heterogeneity in the major simulation units does not affect the quality of the simulation.

Each of these sub-basins except the one representing the main outlet at Geesthacht has a certain other sub-basin into which the discharge is routed further. The complete network of smaller river branches and brooks (not shown in the map) is represented in this way, and the hydraulic properties of the sub-basin reaches are derived from an elevation map. The latter was provided by an interpolation of the Shuttle Radar Topography Mission (SRTM; Farr et al. 2007) data onto the 250 m map raster. No correction for vegetation or built-up areas had been applied: Sub-basin delineation is sensitive to these errors in lowland areas, but as already mentioned the sub-basin map had been obtained independently.

The soil map cut-out (Figure 5) looks rather nice, because there are samples of all major soil texture classes included here. This was in fact one reason to choose this region for the enlarged views.

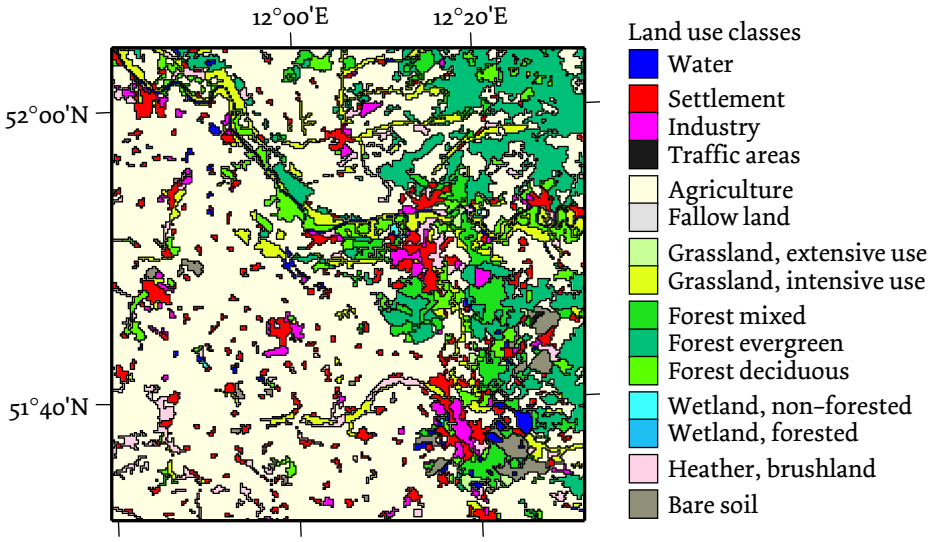

Figure 6: Land use types near Dessau. Reclassification of the CORINE2000 at 250 m raster resolution into the land use classes defined in SWIM. Map location, scale, and coverage are identical to Fig. 4

There are more soil unit boundaries than different colours, because the colours refer to the texture, but the map basis used here (BÜK 1000, Hartwich et al. 1995) differentiates also between soil types.

The inhomogeneity of the soil map regarding the different data sources for Germany and the Czech Republic has already been addressed (Fig. 2). It should be obvious that both the definition of the soil classification and the spatial resolution of the soil map have large impacts on the quality of the model representation and hence the simulation output. Figure 5 compared to Figure 4 suggests that it is rather low here: Individual sub-basin discharges are probably affected by the high degree of soil unit generalisation.

The next map in Figure 6 is the land use map. It is a reclassification of the European CORINE 2000 raster map (CEC 1995, Bossard et al. 2000) to the 15 land use classes of SWIM.

There are two larger agglomerations of settlements and industry in the eastern part of the map. The northern one on the Elbe River is the town Dessau (politically a part of Dessau-Roßlau), the southern one the double-town Bitterfeld-Wolfen. Generally the area is dominated by agriculture and rather equally speckled with smaller villages.

The fourth map shown in Figure 7, locating the wetland areas, would be the last for a standard SWIM set-up. Our wetland map was basically derived from the soil map, defining bog and gley soils characterised by surface-near groundwater as wetlands. A partial refinement had been made by a more detailed wetland map for Brandenburg, provided by Dr. Ottfried Dietrich from the Leibniz Centre for Agricultural Landscape Research (ZALF) in Müncheberg. Although wetlands do not take up

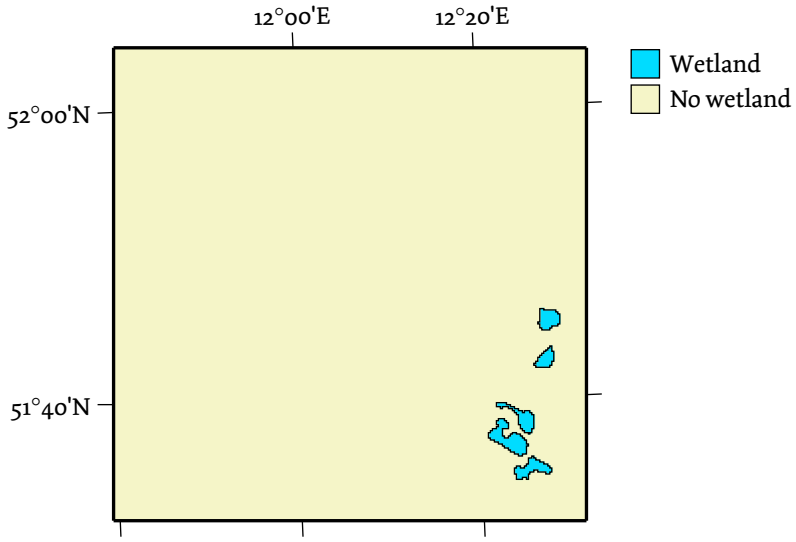

Figure 7: Wetlands near Dessau. Map location, scale, and coverage are identical to Fig. 4

much space in the selected cut-out, they are rather frequent in the northern parts of the Elbe River basin (cf. Figure 3).

A fifth map was required to consider disturbed discharge areas which are inactivated for certain time periods in the scenario simulations due to former open-cast mining activities. It shows the areas of excessive groundwater drawdowns and their projected recession. Details about this special feature are given in Subsection Groundwater drawdown on Page 30, and the respective map is shown in Figs. 8 and 9.

The hydrotopes – basic simulation units that are defined by homogeneous soil profile, land use, wetland property, occasionally a certain time period into which inactivity due to groundwater drawdown is required, and last but not least a definite sub-basin affiliation – can now be delineated by an overlay of these five maps. The result is shown in Figure 10.

The area distribution of the hydrotopes is even more varying than that of the sub-basins: Each of the smallest 11 % covers only one raster cell (0·0625 km²) while the largest 10 % are larger than 6·44 km²; the largest per cent are even larger than 35·91 km², and the largest one of all the 48 146 hydrotopes of the reference set-up covers 220·19 km².

Very large hydrotopes are formed in regions with a dominating land use class (like the agriculture in the example maps) and large soil map units. They may be suggestive of an overly simplification, but they are just mirroring missing heterogeneity of the input data. From the computational point of view, they represent the resource-saving advantage of the semi-distributed approach.

Different travel times of the water from more or less distant parts of very large hydrotopes to the river channel are disregarded, but this problem pertains also to small hydrotopes that are differently remote

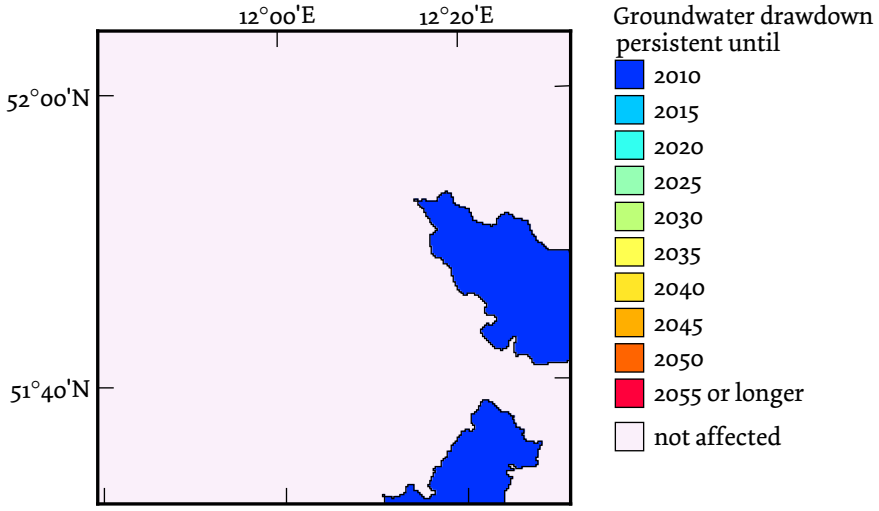

Figure 8: Extent and expected recession of groundwater drawdown areas near Dessau. Map location, scale, and coverage are identical to Fig. 4

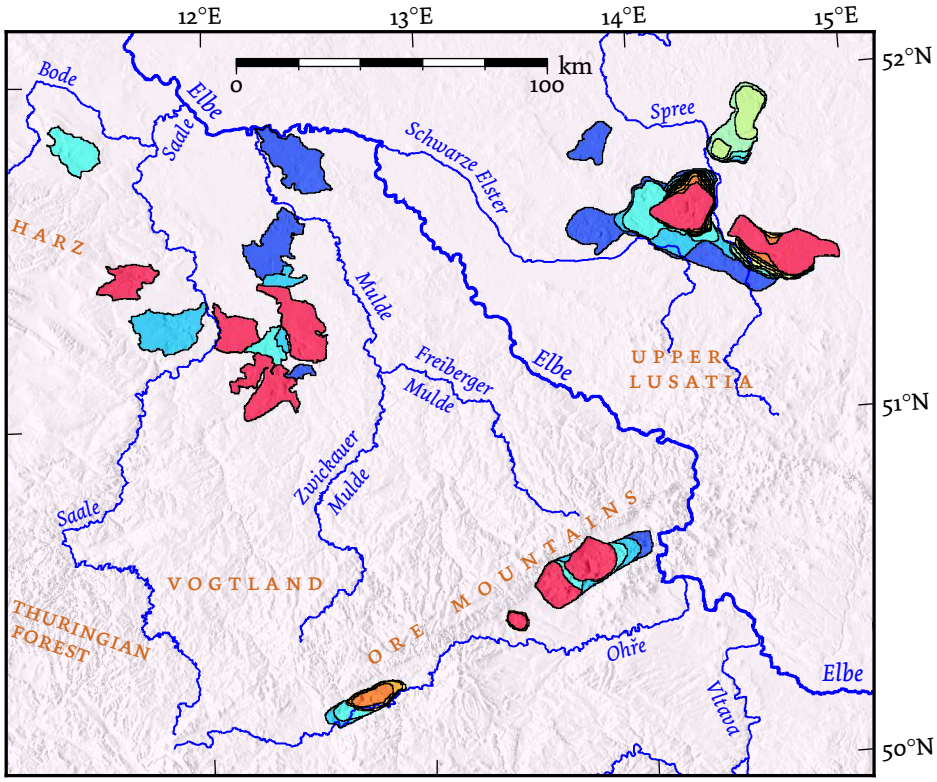

Figure 9: Groundwater drawdown areas and their projected recession in the entire Elbe River basin. This is the raster integration of the ten vector maps for the scenario without enhanced environmental orientation, cf. page 30. The original vector maps were provided by the environmental agencies of Saxony and Brandenburg and the former mining company LAUBAG. The map legend of Fig. 8 applies accordingly.

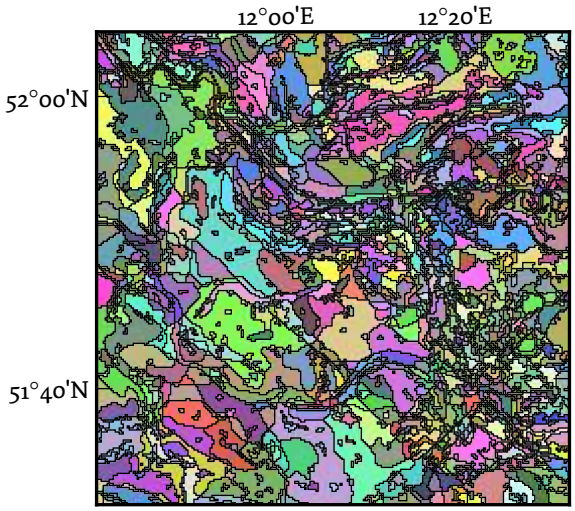

Figure 10: Hydrotope structure near Dessau. This is the overlay map from the five base maps presented in Figs. 4, 5, 6, 7, and 8. Map location, scale, and coverage are identical to Fig. 4.

from the channel – within the sub-basin representing the river reach. Thus, the sub-basins have to be small enough to avoid internal water travel times exceeding the one-day time step of the model.

Brief descriptions of the eco-hydrological modelling within the hydrotopes and the subsequent river runoff routing through the sub-basin structure are given in two Sections of the research papers in the following chapters: 'The eco-hydrological model SWIM' on page 29 and 'General model structure' on page 99.

1.4.2 *Sub-basin discharge deviations*

The already mentioned general problem of the degrading simulation quality for smaller sub-catchments shall be illustrated here: Figure 11 shows a map of the model domain (134 890 km²) with selected gauges and their sub-basins; their main features are listed in Table 1. Comparisons between measured and modelled discharge curves of these gauges are presented in Figure 12.

The good fit at Neu Darchau is partly due to a superposition of over- and underestimated hydrographs. These may consist of even more biased simulations for higher-oder catchments. However, the strong under-estimation at Lübben is due to an anthropogenic effect not considered in the model: There are large open-cast lignite mining activities in the Spree catchment upstream Lübben, for which more than 30 $m^3 s^{-1}$ of groundwater had been continuously pumped into the river in the 1980s (Grünewald 2001).

Figure 11: Sub-basin structure used for spatial calibration (beige pattern) and selected gauges with their catchment areas highlighted by blue tints. The discharge measurements are compared with the results of an only globally calibrated model run; results for the selected gauges are shown in Figure 12.

Table 1: General features of the catchment areas of Neu Darchau plus the five selected sub-basin gauges

Gauge River	Basin characteristics						Discharge 1981–1990			
	Area km²	Elevation m a.m.s.l.			Dominating geology	Typical land use	Runoff m³ s⁻¹			Rate *l* s⁻¹ km⁻²
		Min	Mean	Max			*MNQ**	*MQ*	*MHQ**	*Mq*
Neu Darchau Elbe	131 950	7	280	1602	—	Agriculture and Forest	303	729	2080	5·52
Ravensbrück Hegensteinfließ	180	55	78	124	Weichselian till	Forest	0·51	1·04	1·91	5·78
Wegeleben Bode	1215	70	343	1142	Silurian rock and Mesozoic limestone	Forest and agriculture	2·52	8·22	29·82	6·77
Lübben Spree	4492	48	149	610	Quarternary sands	Agriculture and open cast mining	12·82†	30·54†	67·79†	6·80†
Písek Otava	2914	354	660	1373	Precambrian rock (gneiss and granite)	Forest, pasture, and agriculture	7·77	23·13	157·50	7·94
Tuřice Jizera	2158	179	451	1436	Upper Cretaceous, Precambrian rock	Forest, pasture, and agriculture	7·50	30·90	206·80	14·32

* *MNQ* = Mean annual low flow; *MHQ* = Mean annual flood flow

† The runoff at Lübben was raised by mining activities.

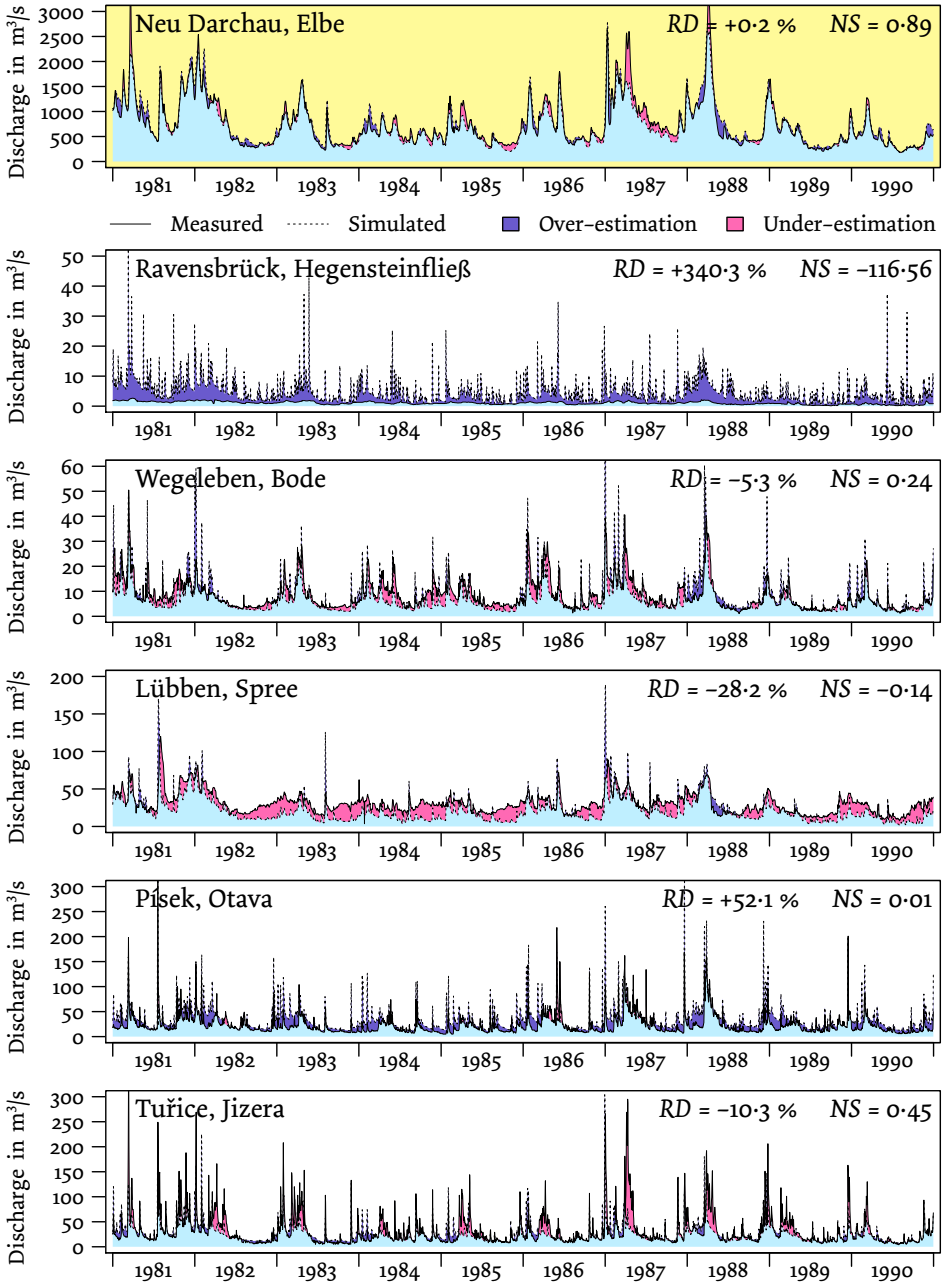

Figure 12: Comparison of measured and simulated hydrographs for selected gauges (cf. Figure 11). The model was only globally calibrated at the outlet. For each graph, relative deviation *RD* and Nash–Sutcliffe Efficiency *NS* of the model are given. Although the global calibration led to least relative errors for the basin outlet hydrograph (gauge Neu Darchau, shown with yellow background on top), the simulation contained large departures for many tributaries.

1.4.3 *The climate scenario*

To conclude the introduction on the Elbe modelling, the climate model that produced the scenario weather data for the SWIM application in Chapter 2 shall be critically appreciated. The '*Sta*tistical *R*egional Model' (STAR, recently renamed to '*Sta*tistical *R*egional *S*imulator'/STARS) had been developed at the Potsdam Institute for Climate Impact Research as computationally fast alternative to dynamical climate models for multi-realisation downscaling of climate change scenarios (Werner & Gerstengarbe 1997, Orlowsky 2007). It served as the scenario basis for the entire GLOWA-Elbe project (Gerstengarbe & Werner 2005, Gerstengarbe et al. 2013).

The basic working principle of STAR is explained in Section 2.2.5.1 on Page 37. Shortly said, the main idea is re-arranging blocks of synoptic measurements (here: daily values) in time in such a way that the new order matches a prescribed trend in one of the climate variables, temperature in our case. The underlying assumption is that future weather situations will be comparable to observed ones, because real-world observations must be in accordance with physical laws and the given orography and land cover which are considered as invariant. Consequently, a temperature increase due to climate change means that STAR more frequently draws warmer days from the pool of observations.

The warmest days in Central Europe are regularly sunny days. Apart from wintertime, temperature and radiation are positively correlated. This means that summer realisations from any any STAR scenario with increasing temperature trend are characterised by growing numbers of high-pressure weather situations with high radiation and low air humidity. Evapotranspiration which is concentrated in the summer months increases while precipitation decreases. Consequently, discharge simulations based on STAR scenarios show typically strong dependencies on the prescribed temperature trend, and increasing temperatures regularly lead to decreasing river runoff – as shown in Chapter 2.

Although hydrological trend projections derived from STAR scenarios are therefore questionable, there are considerable advantages of the algorithm: Due to the comparably low computational burden, 100 or even 1000 scenario realisations can be evaluated, e. g. by visualisation of uncertainty ranges like in Figure 23 on Page 44. Another possible advantage for hydrological modelling is the spatial structure of the scenario output that matches the input locations. The same meteorological stations can be used for calibration and validation with recent measurements as well as for producing scenario projections.

1.5 REMOTE SENSING IN HYDROLOGY

Integrating data from remote sensing into hydrological modelling has become a 'hot spot' in geosciences. This is shown by the bibliometric results illustrated in Figures 13 and 14 which have been obtained by querying one of the major data bases for scientific publications.

Figure 13 shows strong increases for the annual counts of publications (mainly journal articles) concerning hydrological modelling (left panel) and remote sensing (right panel). Of course, these graphs are overestimating the respective increase in scientific interest: Both graphs expose a step upwards in 1991 that indicates very likely an important time-horizon of data base coverage (which seems to be rather incomplete before). And it is also probable that some of the large number of recent publications reference only former hydrological modelling or remote sensing studies without actually contributing to these research fields. However, it seems clear that both topics have largely gained attention during the last decades.

Figure 14 displays the even more sweeping rise of the combination of hydrological modelling and remote sensing: the left panel shows the numbers of publications referencing both topics in their title or abstract, and the right one shows the relative shares of these subsets in the hydrological modelling literature. The simple linear fit might be disputable due to the scarce data basis in the 1980s, but one can say that the share of publications concerning hydrological modelling which are

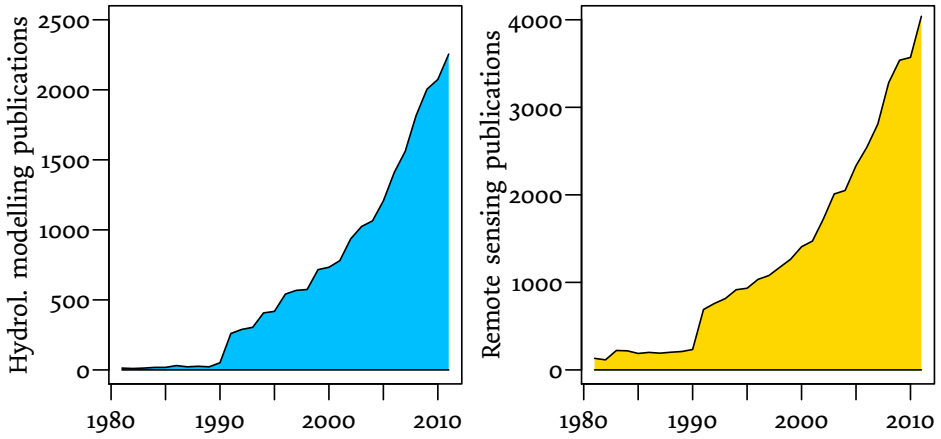

Figure 13: Annual counts of publications about hydrological modelling and remote sensing found in the Thomson Reuters (formerly ISI) Web of Knowledge database (URL http://webofknowledge.com) for the years 1981–2011. Left: number of records displayed for topic search after 'hydrolog* model*'; right: number of records displayed for topic search after 'remote* sens*'. The asterix wildcards cover variants like 'hydrological modelling' or 'models in hydrology'. The search was performed on 1st June 2012.

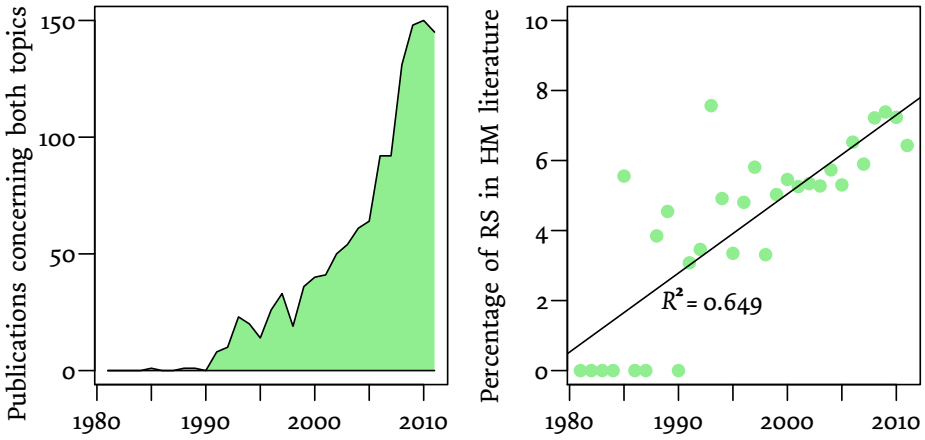

Figure 14: Increasing number of titles combining hydrological modelling and remote sensing research. The left panel shows the result counts for the combined topic search 'hydrolog* model* remote* sens*' (cf. Figure 13), the right panel displays for each year the fractions of these results within the set of publications found by 'hydrolog* model*' alone. The simple linear regression of their increasing trend over time is also drawn.

also related to remote sensing has nearly doubled within the last two decades.

The new research field is explored from two directions and their combination:

A. From the sky: Interpretation of remotely sensed raw data with respect to hydrological features. For example, surface temperatures and vegetation densities can be derived from combining several spectral channels, and hence evapotranspiration (*ET*) maps may be compiled. In many cases, validation is restricted to some pixels containing ground measurement sites. Examples are given by Wloczyk (2007) who validated satellite-based *ET* estimations by lysimeter data, or, to name recent works, by Yang et al. (2012) who applied the SEBAL method (Bastiaanssen et al. 1998a), or Shi et al. (2012) who reviewed the progress in estimating land surface parameters by microwave remote sensing.

B. From the ground: Calculation of hydrological parameters or modelling of hydrological systems principally by ground measured data. But remote sensing products aid in model set-up (especially for land use classification) or are used for subsequent validation. Recent examples include Lei et al. (2012) who modelled a catchment in China incorporating remotely sensed land use information, and Fatichi et al. (2012) who validated the hydrological and vegetation dynamics of their ecohydrological model by remote sensing data.

c. From both: Data fusion or assimilation methods where model system states are controlled or models partly driven by remotely sensed snapshot data. This obviously favourable idea to integrate irregularly available satellite scans was pioneered over two decades ago (Schultz 1988, 1993), but even with the availability of the needed computing power and mathematical concepts (McLaughlin 1995, Reichle 2008), many problems emerge in practical applications, e. g. the correlation of data availability with daylight or clear sky conditions that entails certain bias risks. However, there is a number of studies on assimilating remotely sensed soil moisture information into hydrological modelling; recent examples are: Brocca et al. (2012), Flores et al. (2012), or Hsu et al. (2012).

There are still gaps between these approaches; quite regularly unneglible differences between ground based and remotely sensed 'truths' can be observed. The two final papers of this thesis are devoted to these different perceptions. Although neither a fundamentally new approach nor an easy method to close the gaps between remote sensing, ground measurements, and modelling can be presented, there might emerge some helpful insights by tracing some error sources at the spatial level of selected sub-basins.

RESEARCH ARTICLES AND MANUSCRIPTS

All four research articles of my hereby presented PhD-thesis entitled 'Challenges of regional hydrological modelling in the Elbe River basin' were completely drafted by myself. Unless noted otherwise below, I produced all figures, compiled all tables, and made all calculations using the computer facilities of the Potsdam Institute for Climate Impact Research.

Chapter 2, Page 25:
Original title: *Spatially differentiated management-revised discharge scenarios for an integrated analysis of multi-realisation climate and land use scenarios for the Elbe River basin*
Co-authors: Hagen Koch, Fred F. Hattermann, and Frank Wechsung
Published in 2012 in *Regional Environmental Change:* Volume 12, Issue 3, Pages 633–648. doi:10.1007/s10113-012-0279-4

For this paper, Dr. Hagen Koch organised large amounts of water management data from numerous sources. Using these data, he corrected the measured hydrographs for the spatial calibration of the eco-hydrological model. All co-authors helped in shaping the text to its final form regarding the sectioning and many improvements in single paragraphs and sentences.

Chapter 3, Page 53:
Original title: *Precipitation or Evapotranspiration? Bayesian analysis of potential error sources in the simulation of sub-basin discharges in the Czech Elbe River basin*
Co-authors: Hagen Koch, Fred F. Hattermann and Frank Wechsung
Published in 2012 in *Regional Environmental Change:* Volume 12, Issue 3, Pages 649–661. doi:10.1007/s10113-012-0280-y

This article is the companion paper to the one presented in Chapter 2 and thus shares the same authors. Some runoff time series corrected by Dr. Hagen Koch have also been used here. The direct contributions of the co-authors were limited to smaller improvements of the drafted text.

Chapter 4, Page 71:
Original title: *Measured effects of new lake surfaces on regional precipitation / Mesures de l'impact de nouveaux lacs sur les précipitations régionales*
Co-authors: Zbigniew W. Kundzewicz, Fred Hattermann and Frank Wechsung
Published in 2007 in *Hydrological Sciences Journal:* Volume 52, Issue 5, Pages 936–955. doi:10.1623/hysj.52.5.936

This was the first scientific paper I ever published and I am indebted to all co-authors who had to teach me the art of scientific writing by reviewing several draft versions. The 'Exploratory data analysis' starting on Page 77 was proposed by Professor Dr. Kundzewicz, and he corrected my graphical presentation of wind directions in Figure 39 on Page 88.

Chapter 5, Page 93:
Manuscript title: *Three Perceptions of the Evapotranspiration landscape: Comparing spatial patterns from a distributed hydrological model, remotely sensed surface temperatures, and sub-basin water balances*
Co-authors: Frank Wechsung and Axel Bronstert
Submitted to *Hydrology and Earth System Sciences* on 8th Jan. 2013

My drafting of this article was closely supervised by Professor Dr. Bronstert who suggested the individual analyses on sub-basins with exceptional differences between the evapotranspiration estimations beginning on Page 112 within Section 5.3.2. The findings became finally relevant for the overall discussion in Chapter 6. Professor Dr. Bronstert also pointed out the concept of aleatoric and epistemic uncertainties to me, cf. Section 5.5.1 on Page 119; this uncertainty concept is also picked up in Chapter 6. Dr. Wechsungs contributions can be found in the discussion of possible errors from inaccurate plant cover modelling and the phenomena of global dimming and brightening; Section 5.4.3 on Page 118 addresses these points.

2

SPATIALLY DIFFERENTIATED DISCHARGE SCENARIOS FOR THE ELBE RIVER BASIN

Tobias Conradt, Hagen Koch, Fred F. Hattermann & Frank Wechsung

ABSTRACT A spatially differentiated, management-revised projection of natural water availability up to 2053 was requested for a basin-wide scenario study about the impact of global change in the Elbe River basin. Detailed discharge and weather information of the recent years 1951–2003 were available for model calibration and validation. However, the straightforward "classic" approach of calibrating a hydrological model on observed data and running it with a climate scenario could not be taken, because most observed river runoffs in Central Europe are modified by human management. This paper reports how the problem was addressed and how a major projection bias could be avoided. The eco-hydrological model SWIM was set up to simulate the discharge dynamics on a daily time step. The simulation area of 134 890 km² was divided into 2278 sub-basins that were subdivided into more than 47 500 homogeneous landscape units (hydrotopes). For each hydrotope, plant growth and water fluxes were simulated while river routing calculation was based on the sub-basin structure. The groundwater module of SWIM had to be extended for accurate modelling of low flow periods. After basin-scale model calibration and revisions for known effects of lignite mining and water management, evapotranspiration and groundwater dynamics were adjusted individually for more than 100 sub-areas largely covering the entire area. A quasi-natural hydrograph was finally derived for each sub-area taking into account management data for the years 2002 (extremely wet) and 2003 (extremely dry). The validated model was used to access the effect of two climate change scenarios consisting of 100 realisations each and resembling temperature increases of 2 and 3 K, respectively. Additionally, four different land use scenarios were considered. In all scenario projections, discharge decreases strongly: The observed average discharge rate in the reference period 1961–1990 is 171 mm/a, and the scenario projections for the middle of the twenty-first century give 91–110 mm/a, mainly depending on the climate scenario. The area-averaged evapotranspiration increases only marginally within the scenario period, e. g., from about 570 to about 580 mm/a for the temperature increase of 2 K, while potential evapotranspiration increases considerably from about 780 to more than 900 mm/a. Both discharge and evapotranspiration changes vary strongly within the basin, correlating with elevation. The runoff coefficient that globally decreases from 0·244 to 0·160 in the 2 K scenario is locally

governed primarily by land use; 68 % of the variance of the decreases can be attributed to this factor.

KEY WORDS Elbe River basin, Regional impacts of climate change, Natural water availability, Spatially distributed hydrological modelling, Spatial calibration, SWIM

2.1 INTRODUCTION

For a comprehensive assessment of global change effects on the regional water cycle in the Elbe River basin – the GLOWA-Elbe scenario study – future changes in water availability based on different climate and land use scenarios had to be projected. The considered scenario period covers the years 2004–2053. The projections should be spatially differentiated and referenced by river discharge observations that were revised to remove the effects of past water management practices.

The level of spatial resolution was defined by the requirements of subsequent assessments. These assessments included simulation studies about regional water management effects (Kaltofen et al. 2013a, Koch et al. 2013a,b) in general and for wetlands in particular (Dietrich et al. 2008, 2012, 2013), about nutrient loads (Venohr et al. 2013) and about metabolic alterations in the main stream channel (Quiel et al. 2011, 2013).

The subsequent studies needed projections of quasi-natural discharge (cf. Finke & Bjarsch 1996) in order to explore the effect of different management regimes and to avoid biasing by the implicit extension of past management measures into the future.

Water availability is an important issue for the Central European Elbe River basin (148 268 km², Fig. 15) as in many other river basins. The daily per-capita water availability is about 3 m³ (cf. data given by Simon et al. 2005). According to the 2005 Report of the International Commission for the Protection of the Elbe River (ICPER 2005), 29 % of precipitation is discharged. These numbers are probably too high, because the total basin runoff has been continuously biased upward for several decades as a result of mining activities (Grünewald 2001).

For the German part of the Elbe River basin, climate change effects on landscape hydrology and agricultural yields had already been assessed in a former scenario analysis using SWIM (Hattermann et al. 2005b, Krysanova et al. 2005). However, this former projection was based on unrevised runoff records and simplifying assumptions about the Czech tributaries.

The climate scenario used back then (Gerstengarbe & Werner 2005) postulated a decrease in mean precipitation of 10·4 % from 687 mm/a for the reference period 1961–1990 to 616 mm/a for the middle of the twenty-first century (2046–2055). The mean temperature was assumed to increase by 1·4 K within the scenario period (2001–2055). The resulting actual evapotranspiration slightly increased from 527 to 536 mm/a

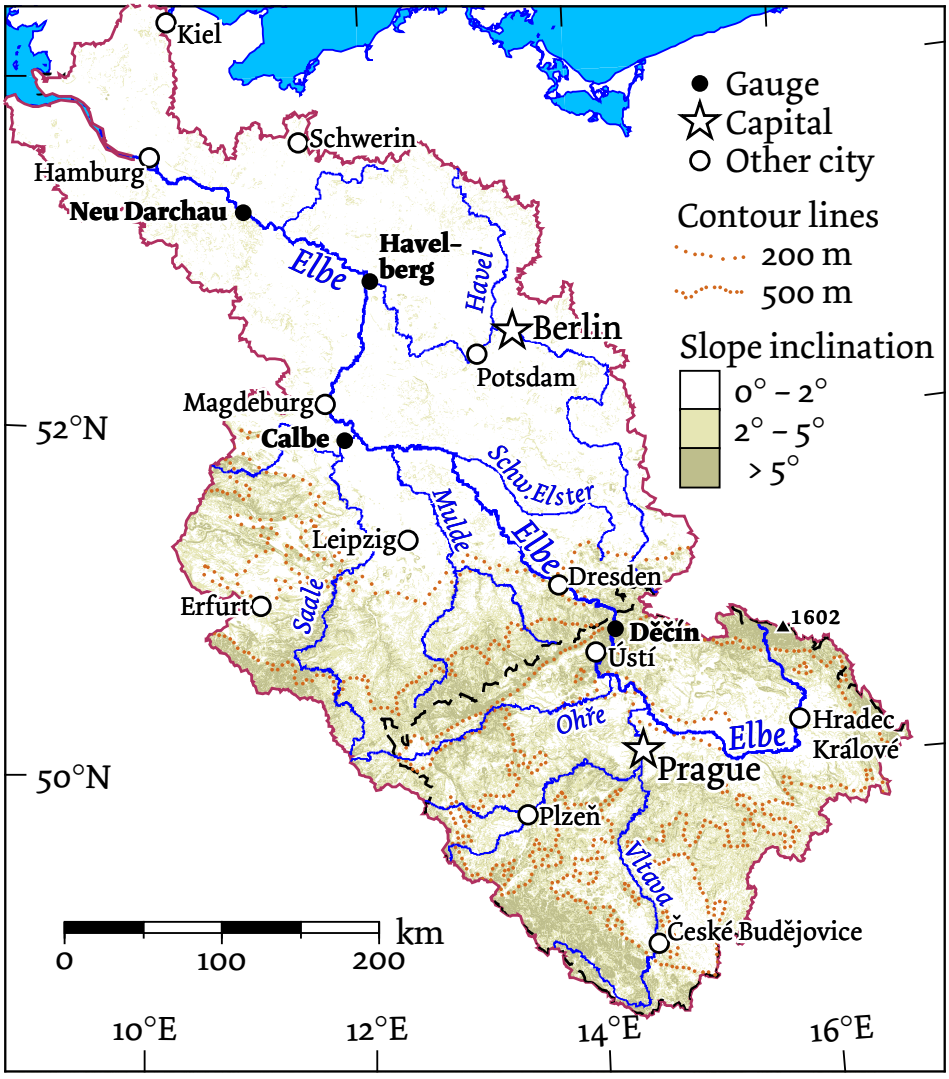

Figure 15: Map of the Elbe River basin. The catchment area can be separated into lowlands (typically below 200 m a.m.s.l.), hilly areas, and mountainous regions (above 500 m a.m.s.l., gradients over 5°). The highest spot is the Snezka Mountain (1602 m a.m.s.l.).

(+1·8 %), and the runoff rate showed a generally strong but regionally differentiated decrease from 172 to 101 mm/a (–41·4 %). The relative decrease did not differ among runoff components. Details of the evapotranspiration calculus that does not regard the CO_2 effect on transpiration are given below under 'Material and Methods'. Further information about the former study including sensitivity and uncertainty analyses can be found in Hattermann et al. (2005c).

The eco-hydrological model SWIM (Krysanova et al. 1998, 2000) is used also for the analysis presented here. It simulates water and matter fluxes as well as plant growth on a spatially semi-distributed basis. Therefore, it is suitable for both domain-wide application and the adequate representation of possible interactions between climate and land use such as a shifting vegetation period or combined effects of rain storms and sealed surfaces.

For this study, we extended the simulation domain of SWIM to include the Czech, Polish, and Austrian parts of the Elbe River basin. Accordingly, the climate scenario had to be extended in space. Compared to the previous study, we assumed stronger increases in temperature (+2·1 and +3·0 K) until 2055 and considered also four land use scenarios, described by Hoymann (2010b) and Hoymann et al. (2013). Moreover, the model was calibrated on revised discharge observations.

Several factors had to be taken into account for the revision of observed hydrographs. Among them were the influence of the mining activities in the region, the management of major reservoirs, and water transfers between sub-basins. For example, the drainage from the Lusatian mining district exceeded rates of 30 m^3/s in the 1980s and created a groundwater deficit of more than 12×10^9 m^3 at the end of the 1980s affecting an area of about 2100 km^2 (Grünewald 2001, 2003, Koch 2005).

The request for spatially representative runoff simulations in a multitude of tributaries as well as in the main stream runoff meant an additional challenge for calibration. Studies addressing watershed model fidelity at interior points report lower prediction accuracies, nearly without exception. The model fit of discharge simulation usually becomes worse the smaller the sub-catchment is (Andersen et al. 2001, Güntner 2002, Reed et al. 2004, Moussa et al. 2007) This even holds if spatial calibration has been applied (Fernandez et al. 2000, Cao et al. 2006, Bekele & Nicklow 2007, Artinyan et al. 2008). Two alternative options for spatial calibration in the Elbe River basin are analysed in a companion paper (Conradt et al. 2012a, Chapter 3).

This paper summarises how SWIM can be parameterised for runoff simulation when the measured hydrographs are heavily modified by anthropogenic influence, and accuracy is requested not only at the outlet of the river system but also at several sites within the basin. Using the parameterised model, we analyse the consequences of the climate and land use scenarios for water availability. Limitations of

the modelling approach during low flow periods will be particularly addressed.

2.2 MATERIAL AND METHODS

2.2.1 *The eco-hydrological model* SWIM

The functional principles of SWIM have already been described elsewhere (cf. Krysanova et al. 1998, 2000, Hattermann 2005). In brief, SWIM has been developed on the basis of the globally established model SWAT (Arnold et al. 1993, 1998, Gassman et al. 2007). Both models share the sub-basin approach with the sub-basins also representing river reaches. In SWIM, the sub-basins consist of so-called hydrotopes, the principal simulation units. These are homogeneous landscape patches with respect to land use, soil profile, and wetland characteristic.

All relevant eco-hydrological processes including plant growth are calculated for each hydrotope on a daily time step. Storages taken into account are interception, snow cover, soil water content (for up to 10 soil layers), and groundwater. The hydrotopes' runoff contributions are summed up to the sub-basin discharges. The latter are routed through the virtual river system by the Muskingum method (Maidment 1993).

SWIM had already been applied and validated for the Elbe River basin in different contexts (e. g. Hattermann et al. 2005c, Post et al. 2008). Examples for the development of SWIM modules applied to parts of the basin are given by the contributions of Hattermann et al. (2004a, 2006), Habeck et al. (2005), and Voß (2007).

2.2.2 *Spatial and climate input data*

The model domain of 134 890 km² is the part of the catchment area of the Elbe River upstream the Geesthacht Weir (cf. Figs. 19, 20, 21). It had been divided into 2278 sub-basins. This division was based on a digital catchment map of the German Federal Environment Agency (Umweltbundesamt) and on masters of the Czech water management authorities (Povodis). The relief characteristics of the sub-basins had been derived from NASA's freely available SRTM data (Farr et al. 2007).

In order to obtain a soil map for the Elbe River basin, we combined the general soil map of Germany ('BÜK 1000'; Hartwich et al. 1995) with a comparable Czech soil map (cf. Němeček & Kozák 2003). While there are characteristic soil profiles given for the 72 BÜK 1000 map units, profile data for the 20 units of the Czech map had to be copied from their likely counterparts in the German map in accordance with Tomášek (2003). Groundwater-influenced soil units were classified as wetlands where vegetation was modelled with direct access to groundwater. Recent land use had been reclassified from the CORINE2000 map (CEC 1995, Bossard et al. 2000) to the 15 land use classes of SWIM.

More than 47 500 hydrotopes were made up by an overlay of five maps: In addition to sub-basins, soil, wetland, and land use units, groundwater drawdown areas were also considered.

For each sub-basin, precipitation, global radiation, relative humidity, and the maximum, minimum, and average temperatures of that day are required. These variables were interpolated to the sub-basins from daily meteorological station data. Precipitation measurements were corrected for systematic bias (Richter 1995). There were 853 meteorological stations in the data pool, of which 783 are located in Germany and only 70 in the Czech Republic. This inevitably leads to decreased spatial fidelity of the interpolated data and the simulation results in the Czech part of the basin.

2.2.3 *Modifications of the standard version of* SWIM

2.2.3.1 *Groundwater drawdown*

The large-scale groundwater drawdowns in regions affected by lignite mining generated interior catchment areas. Any runoff formation in these areas is directed into filling the groundwater deficit until quasi-natural runoff conditions are successively re-established. Because a large number of mines are shut down, these interior catchments are shrinking. Ten maps predicting the shrinkage at five-year intervals had been compiled on the basis of projections of the environmental agencies of the German federal states Saxony and Brandenburg and of the former mining company LAUBAG (today Vattenfall Mining AG). These maps were integrated into one map with ten categories for hydrotope discretisation determining the years of switching the affected hydrotopes from inactivated runoff to the standard contribution scheme.

2.2.3.2 *Evapotranspiration calculus*

To maintain consistency with the SWIM set-up of Hattermann et al. (2005b), the standard method for calculating reference evapotranspiration was a Turc–Ivanov approach (cf. DVWK 1996), using net radiation, air humidity (for cold days), temperature, and monthly factors given by Glugla & König (1989).

The further computations to determine actual evapotranspiration include linear modifications of this reference evapotranspiration with respect to land use (ATV-DVWK 2002) and air humidity. Plant transpiration and soil evaporation are calculated separately according to Ritchie (1972). Finally, water stress is calculated from the water contents of rooted soil layers, and actual evapotranspiration and plant growth are reduced accordingly.

Modelling of the impact of increased CO_2 on plant transpiration is optionally switchable in SWIM but has not been activated so far.

Additional research is needed to evaluate the results of Hattermann et al. (2005b) and this study with respect to this CO_2 effect.

2.2.3.3 *Groundwater modelling*

The hydrographs of most tributaries and from gauging stations along the Elbe River itself could be reproduced with Nash–Sutcliffe efficiencies (Nash & Sutcliffe 1970) over 0·7 after rough calibration. An exception was the Havel River: Even a separate set of parameters for the catchment area of this important tributary could hardly raise the Nash–Sutcliffe value above 0·5. Noticeable was a delay of the low flow periods in late summer of 2–3 months, shown in Figure 16(a).

We assumed that the simulated plant water uptake at sites with a near-surface groundwater table (wetlands and riparian zones) was the probable cause of the unsatisfactory model behaviour for this tributary. While SWIM originally did not account for plant roots accessing the groundwater at all, Hattermann et al. (2006) implemented groundwater modelling in hydrotopes including groundwater table-dependent control of plant water and nutrient uptake for the Nuthe catchment area (1803 km²) south of Potsdam (cf. Fig. 15).

Such a detailed modelling was not feasible for the Elbe River basin which is more than 70 times as large as the Nuthe basin. Here, groundwater tables and discharges are computed on sub-basin scale. Although the model accounted for vegetation having direct groundwater access, the relatively sluggish reaction of the sub-basin groundwater storages caused part of the delay in Figure 16(a).

In the first place, SWIM was changed in order to meet the water demand of the riparian vegetation directly from the sub-basin discharge. The result is displayed in Figure 16(b). The amplitude of the seasonal cycle is still not rendered satisfactorily. Groundwater runoff is the dominating discharge component in the relatively plain Havel catchment area. Thus, the groundwater module was altered to improve the seasonal discharge dynamics.

In the standard version of SWIM, groundwater recharge is simulated from percolation into a first linear storage. Another linear storage representing the "shallow" groundwater component receives 95 % of this recharge and contributes to runoff. A deep groundwater storage does not exist; the remaining 5 % of "deep" groundwater is assumed to bypass the river system subterraneously. Our model version uses the "shallow" storage for a quick groundwater runoff component and has been extended by a third linear storage which contributes the respective slow component to river runoff. There is no groundwater bypassing the model river system any more.

The following equations show the new mode of calculation in detail with

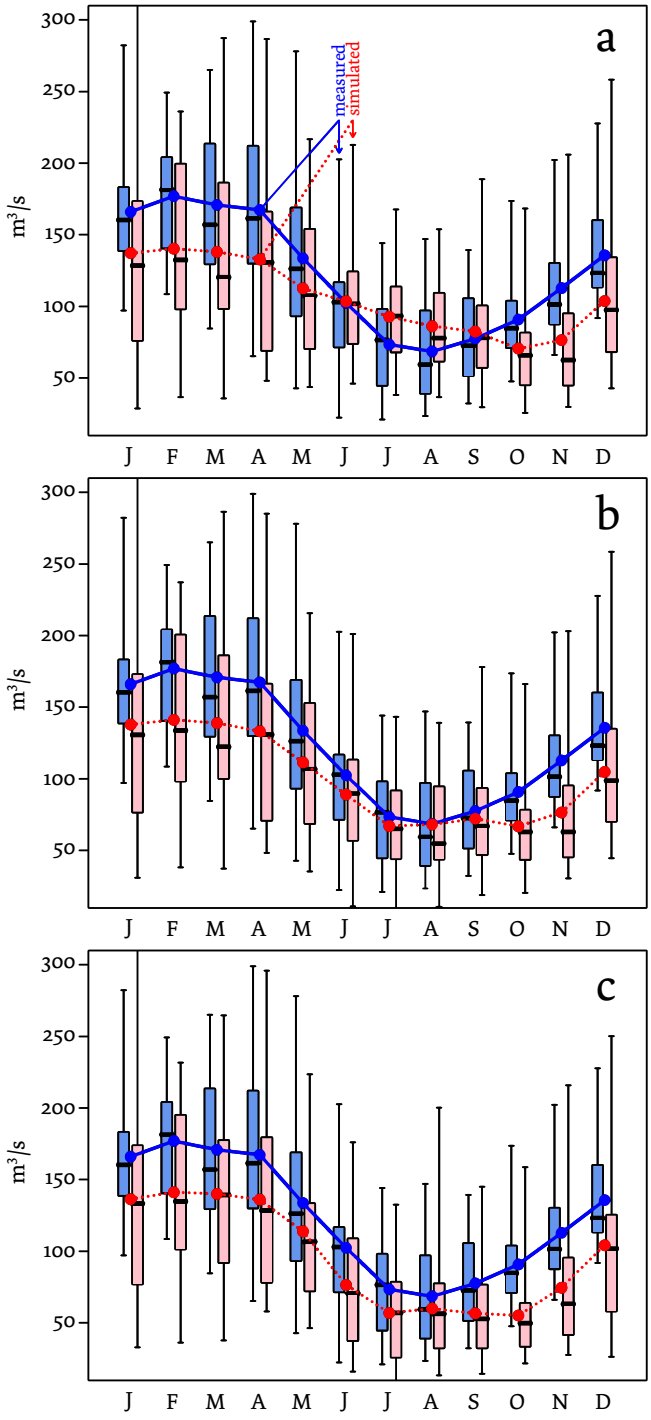

Figure 16: Improvements of the fit of simulated runoff for Havelberg (Havel River) to measurements for the reference period 1961–1990. a) Initial run; b) with direct impact of plant water uptake in riparian zones; c) ditto, with enhanced groundwater module. (The difference between the hydrographs approximately equals the input from lignite mining activities which do not show seasonality.) The box plots show the distributions of the monthly values, and the connecting lines show their average values.

$Q_S^{(t)}$	Percolation on day t
$Q_R^{(t)}$	Groundwater recharge on day t
α_{rchg}	Groundwater recharge parameter
d	Reaction time of groundwater recharge in days
$R_{\text{fast}}^{(t)}$	Fast component of groundwater recharge on day t
$R_{\text{slow}}^{(t)}$	Slow component of groundwater recharge on day t
c	Splitting parameter between fast and slow component
$Q_{\text{fast/slow}}^{(t)}$	Fast/slow component of groundwater discharge on day t
$Q_{\text{fast/slow}}^{(t-1)}$	Fast/slow component of groundwater discharge on the day before
$\alpha_{\text{fast/slow}}$	Fast/slow groundwater release parameter, here: $\alpha_{\text{fast}} = 0{\cdot}0260$, $\alpha_{\text{slow}} = 0{\cdot}0016$
$Q_{\text{GW}}^{(t)}$	Groundwater runoff on day t

The groundwater recharge is a linear storage function of percolation like in the original model version:

$$Q_R^{(t)} = \alpha_{\text{rchg}} Q_R^{(t-1)} + (1 - \alpha_{\text{rchg}})\, Q_S^{(t)} \tag{1}$$

$$\alpha_{\text{rchg}} = \exp\left(-\frac{1}{d}\right). \tag{2}$$

The model modification starts with the adjustable distribution of the groundwater recharge between the quick 'shallow' and the sluggish 'deep' aquifer:

$$\left.\begin{aligned} R_{\text{fast}}^{(t)} &= c\, Q_R^{(t)} \\ R_{\text{slow}}^{(t)} &= (1-c)\, Q_R^{(t)} \end{aligned}\right\} \text{ with } \quad c \in [0, 1] \tag{3}$$

We assumed equal shares for all simulations ($c = 0{\cdot}5$). Both linear storages of the groundwater components in Equation 4 are in analogy to Equation 1, and both their releases are finally added to the groundwater discharge in Equation 5.

$$\left.\begin{aligned} Q_{\text{fast}}^{(t)} &= \alpha_{\text{fast}} Q_{\text{fast}}^{(t-1)} + (1 - \alpha_{\text{fast}})\, R_{\text{fast}}^{(t)} \\ Q_{\text{slow}}^{(t)} &= \alpha_{\text{slow}} Q_{\text{slow}}^{(t-1)} + (1 - \alpha_{\text{slow}})\, R_{\text{slow}}^{(t)} \end{aligned}\right\} \text{ with } \quad 0 \ll \alpha_{\text{fast}} < \alpha_{\text{slow}} < 1 \tag{4}$$

$$Q_{\text{GW}}^{(t)} = Q_{\text{fast}}^{(t)} + Q_{\text{slow}}^{(t)} \tag{5}$$

Figure 16(c) shows the annual hydrograph simulated with the enhanced groundwater module. Nash–Sutcliffe efficiencies for Havelberg finally reached 0·75 without individual parameter settings. Simulated runoff is below the measured reference values throughout, but this is caused by the mining activities not considered here. The mean drainage input of the reference period (1961–1990) was just over 20 m³/s (Grünewald 2001), approximately equalling the shift in Figure 16(c).

2.2.4 *Calibration and validation*

Assigning optimum parameter values found for a few selected sub-basins which are largely free from human impacts to the entire river basin did not produce realistic output. There are numerous reports of this regionalisation problem in hydrology (e. g. Heuvelmans et al. 2004, Lee et al. 2006, Cole et al. 2008, Snelder et al. 2009). Alternatively, a two-stage approach consisting of a basin-scale calibration and a subsequent spatially distributed calibration was chosen. Almost all measured hydrographs are distorted by human management; therefore, the reference data had to be revised extensively to exclude management effects, i. e., reservoir releases, discharges from wastewater treatment plants, etc., before they could be used for calibration.

2.2.4.1 *Basin-scale calibration*

The model was calibrated globally for the entire basin at the lowermost gauge station Neu Darchau (Elbe) (see Fig. 15). Only continuous anthropogenic groundwater inputs and low flow supplements were considered for management correction of the runoff observations for this gauge station. The calibration time period of 1981–1990 represents the longer climate basis period 1961–1990 regarding water balance and extreme years (dry: 1989 and 1990, wet: 1981 and 1988). The regional climate change compared to pre-industrialised conditions can still be neglected for the 1980s.

Six global model parameters that were known to be most sensitive were adjusted for this time period: an evapotranspiration correction factor, a correction for the hydraulic soil conductivities, and two groundwater and two river routing parameters. Besides manual parameter estimation, 50 combinations of parameter values were tested by Latin hypercube sampling (McKay et al. 1979, Iman et al. 1981). The best fit was further optimised with an iterative gradient method (cf. Blobel & Lohrmann 1989) using the program PEST ('Parameter EStimation Tool', Doherty 2004).

2.2.4.2 *Basin-scale validation*

The observed and simulated hydrographs at gauge station Neu Darchau (Elbe) for the years 1971–2000 based on the basin-scale calibration of 1981–1990 are depicted in Figure 17. As could be expected, the Nash–Sutcliffe efficiencies are highest for the central decade used for calibration (Table 2).

SWIM overestimates the runoff for the last validation decade 1991–2000 by 13.5 % as can be seen also in the lowermost panel of Fig. 17.

The average simulated runoff of that period was 87 m^3/s higher than the observed mean of 642 m^3/s. However, the low flow periods are simulated with only small errors. The absolute volume departure of all

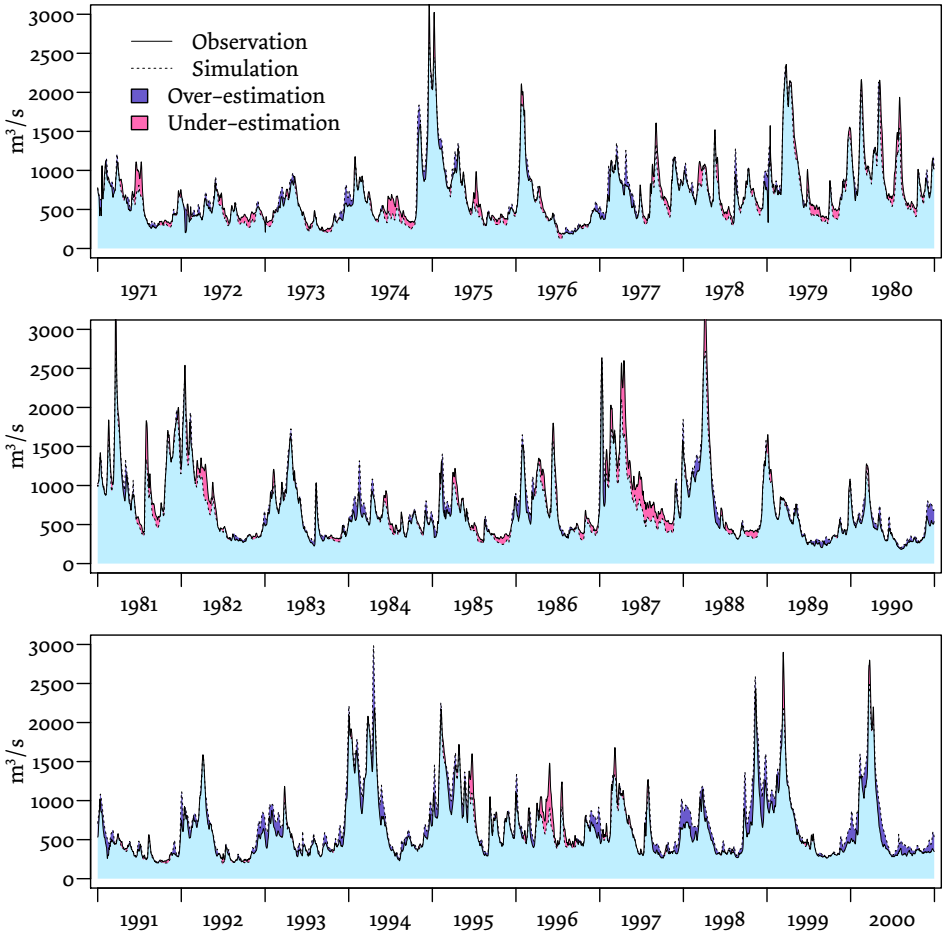

Figure 17: Measured and simulated hydrographs for the gauge Neu Darchau (Elbe) in the years 1971–2000, based on basin-scale calibration for the central decade 1981–1990.

Table 2: Results of the model validation at gauge Neu Darchau (Elbe)

Fidelity measure of the simulation	1971–1980	1981–1990	1991–2000
Nash–Sutcliffe efficiency (daily data)	0·905	0·924	0·825
Nash–Sutcliffe efficiency (monthly data)	0·940	0·945	0·848
Relative departure from water volume (%)	±0·0	−1·3	+13·5

days in the previous decade 1981–1990 with runoffs lower than 300 m³/s at gauge station Neu Darchau (Elbe) is just −9·7 m³/s (observation average: 260 m³/s, n = 300), and in the decade 1991–2000, it is only +4·3 m³/s (observation average: 263 m³/s, n = 427).

2.2.4.3 *Spatially distributed calibration*

After basin-scale calibration, sub-area-specific parameter adjustments were carried out. Measured runoff data of more than 100 gauges from all parts of the river basin could not be used directly as reference due to management impacts. Revision of the data by subtracting the management-induced flows was necessary, as mentioned before (cf. Koch et al. 2010). Limited data availability restricted this work for most sites to the years 2002 and 2003. Both years were fortunately extremely different. While 2002 was characterised by high runoffs and a centennial flood of the Elbe River, 2003 was dominated by low flow situations as a consequence of an extremely dry and hot summer (Table 2).

The calibration parameters used for the sub-regions are an evapotranspiration factor for adjusting the water balances and a tuning factor for the groundwater α-parameters (cf. Eq. 4). The latter primarily controls the seasonality of discharges via the recession time of the base flow in summer which seemed to be the main reason for deviations with respect to the hydrograph shape.

2.2.4.4 *Spatially distributed validation*

Due to missing reference data, no hydrograph-oriented validation for all sub-areas was possible. Since the discharge time series of the gauge Děčín (Elbe) (see Fig. 15) dates back to November 1887, it was at least possible to compare historical exceedance frequencies of monthly discharges measured before the system of reservoirs in the Czech Republic was built to those simulated by SWIM. The result is shown in Figure 18.

The resulting graphs shown in Fig. 18 are similar, but the simulated discharges are lower. At low flows, the differences are relatively small. Any interpretation of this result (see the Discussion) has to consider the differing reference periods.

2.2.5 *Discharge simulation under scenario conditions*

2.2.5.1 *Climate scenarios from the scenario model* STAR

This research uses climate scenarios from the statistical downscaling model STAR (Werner & Gerstengarbe 1997, Orlowsky 2007) as input. Readers who would like to know more about the assumptions and

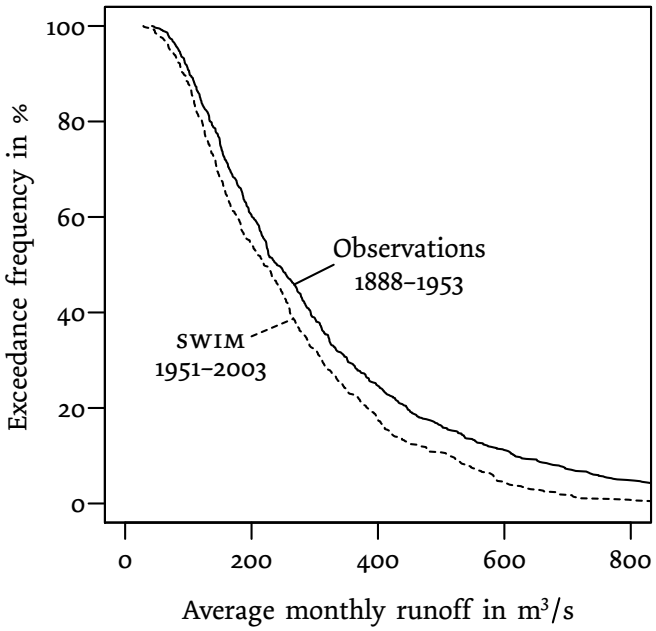

Figure 18: Measured and simulated exceedance frequencies of average monthly discharges at the gauge Děčín (Elbe)

settings in the climate scenario generation summarised below should consult the cited literature, especially Gerstengarbe et al. (2013).[1]

All STAR climate scenarios for the Elbe River basin consist of extrapolations of recent climate station time series (1951–2003) into the scenario period of nearly the same length (2004–2055; SWIM simulations only until 2053). A scenario is based on a prescribed temperature trend. Blocks of twelve subsequent days of recent measurements are assigned new calendar dates in the future by a heuristic approach using a random number generator. The seasonal position of a twelve-day block is not allowed to shift arbitrarily within the year. The resulting temperature trends of a large number of generated realisations differ more or less from the prescribed trend; hence, 100 realisations are finally selected resembling the temperature trend within close limits. For the other meteorological variables, STAR retains the range of natural variability. Therefore, the 100 realisations provide a distribution of precipitation and discharges showing the uncertainty range of a single scenario projection. This constitutes a special strength of the applied approach.

We will analyse the consequences of two climate scenarios produced by the current STAR version (Gerstengarbe et al. 2013): STAR T2 and STAR T3. The acronyms T2 and T3 denote 2·1 and 3·0 K temperature rise, respectively.

1 Note also the remarks in the introductory Section 1.4.3 on Page 18.

2.2.5.2 *Land use and lignite mining scenarios*

In addition to recent land use, four land use scenarios are considered. The land use scenarios had been developed using the model LandUse-Scanner (Hoymann 2010a,b) according to a set of development frames (Hartje et al. 2013). These consist of four possible combinations (A1^0, A1$^+$, B2^0, and B2$^+$) of two binary factors: the IPCC storylines (Nakicenovic et al. 2000) with the specifications 'globalisation' (A1) and 'differentiation' (B2) and the environmental policy with the two levels 'not enforced' (0) and 'enforced' (+). The largest contrasts can be found between the scenarios A1^0 and B2$^+$. In the first case, settlement growth is maximised, and in the other one, it is minimised. Mining activities differ as follows: Lignite mining is continued on a large scale in scenario A1^0, while it clearly declines in scenario B2$^+$. This affects the process of shrinking of the areas without runoff generation due to groundwater drawdown.

Future population trends are not considered directly. Firstly, there are only small changes to be expected for both IPCC storylines (Blazejczak et al. 2013), and secondly, water consumptions by industry and households are not covered by SWIM anyway.

2.3 RESULTS

2.3.1 *Water balance simulations*

The simulation results are summarised in Table 3. The runoff coefficient of 0·24 for the revised water balance during the period 1961–1990 differs from that of 0·29 reported for unrevised conditions (cf. Introduction).

The mean scenario runoff is always lower than during the observation period (Tab. 3). This holds already at the beginning of the scenario period (T2, 2004–2013). The water balance numbers in Table 3 confirm that small relative changes in precipitation and evapotranspiration may cause striking reductions in runoff and groundwater recharge. Drier climate scenarios with higher temperature increase and thus higher potential evapotranspiration rates do not lead to comparably higher actual evapotranspiration due to the limitations in water availability.

Global runoff variations caused by the different land use scenarios were negligible. The most extreme land use scenarios regarding runoff effects were A1^0 (globalisation without enforced environmental policy) and B2$^+$ (differentiation with enforced environmental policy). The differences in runoff were limited to 4 % higher discharge in A1^0 compared to B2$^+$ due to the difference between the fractions of sealed surface (cf. Hoymann 2010a, 2011, Hoymann et al. 2013). Hence, only results from the scenario A1^0 are presented.

Table 3: Changes in the mean annual water balance numbers for the model domain

	Obs.	STAR climate scenarios					
	1961–1990	2004–2013		2044–2053			
		T2		T2		T3	
	mm	mm	Δ%	mm	Δ%	mm	Δ%
Precipitation	701·2	710·6	+1·3	691·4	−1·4	675·5	−3·7
Evapotranspiration	530·3	570·1	+7·5	581·0	+9·6	584·7	+10·3
Direct runoff	53·4	41·5	−22·3	29·5	−44·8	21·1	−60·5
Groundwater recharge	117·5	99·0	−15·7	80·9	−31·1	69·6	−40·8
Total runoff*	170·9	140·5	−17·8	110·4	−35·4	90·7	−46·9
Runoff coefficient	0·244	0·198		0·160		0·134	

*without draining from mines

Figures for 1961–1990 are based on measurements; scenarios are averages of all simulation runs of 100 STAR climate realisations, using the land use scenario A1[0]. Results for the first scenario decade 2004–2013 are given for T2 only, because differences to T3 are negligible.

2.3.2 *Landscape hydrology*

In general, the precipitation pattern governed by orography affects the spatial distribution of runoff contributions. In Figure 19, light tints show dry regions like the area to the south and east of Magdeburg, and water surfaces and wetlands can even have negative values (e. g. the Müritz Lake at the northern edge of the area or the Spreewald wetland, 80 km south-east of Berlin) while large urban agglomerations like Berlin show up darker than their surroundings due to increased direct runoff (for location of the named cities, see Fig. 15).

The partly drastic decreases in runoff generation are distributed over the entire Elbe River basin (Figure 20). Hot spots are mountain ranges but also water surfaces and wetlands which are characterised by negative runoff contributions (evapotranspiration exceeds precipitation). These negative runoff contributions require surface or groundwater exchange to compensate the losses.

Comparing Figure 20 with a scenario map of the changes in the climatic water balance (Gerstengarbe et al. 2013) reveals important differences. The small-scale variability of changes is much higher in discharges than in the climatic water balance, and the mountain ranges show up much more distinctly in Fig. 20 through strong declines in runoff.

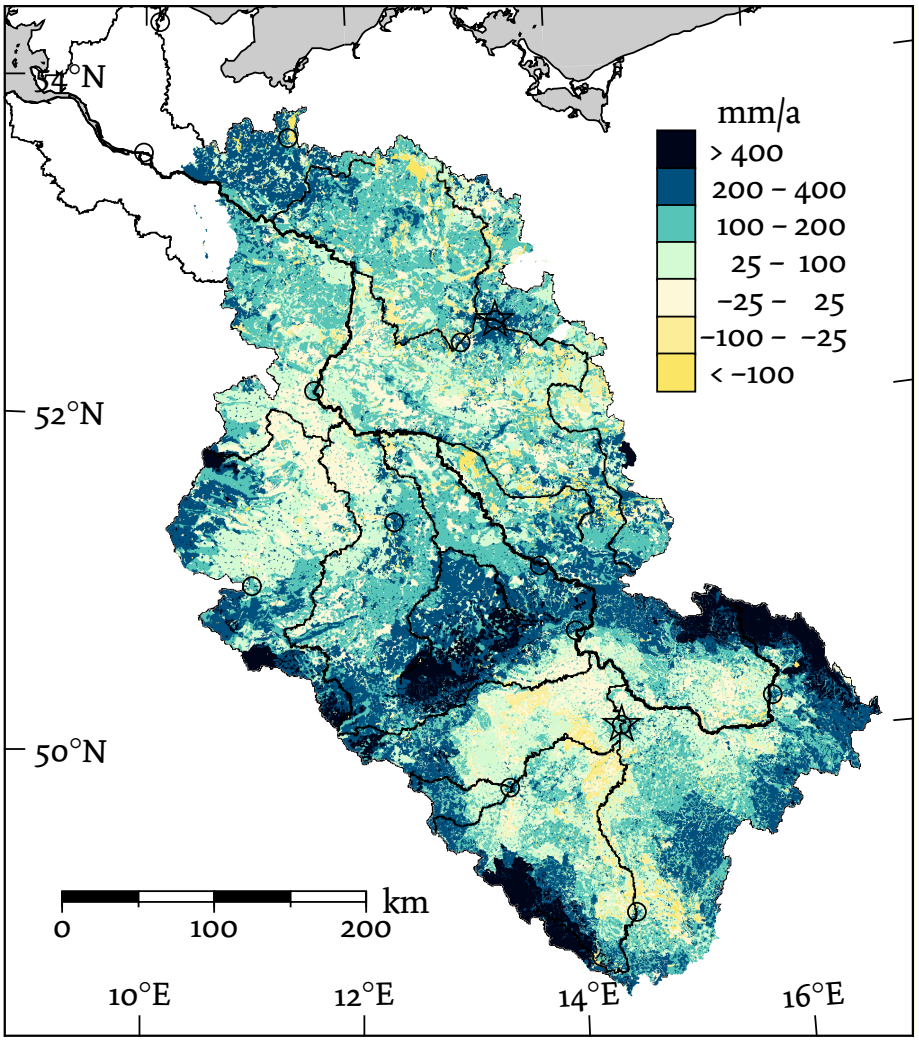

Figure 19: Spatial distribution of runoff contributions. Values of the first 10 years of the scenario period (2004–2013) averaged from all 100 climate realisations of the T2 scenario.

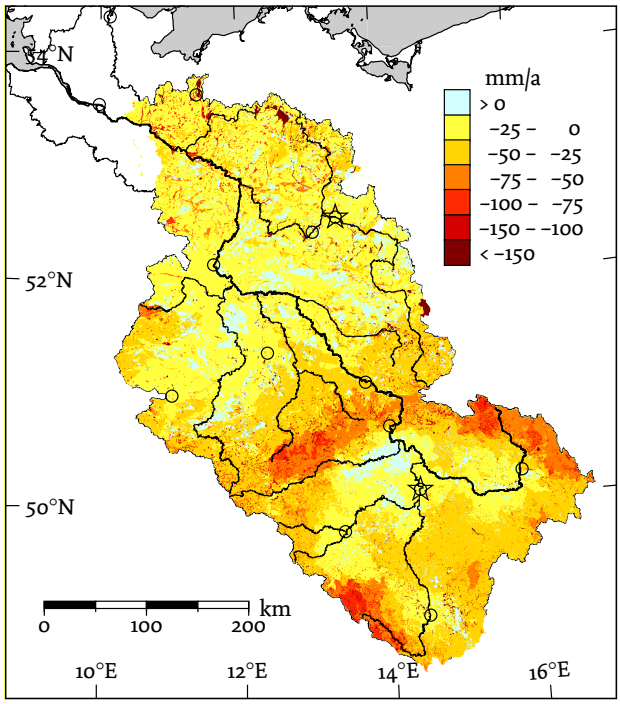

Figure 20: Change in average runoff contributions within the scenario period: differences between runoff contributions in the years 2044–2053 and 2004–2013. Basis: 100 climate realisations of the T2 scenario.

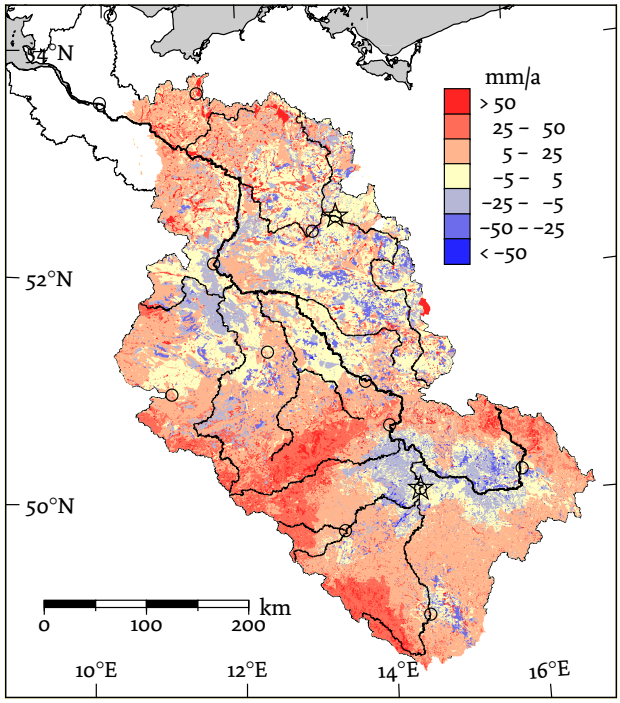

Figure 21: Development of evapotranspiration depths within the scenario period: differences between the average daily evapotranspiration in the years 2044–2053 and 2004–2013. Basis: 100 climate realisations of the T2 scenario

The weak increase in area-averaged evapotranspiration splits into stronger increases along mountain ranges and wetlands, especially in the north-west, and decreases in the lowlands, where the difference between potential and actual evapotranspiration increases (Figure 21). It has to be noted that the spatial pattern of changes (Figs. 20 and 21) is stable throughout all climate realisations.

The strong dependency of hydrologic response on the local (hydrotope) differentiation also becomes evident in alterations of the runoff coefficient. A multivariate linear regression model depending on continuous and factor variables for the changes in hydrotope runoff coefficients between the first and last decade of the scenario period explains the latter mainly by land use (factor, 68.0 %); i. e., the land use of a hydrotope determines strongly how runoff processes change during the scenario period. The other independent variables are of high significance ($p \leq 10^{-6}$) but minor influence: soil type (factor, 4·4 %), climatic water balance change (continuous, 1·2 %), and elevation (continuous, 0·3 %). This leaves an unexplained part of 26·1 % of the total variance. Including precipitation change into the set of independent variables increases the explained part only by 0·01 %.

Regarding the area-averaged runoff coefficient, there are drastic decreases. The values of 0·243 for the reference period (1961–1990) and of 0·160 for the middle of the twenty-first century in the T2 scenario given in Table 3 nearly match the results given by Hattermann et al. (2005b) for an average STAR realisation for the German Elbe River basin: 0·250 for the reference period and 0·163 for the middle of the century.

2.3.3 *Evapotranspiration and runoff scenarios*

While the potential evapotranspiration averaged from all 100 realisations clearly rises in the scenario period, the actual evaporation changes only marginally due to the decreasing water availability. The range of annual potential evapotranspiration values is larger than the shift of the mean during the scenario period, though (Figure 22, left and middle panel). There is no correlation between the monthly area-averaged potential and actual evapotranspiration depths (Fig. 22, right panel).

The impacts of climate change can explicitly be seen in the temporal runoff projections. The observations and simulated distributions for monthly discharges at four main gauges are shown in Figure 23. It should be noted that the scenario simulations represent a quasi-natural, unmanaged situation. Subsequent implications for the managed runoff are considered by Koch et al. (2013a) and by Kaltofen et al. (2013a).

All projected runoff distributions for the Elbe River, Saale River, and Havel River drift towards drier conditions. The drastic decline between measurements and simulation at gauge station Havelberg (Havel) is caused by not considering the mine discharges in the simulation (cf. the calibration in Figure 16(c)). But the decreases in runoff at the other

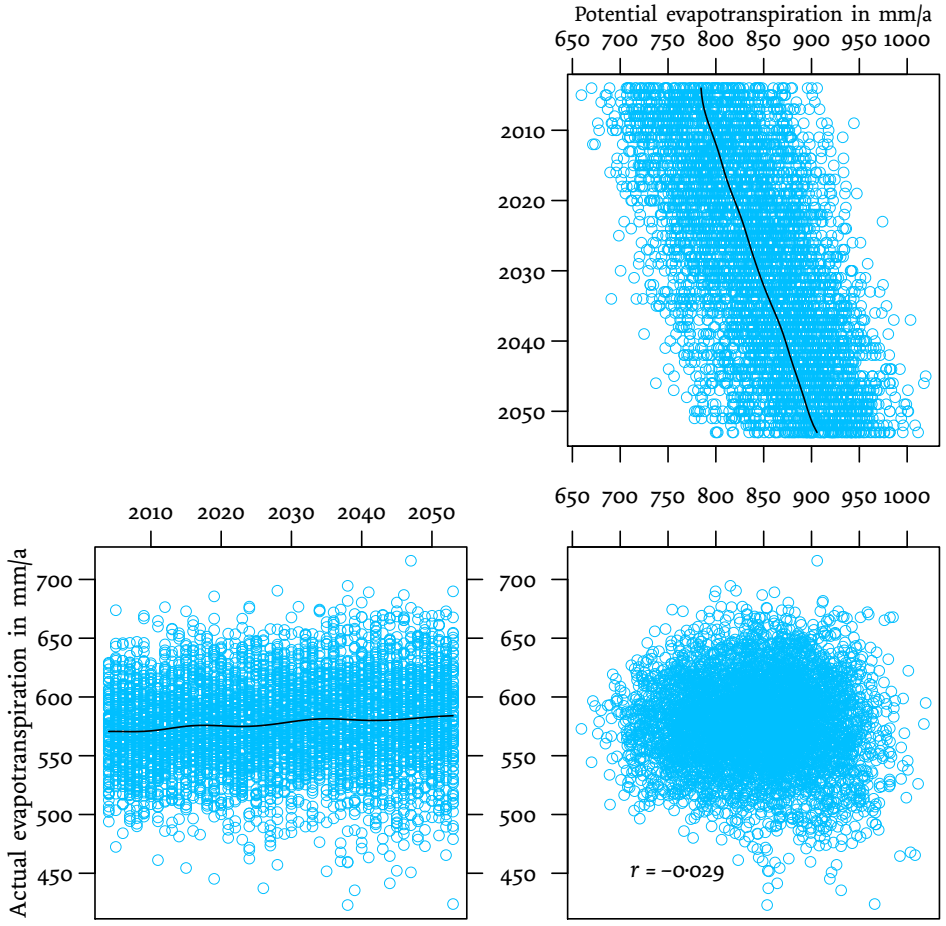

Figure 22: Development of evapotranspiration in the T2 scenario. Top right: annual potential evapotranspiration depths (model domain averages) of all 100 realisations over time; the black line is the smoothed mean (Gauß-kernel, bandwidth 3 years). Bottom left: the same for actual evapotranspiration depths. Bottom right: correlation between potential and actual evapotranspiration depths of the 5000 scenario years.

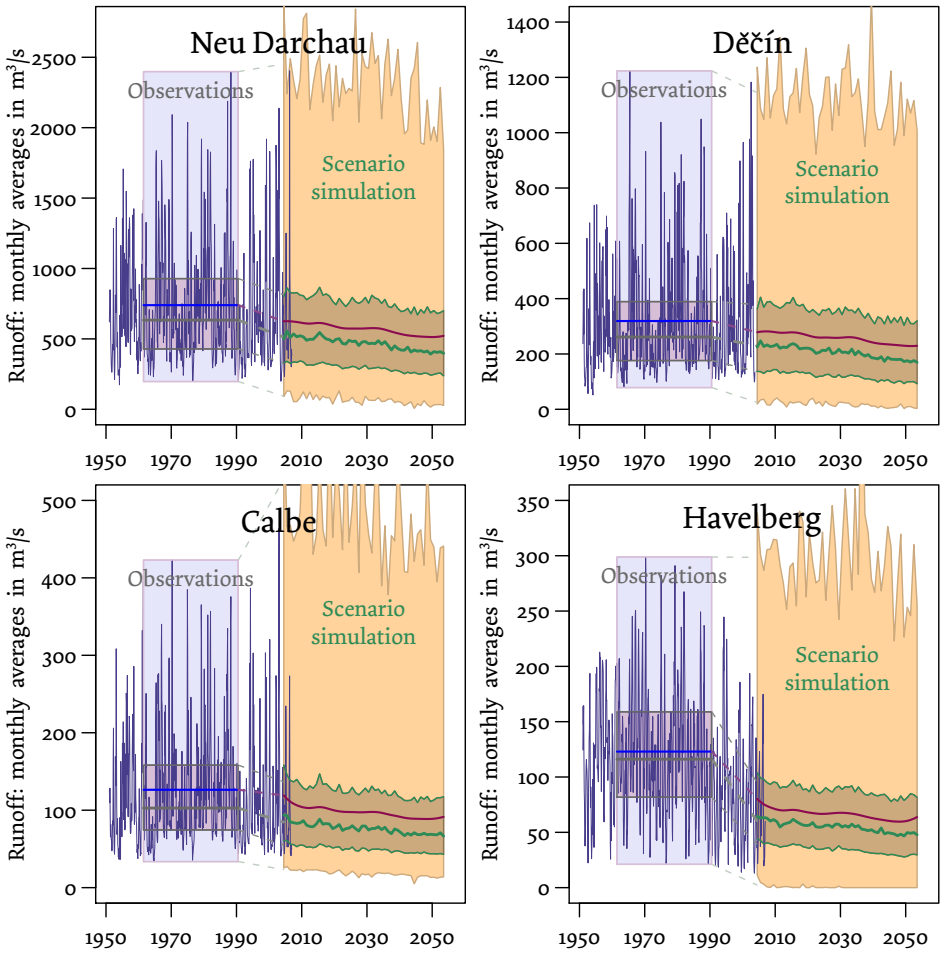

Figure 23: Shifts of runoff distributions for the gauge stations Neu Darchau (Elbe), Děčín (Elbe), Calbe (Saale), and Havelberg (Havel). Each subfigure shows ranges, inner quartiles, median, and average values for measurements of the reference period (1961–1990) by the boxes to the left and for the scenario simulation by the bands to the right. The bands are produced from the respective annual distributions of the 100 realisations.

gauges are also strong compared to precipitation reductions. Depending on the climate scenario, the runoff coefficient declines from formerly about one quarter to the sixth part or less (Table 3).

For all gauge stations, the variability in the scenario simulations covered by the 100 realisations seems to be larger than the variability in the observations during the reference period (1961–1990). However, it has to be taken into account that the reference period spans only 30 years, while the 100 realisations produce over three times larger samples for each year of the scenario.

2.3.4 *Negative runoff: the limits of model validity*

Although the model delivers almost invariably realistic outputs when driven by measured climate data, negative river runoffs occurred in some reaches under scenario conditions. This affected primarily the Spree River, the Havel River, the Schwarze Elster River (which occasionally falls dry in reality), and the Vltava River.

The STAR climate model increases the frequency of longer periods (>14 days) of dry days compared to the measured input. In combination with the unlimited model evapotranspiration from the riparian hydrotopes within SWIM, the model is driven beyond the state of validity.

Of course, negative river runoffs are due to a fundamental error – lacking limitation of evapotranspiration from riparian zones and wetlands – which should have been fixed. But this version of SWIM reproduced the observed (and revised) hydrographs with higher Nash–Sutcliffe efficiencies than any former modelling without or only limited extra evapotranspiration. Therefore, we accepted this misbehaviour, as it did not affect the follow-up analyses.

The problem became invisible for most cases by aggregating daily to monthly values. An exception is gauge station Havelberg (Havel), where the range of monthly scenario runoff touched zero (Fig. 23, lower right corner). Here and in analogous cases, negative values have been set off against simulated runoff from below the next confluence in order to keep the balance.

2.3.5 *Exceedance frequencies of minimum runoffs*

Negative discharges within the simulation are of no relevance to the frequency of runoff threshold exceedances. This allows for analyses of non-aggregated daily data as shown here for the gauge station Dresden (Elbe). Apart from that, the gauge Dresden (Elbe) receives negative model runoff on less than one day per year, even in the scenario period.

Navigation standards for the Elbe River including construction and maintenance have long been based on reference low flow levels. We used a former reference standard of 1959 as threshold for our analysis, because recent reservoir management is not modelled by SWIM. The respective

runoff threshold of 101 m³/s at Dresden (Faulhaber & Willamowski 2002) represents low flow conditions without releases from Czech reservoirs.

Figure 24(a) compares counts of the days on which the threshold had been met or exceeded in the years 1981–2003 by the reference simulation to the observations. For comparability, we set the observational threshold 30 m³/s higher to account for the bias caused by recent measures to raise water levels under low flow conditions. There is a significant correlation between model and (managed) reality.

Figure 24(b) and (c) show the effects of both climate scenarios. While there are still 10 realisations remaining above the threshold towards the end of the scenario period under T2-climate, the T3-scenario leads to extensive low flow periods in each year in the near future. The remaining time periods with a runoff above the threshold shrink on average to two-thirds of the year.

Although the results indicate a deterioration of navigation conditions under the supposed climate change, further quantitative analyses considering water management effects (cf. Koch et al. 2013a,b, Kaltofen et al. 2013a) are needed before final conclusions can be reached.

2.4 DISCUSSION

Although similar models had been successfully applied on even larger scales (e. g. Arnold et al. 1999, Gerten et al. 2004), the application presented here is characterised by the very high spatial discretisation. This includes not only the sum of hydrotopes, but also the explicit task to deliver valid scenario data for hundreds of sites within the model domain.

2.4.1 *Model fidelity in sub-basins*

As mentioned before in the introduction, the problem of the decreasing fidelity of model outputs with decreasing size of sub-areas has been reported by practically all authors who validated distributed hydrological models not only at the outlet but also at interior points. Uncertainty due to necessary generalisations and erroneous assumptions is unavoidable. This might also include the subset of parameters chosen for calibration.

In order to test the validity of the chosen parameter set for regional calibration, a separate study has been conducted (Conradt et al. 2012a, 2013b, Chapter 3). The main result was that model validity would have decreased in most sub-basins if a precipitation correction instead of the chosen evapotranspiration tuning had been used for water balance calibration.

Concerning the quality and resolution of input data, there were numerous sources of uncertainty:

Higher spatial density of climate station data in the Czech part of the basin would have been essential to obtain more realistic results for the

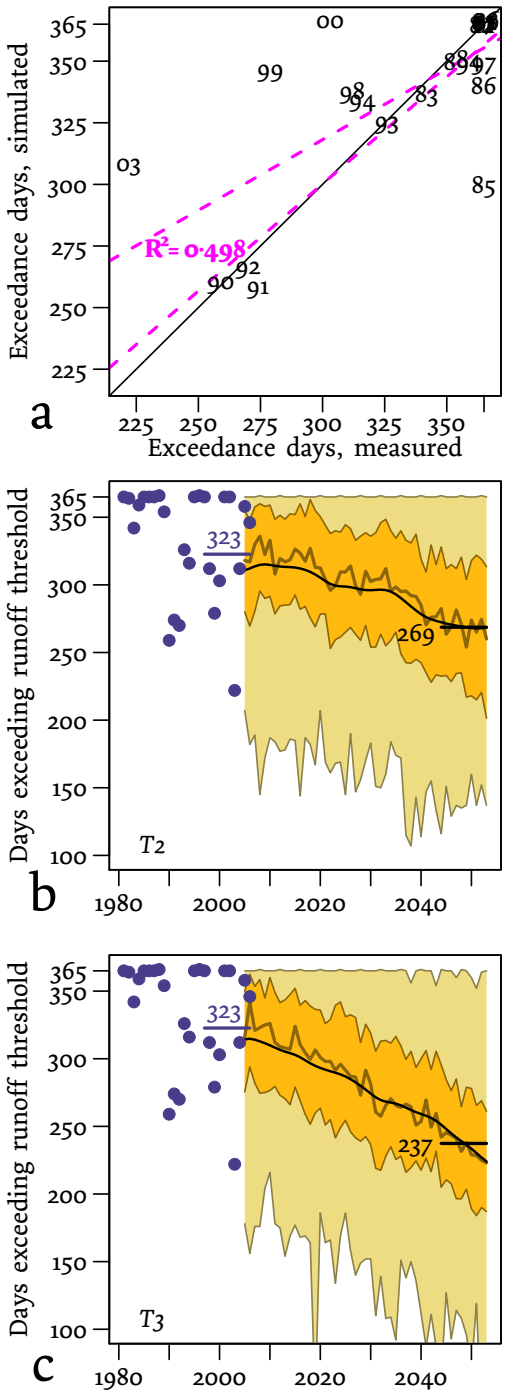

Figure 24: Recent observations (corrected by subtraction of 30 m³/s due to the supplemental discharges from Czech reservoirs under low flow conditions), simulations, and scenario projections of exceedance durations of a runoff threshold of 101 m³/s at the Dresden gauge. a) Scatter-plot of observations and simulations of 23 years of the past. The annual data points are marked by two-digit year numbers; dashed lines indicate the two-way linear regressions. b,c) Recent observations and scenario projections. The shaded bands show the quartiles of the duration distributions given by the respective samples of 100 realisations for the T2- and the T3-scenario. The black curves are their smoothed averages over time. The horizontal, numbered lines are the averages of the decades 1997–2006 (observations) and 2044–2053 (scenario projection).

Czech sub-basins. There are in fact more stations, but the data could not be made available.

The German general soil map (BÜK 1000) with a reference scale of 1 : 1 000 000 (Hartwich et al. 1995) had been used to determine wetland sites with near-surface groundwater. This did not sufficiently reflect the small-scale heterogeneity: Depending on soil unit boundaries, simulated runoff contributions from neighbouring sub-basins with similar landscapes could differ over a magnitude. Improvements can be expected by use of a more detailed German soil map, called BÜK 200 (reference scale 1 : 200 000), but some sheets covering the Elbe River basin are still to be completed.

Land use classification and parameterisation led to inaccuracies, too. There were conspicuous underestimations of discharge from large parts of the Ore and Giant Mountains. This was very likely caused by a discrepancy between the model land cover of perfect forests and the reality of rocky heights that were heavily marked by forest dieback in the 1980s.

However, although simulating local behaviour by a large-scale model implies operating on different scales, this will remain the only feasible approach to link the regional hydrological effects of global change to local water management issues within the foreseeable future. Finally, it has to be noted that the Nash–Sutcliffe efficiencies exceed 0·7 for any decade of daily discharges of the Elbe River at any point downstream of the Vltava River confluence (cf. Fig. 15). In order to maintain that level of model fidelity, Nash–Sutcliffe efficiencies of over 0·9 had to be achieved for the outlet gauge Neu Darchau (Elbe).

2.4.2 *Basin-scale validation*

In the basin-scale validation, the comparison of simulated and observed runoff values for the third validation decade 1991–2000 revealed a simulated water surplus at the gauge Neu Darchau (Elbe) of 87 m^3/s. Between 20 and 30 m^3/s of this surplus can be ascribed to decreasing mining activities (cf. Grünewald 2001).

The remaining difference could be related to three phenomena: the regional re-dimming, the re-filling of accumulated groundwater deficits, and the flooding of abandoned open-cast mines.

Global radiation had been decreasing since the 1950s due to aerosol emissions from lignite usage. This trend was stopped in 1989 and finally reversed by closing down old industries and introducing new technology (Wild et al. 2005). Although global radiation is one of the input data used in SWIM, intensity variations may have been captured insufficiently, because most climate stations measured only sunshine duration (Werner 2007) leading to underestimations of evapotranspiration after 1989.

The flooding of mines and the re-filling of the accumulated groundwater deficits started in the early 1990s. Both activities might have further

reduced the runoff from the German tributaries Mulde, Schwarze Elster, Saale, and Havel.

During low flow phases, the model runoff error differs only by 14 m^3/s between the 1980s and the 1990s. This difference has to be entirely ascribed to the discontinuation of mine draining which should be observable independent of the runoff stage. Thus, the disappearance of the remaining difference needs to be explained. Only a minor part is clear: The flooding of abandoned mines at a rate of around 5 m^3/s is controlled and is usually shut down during low flow phases. Regarding the conjecturable radiation effect, we can only assume that groundwater discharge that dominates low flow conditions may not react quickly enough to retrace the effect.

It has to be admitted that the change in runoff dynamics which occurred in the Elbe River basin around 1990 has not been fully understood yet.

2.4.3 *Spatially distributed validation*

The comparison of a simulated runoff distribution for the gauge Děčín with another distribution drawn from historical measurements shown in Figure 18 depicts growing differences in the discharge volume. However, the direction of these differences is consistent with the dominant climate and land use change between both periods as there are higher temperatures and intensified agricultural land use. Both can be expected to result in a runoff decrease.

Thus, the results do not question the model calibration undertaken for the Czech part. The relatively small differences in low flows could indicate a delayed groundwater discharge reaction. Such an interpretation is supported by the scenario simulation for the entire basin: the relative decreases of groundwater discharge are smaller than those for total runoff which may also indicate a delayed reaction to the climate scenario.

2.4.4 *Scenario results*

The scenario projection of the broad runoff recessions in the main channel of the Elbe River clearly results from the warmer and (with respect to precipitation) drier STAR climate scenarios (cf. Gerstengarbe et al. 2013). However, only simulations allow the discharge alterations to be estimated quantitatively in space and time. While the climatic water balance (which is only the difference between long-term means of precipitation and potential evapotranspiration) sufficiently characterises climatic conditions, the hydrological conditions depend on soil conductivity, depth of the groundwater table, and actual evapotranspiration ration which is also governed by plant cover characteristics, soil wetness profile, and further factors.

According to a prequel study by Hattermann et al. (2005b) for the German part of the Elbe River basin, the change in total runoff in the middle of the twenty-first century was estimated to be –41·4 % compared to the reference period 1961–1990. This ranges in between the respective values given in Table 3 for the T2 and the T3 scenario. However, the relative decrease in the groundwater component was larger (–49·6 %), while we observed minor relative reductions for this component compared to total runoff (Table 3). Our differing result is very likely an outcome of the groundwater module enhancement and may indicate a delayed reduction of groundwater discharge to climate change (see above). While the improved model fidelity in simulating recent low flow periods dominated by baseflow maintains this interpretation, the higher plausibility of a delayed groundwater reaction itself justifies the enhancement of the groundwater module.

Apart from the former study being restricted to the German part of the Elbe River basin, it has to be noted that management effects on reference observations had not been considered and that it was based on a single climate realisation only. This differed from the average characteristics of our climate scenarios: There was much less precipitation than measured in the reference period (–10·4 %) and a temperature trend of +1·4 K from 2000 to 2055. Hattermann et al. (2005a) found in another analysis for the German part based on 100 climate realisations with the same temperature only a moderate discharge decrease (–15 %). The average level of precipitation was rather stable (–1·5 %).

The comparability of our results to the finding of these former studies shows that modelling these parameters in detail is feasible and allows a general conclusion to be drawn: With respect to the differences in model domains and temperature trends, a temperature increase of 1 K seems to have a similar impact on runoff as a 10 % decrease of precipitation.

It has to be considered that such reasoning and all model results still disregard some effects of climate change which indirectly affect the runoff behaviour. These include the fertilisation effect of increased atmospheric CO_2 content and the combined reduction of plant transpiration (Gedney et al. 2006).

However, there is much evidence of a strong change towards much drier conditions with extended low flow phases in the Elbe River basin. This trend already commenced in the past but was masked by the releases from Czech reservoirs during low flow conditions since the 1960s (Wechsung et al. 2006).

The 100 climate realisations per scenario leading to 100 realisations of the eco-hydrological conditions make possible both uncertainty tracking and the illustration of probabilities and stochastical relations: The correlation between potential and actual evapotranspiration (Fig. 22) can be studied not only over time but also across realisations. Probability

distributions are accessible as quantile delineations over time as shown for runoffs (Fig. 23) or for threshold exceedances (Fig. 24).

The basic importance of land use changes for alterations of the runoff coefficient is high, especially in the process of urbanisation (e. g. Cheng 2011, Liu et al. 2011, Notebaert et al. 2011). Therefore, different land use scenarios have been considered. The impact of urban areas on runoff generation can also be seen directly in Figure 19, and on hydrotope level, over two-thirds of the variance of the runoff coefficient alterations during the scenario period can be explained by the land use factor. On the other hand, it has been stated that the differences in global runoff (i. e. at the outlet) between the different land use scenarios are negligible, which was the reason to restrict this analysis to the A1^0 land use scenario.

The reason for this apparent contradiction is the small fraction of land cover which actually differs between the land use scenarios (Hoymann 2010a,b, Hoymann et al. 2013). While the most extreme variant regarding urbanisation, A1^0, shows 4·97 % residential areas in the Czech part and 7·03 % in the German part of the Elbe River basin, the respective numbers are 4·28 and 6·50 % for the B2$^+$ scenario (Hoymann 2011). Thus, effective differences are restricted to about 0·6 % of the area.

As the intensity of urbanisation is not spatially homogeneous, larger relative differences in runoff between land use scenarios have to be expected on the sub-area or sub-basin level. This may need further research into local hydrological consequences of combined climate change and landscape planning effects.

ACKNOWLEDGEMENTS The authors would like to express their gratitude tude to all project partners involved for the good cooperation, especially for numerous valuable remarks during the process of calibration and validation. Sincere thanks are given to the German Federal Ministry for Education and Research (BMBF) and the project management agency at the German Aerospace Center (PT-DLR) for the funding of the GLOWA-Elbe project (grant no. 01 LW 0603 A2).

3

CALIBRATING PRECIPITATION OR EVAPOTRANSPIRATION?

Tobias Conradt, Hagen Koch, Fred F. Hattermann & Frank Wechsung

ABSTRACT A global change assessment required detailed simulation of water availability in the Elbe River basin in Central Europe (148 268 km²). Using the spatially semidistributed, eco-hydrological model SWIM, spatial calibration was applied. For 225 sub-areas covering the model domain (134 890 km²), evapotranspiration and groundwater dynamics were individually adjusted. The calibration aimed at good correspondences with long-term runoff contributions and the hydrographs for two extreme years. Measured runoff was revised from water management effects to produce quasi-natural discharges for calibration. At some gauges, there were large volume differences between these reference data and the simulations of the spatially uncalibrated model. Most affected were some sub-basins in the Czech part of the basin where the density of available climate stations was much lower than the German part. Thus, both erroneous precipitation data and systematic flaws in the evapotranspiration module of SWIM could have caused the differences. In order to identify the major error source and to validate the choice of spatial calibration parameters (evapotranspiration and groundwater dynamic corrections), MCMC analyses were made for three Czech areas. Optional precipitation correction had been considered by a third calibration parameter in the MCMC assessment. In two of the three cases, it can be shown that evapotranspiration corrections are preferable as precipitation errors are negligible. In the third case, where the analyses indicate a substantial error in precipitation data, an interpolation problem of the climate data at the edge of the model domain could be found. Hence, the applied method shows its potential to identify specific sources of uncertainty in hydrological modelling.

KEY WORDS Bayesian uncertainty analysis, Elbe River basin, Error signature, Error sources, MCMC, Metropolis algorithm, Spatial calibration, Spatially distributed hydrological modelling, SWIM

3.1 INTRODUCTION

In order to investigate the changes in natural water availability within the Elbe River basin under climate and land use change, scenario simulations with the eco-hydrological model SWIM (Krysanova et al.

1998, 2000) had been made. The general approach and the simulations for the Elbe River basin are described in Conradt et al. (2012b, 2013a).

Local uncertainties and systematic errors had to be reduced as much as possible. Studies devoted to simulation fidelity of spatially distributed hydrological models invariably report larger relative errors for gauge stations within the model domain than for the outlet. It is often observed that the smaller the sub-catchment in question is the worse the fit (cf. e. g. Andersen et al. 2001, Güntner 2002, Reed et al. 2004, Moussa et al. 2007). This also holds true if spatial calibration was explicitly applied (Fernandez et al. 2000, Cao et al. 2006, Bekele & Nicklow 2007, Artinyan et al. 2008). In the model set-up presented here, many sub-basins cover only a few thousandths of the entire area; hence, spatial calibration was a major issue.

Comparisons of hydrographs from sub-areas modelled without spatial calibration to reference hydrographs from measurements adjusted by anthropogenic influences often evinced one or both of the following deviation patterns:

- Generally higher or lower level (global volume error)
- Seasonal deviations (seasonality error)

Given a water balance without extensions by lateral components like subsurface groundwater runoff, a hydrological model should only produce a global volume error if the precipitation input data are biased, if the evapotranspiration is modelled erroneously, or if both errors are combined. This study neglects lateral fluxes accordingly; the runoff from a "deep" groundwater storage which is assumed in the standard version of SWIM had been eliminated.

Seasonality errors can have considerably more potential causes like a combination of an upward bias in precipitation input with systematic over-estimation of evapotranspiration. At least in Central Europe, this would cause a seasonality error, because here precipitation is rather equally distributed throughout the year, while evapotranspiration follows a distinct seasonal cycle.

The modelling of vegetation growth or groundwater dynamics could possibly provide other reasons for seasonality errors. Groundwater modelling would be a first-rate candidate, because the groundwater runoff component (baseflow) reacts only slowly on groundwater recharge. Sluggish baseflow behaviour can thus account for smoothing the seasonal hydrograph.

The basic idea of this investigation is that each of these error sources produces a specific signature in the simulation errors. Taken on its own, this does generally not allow for unambiguous identification of error sources. But during model calibration, this signature transforms into specific parameter combinations that minimise errors optimally and make it possible to determine the sources of error or uncertainty.

It is conceivable that a seasonality error, caused by a combined precipitation bias and evapotranspiration adjustment as described above, can be mitigated by a "correction" of groundwater dynamics. Such a model would only seem to be calibrated optimally but would be unable to reproduce the behaviour of the real system before or after the calibration period.

Even the early users of numerical, process-based hydrological models were confronted with different parameter combinations leading to comparable and equally eligible fits to measured data; often physically nonsensical parameter values delivered the best results (e. g. Bultot & Dupriez 1976, Pickup 1977, Kitanidis & Bras 1979). Beven & Kirkby (1979) displayed such response relations by isolines of a target function in a two-dimensional parameter space. citetbeven1993 finally adopted the term "equifinality" for this problem.

Beven & Binley (1992) promoted the idea of an extensive sensitivity analysis for hydrological modelling using a Monte Carlo approach named "Generalized Likelihood Uncertainty Estimation" (GLUE). The basic concept of illuminating the multi-dimensional distribution of optimal parameter combinations by Monte Carlo methods had been applied to water quality modelling before (cf. Spear & Hornberger 1980, Hornberger & Spear 1981, Halfon & Maguire 1983, Fedra 1983). These and similar approaches aimed primarily at investigating the validity and forecast capabilities of numerical models and at defining confidence intervals for their outputs.

The aim of this investigation is to evaluate the individual shares of systematic over- or underestimations of precipitation and evapotranspiration in the errors of hydrograph simulations for three Czech sub-catchments. The results are intended either to validate the spatial calibration without precipitation corrections or to encourage repeating it with adequate parameters.

We used a maximum likelihood-based Markov Chain Monte Carlo (MCMC) approach in order to narrow down possible sources of the differences between simulations and observations. The assessments were restricted to three calibration parameters for precipitation, evapotranspiration, and groundwater discharge.

In the following, we present first the eco-hydrological model SWIM, its application in the Elbe River basin, and the options for spatial calibration. After introducing our MCMC approach, the results and their interpretation for three Czech sub-catchments follow. Finally, some conclusions regarding the parameters for spatial calibration can be drawn.

3.2 MATERIAL AND METHODS

3.2.1 *The eco-hydrological model* SWIM

For a detailed description, the reader may refer to the companion paper on the simulation of discharges under scenario conditions in the Elbe River basin (Conradt et al. 2012b, Chapter 2). The summary below is mainly devoted to calibration issues.

SWIM (Soil and Water Integrated Model) is a spatially semi-distributed, eco-hydrological research model, which simulates natural water and matter fluxes (Krysanova et al. 1998, 2000). The model was developed at the Potsdam Institute for Climate Impact Research on the basis of SWAT (Arnold et al. 1993, 1998, Gassman et al. 2007) and had already been applied and validated several times for the simulation of the German Elbe River basin (e. g. Hattermann et al. 2005c, Post et al. 2008).

For each daily time step, spatially distributed climate data are needed. These are generated from station data interpolated to the centres of the sub-basins.

Elementary simulation entities are landscape units, so-called hydrotopes. These are defined by uniform hydrological properties, usually with respect to soil profile and land use. For each hydrotope, all vertical eco-hydrological processes are computed. These include plant water uptake, plant growth, potential and actual evapotranspiration, seepage, runoff formation, and groundwater recharge. Also nutrient cycles are modelled, but were of no interest for this study.

Evapotranspiration calculation is based on reference evapotranspiration determined by the Turc–Ivanov approach after DVWK (1996) using the month factors of Glugla & König (1989) and land use factors according to ATV-DVWK (2002). Actual evapotranspiration values are computed depending on soil water availability and the state of the vegetation.

The hydrotope runoff contributions are summed up within sub-basins that also represent the river system. The sub-basin discharges are subsequently routed through the sub-basin structure by the Muskingum approach (Maidment 1993).

3.2.2 *Representation of the Elbe River basin in* SWIM

The entire Elbe River basin covers an area of 148 268 km², but only the catchment area upstream of the Geesthacht Weir has been modelled. This excludes the tidally influenced lower part of the stream (Figure 25). The model domain (134 890 km²) had been split into 2278 sub-basins using a digital catchment map of the German Federal Environmental Agency and, for the Czech part, masters of the Czech water authorities.

From an overlay of a soil map (in the German part based on the general soil map BÜK 1000, Hartwich et al. 1995), a land use map derived

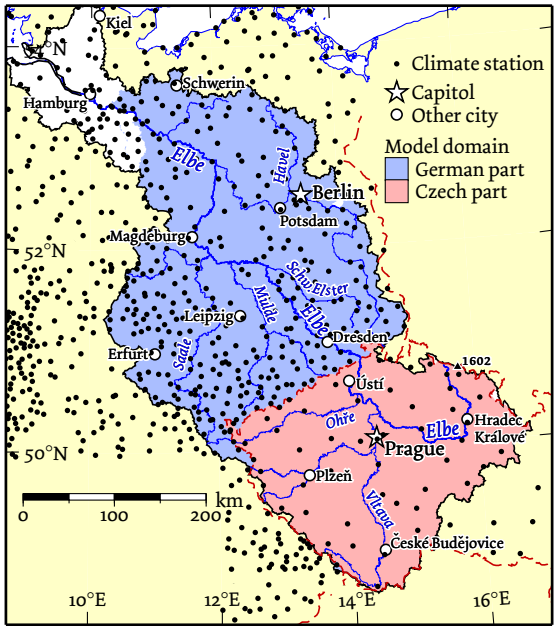

Figure 25: The Elbe River basin and the model domain simulated by SWIM. Climate stations are marked by black dots; clearly visible is the comparably low station density in the Czech part

from the CORINE 2000 (CEC 1995, Bossard et al. 2000), and some maps of areas affected by artificial groundwater depletion about 47 500 hydrotopes were identified.

The recent climate data used for model calibration were based on measurements from 853 stations with 501 thereof reporting precipitation only. All meteorological variables had been interpolated to all locations, though. Data gaps had been cleared with neighbouring measurements by statistical means (Oesterle 2001, Österle et al. 2006). As can be seen from Figure 25, the spatial density of the stations available in the Czech Republic is much lower than in the rest of the Elbe River basin.

3.2.3 *Calibration*

As described in the companion paper on the scenario study (Conradt et al. 2012b, Chapter 2), the calibration had to provide minimal errors in both water balance and runoff seasonality simulations not only for the outlet gauge but for each sub-basin. Errors in this application were the deviations from hypothetic, quasi-natural discharges that would occur without water management.

First, the model was calibrated at the lowermost runoff gauge Neu Darchau. In a second phase of spatially distributed calibration, the model was adjusted to average runoff contributions of 225 sub-areas covering the entire area, by means of local evapotranspiration corrections. This implied the assumption of unbiased precipitation data. Limiting

the spatial calibration to water volume follows the approach of Santhi et al. (2008).

Reference values were generally long-term runoff means (primary source: DGJ 1995a,b,c); estimations were used for areas without a terminating gauge or within the hydrologically disturbed open-cast lignite mining landscape. For comparison, 30 years of the past (1961–1990) were simulated.

This approach had several flaws, though:

1. The long-term reference data referred to different time periods. Even under the assumption of stationarity for average discharges, most time series are too short (some only 10 years) to be a reliable basis.

2. Stationarity does not exist in hydrological time series. This holds for all time scales and is known as the Hurst effect (Hurst 1951, 1957, Mandelbrot & Wallis 1968, 1969, Klemeš 1974). Thus, the comparison of average values of different time periods must produce errors.

3. The estimations for areas without utilisable gauge data are based on the N-A-U-Map (IfWW 1958) that was compiled from station measurements of the years 1921–1940. The sub-catchments in question primarily became open-cast lignite mining areas whose water balances have drastically been changed. Groundwater drainage is not included in the model, and the areas are simulated as open pits without vegetation. This shifted their hydrological properties strongly compared to the model representation.

4. In the presence of systematic errors in precipitation data, the water volume calibration of runoff via evapotranspiration correction may lead to biased representations of the real processes.

5. Large differences in the simulated run-off contributions of neighbouring sub-basins are frequently found where the generalised soil map shows groundwater influenced sites with high evapotranspiration rates for one sub-basin but not for the neighbouring one. These artefacts cannot be corrected by water volume calibration, because the calibration areas are often too large to affect single sub-basins.

6. Lateral water fluxes besides the natural river systems are neglected. This includes artificial passages or natural groundwater movements (Schaller & Fan 2009). In the heavily managed city area of Berlin, these cannot be broken down despite regular runoff measurements (Senatsverwaltung 1992).

The automatic evapotranspiration calibration in the sub-basin delivered in some cases extreme factor values. This could be expected due to the

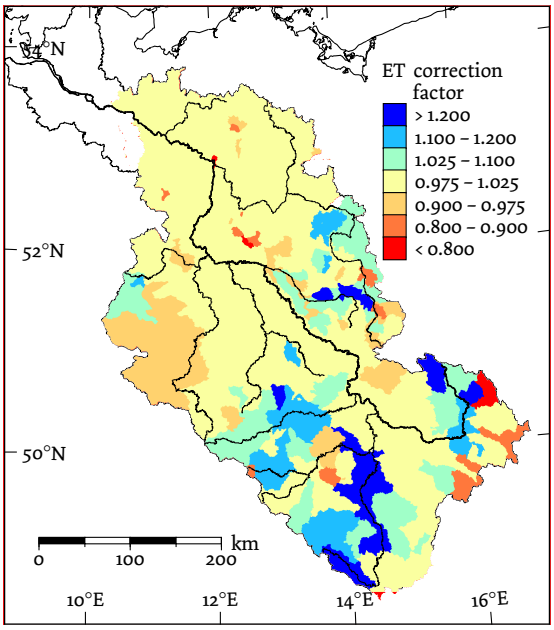

Figure 26: Map of the evapotranspiration correction factors after manual spatial calibration. The primarily modelled evapotranspiration had been multiplied by these sub-basin-related correction factors

flaws of the approach and the possible input errors. The hydrograph shapes often differed strongly from the available reference hydrographs.

The spatial calibration for the sub-basins was therefore repeated manually. This calibration aimed not only at reproducing long-term runoff means but also at matching hydrograph dynamics. Therefore, corrections on the recession parameters of the linear groundwater reservoirs were introduced into the set of area-specific calibration parameters. The spatial distributions of the resulting factor values that optimally minimised the errors between simulation and reference hydrographs are shown in Figs. 26 and 27.

Additionally, a runoff data basis containing not only average values was necessary. In the Czech Republic, monthly values corrected for management effects were available for most areas for the years 2002 and 2003. These contained a centennial flood (2002) and an extensive low-flow period (2003). For the German Havel Catchment and the Schwarze Elster River quasi-natural, monthly runoff data could be obtained from water management models of the German federal states, and for the Saale River basin, there were respective data from the Federal Institute of Hydrology.

For some regions, the fit of the modelled data remained unsatisfactory despite all efforts. This holds especially true for the Czech part of the model domain, in which the spatial density of climate stations was comparably low (cf. Fig. 25). One Czech station represents the weather pattern for an area of approximately 1200 km².

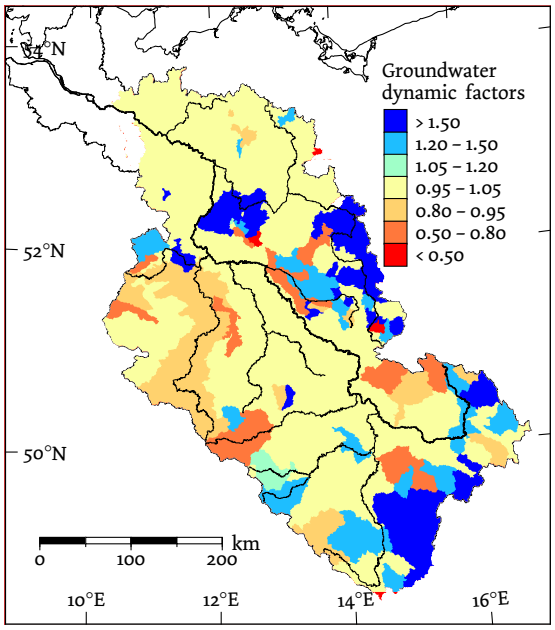

Figure 27: Map of the groundwater dynamic parameters after manual spatial calibration. The groundwater recession coefficients (α values) that had primarily been set uniformly for the entire model domain were multiplied by the squares of the correction parameters shown here (cf. Equation 9). Values > 1 represent longer effective storage times and values < 1 shorter effective storage times

3.2.4 *Bayesian validation of the spatial calibration approach*

Calibrating water volumes by evapotranspiration corrections is a logical consequence of a common assumption in hydrological modelling. Measured climate and runoff data are generally assumed to render the real conditions in an unbiased way. Hence, the remainder term of evapotranspiration which is not measured directly has to be adjusted in order to close the modelled water balance.

We also made this assumption for our calibration – precipitation correction factors remained neutral – but as station density is very low in the Czech part of the basin, it should be validated in the framework of this study. Technically, an alternative or additional spatial calibration by precipitation correction factors would be a realistic option.

Because the method described in detail below requires several thousands of model runs, a basin-wide validation was not feasible. Therefore, three Czech catchments consisting of only three or four model subbasins were extracted as independent mini models; these are listed in Table 4 and shown in Figure 28.

In order to evaluate our calibration approach with precipitation corrections, we applied the Bayesian method with the Markov Chain Monte Carlo (MCMC) approach. In recent years, this has been utilised by many authors in the field of hydrological modelling for estimating

Table 4: The three catchments in which the model behaviour was analysed

Gauge name	River name	Gauge location	Catchment area km²
Chlum Volary	Vltava	48°51·7′N, 13°53·9′E	347·01
Stará Lhota	Úhlava	49°15·9′N, 13°09·0′E	81·18
Žlutice	Střela	50°05·2′N, 13°07·6′E	213·75

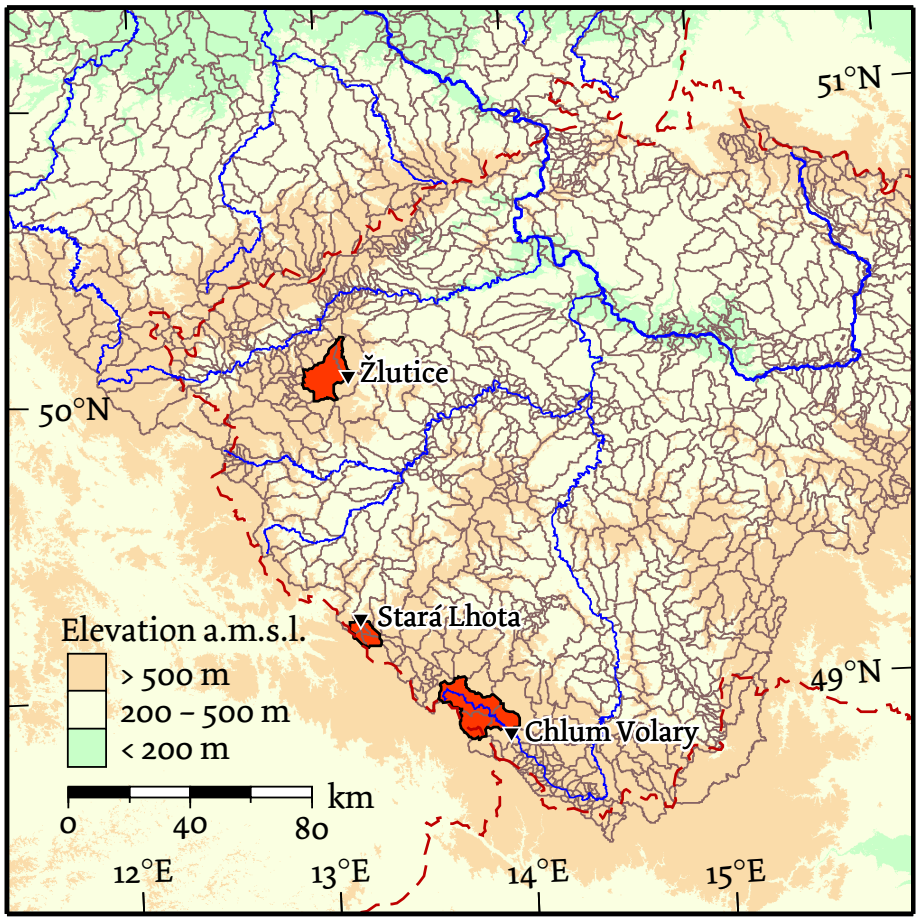

Figure 28: The catchment areas investigated by the Bayesian method in a map section. Also shown are the boundaries of the model sub-basins (grey solid lines) and national boundaries (black dashed lines).

parameter distributions or even assessing errors in input data (e. g. Engeland & Gottschalk 2002, Vrugt et al. 2003, Engeland et al. 2005, Kavetski et al. 2006a,b, Yang et al. 2007).

The Bayesian method produces a multi-dimensional posterior probability distribution $p(\boldsymbol{\theta}, \phi|Q_{\text{obs}})$ for hydrological or statistical parameter vectors, denoted by $\boldsymbol{\theta}$ and ϕ. In our case, the parameter space was defined by three correction factors for precipitation, evapotranspiration, and groundwater dynamics. These had to be conditioned on the measured run-off values Q_{obs} (which had been corrected for water management effects not regarded by the model). According to Bayes's theorem, it holds that:

$$p(\boldsymbol{\theta}, \phi|Q_{\text{obs}}) = \frac{p(Q_{\text{obs}}|\boldsymbol{\theta}, \phi)p(\boldsymbol{\theta}, \phi)}{\int (Q_{\text{obs}}|\boldsymbol{\theta}', \phi)p(\boldsymbol{\theta}', \phi)\mathrm{d}\boldsymbol{\theta}'} \tag{6}$$

Here, $p(\boldsymbol{\theta}, \phi)$ is the so-called prior, the probability density of the parameters before information or an information update from the comparison between simulation and measurements is present. We conceived equal distributions on the interval $[0, \infty)$ for all parameters as noninformative prior. With given measurement data, $Q_{\text{obs},p(Q_{\text{obs}}|\boldsymbol{\theta},\phi)}$ resembles a likelihood function $L(\boldsymbol{\theta}, \phi|Q_{\text{obs}})$ for the parameter vectors $\boldsymbol{\theta}$ and ϕ. The integral over the entire space of the model parameters in the nominator normalises the resulting probability density.

There are a large number of suggestions for the formulation of reasonable likelihood functions in uncertainty assessments for hydrological modelling. While Beven & Binley (1992) request merely $L(\cdot) = 0$ for all simulations whose results are "dissimilar" to the measurements and a monotone increase of the likelihood for increasing similarities in their concept of Generalized Likelihood Uncertainty Estimation (GLUE), other authors (Mantovan & Todini 2006, Stedinger et al. 2008) advocate more formal definitions based on an error model. Without such an error model describing the distribution of the errors and possibly their auto-correlation, no quantitative statements on the uncertainty of simulation results can be made. However, likelihood functions regarding auto-correlation can be rather complex, cf. Yang et al. (2007).

We do not define the differences between simulated and measured discharges as simulation error ϵ but the relative departures between simulation and measurement:

$$\epsilon := \ln\left(\frac{Q_{\text{sim}} + c}{Q_{\text{obs}} + c}\right) \tag{7}$$

Thus, absolute differences in flood flow months are weighted less and a high standard for model fidelity during low-flow operation is maintained. The additive constant c is usually zero, but has been set to $0{\cdot}1\ \mathrm{m^3 s^{-1}}$ for the gauge Žlutice (Střela), because only $0{\cdot}01$ viz. $0{\cdot}00\ \mathrm{m^3 s^{-1}}$ had been observed here in August and September 2003. The resulting errors have an approximate Gaussian distribution, which allows for

using the normal distribution as error model. Auto-correlation had not been taken into account, because only monthly values with negligible autocorrelation were evaluated. The respective likelihood function with the standard deviation as the only statistical parameter is:

$$L(\theta, \sigma|Q_{obs}) = \prod_{t=1}^{n} \left[\frac{1}{\sqrt{2\pi}\sigma} \exp\left(-\frac{1}{2\sigma^2}(\epsilon_t(\theta))^2 \right) \right] \tag{8}$$

The vector of hydrological parameters θ whose interaction in the area of optimal model calibration shall be revealed consists of an evapotranspiration correction factor, a respective multiplier for precipitation, and a groundwater dynamics parameter g that alters the groundwater runoff coefficients α as follows:

$$\tilde{\alpha} = e^{(-\alpha g^2)} \tag{9}$$

Regarding the principal question of this research, only the corrections for precipitation and evapotranspiration seem to be relevant, because they govern the runoff volume. But also dampening and hysteresis of the runoff seasonality by the groundwater component are important for the error signature explained above. Therefore, it was important to include the groundwater dynamics parameter, too.

The standard deviation parameter σ in Equation 8 should approximately equal the error dispersion of an optimally parameterised model run and was adjusted accordingly.

As monthly averages of runoff measurements with corrections for water management effects were only available for the years 2002 and 2003, the number of reference data to be considered was $n = 24$. This allowed the likelihood for each model run to be calculated directly by Eq. 8 and not as log-likelihood.

The idea of tracking precipitation errors by Bayesian analysis has already been addressed in publications by Kavetski et al. (2003) or Ajami et al. (2007). The approach chosen by these authors was to define individual correction factors for each precipitation event. In the present study, we assume a systematic bias of all data; thus, a constant multiplier is applied to all precipitation events for correction.

3.2.5 MCMC: *the Metropolis algorithm*

The joint probability distribution of the posterior does not have a closed form, but the Markov Chain Monte Carlo (MCMC) approach implemented by the classical Metropolis algorithm constitutes an established numerical solution method (cf. Cowles & Carlin 1996). MCMC approach is the term for obtaining a sample from the probability distribution by constructing a Markov Chain based on (pseudo) random numbers, which converges to the target distribution. A Markov Chain is a (time) series of state or parameter vectors forming a stochastic

process. Switching from one state to its successor depends solely on the actual state and given probabilities of transition; previous states have no influence on the progression of the process.

Such a Markov Chain is produced by the Metropolis algorithm (Metropolis et al. 1953, Hastings 1970). It is started by defining an initial state θ_0, a combination of precipitation and evapotranspiration correction factors and groundwater dynamics parameter in our case, which preferably yields a relatively high likelihood value, that is, high density of the probability distribution. If the initial parameter vector is distant from the regions of higher density of the distribution, a lengthy burn-in phase may result.

For the subsequent state θ_1 and the further successors θ_i with $i = \{2, 3, 4, \cdots, n\}$, the parameters are changed by random amounts. These random amounts are drawn from a so-called jump distribution using (pseudo-) random numbers. The model is run with the modified parameter vector θ_i^*, and the likelihood is calculated. It holds that:

$$\theta_{i+1} = \begin{cases} \theta_i^* & \text{with} \quad p = \min\left\{\frac{L(\theta_i^*)}{L(\theta_i)}, 1\right\} \\ \theta_i & \text{otherwise} \end{cases} \tag{10}$$

If the jump led the chain to a realisation with higher likelihood, this is accepted as the new state of the chain. If the new likelihood is lower than the last one, the acceptance probability of the jump equals the likelihood ratio. The actual acceptance is then decided on another random number sample. If the jump is not accepted, the parameter vector remains unchanged and the next trial starts from the same position.

To minimise the steps for obtaining a satisfactory sample of the target distribution, much depends on the definition of the jump distribution. A jump distribution with small variance compared to the target distribution leads to slow transition of the latter; this can be detected by high acceptance rates of the jump trials. On the contrary, a too wide jump distribution leads to low acceptance rates, because it often hits areas distant from the target distribution. The ideal jump distribution resembles the target distribution and may also have correlated parameters.

For the analyses presented below, only the orthogonal variances of the jump distribution were optimised; this was a three-dimensional (according to the number of parameters) and symmetrical (no covariances) normal distribution, the realisations were drawn by a function of R (R Development Core Team 2011), which is based on the Mersenne-Twister algorithm (Matsumoto & Nishimura 1998).

The Markov Chains were computed up to a length of 10 000 elements for each gauge with the exception of Stará Lhota where two such chains generated with different variances of the jump distribution were concatenated. Burn-in phases were not removed, because in all cases, the chains were started near the modi of the respective distributions.

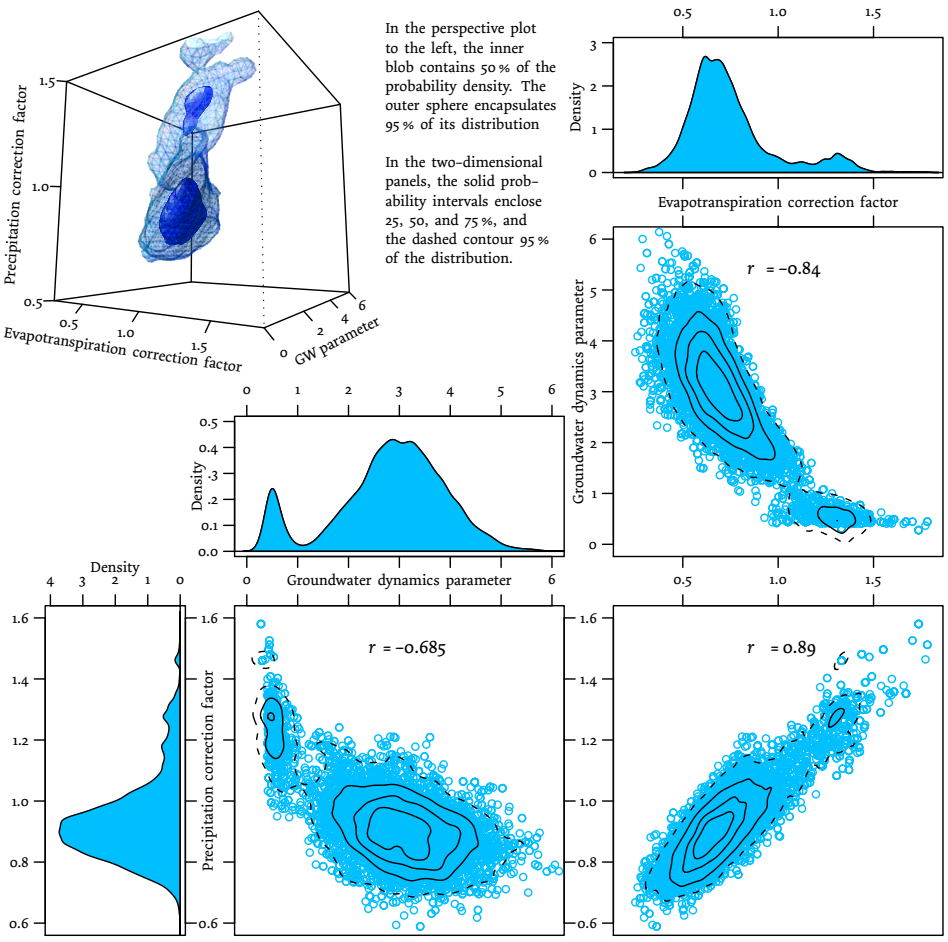

Figure 29: Multiple views of the probability distribution for the local calibration parameters at gauge Stará Lhota, Úhlava. The underlying Markov Chain has a length of 20 000 elements.

3.3 RESULTS

3.3.1 *Stará Lhota, Úhlava*

The three-dimensional probability distribution of the parameters evapotranspiration correction, precipitation correction, and groundwater dynamics factor that is shown in multiple views in Figure 29 has a dominant major maximum at an evapotranspiration correction factor of about 0·6. This means a distinct reduction in the model evapotranspiration affected by global calibration only. The marginal distribution of the precipitation correction factor shows the same major maximum at a value of 0·9 which merely means a reduction in a tenth of the precipitation input data. The groundwater dynamics parameter takes the value 3·0, but this has no meaning with respect to the question whether precipitation or evapotranspiration should be corrected.

The key message is that optimal simulation results do not depend on a shift in precipitation data but on evapotranspiration calibration. This is

confirmed by the observation of the distribution showing a remarkable density even when the precipitation correction is neutral (factor 1·0). The core of the distribution is located between evapotranspiration corrections in the range of 0·7–0·9. The neutral evapotranspiration factor of 1·0 is correlated with a small, but not fully neglectable probability.

However, the high correlation (the correlation coefficient is at 0·89) of the two-dimensional marginal distribution of the precipitation and evapotranspiration calibration parameters supports a complete scale of preferable parameter combinations; this illustrates how similar these parameters affect the model output.

In the course of the main axis of the correlation, there is an ancillary maximum of the distribution. It corresponds to equivalent increases of precipitation and evapotranspiration by a factor of 1·3 and a groundwater dynamics parameter of 0·5. Since it does not represent a larger fraction of the distribution, it is simply a nice example for the equifinality of different parameter combinations (Beven 1993, 2006, Ebel & Loague 2006). Besides, such a secondary peak of the distribution is a challenge for the Metropolis algorithm, because it is poorly interlinked to the main mass that hampers transitions of the Markov Chain in between. This is the reason why we applied a chain of double length compared to the other cases.

3.3.2 *Žlutice, Střela*

The gauge Žlutice also produces a tubular distribution that is also bimodal (Figure 30). However, the areas of higher density are less clearly separated from each other here (with the exception of the marginal distribution of the groundwater dynamics parameter), and there is not such a clear hierarchy. Thus, transitions of the Markov Chain between the two centres of density are much more frequent than they were at Stará Lhota.

The preferred combinations of precipitation and evapotranspiration correction factor are oriented along a straight line and highly correlated (r = 0·939), whereas the interrelations with the groundwater dynamics parameter are clearly nonlinear. The modi of the two-dimensional marginal distribution show stronger preferences towards a low increase of evapotranspiration (correction factor values between 1·0 and 1·2) in combination with practically unchanged precipitation. Alternatively, there is a certain preference towards precipitation increases of about 20 % combined with evapotranspiration multipliers of 1·4–1·5.

On one hand, this means a certain preference of evapotranspiration over precipitation correction. On the other hand, it exemplifies again the difficulty to finally choose from the different combinations of correction possibilities with higher probability that one which matches the real conditions best. The global density maximum slightly above the neutral precipitation correction suggests that a pure evapotranspiration

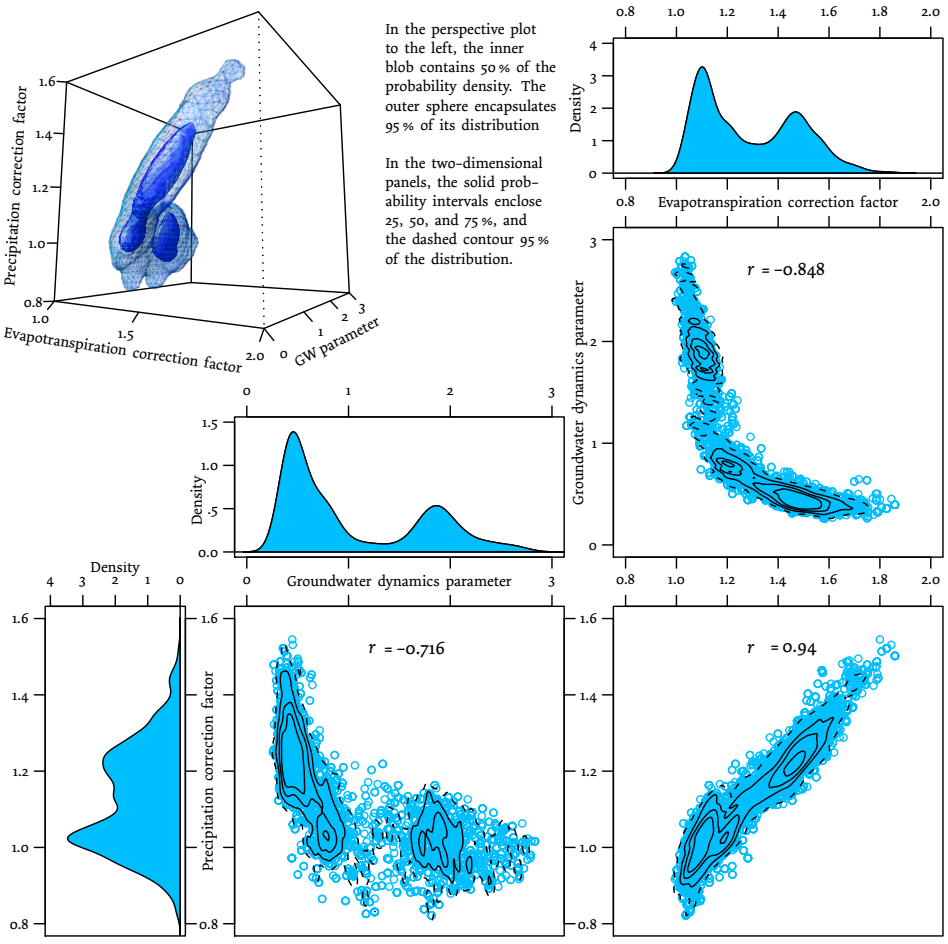

Figure 30: Multiple views of the probability distribution for the local calibration parameters at gauge Žlutice, Střela. The underlying Markov Chain has a length of 10 000 elements.

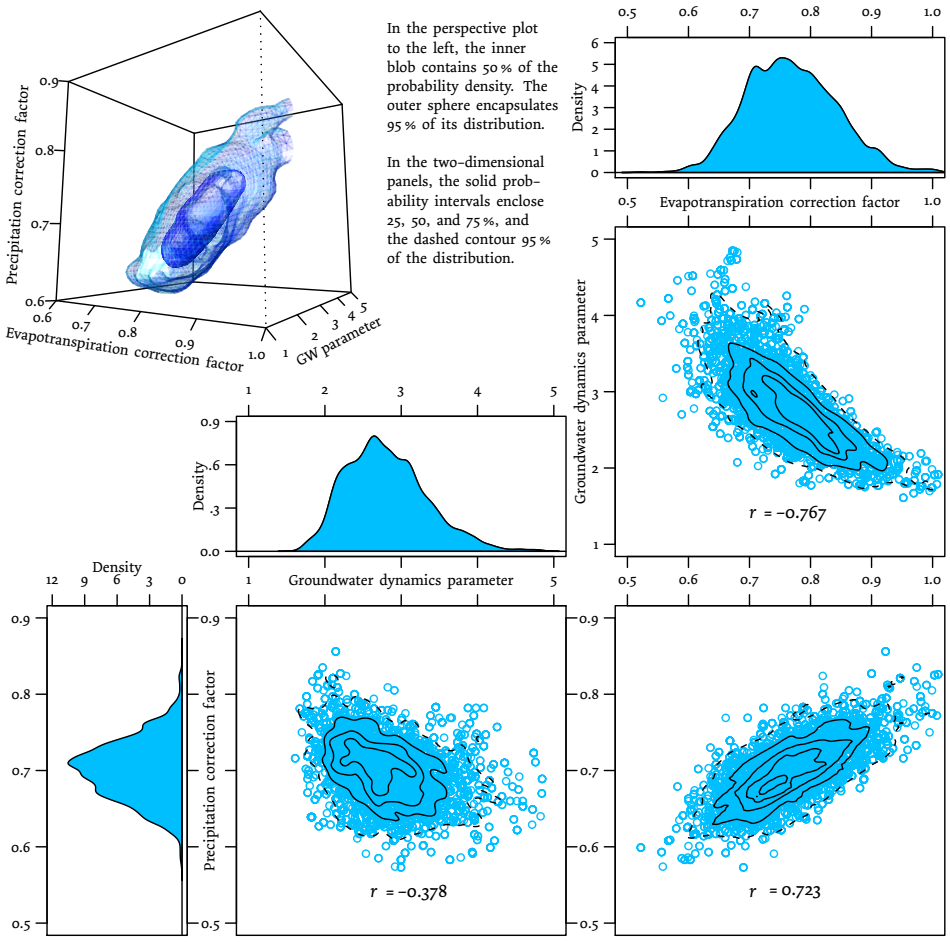

Figure 31: Multiple views of the probability distribution for the local calibration parameters of gauge Chlum Volary, Vltava. The underlying Markov Chain has a length of 10 000 elements.

correction is most probable, but the possible alternatives cannot be categorically rejected.

However, it has to be stated that a run-off correction for gauge Žlutice by evapotranspiration correction alone does not conflict with these results.

3.3.3 *Chlum Volary, Vltava*

In the spring area of the Vltava, the marginal distributions of evapotranspiration and precipitation correction factors are also strongly correlated (r = 0·723). While mode, median, and mean of the relatively symmetrical marginal distribution for the evapotranspiration correction are grouped around 0·75 (Figure 31), an even stronger reduction is required for precipitation. The respective central values of the marginal distribution for the precipitation correction factor are around 0·7.

This promotes a general over-estimation of the interpolated precipitation in combination with an over-estimation of actual evapotranspiration by SWIM. The local evapotranspiration correction from spatial water balance calibration of the entire model leads to a factor of 1·3, which may cause realistic discharge volumes but is likely to increase the local over-estimation of actual evapotranspiration.

More evidence for an upward bias in precipitation data is given by the tail of the distribution near the neutral evapotranspiration correction of 1·0. Here, the most probable values for the optimal precipitation correction factor concentrate at 0·8; vice versa, no optimal correction factor can be given for uncorrected precipitation, as the model is unable to produce acceptable simulations without precipitation reduction.

3.4 DISCUSSION

According to these analyses, there are two gauges, namely Stará Lhota and Žlutice, where the applied method for local water balance calibration by evapotranspiration corrections can be confirmed. Only the simulation of Chlum Volary would probably have been more realistic if precipitation had been corrected before. In the case of Chlum Volary, the reason for the obviously upwardly biased precipitation data can indeed be attributed to a problem in the interpolation of station data.

In the boundary region between the Czech Republic and Germany, both the national boundary and the Elbe River basin boundary run along the crest of the Bohemian Forest. There were data from numerous weather stations on the German side, outside the basin. On the Czech side, where also the catchment areas of the gauges Stará Lhota und Chlum Volary are located, the density of available stations was much lower. The map in Figure 32 shows how the overweight of stations on the rain-laden windward of the mountain ridge affects the interpolations for many Czech sub-basins.

For Chlum Volary, the Bayesian analysis confirms the suspicion that the interpolated precipitation is biased upward due to the windward stations outside the basin. The catchment area of Stará Lhota is comparably located and receives high precipitation amounts, too. However, according to the Bayesian analysis, the interpolated precipitation is only slightly biased here.

This example shows how heterogeneous some sources of uncertainty may be. Unfortunately, it is impossible to assess and optimally eliminate individual errors and comparable flaws in the input data with maintainable efforts for each sub-basin. It has also to be taken into account that any input uncertainty assessment using model residuals implicitly relies on the assumptions of the model. However, respective interpolation errors should be restricted to this section of the basin boundary. Thus, the applied practice of realising the spatial calibration

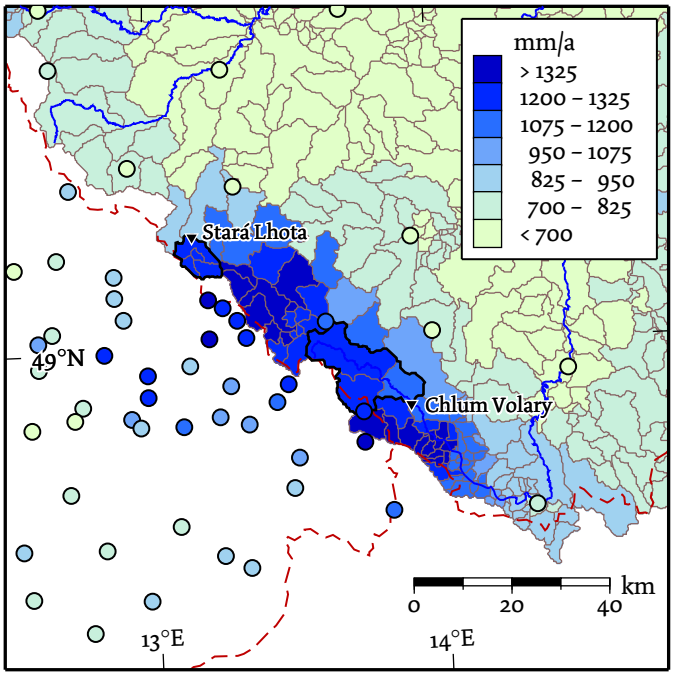

Figure 32: Mean annual precipitation depths in the south-west of the Czech Republic during the reference period 1951–2003. Climate stations are coloured according to their measurements, and the model sub-basins are coloured according to the values that were interpolated on them and used for the simulation.

of run-off volumes by evapotranspiration corrections is supported by this study.

Finally, the assessments presented here exemplify how Bayesian analyses using MCMC methods can be utilised for isolating specific error sources in hydrological modelling applications.

ACKNOWLEDGEMENTS The authors would like to express their gratitude to all project partners involved for the good cooperation. Sincere thanks are given to the German Federal Ministry for Education and Research (BMBF) and the project management agency at the German Aerospace Center (PT-DLR) for the funding of the GLOWA-Elbe project (grant no. 01 LW 0603 A2).

4

LAKE EFFECTS ON REGIONAL PRECIPITATION

Tobias Conradt, Zbigniew W. Kundzewicz, Fred F. Hattermann & Frank Wechsung

ABSTRACT Although often modelled, empirical evidence for regional water balance shifts, due to local land-use changes, is rare. The same holds for quantification of such effects by measurement. The flooding of former open-cast mining areas in Lusatia, eastern Germany, delivers an unique opportunity to address this topic in a well-gauged region. During two decades, flooding changed about 60 km² of lignite pits to lake surfaces. To quantify possible shifts in the regional precipitation pattern, the background of general precipitation dynamics within the research area was separated from all rain gauge records by principal component analysis (PCA). Linear models with the dominating PCA-component as independent variable were fitted to the single station records. The residuals of these fits represent the local deviations from the general dynamics, and they contain the signals of climate alterations within the region. The analysis of these residuals revealed a shifting precipitation pattern with significant increases (up to 10 % of the former mean annual precipitation, which is approximately 650 mm) on the lee side of the developing lake area. Further analysis showed that most of the observed changes are due to more frequent and intense convective storms. Water balance estimations indicate that the additional evaporation approximately equals the precipitation increase.

KEY WORDS flooding; land-use change; Lusatia; precipitation; principal component analysis; regional climatic change; thunderstorm activity; water balance

4.1 INTRODUCTION

The significant influence of land-use or surface patterns and their alteration on local or regional climate has been shown by a number of studies. Review articles by Pielke (2001) and Moorcroft (2003) cite publications on the coupling between surface and atmosphere. Examples of effects on local or regional scales have been reported by Baidya Roy & Avissar (2002), Clark et al. (2004), Pitman et al. (2004), Pitman & Narisma (2005), Sen et al. (2004), Marshall et al. (2004), and Cooley et al. (2005). The point made in these studies is the triggering and support of local convection processes by landscape patterns or surface characteristics.

However, many of these studies lack verification from empirical observations and, in general, analyses devoted to field-measured data are rare. The available literature on the effects of landscape on precipitation can be classified into three categories:

A. climate effects of static water bodies (lakes) on the surrounding region;

B. spatial changes in precipitation without accounting for landscape alterations; and

C. effects of urbanization on regional precipitation.

Observational studies on the precipitation changes caused by land-to-water alterations are also rare. The present study aims to colonize this information niche. Before proceeding to our research objective, we firs discuss each of the categories listed above.

Precipitation effects of lakes have been extensively studied at Lake Kinneret in Israel and the Great Lakes in North America. In an early study, Day (1926) presented elevated rainfall in the neighbourhood of the latter. Wilson (1977) found little increase in precipitation within 30 km of the shore of Lake Ontario restricted to the warm season, whereas Scott & Huff (1996) reported doubling of precipitation in downwind areas of Lake Superior during winter. The effects involved are a combination of moisture transport and an influence of surface characteristics on the atmosphere. During spring and summer, water surfaces cool the air layer above them. This leads to stabilization of the overlying atmosphere and subsequent reduction in the number of showers. Wilson (1977) reports this mechanism for the lake region, but the adjoining land showed strong increases in shower activity.

Surveys of regional changes in rainfall were presented by de Luís et al. (2000) for a part of Spain, by Gong & Ho (2002) for the Yangtze area, and by Drogue et al. (2006) for the Rhine–Meuse Basin. However, none of these studies attributes its findings to land-cover changes.

The few precipitation studies linked to land-use change concentrate on urban effects. Studies for bigger cities, e.g. Atkinson (1968) for London, or Changnon (1980), Changnon & Huff (1986), Dixon & Mote (2003), and Burian & Shepherd (2005) for cities in the USA, generally show increased convective activity and thunderstorms over the urbanized areas at their downwind part. Jaurequi & Romales (1996) investigated rainfall in Mexico City and presented results on the effect of urban sprawl on the increased convective activity. Other urban area precipitation studies not limited to a single city report the same effect of increasing convective rainfall (see Huff & Changnon 1973, Shepherd et al. 2002).

Observed effects of land-use alterations not directly related to urbanization were reported by Stidd (1975). This study found increased

precipitation within a radius of approximately 200 km of an irrigation project.

Here, we study former open-cast lignite mining pits in the Lusatian region of eastern Germany. Within the post-mining recultivation activities, abandoned pits are being flooded. About 60 km² of sandy dumping grounds have been converted to water surfaces within two decades. Therefore, this region offers a unique opportunity to study how the transformation of dry areas into lakes might affect the precipitation pattern in a temperate climate.

What are the meteorological effects of such extensive changes? How far do those effects extend? Lake studies do not give a very clear picture, and there are at least two major mechanisms to be considered: hydrological recycling by the increased evaporation from the lake, and convection triggering.

Local hydrological recycling means that evaporation from a certain area is a source of precipitation in its neighbourhood (see Eltahir & Bras 1996, for a comprehensive introduction into the topic). Accordingly, there are several different estimates for the 'recycling rate', defined as the share of local evaporation in the precipitation of a certain place or area.

One valuable approach for precipitation source studies is that of isotope investigations, such as those reported by Bosilovich & Schubert (2002) and Yamanaka et al. (2002). However, the spatial selectivity of these methods is too weak for application within the area of this study, since isotopic gradients of surface waters can only be detected at much larger scales than a few kilometres. The relatively small extent of our investigation area (12 100 km²) may also exclude recycling in the strong sense, i.e. with the same water particles.

Convection triggering is the driving force of convective precipitation in urbanized areas, since evaporation is depressed by sealed surfaces. The trigger, in this case, is the relative 'heat island' effect of settlements in contrast to the surrounding landscape. In an unstable atmosphere, the resulting convection accelerates without further external drivers and may induce shower or thunderstorm activity.

In our case, where water surfaces replace dry sandy dumping grounds, evaporation displays a net increase and strengthens the probability for local recycling. A number of meso-scale climate modelling results on similar land-use alterations have been reported; see, for example, Miller et al. (2005) on the Three Gorges Dam in China and Mölders & Raabe (1997), Mölders (1998, 1999a,b,c), and Mölders & Rühaak (2002) on the Lusatian post-mining landscape alterations.

While Miller et al. (2005) conclude that, by submerging about 1000 km², the Three Gorges project will not affect the regional climate (i. e. warm temperate with dry winter and humid summer), the results of Mölders and co-authors indicate significant changes for Lusatia. Higher evaporation from water surfaces relative to dry dumping grounds led to a slight

raise in simulated precipitation on the lee side of the flooded mining pits. This effect was mostly restricted to autumn conditions with higher water temperatures. In spring, cool water surfaces stabilize the model atmosphere and shower intensity decreases compared to non-flooded conditions. Notice, however, that the model was applied only to single, sample days, and could not be validated.

In the present study, we use measured data to explore the change in the precipitation pattern caused by the flooding of former open-pit areas. Attention is given not only to changes in annual precipitation amounts, but also to seasonal effects and the role of convective storms.

4.2 THE STUDY AREA

The area under investigation is a square of 110 km × 110 km in Lusatia, eastern Germany, a region adjoining the borders of Poland and the Czech Republic. The most prominent city within the study area is Dresden on the River Elbe, located in the southwestern corner of the square. Figure 33 shows a map including the locations of the 25 precipitation stations.

The elevation ranges from 39 m a.m.s.l. near the River Neisse in the northeast to a mountain top of 587 m a.m.s.l. at the southern edge of the area. In general, there is a rather uniform increase in elevation from about 50 m a.m.s.l. in the north to a hilly strip in the south, with typical values ranging between about 200 and 400 m a.m.s.l.

In Fig. 33, all new water surfaces (flooded mining areas), which emerged between 1990 and 2000, are indicated in black. This information was taken from the German part of the CORINE land-use database provided by the European Environmental Agency (EEA, http://www.eea.europa.eu). Detailed documentation about the CORINE data is given by Bossard et al. (2000), Büttner et al. (2002), and Mohaupt-Jahr et al. (2004).

Open cast mining has a long history in this region. It was most intensive before 1990, when it yielded nearly 200 × 10^6 t of lignite per year, this being the main energy source for the former German Democratic Republic. Each year, nearly 40 km² of landscape were devastated, and in Lusatia 7 m³ of groundwater had to be pumped for each ton of lignite. There had already been some recultivation activities, but the devastation largely exceeded the recultivated area (Berkner 1989).

According to the statistics of the German brown coal mining association (DEBRIV, http://www.kohlenstatistik.de), 23·6 km² of water surfaces had emerged in the mid-1980s and 32·6 km² by the beginning of the 1990s. After the German reunification, mining activities were reduced, while recultivation was enhanced considerably. New water surfaces emerged, with the total area in the year 2000 being 79·0 km². This means that there was an increase of about 60 km² between 1984 and 2002, the main time frame of this study. There are other open cast

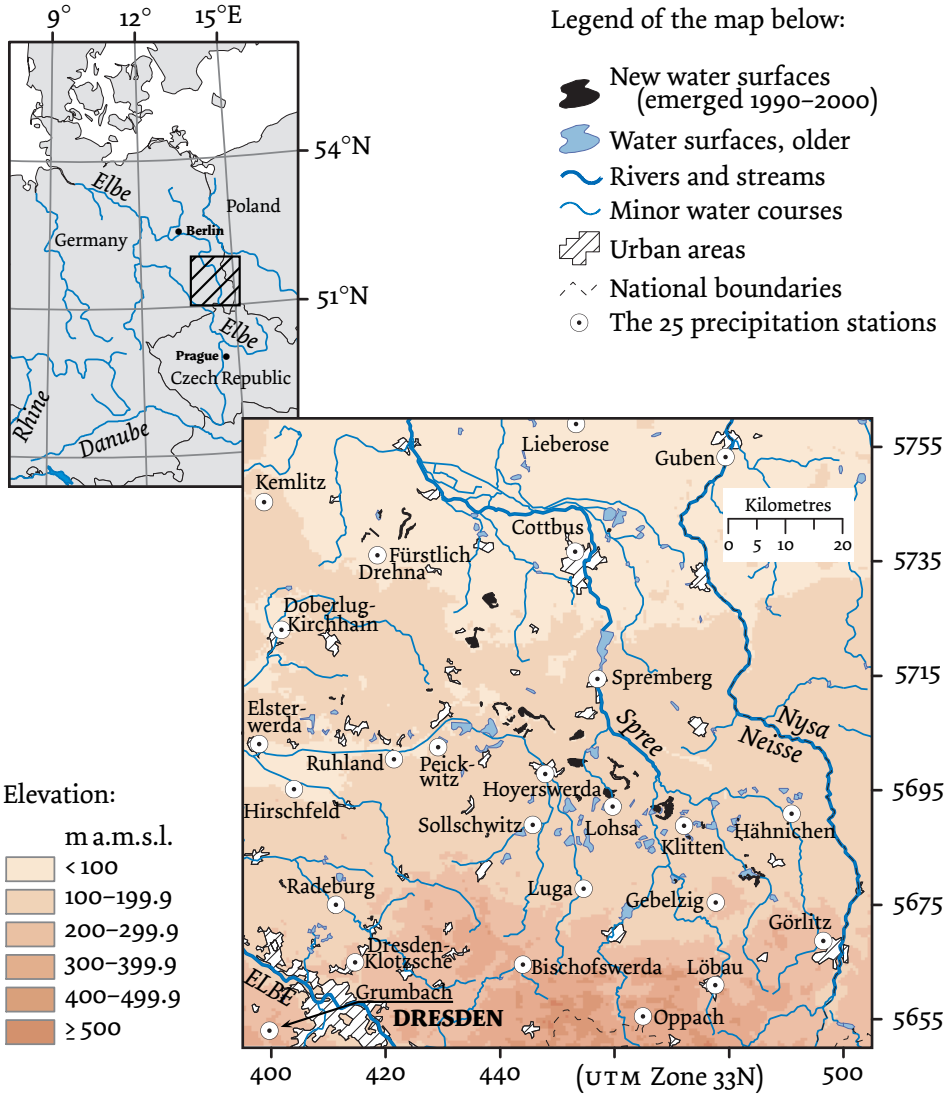

Figure 33: The study area with precipitation stations

Table 5: List of the 25 precipitation stations whose data are used in this study

DWD-ID	Lat °N	Long °E	Elevation m a.m.s.l.	Name	Data gaps Year: month(s)	Gap subst. DWD-ID(s)
3358	14·32	51·78	69	Cottbus		
3386	13·78	51·13	222	Dresden-Klotzsche		
11405	14·95	51·17	237	Görlitz		
11455	14·7	51·93	46	Guben		
41254	13·57	51·02	290	Grumbach		
41409	14·22	51·35	132	Sollschwitz		
41433	14·2	51·13	300	Bischofswerda		
41442	14·35	51·25	155	Luga	1999: 10–12	41409, 46224
41451	14·25	51·43	135	Hoyerswerda		
41466	13·98	51·47	102	Peickwitz		
41469	13·87	51·45	98	Ruhland		
41515	13·62	51·4	105	Hirschfeld		
41527	13·73	51·22	153	Radeburg		
41603	13·53	51·47	91	Elsterwerda		
41609	13·58	51·65	97	Doberlug-Kirchhain	1992: 01–05	41603, 46603
46203	14·5	51·05	320	Oppach	1991: 08	46236
46224	14·42	51·38	125	Lohsa	92:05, 97:04, 98:06, 00:06	41451, 46251
46236	14·68	51·1	249	Löbau	1984: 11	46203
46245	14·68	51·23	190	Gebelzig		
46251	14·6	51·35	132	Klitten		
46272	14·87	51·37	155	Hähnichen	2001: 11	11405, 46245
46310	14·38	51·58	96	Spremberg		
46415	14·32	51·98	58	Lieberose		
46436	13·82	51·77	77	Fürstlich Drehna	1991: 02–05	41609, 46603
46603	13·53	51·85	108	Kemlitz		

lignite mining areas with similar development in Germany, but Lusatia has the strongest clustering of residual lakes; this is why this region was selected. The long term planning by the company responsible for the landscape rehabilitation (LMBV, http://www.lmbv.de) proposes 146 km² of flooded area in the long run, but this may still take some decades, as only about half of the groundwater deficit of 7×10^9 m³ had been restored by 2005.

There were more precipitation stations within the map area than the 25 used for this study, but some had to be excluded due to discontinued measurements. Smaller data gaps, summing up to a maximum of five months per individual station, were filled with averaged data from neighbouring stations. The station details are listed in Table 5.

Typical values of mean annual precipitation range from 550 mm year^{-1} in the northwestern corner of the area to 800 mm year^{-1} at its southern edge, and are typically correlated with elevation. On average, summer precipitation with dominating convective rainfall is slightly higher than in the rest of the year (monthly values around 70 mm compared to approximately 50 mm). Runoff maxima typically occur in winter or early spring due to high evapotranspiration in summer. Both phenomena are very common for the whole of Central Europe and other temperate zones.

4.3 EXPLORATORY DATA ANALYSIS

Before discussing the spatial trend distribution, the general increase in precipitation on the lee side of the residual mining areas coinciding with the flooding process is presented. Figure 34(a) shows precipitation data for 1951–2002. The solid line (A) marks annual averages of five neighbouring rain gauges in the northwest of the area: Cottbus, Doberlug-Kirchhain, Lieberose, Fürstlich Drehna, and Kemlitz (see Fig. 33 for the locations of these gauges). The dashed line (B) displays the same information but for Luga, Lohsa, Gebelzig, Klitten, and Hähnichen stations. These latter stations form a group in the southeast, downwind of the flooded areas.

To compare the development of these well correlated time series, one could simply analyse their differences. But with Group B having higher elevations and respectively higher precipitation values (and variations) than Group A, it is advisable to project one time series on the level of the other before carrying out the comparison. This was done by linear regression of the 52 annual values from Group B on their complements from Group A, which yielded linear estimates for B_i as $\hat{B}_i = 1{\cdot}0323\, A_i + 73{\cdot}7$ mm. ($R^2 = 0{\cdot}788$; the index i refers to the year of the annual values.) With these estimates being just a transformation of the A_i, the notation $\tilde{A}_i$ instead of $\hat{B}_i$ is applied in Fig. 34(a).

The resulting line of differences is plotted in the lower part of the same diagram. Wide variations reaching up to 198·5 mm in 1981 make

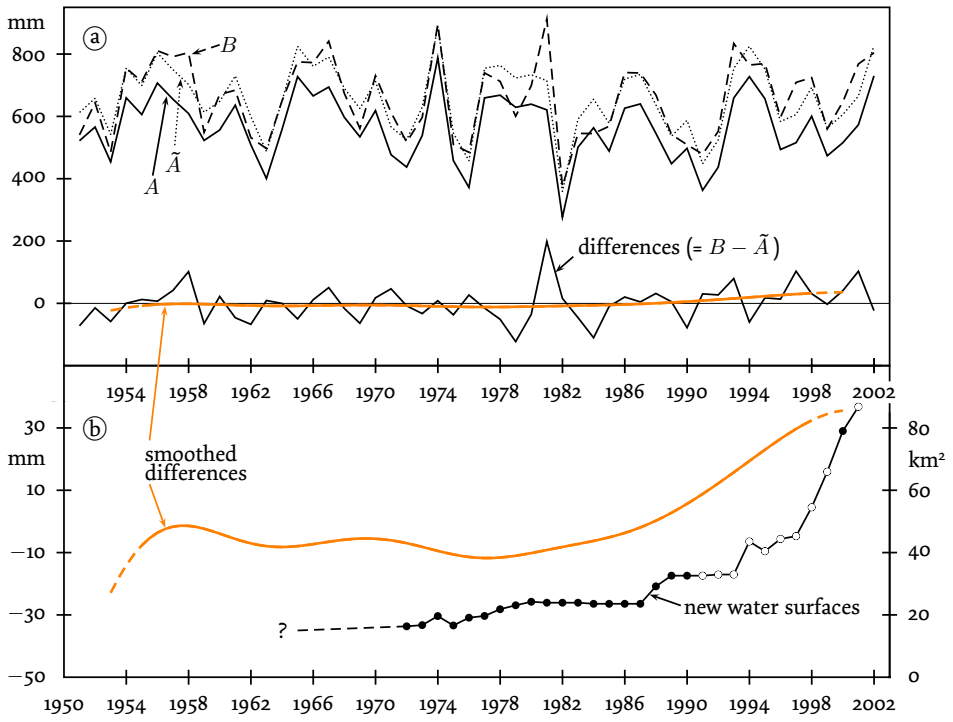

Figure 34: Comparison of precipitation measurements in different sub-regions (annual averages of the two rain gauge groups A and B) and the evolution of the new water surfaces. Surface values indicated by hollow dots are estimated from a statistic covering all lignite mining recultivation areas in eastern Germany.

it hard to perceive any tendency directly. These variations seem to manifest at least one periodicity of 4–5 years, which might be caused by the North Atlantic Oscillation (NAO) or the El Niño Southern Oscillation (ENSO), (see Marković & Koch 2005), but this hypothesis was not validated further.

Smoothing by a Gaussian kernel of 4·2 years bandwidth reveals an upward trend towards the end of the time series, shown as an orange curve. The smoothing levels out the strong oscillation around 1981. Figure 34(b) shows the same smoothed curve on a zoomed precipitation scale, which makes it easy to compare the final relative increase in precipitation measured for Group B with the development of new water surfaces by post-mining recultivation. The axis on the right-hand side of Fig. 34(b) refers to the flooded area (km^2). Obviously, the precipitation increase started concurrently with the acceleration of the flooding process, in about 1987.

As the magnitude of changes in precipitation is clearly below the annual variability, the natural interannual variability has also to be considered. Therefore, Fig. 34(b) may not show a cause–effect relationship but the so-called Hurst effect, cf. Koutsoyiannis (2005).

A more in-depth validation of this hypothesis is beyond the objective of this explanatory analysis, which mainly provides a first glance at the precipitation shift within the region.

4.4 SPATIAL TREND ANALYSIS

4.4.1 *Methodology*

4.4.1.1 *Steps of the Analysis*

In order to separate the local influences from external ones on the spatial precipitation pattern, and to quantify the temporal changes, we pursued the following analysis:

1. Principal Component Analysis (PCA) was applied to daily measurements of all 25 utilizable precipitation stations within the area from 1984 to 2002. The time frame was taken with respect to the process of flooding which was negligible before the late 1980s (and restricted by data availability, as well). All data were first transformed to unit variance to achieve equal weighting for each station. The PCA technique was used mainly to yield the values of the first principal component as a time series variable, providing an objective regional measure of precipitation.

2. This general intensity measure was then used as the independent variable to compute linear regressions with the individual measurements of each station. The residuals of these fits provide the stations' individual deviations from the common dynamics of

all time series. These are thought to contain the signal of local changes within the area (superimposed by statistical noise). The linear estimates themselves are less interesting in this context. Their strong correlation with R^2 values around 0·7 to the first principal component illustrates the dominance of the general dynamics for the whole area.

3. Changes in the mean value of the deviations over time were revealed by another application of linear regression. The results may be interpreted as local trend anomalies of precipitation, separated from the general influence of climate variations.

4. The significance of the regression estimates was checked for each station separately by non-parametric trend tests, which led to further statistical analysis of the deviations.

5. The 25 linear estimates of increase or decrease were interpolated and mapped by ordinary kriging.

6. Trend estimations and mapping were repeated with restriction to data from selected parts of the year to investigate intra-annual variations in the spatial pattern found; the mapped results are compared to seasonally dominating wind directions.

7. Finally, the alterations of the regional water balance were calculated.

All computations and most figures in this paper were made using the open-source R programming language (http://www.r-project.org).

4.4.1.2 *Why PCA?*

Originally introduced by Pearson (1901) and Hotelling (1933), PCA condenses information given redundantly by measurements of different variables to a set of, preferably few, dominating factors. Detailed description of the method is provided in many books on multivariate statistics and factor analysis; a comprehensive reference is Jolliffe (2002). In order to understand why PCA was used in preference to simple averaging to obtain one variable of general regional precipitation activity, the following example illustrates the basic idea of the method.

Any multivariate set of observations can be analysed and transformed by PCA, provided there are no missing values; it is a coordinate transformation. As shown in Fig. 35, the three-dimensional data sets can be reproduced by combinations of the so-called principal components, shown as arrows. This transformation is not done arbitrarily, but results from the calculation of the eigenvector directions of the covariance matrix. Thus, the first principal component, shown by thicker arrows

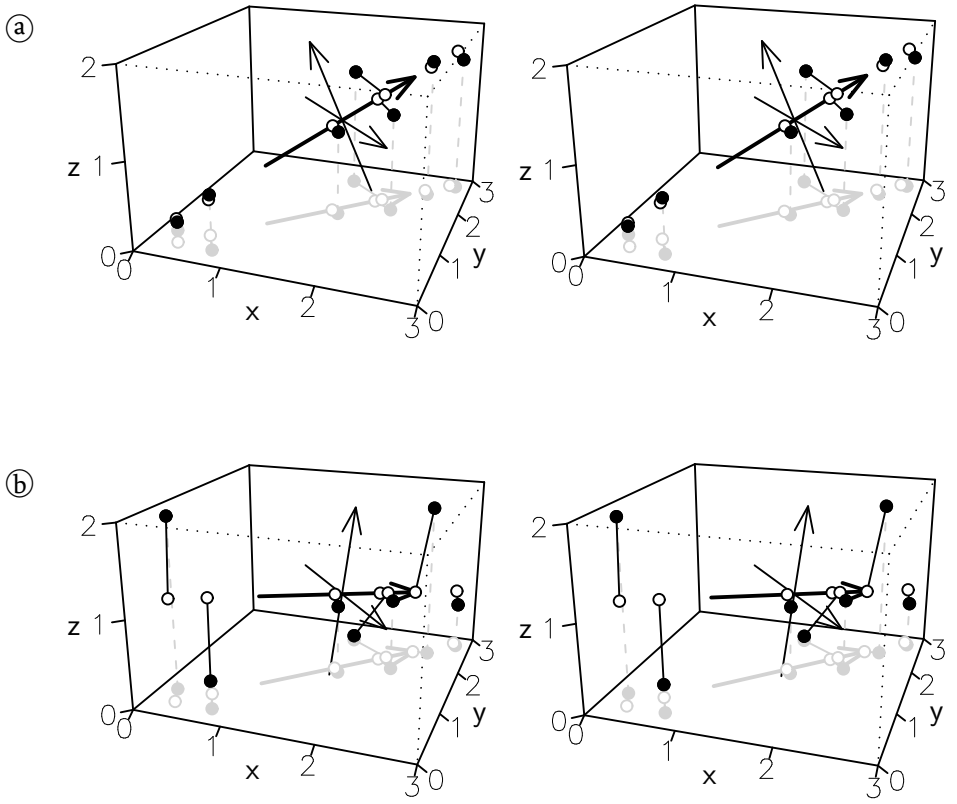

Figure 35: Stereoscopic views of PCA: (a) applied to three correlated variables and (b) the same situation with the z variable being uncorrelated noise. The arrows show the transformed coordinate system. Data representation on the main component (white dots on the thicker arrow) is hardly influenced by the z noise (in b), which maps to its own component. Projections of points and main component on the x–y plane are shown in grey. Both graph pairs can be seen with depth by 'overcrossing' the eyes, i. e. focusing the right eye on the left and the left eye on the right graph. This works best from 50–70 cm distance.

in Fig. 35, is always oriented along the leading direction of data variance in the input variable space and contains most of the information, represented by the white dots.

In higher-dimensioned systems with many correlations, PCA can map the data to a few leading principal components with negligible information losses. This enables PCA to effectively separate common patterns from individual data vectors, e. g. time series.

Consider PCA applied on measurements of 25 rain gauges within the same region. The first principal component of the 25-dimensional system will rise and fall with the rainy periods affecting all gauges in the region simultaneously.

Notice that if all rain gauges delivered highly correlated data, PCA would not be more efficient relative to daily averaging. But, if some of

the gauges recorded patterns deviating from the majority of measurements, e. g. due to local weather effects, the first principal component would still preserve the dominating pattern, while the deviations would be mapped to higher components. The PCA-principle is shown for a three-dimensional system by Fig. 35(b), with the third input variable being uncorrelated noise.

It is important to emphasise the caveat that, since PCA is a second moment technique, while daily precipitation is a highly skewed and intermittent process, statistical inference is limited to broad features.[1]

4.4.2 *Results and Discussion*

4.4.2.1 *PCA and Station Trends*

The first principal component explains 71·3 % of the total variance, which is a magnitude above the information content of the subsequent principal components; the second component explains 6·2 % and the third 4·4 % of the total variance.

The column vectors of the rotation matrix (which is used to compute the coordinate transformation in the 25-dimensional space) contain the so-called 'loadings' representing the linear correlations between the principal components and the individual station time series. All 25 loadings of the first principal component are in an interval between 0·176 (Kemlitz in the northwestern corner of the study area) and 0·213 (Luga, about 30 km south of the centre).

The other column vectors contain fair mixes of positive and negative loadings, showing spatial sub-structures. The second one ranges from –0·298 (Kemlitz in the northwest) to 0·340 (Löbau in the southeast) and the third one from –0·393 (Grumbach in the southwestern corner) to 0·422 (Guben in the northeast). These are associated to low eingenvalues, viz. components with low information content.

The dominance of the first principal component and the small variance of its loadings are empirical evidence for the assumption of one general precipitation regime affecting all stations in a similar way.

Figure 36(a) depicts a cloud of tiny dots, the daily residuals for the station Hoyerswerda (in the centre of the study area) obtained by the linear regression of the measured precipitation at Hoyerswerda against the first principal component values for all stations. Here, the residuals are plotted against time. Positive values mean more precipitation at this site than expected from the entire measurements of the specific day. What looks like a horizontal line slightly above zero is formed by all those dots on dry days without precipitation at any of the stations.

1 One of the reviewers insisted in having this sentence included. I doubt that there is a limitation to broad features in our application, since we do not analyse the variance components but concentrate on residuals of the original measurements.

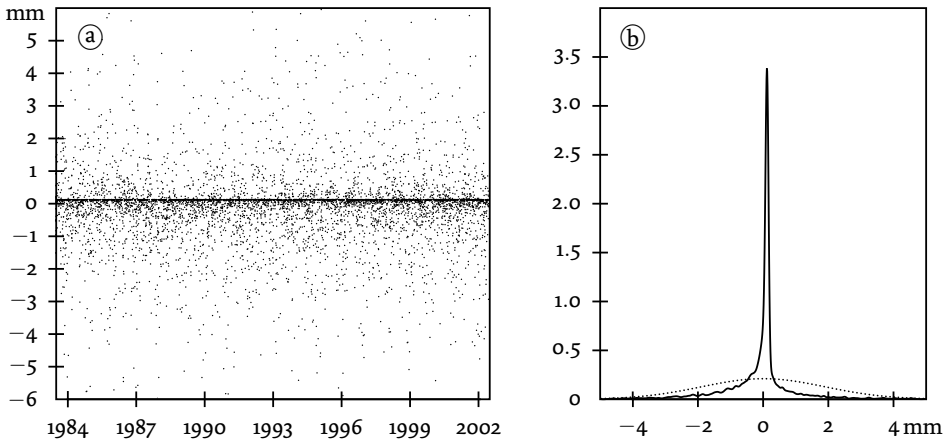

Figure 36: (a) Daily residuals of Hoyerswerda and (b) their density function estimated by kernel smoothing. The dotted line on the density graph shows the normal distribution with the same standard deviation of 1·89 mm for comparison.

These days led to the most frequent value of the residuals' distribution, which is heavily peaked and long tailed.

Figure 36(b) shows an estimate of the density function, smoothing away the principally infinite heigth at the often repeated dry-day value. The inner quartiles range from –0·27 to 0·14 mm, while the most extreme values are –20·11 and 39·95 mm, respectively; the numerical kurtosis has been computed as 95·6. Additionally, the distribution has a skewness of 5·56: a possible explanation for this could be isolated showers producing higher positive residuals at the affected stations being more frequent than their opposite, distinct dry areas on rainy days.

In order to test the residuals for significant trends, the non-parametric Mann-Kendall and Spearman rank correlation tests were applied. Both tests do not require assumption of normally distributed data.

Table 6 lists the results for the 25 precipitation stations, the first column of trend values giving the linear fit for the raw data (including the background increase) for comparison. The linear trend estimates of the residuals are listed in the next column and are referred to as 'trend anomalies', as they must not be mixed up with the linear trends of the raw precipitation measurements being addressed as 'base trends'. Of course, the significance tests have only been calculated on the background-independent residuals of the PCA method.

Both trend tests yield very similar results indicating significance at the 95 %-level for nine stations and at the 99·9 %-level for five out of the 25 stations. Except for Guben, only negative trends are found to be significant, and in the case of Sollschwitz, the positive linear trend in the anomaly was found to be negative in the data ranks (cf. the negative values of τ and ϱ).

Table 6: Linear trend estimates for the raw data of the 25 locations (base), their PCA-filtered residual trends (anomaly), and the results of two non-parametric trend tests for the trend anomalies

		Trend estimates		Non-parametric trend tests of the anomalies			
		Base	Anomaly	Mann-Kendall		Spearman	
				τ	p-value	ϱ	p-value
DWD-ID	Name	mm year^{-1}	mm year^{-1}	10^{-3}	%	10^{-3}	%
3358	Cottbus	3·516	−1·296	1·27	87·6	1·94	87·2
3386	Dresden-Klotz.	1·708	−4·267	−49·3	< 0·001***	−71·0	< 0·001***
11405	Görlitz	2·890	−2·278	−27·5	0·077***	−40·5	0·074***
11455	Guben	5·501	0·989	19·8	1·56 *	28·8	1·63 *
41254	Grumbach	4·876	−1·170	−29·7	0·028***	−42·9	0·035***
41409	Sollschwitz	7·166	1·393	−26·9	0·097***	−39·3	0·106**
41433	Bischofswerda	3·963	−1·793	−19·0	2·03 *	−27·7	2·09 *
41442	Luga	7·520	2·266	6·22	44·7	9·14	44·6
41451	Hoyerswerda	7·024	1·283	−9·15	26·3	−13·2	27·1
41466	Peickwitz	−2·014	−7·285	−66·1	< 0·001***	−96·8	< 0·001***
41469	Ruhland	3·257	−2·035	−5·46	50·3	−7·62	52·6
41515	Hirschfeld	5·117	0·232	−1·17	88·6	−1·35	91·1
41527	Radeburg	7·550	2·040	1·14	88·9	2·14	85·9
41603	Elsterwerda	8·477	3·564	6·34	43·8	9·72	41·8
41609	Doberlug-Kh.	2·950	−1·774	−23·9	0·339**	−36·0	0·269**
46203	Oppach	6·458	0·695	2·34	77·5	3·36	77·9
46224	Lohsa	9·486	3·714	−12·3	13·2	−17·7	14·1
46236	Löbau	8·554	3·059	−9·77	23·2	−13·7	25·3
46245	Gebelzig	9·402	3·969	14·5	7·50	21·4	7·45
46251	Klitten	7·104	1·663	4·52	58·0	6·96	56·2
46272	Hähnichen	8·635	3·172	3·62	65·8	5·47	64·9
46310	Spremberg	2·937	−2·248	−46·4	< 0·001***	−67·5	< 0·001***
46415	Lieberose	3·011	−1·167	−14·4	7·83	−20·8	8·36
46436	Fürstl. Drehna	4·076	−0·661	0·32	96·9	0·64	95·8
46603	Kemlitz	7·104	−1·632	−12·9	11·6	−18·5	12·3

Significance levels: * 95 %, ** 99 %, and *** 99·9 %.

4.4.2.2 *The Role of Summer Thunderstorms*

The non-parametric tests are based on data ranks; they show a falling pattern formed by the majority of data points while a few positive outliers at the end of the time series lead to an increasing linear fit. A likely source for respective extreme values in these data are convective storm events with locally very high precipitation sums.

Figure 37 shows station residuals of 5 mm or more. The inference that these are the fingerprint of convective precipitation events can be validated by their prevailing occurence during summer, the season in which most of the regional precipitation is of the convective kind, extreme events typically being thunderstorms. Note that the dots are clustered on top of the time-axis tickmarks indicating the middle of the respective year. With the exception of Peickwitz, the examples

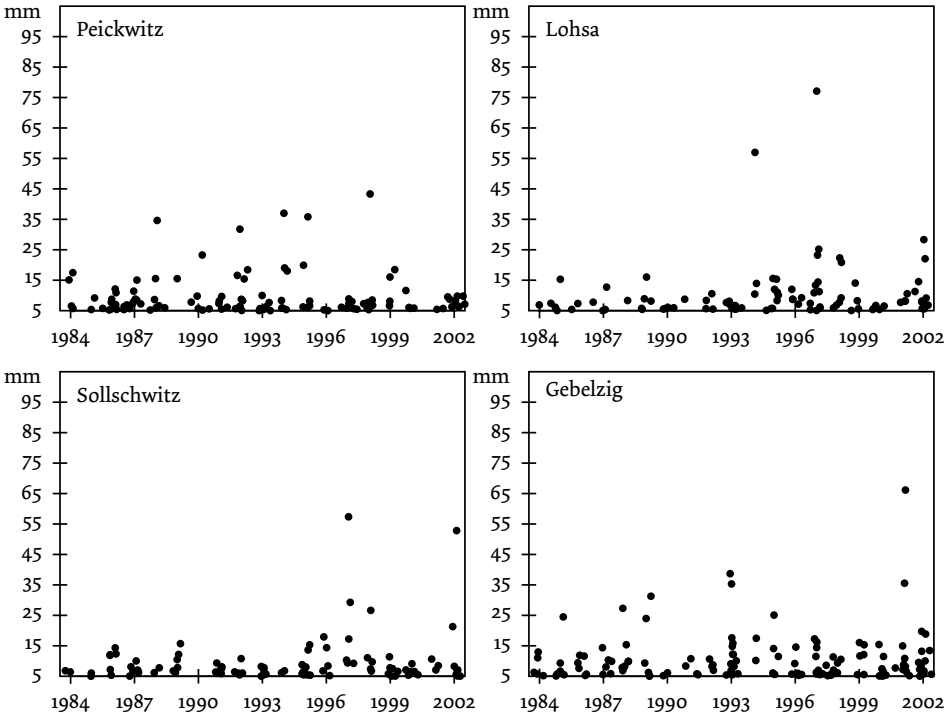

Figure 37: Daily residuals ≥ 5 mm of four selected raingauge stations. Apart from Peickwitz, they show substantial increases of very heavy local storm events during the second half of the time period investigated.

show higher frequencies and intensities in the second half of the time window.

To validate this increase, all positive residuals exceeding thresholds of 5 and 10 mm were counted within two time windows for all stations. The sampling periods are 1984–1992 and 1994–2002, representing the first and the second halves of the entire time frame. The middle year, 1993, was excluded and not split, because the events do not cluster exactly in the middle of the year but in the beginning of the second half.

Due to the lesser counts for individual stations, single χ^2-tests contradict the null hypothesis of equally expected frequencies only in few cases, but a general increase of events exceeding both thresholds is clearly significant. The following numbers in the format *a*:*b* refer to the first and second time spans: For the 5 mm threshold, the respective residuals of all 25 stations sum up to 1430:1707, and the counts for the 10 mm threshold are 366:540. General χ^2-tests yield p-values lower than 10^{-6} for both cases, meaning that sampling such increases by mere accident is extremely improbable. The pattern can be traced through the minima of the stations' counts, 26:42 and 4:7, the median values, 58:66 and 14:21, and the maxima, 89:100 and 29:39, respectively.

However, Pearson's χ^2-test for homogeneity of contingency tables reveals that these counts are likely to contain more than a general increase in thunderstorm frequencies. It can be applied to all counts of each threshold. The p-values of the test are only 0·120 for the 5 mm

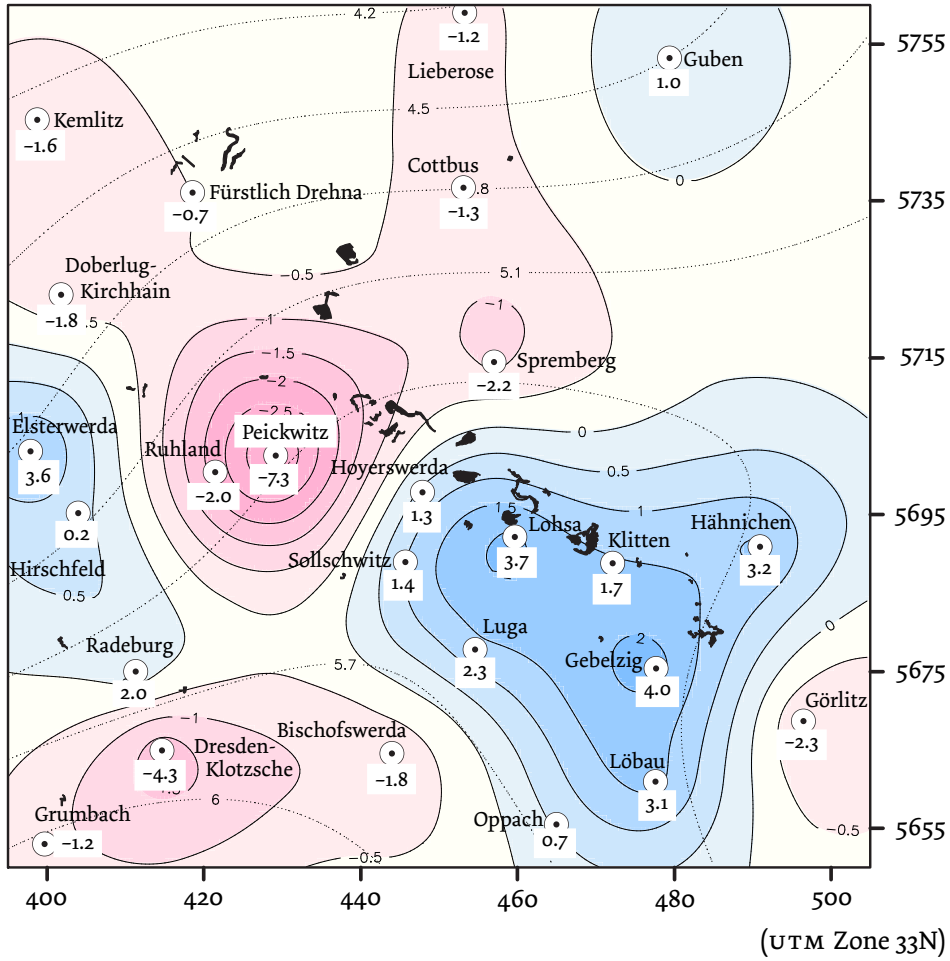

Figure 38: Contour map of the trend anomalies for annual precipitation change in mm year^{-1} for 1984–2002. The dotted lines indicate the differences from the (within that time) generally more increasing base trends of the raw data.

threshold and 0·052 for 10 mm, while, according to the test design, p-values close to one are needed to confirm the null hypothesis of homogeneity. Therefore, it is necessary to report the most obvious deviations from the general pattern.

Two neighbouring stations show decreases at both thresholds: Peickwitz, 58:50 and 14:9, and Ruhland, 50:42 and 13:12. Peickwitz, already presented in Fig. 37, is also the station with the most negative trend anomaly (cf. Table 6). Bischofswerda's counts, 65:75 and 21:7, decrease only for the higher threshold, and Fürstlich Drehna has a slight decrease at the lower one, 66:61 and 17:21. Accordingly, a combination of a negative trend anomaly and low but positive values for τ and ϱ can be found for this station. All this supports our hypothesis of a dominating role of intense convective storms in the precipitation changes observed within Lusatia.

4.4.2.3 *The Spatial Pattern*

The station trend anomalies are mapped in Fig. 38. Additionally, Fig. 38 presents shaded contours of the anomaly pattern interpolated from the station estimates by ordinary kriging. The contour values remain within a low range compared to the station values, because the interpolation assigns uncertainty to the point values and takes their spatial correlation into account. This leads to higher abatements at isolated extrema, most obvious at the Peickwitz location.

The shaded contour plot demonstrates the spatial pattern of precipitation changes, not explicitly giving exact measures. The number of 25 raingauges within the area of 12 100 km² is simply too low for a reasonable analysis of spatial uncertainty. Thus, the spherical variogram model was used with a range of 30 km and nugget and additional sill values of 5 mm² year⁻².

A map with the unfiltered base trends would have shown nearly the same pattern, just with higher values. For comparison, Fig. 38 maps the distance between both trend surfaces as dotted contour lines. Due to the general upward trend of precipitation within the years 1984–2002, the base trends show annual increases of 4·2 to 6 mm higher than the filtered anomalies. The dotted contours had also been generated by kriging, but in this case the spatial correlation was very strong, and the variogram could be fitted very well by a Gaussian model with a range of 60 km, a sill of 0·4, and a nugget of only 0·01 mm² year⁻².

It has to be recalled that the general increase in the raw data must be interpreted on the background of the high inter-annual variability in combination with the rather short observation period of 19 years (cf. 1965–1983 in Fig. 34 comprising a strong decrease). There is no climate signal to be detected, and all that can be shown here are relative changes within the station cluster.

Clearly, the gauges with stronger positive trend anomalies are clustered in the southeastern part of the map, the only exception being Elsterwerda in the west. Of course the heavy decrease at Peickwitz is striking, but there is a good reason for not excluding this station as an outlier with measurement error: the neighbouring Ruhland gauge also shows a negative anomaly and well correlated seasonal dynamics. On the one hand, it has to be considered that these decreases are just relative to the PCA background and, although the base trend for Peickwitz is negative as well, its absolute numbers are much less pronounced. On the other hand, these local inhomogeneities may be due to effects from the station's close neighbourhood. In order to explain these divergences, further research is needed.

The main impression given by the map in Fig. 38 is the following: the area with relatively increasing precipitation does not overlap with the belt of flooded mining holes. Following the hypothesis of local evaporation recycling, there must be wind frequently blowing from northwesterly directions shifting the water vapour, the area receiving

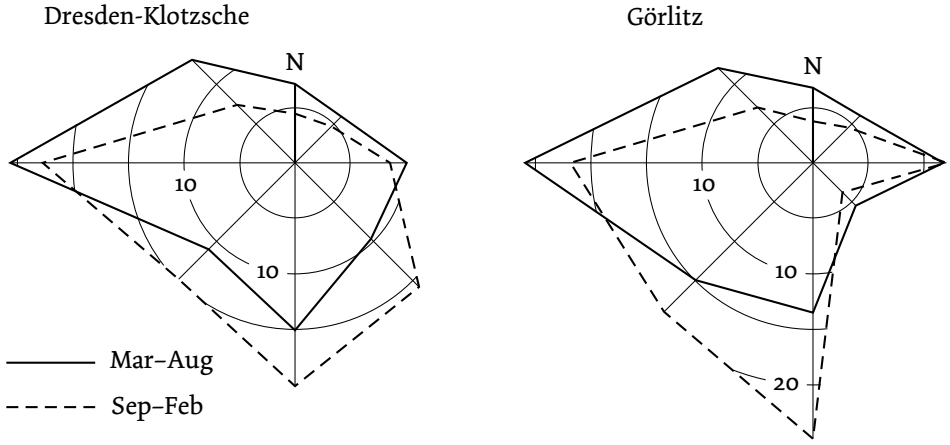

Figure 39: Frequencies of wind directions in opposing halfyears

the surplus of precipitation correspondingly. And this is just what can be observed: the main wind direction is west at the ground (see Fig. 39), implying more northwesterly directions at height, due to more geostrophic conditions in the absence of surface friction.

This is, of course, no proof for hydrological recycling in the strong sense, nor can our analysis alone validate the assumption of a surplus of thunderstorms triggered by the newly established lake–land pattern and drifted with the wind afterwards. However, the spatial clustering of stations showing upward trends is unlikely to be completely random.

4.4.2.4 *Seasonal Variations*

The main questions which lead to investigations restricted to seasons were:

1. Can similar spatial patterns be found on the basis of separate subsets of the data? This would be further evidence against the fortuitousness of the results.

2. Are there stronger effects during autumn than in springtime? Modelling results by Mölders (1999a) can be explained by the hysteresis of water bodies to seasonal temperature variations. In springtime the water is colder, stabilizing the atmosphere. This leads to a net decrease in convection and shower activity. During autumn, the warmer water surfaces evaporate much more and provide less stabilizing effects. This favours shower activity.

3. Can intra-annual displacements of the area with increasing trends be observed, and do they coincide with seasonal shifts of preferred wind directions?

Figure 40 shows four contour maps comprising the spatial trend patterns within the four seasons. The first question may be easily

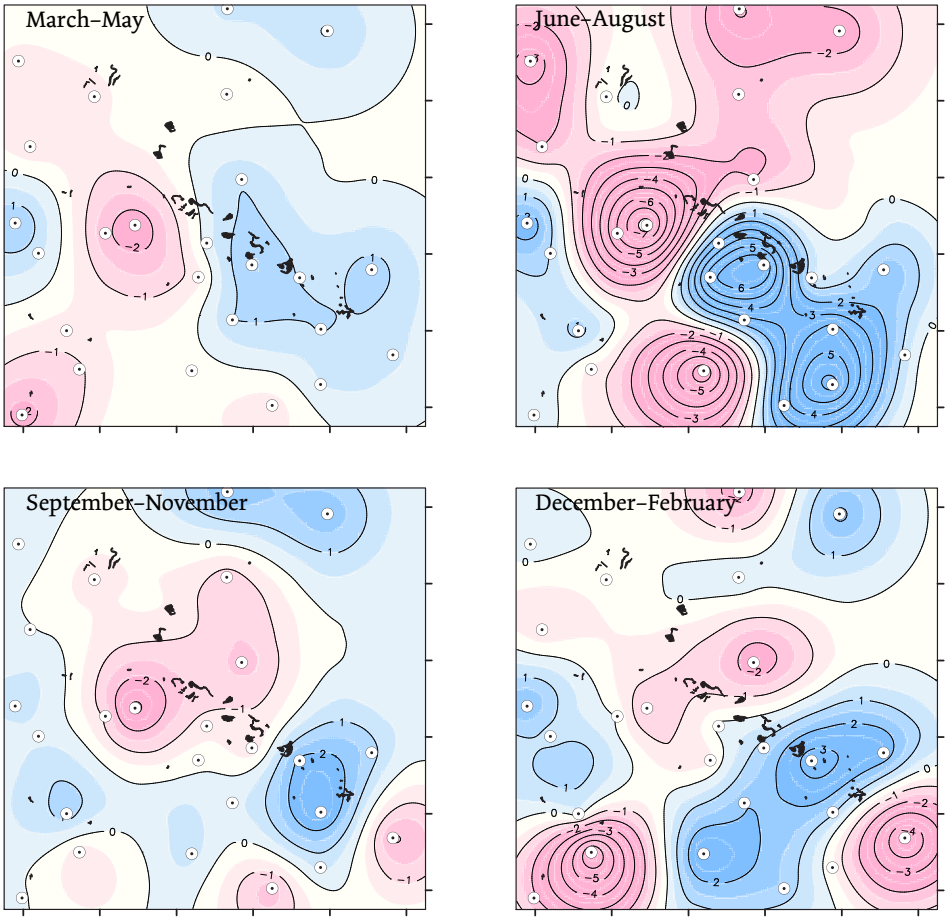

Figure 40: Spatial anomaly patterns for the meteorological seasons. Contour values indicate changes within the sub-datasets containing only the selected months in mm year^{-1}.

answered: a pattern of increasing values in the southeast of the map area is shown by all subsets of data. But, for the theory behind the second question there is no clear verification. In both spring and autumn there are only weak spatial differences. The highest contrasts between the upward trend area in the southeast and its surroundings can be found in the summer period. The reason for this is likely to be the dominating regime of thunderstorms, already discussed.

Wind direction frequencies and their seasonal variations could be obtained for the climate stations Dresden-Klotzsche (airport) and Görlitz, which can be found in the southern corners of the map. In both cases, observations from the years 1991–1999, measured three times a day, gave at least a rough picture of typical wind directions. Monthly grouping of the data showed the highest percentages for the southern direction at Dresden in October, November and December, accompanied by a secondary preference of the southeastern sector. At Görlitz, the southeastern direction is always less frequent, whereas the southern direction is dominant from October to January. Figure 39 presents the wind roses with the average direction distributions for Dresden and Görlitz within the associated half years.

Comparison of the respective pairs of maps in Fig. 40 gives little evidence for the theory of wind related precipitation shifts. The structures of spring and summer dominated by (north)westerly winds shown in the upper two maps are slightly northwest–southeast oriented, and those of the lower pair, influenced by winds from south(east), contain more southwest–northeast directions.

4.4.2.5 *Water Balance*

Here we attempt to answer the question: how much additional precipitation is produced within the study area by flooding of one square kilometre of land? At this point, a systematic limitation of the method becomes apparent: Any regional effect affecting a larger part of the raingauges introduces a bias to the background of the study area. Hence, it is impossible in principle to calculate an exact value.

Under the assumptions that only internal effects such as land-use change produce the local trends observed, and that the affected regions are relatively small compared to the study area (or there are opposing trends within the area), a rough estimation may be possible.

According to the results mapped in Fig. 38, about one sixth of the map area of $A_{map} = 12\,100 \times 10^6\ m^2$ seems to receive additional precipitation. Taking the relative precipitation increase ΔP within this area of approximately 1 mm year^{-1}, the increase in annually transported water volume would be:

$$\Delta V = \frac{1}{6} A_{map} \cdot \Delta P \approx 2 \cdot 10^6\ m^3\ year^{-1} \qquad (11)$$

According to the numerical values given earlier, the mean annual growth of water surfaces ΔA_{surf} between 1984 and 2002 was $3{\cdot}2 \times 10^6$ m², and hence the effect per unit surface changed from land to water is given by:

$$\frac{\Delta V}{\Delta A_{surf}} \approx 0{\cdot}625 \frac{\text{m}^3}{\text{year} \cdot \text{m}^2} = 625\,\text{mm}\,\text{year}^{-1} \quad (12)$$

To comply with the recycling hypothesis, this should be a fraction of the difference between the evaporation from the new water surfaces and the former value when there were dry mining areas.

Biemelt (2001) examined exact water balances in the residual pit landscape of Lusatia and gave an average evapotranspiration value of 325 mm year⁻¹ for the dumping areas. For the evaporation of the water surfaces, there are a couple of differing estimations. Indirect approaches by isotope measurements done by Fauville (2002) and Hofmann et al. (2008) in selected pit lakes yielded the lowest results of about 700, an often-quoted 'rule-of-thumb' value is 800 (cf. Reichel & Uhlmann 1995), while Pfützner (1997) estimates 900–1000 mm year⁻¹. Wendling et al. (2000) depict Lusatia in their map of potential evapotranspiration at the top of the range within Germany, with typical values of 800–860 mm year⁻¹ for grassland.

Taking into account all these findings, 500 mm year⁻¹ seems to be an appropriate lower estimate for the increase in evapotranspiration at each location changed from dry dump into water surface. This is somewhat lower than the estimated increase in local precipitation of 625 mm year⁻¹ and would mean a theoretical recycling rate of more than 100 %. Including the higher evaporation from the landscape around the lakes (benefiting from the groundwater level rise) in the calculation could close this balance, but total recycling on such a small scale is unrealistic. More likely is the other hypothesized mechanism – the lake pattern triggers the occurence of convective precipitation, thus draining the atmosphere of water transported from remote regions. In any case, an increase in partly intensive thunderstorms in summertime leads to numerous consequences for hydrological and landscape planning, particularly since most climate change scenarios predict the opposite trends of drier and hotter summer seasons for this region.

4.5 CONCLUDING REMARKS

The main findings of this study are that:

- precipitation increases downwind of the emerging lake landscape in Lusatia, and
- this increase can be explained by more frequent and intense summer thunderstorms.

One aim of this study was to verify the climate model results obtained by Mölders (1998, 1999a). The observed precipitation increases did not

show higher intensities for autumn and lower or opposite effects for spring as predicted, but only higher extremes in summer. This could mean that the temperature effects were over-estimated in the model.

The calculated balance of additionally dissipating evaporation and precipitation increase needs further investigation, espechially whether local hydrological recycling takes any part in it. Our interpretation of the results ist that the newly established lake–land pattern triggers local convection cells promoting the increase in summer thunderstorms.

Regarding these observations and inferences and considering the drought risk in the Elbe basin, (Gerstengarbe & Werner 2005, Wechsung 2005, Hattermann 2005), landscape management decisions have to be made very carefully. Although scattered further flooding and inundations in this region would rather likely strengthen the local water fluxes in a similar way, there might be some limitations for changing the regional hydrological conditions.

More lakes could also cause net losses of water during dry periods when most of the additional evaporation would simply dissipate. And if triggering of convective showers were (as it seems) the dominant effect, associated torrential rain erosion and flood events might cause problems.

Finally, it has to be mentioned that appropriate policy decisions should be based on adequate modelling, despite all the model shortcomings. The special value of observation studies, such as this one, is not only to make specific statements about the investigation areas; they also encourage improvements of models to be used. As Bronstert et al. (2005) pointed out, there is still lack of adequate hydrological modelling concepts. Not only including soil and surface properties, but parameterizing meteorological effects of surface alterations, would improve runoff models and thus provide support within an important policy field.

ACKNOWLEDGMENTS The authors would like to thank Andreas Langousis and Konstantine P. Georgakakos who reviewed the manuscript and made many constructive proposals and valuable critical remarks. This work was carried out in the framework of the GLOWA-Elbe II Project, funded by the German Federal Ministry of Education and Research.

5

THREE PERCEPTIONS OF THE EVAPOTRANSPIRATION LANDSCAPE

Tobias Conradt, Frank Wechsung & Axel Bronstert

ABSTRACT A problem encountered by many distributed hydrological modelling studies is high simulation errors at interior gauges when the model is only globally calibrated at the outlet. We simulated river runoff in the Elbe River basin in Central Europe (148 268 km²) with the semi-distributed eco-hydrological model SWIM. While global parameter optimisation led to Nash–Sutcliffe efficiencies of 0·9 at the main outlet gauge, comparisons with measured runoff series at interior points revealed large deviations. Therefore, we compared three different stategies for deriving sub-basin evapotranspiration: (1) modelled by SWIM without any spatial calibration, (2) derived from remotely sensed surface temperatures, and (3) calculated from long-term precipitation and discharge data. The results show certain consistencies between the modelled and the remote sensing based evapotranspiration rates, but there seems to be no correlation between remote sensing and water balance based estimations. Subsequent analyses for single sub-basins identify input weather data and systematic error amplification in inter-gauge discharge calculations as sources of uncertainty. Further probable causes for epistemic uncertainties could be pinpointed. The results encourage careful utilisation of different data sources for calibration and validation procedures in distributed hydrological modelling.

5.1 INTRODUCTION

5.1.1 *Improving spatial representativeness of distributed models*

A distributed hydrological model which accurately simulates discharges at the basin outlet while producing poor results at interior points seems to be a paradox. But this feature has been shown by many studies on distributed modelling where inner point discharges were evaluated. Examples for larger simulation errors within the model domain give Andersen et al. (2001), Güntner (2002), Ajami et al. (2004), Ivanov et al. (2004) (suggesting a synthesis of modelling with remote sensing data to realise "the true value of the distributed approach"!), Mo et al. (2006), Moussa et al. (2007), Feyen et al. (2008), or Merz et al. (2009). Bergström & Graham (1998) and Das et al. (2008) report better model performances with increasing basin size for (semi-)lumped approaches, too. Pokhrel & Gupta (2010) and Pechlivanidis et al. (2010) tried parameter-sparse

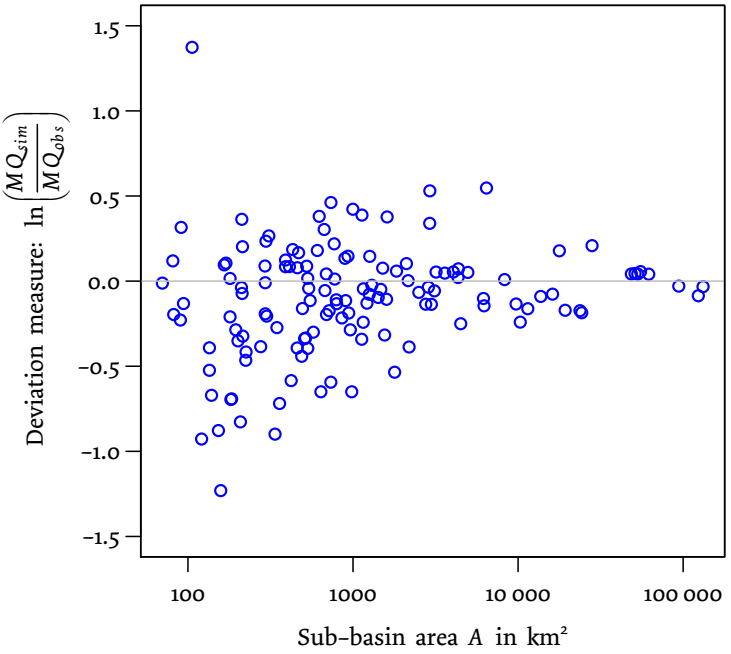

Figure 41: Dependency of model discharge deviation on sub-basin size. For compatibility of positive and negative deviations, the logarithm of the relation of simulated to measured mean discharge has been used as error measure.

approaches for multi-site calibration but achieved generally poor model performances at interior points. Finally, respective results obtained from numerous models in the first phase of the 'Distributed Model Intercomparison Project' (Reed et al. 2004) gave rise to adding more stream gauges at interior points for the second project phase (Smith et al. 2012a) which confirmed the observed trend of model fidelity increasing with basin size (Smith et al. 2012b).

Yet another example from the Elbe River basin in Central Europe (148 268 km²) gave reason to this study: For estimating water-related climate change impacts, the semi-distributed eco-hydrological model SWIM had been applied to project natural water discharges under scenario conditions (Conradt et al. 2012b, 2013a, Chapter 2). Single global calibration by measured discharges at the basin outlet appeared to be insufficient: Comparing the simulated discharges from higher-order tributaries to respective gauge data often revealed grave deviations in water volume. Figure 41 shows the relative volume errors decreasing with increasing sub-basin area. Other comparisons showed poor model performance in simulating peak or low flow phases for some sub-areas of the basin. Nevertheless, a Nash–Sutcliffe efficiency of 0·9 had been achieved for long-term series of daily discharge at the main outlet gauge Neu Darchau.

While studies devoted to spatial representativeness of distributed models have not received much attention yet, the related general mod-

elling problem 'to be right for the wrong reasons' (cf. Klemeš 1982) has incited a broad and still ongoing discussion among hydrologists about the representativeness of their models in general (e. g. Klemeš 1986, Beven 1989, 1996, Grayson et al. 1992, Blöschl 2001, Andréassian et al. 2007, 2012, Sivakumar 2008, to name just a few out of dozens of contributions).

Spatial calibration might minimise sub-catchment uncertainties through increasing site-specific representativeness of the model. In conjunction with distributed hydrological modelling, spatial calibration usually means individual multi-site calibration (Santhi et al. 2008, Zhang et al. 2008). This study uses the term in the same line; it should not be confused with either multi-objective calibrations of global model parameters based on sub-catchment spatio-temporal data (e. g. Zhang et al. 2010, Xie et al. 2012) or data assimilation of which Schuurmans et al. (2011) give an example with weighted averages from satellite-derived and modelled evapotranspiration (*ET*).

Spatial calibration in the narrower sense provides specific research opportunities. Seibert et al. (2000) found optimal sub-catchment modelling results for individual parameter settings, while Khakbaz et al. (2012) explain their opposite finding by a homogeneous basin. In any case, regional patterns of optimised sub-basin parameters as observed by DeMarchi et al. (2011) or Conradt et al. (2012a) (Chapter 3) add credibility to the approach and can be object of further investigation. Partial spatial calibration is also possible: Bronstert et al. (2007) concentrated calibration efforts on some few selected small sub-catchments and on a number of main stream gauges of the Rhine.

Pokhrel & Gupta (2011) argue that enhancements of spatial model representativeness are not necessarily seen in the outlet hydrograph. But they agree with other researchers that incorporating additional site-specific information in a distributed hydrological model increases its robustness (Stisen et al. 2011). Especially remote sensing data are valued as useful complement to station based time series (Finger et al. 2011, Liu et al. 2012).

In our case of semi-distributed eco-hydrological modelling of the Elbe River basin (Conradt et al. 2012a,b, Chapters 2 and 3), sub-basin discharges were fitted to (management corrected) gauge observations by individual evapotranspiration corrections. Having calibrated the model globally beforehand, most sub-basin *ET* adjustment factors differed significantly from one. High and low values were spatially clustered, but no functional relationship to certain land use classes or soil types could be identified. An independent mapping of the spatial *ET* pattern by means of remote sensing could probaby explain these observations and help to identify probable error sources

5.1.2 *Hydrological modelling and remote sensing*

The idea of integrating remote sensing into hydrological modelling is relatively old (e. g. Klemeš 1983, 1988, Schultz 1987, 1988), and despite many systematic and practical problems (cf. Kite & Pietroniro 1996, Beven 1996, 2001) a lot of modellers continued working with remotely sensed data in recent years. As satellite data availability has much been increased within the last decade, current research is finally measuring up with many expectations of the 1980s (Nagler 2011). For example, an operational, multiple-source data assimilation system integrating remote sensing information is currently being put into service in Australia (van Dijk & Renzullo 2011, Glenn et al. 2011).

We use remotely sensed land surface temperatures to map the *ET* pattern in the Elbe River basin. Recent studies that also make use of thermal and optical sensors range from 'classical' rainfall-runoff modelling with remotely sensed pattern comparison (like our contribution) to integrated data assimilation systems. Examples of the former are Boegh et al. (2004) for 10 km² of agricultural landscape in Denmark or Vinukollu et al. (2012) with a global *ET* pattern comparison. A substantial contribution is also Schuurmans et al. (2011) who first compare and then assimilate the modelled and remotely sensed actual *ET* patterns of an area of 70 km² in the middle of The Netherlands; observed differences between the two data sources remain partly unexplained, however.

Despite the fact that remote sensing does not directly provide measurements that a hydrological model could be calibrated to, the idea of using the additional spatial information for improving distributed models seems to be an elegant way between the extremes of validation only and direct data assimilation.

Immerzeel & Droogers (2008), for example, applied the SWAT model to the Upper Bhima catchment in southern India (45 678 km²) and adjusted the monthly evapotranspiration for each sub-basin to the ET_a-estimates of the SEBAL-algorithm (Bastiaanssen et al. 1998a,b) applied to thermal imagery from the MODIS satellite. Singh et al. (2010) and Jhorar et al. (2011) used remotely sensed *ET* rates for improving agro-hydrological models on irrigated plots. And Githui et al. (2012) demonstrated a multi-objective and spatial calibration of a semi-distributed model using data from two runoff gauges and remotely sensed *ET* for 59 sub-basins of the 600 km² Barr Creek catchment in northern Victoria, Australia.

5.1.3 *Objectives of this study*

Originally, our intention was to present an alternative spatial calibration of our Elbe River basin model by means of remote sensing. But we will make a more fundamental assessment by comparing annual evapotranspiration patterns in space derived by:

1. the semi-distributed eco-hydrological model SWIM,
2. an approach based on remotely sensed land surface temperatures, and
3. the water balance method.

The objectives are to show the feasability of our remote sensing approach, to evaluate the correspondencies and differences between the results of all three methods, and to find reasonable explanations for systematic or individual sub-basin deviations. The potential of the remote sensing approach for alternative spatial calibration of the hydrological model may be fathomed as well.

5.1.4 *The Elbe River basin*

Before we present the three methods in detail, the research domain shall be introduced. The Elbe River basin, located in central Europe covers 148 268 km² (FGG Elbe 2005), thereof approximately one third within the Czech Republic and two thirds within Germany; less than 1 % belong to Austria and Poland. Figure 42 provides two maps of the basin.

The model domain was restricted to 134 890 km², including the drainage area of the main outlet gauge Neu Darchau (131 950 km²). The lower part of the stream is influenced by tide, which renders continuous discharge measurements impossible.

Approximately 50 % of the area are lowlands below 200 m a.m.s.l. This landscape dominates the north of the basin. Formed by the last glaciations, it is characterised by sandy plateaus with loam-covered riparian zones and wetlands in between. Due to the low slopes, sandy soils, and comparably low-intensity rainfall, the hydrological behaviour is governed by groundwater dynamics. Major land uses are grassland, forestry, and agriculture, often on poor soils.

The higher elevated regions can be divided up into hilly mountain forelands (32 %, 200–500 m a.m.s.l.) and mountaineous areas (18 %, above 500 m a.m.s.l.). The hilly mountain forelands are covered by loamy–silty substrates and loess areas of highest field capacities. These productive soils are mainly used for agriculture. The mountaineous areas have relatively poor soils, typically thin cambisols from weathered rock sediments. Their major land use are coniferous forests. The highest point of the basin is marked by the mountain Sněžka (Czech) or Śnieżka (Polish) on the border between the Czech Republic and Poland. It reaches an altitude of 1602 m a.m.s.l.

Climatically, the Elbe River basin is located at the transition of the maritime temperate zone towards continental climate. Precipitation shows a rather uniform intra-annual distribution. The long-term mean is 702 mm a^{-1}, and the average discharge at the river mouth of 861 m^3 s^{-1} equals 183 mm a^{-1}, which means an average evapotranspiration

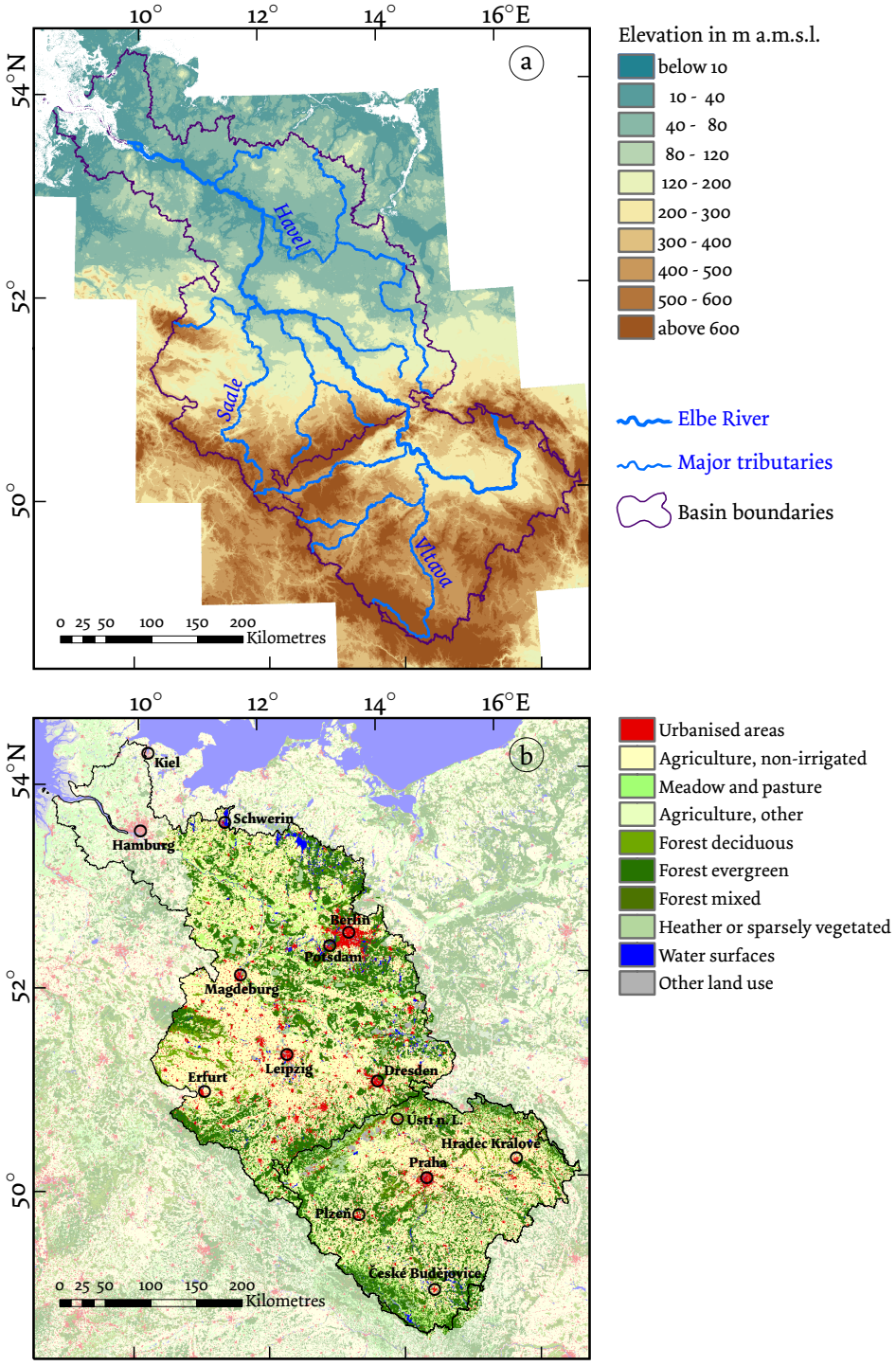

Figure 42: The Elbe basin in central Europe: (a) Elevations and major tributary streams. (b) Land use according to the CORINE 2000 classification; saturated tints indicate the model domain.

of 519 mm a^{-1} (FGG Elbe 2005, and own calculations). The spatial distribution of precipitation depends strongly on topography: Near Magdeburg, in the lee of the Harz Mountains, less than 500 mm a^{-1} are measured, while more than 1200 mm a^{-1} can be observed within the mountaineous regions. Evapotranspiration follows a distinct annual cycle. Negligible in winter, local *ET* rates reach up to 7 mm d^{-1} in summertime.

There are huge lignite open cast mining areas in the sub-basins of the rivers Spree, Schwarze Elster, and Weiße Elster. These are hydrologically important: a groundwater deficit of $13 \cdot 10^9$ m^3 had been created by draining (Grünewald 2001), and ongoing recultivation activities shall produce over 200 km^2 of new water surfaces. Besides direct effects on river discharge, the landscape alterations affect local hydrometeorology (Conradt et al. 2007, Chapter 4).

The spatial pattern of climatic inputs and a multitude of different landforms, soil characteristics, and land uses within the Elbe River basin make it an interesting large-scale domain for distributed hydrological modelling. Examples are the contributions by Krysanova et al. (1999), who observed unsatisfactory model performance in the lowlands (in particular the Havel River) where the runoff regime is dominated by river–groundwater interactions and the related transpiration fluxes in the riparian areas, or Krause & Bronstert (2007) who focused their investigation on these processes.

In contrast to the similar studies of Immerzeel & Droogers (2008) and Githui et al. (2012), records from 133 gauging stations within the Elbe area could be utilized for comparison. As the water balance method requires long-term observations, mean discharges of 1961–1990 were used where available. Some gauge data were restricted to shorter periods that fell into this time-span.[1] Comparisons with model results were always made for matching periods, this applies accordingly for the remote sensing estimations.

5.2 METHODS

5.2.1 *Evapotranspiration modelling*

5.2.1.1 *General model structure*

The semi-distributed eco-hydrological model SWIM (Krysanova et al. 1998, 2000) is a variant of the well-known SWAT (Arnold et al. 1993, 1998, Srinivasan et al. 1998, Gassman et al. 2007). Semi-distributed means that the model domain is not represented in gridded manner (fully distributed) but by landscape patches with uniform hydrological behaviour, the so-called hydrotopes. For this study, the model domain

1 A complete list of the calibration gauges with data sources is given in Appendix A. These data were not submitted for journal publication.

had initially been divided up into 2278 sub-basins. In the following, they shall be addressed as 'model sub-basins' to distinguish them from (gauged) sub-basins in general. 133 calibration sub-basins are gauged aggregations of these model sub-basins. The hydrotopes are sub-units of these model sub-basins, defined by an intersection of soil and land use maps so that each hydrotope is a unique combination of sub-basin, soil type and land use.

For each hydrotope, vegetation growth and water and nutrient fluxes between various storages are modelled. This comprises e. g. water seepage and capillary rise between soil layers, water and nutrient stress for plants, or evapotranspiration. Discharge components are accumulated and routed through the sub-basin structure by the Muskingum approach. The model works on a daily timestep.

Daily climate input was provided by measurements of 853 climate stations, 352 thereof fully instrumented, and 501 rain gauges. Input variables were precipitation, global radiation, air humidity, and maximum, minimum, and mean air temperature. These data were interpolated to the model sub-basins with inverse-distance weighting. Elevation dependencies were considered individually for each variable: When a linear regression on elevation yielded a coefficient of determination exceeded of at least 0·4, only the residuals were interpolated and the trend component added afterwards.

5.2.1.2 *The evapotranspiration calculus*

A modified Turc–Ivanov approach (Richter 1984, Wendling & Schellin 1986, DVWK 1996) which is applicable without wind speed data was used for calculating reference evapotranspiration. The original formula by Turc (1961) is replaced by another approach originally proposed by Ivanov (1954) when the daily average temperature T remains below 5°C:

$$ET_p = \begin{cases} 0{\cdot}0031 \cdot \Omega \cdot (R_n + 209{\cdot}4) \cdot \left(\frac{T}{T+15}\right) & \text{for} \quad T \geq 5 \\ 0{\cdot}000036 \cdot (T + 25)^2 \cdot (100 - rF) & \text{for} \quad T < 5 \end{cases} \tag{13}$$

This combined equation yields daily potential or reference evapotranspiration ET_p in mm from average temperature T in °C, net radiation R_n in J cm^{-2}, and relative humidity rF in per cent. The dimensionless factor Ω varies monthly between 0·7 for December and January and 1·25 for May.

According to ATV-DVWK (2002), the reference ET_p values from Equation 13 were modified by land use specific factors ranging between 0·9 for cropland and 1·3 for water surfaces.

Daily actual evapotranspiration ET_a is then calculated for each hydrotope as sum of soil evaporation ES and plant transpiration EP with an approach similar to that of Ritchie (1972).

Plant transpiration is calculated from the reference ET_p depending on the leaf area index LAI:

$$EP_o = \begin{cases} \frac{ET_p \cdot LAI}{3} & \text{for} \quad 0 \leq LAI \leq 3 \\ ET_p & \text{for} \quad LAI > 3 \end{cases} \tag{14}$$

This preliminary value EP_o is reduced to EP according to the plant actual plant water use which is calculated for each soil layer separately according to the approach of Williams & Hann (1978): A potential water use WUP_i for layer i is estimated with the equation

$$WUP_i = \frac{EP_o}{1 - \exp(RDP)} \cdot \left[1 - \exp\left(-\frac{RDP \cdot RZD_i}{RD}\right)\right] \tag{15}$$

where RDP refers to a 'rate depth parameter', RZD_i means 'root zone depth parameter of layer i', and RD is the fraction of the root zone that contains roots. The actual water use from that layer WU_i depends on the ratio of available soil water SW_i to the field capacity FC_i:

$$WU_i = \begin{cases} WUP_i \cdot \frac{SW_i}{0{\cdot}25 \cdot FC_i} & \text{for} \quad SW_i \leq 0{\cdot}25\, FC_i \\ WUP_i & \text{for} \quad SW_i > 0{\cdot}25\, FC_i \end{cases} \tag{16}$$

Soil evaporation is treated in similar steps; starting with potential soil evaporation which depends on LAI, the value is reduced according to the extent of dry periods and available water in the top 30 cm of the soil.

The amount of evapotranspirated water is subtracted from the soil layer storages and accordingly reduces percolation and subsurface and ground water runoff and, subsequently, the accumulated discharge.

5.2.2 *Estimating ET from land surface temperatures*

Evapotranspiration can not be measured directly from space, but several methods exist to estimate ET values by means of remote sensing. One common approach is based on surface temperature, which can be inferred from thermal radiation and is partly governed by energy partitioning into sensible and latent heat. Most studies following this approach aimed at estimating evapotranspiration more or less solely from remotely sensored data; their comparisons with ground measurements show correlations, but typically high noise levels (Moran et al. 1994, Kite & Droogers 2000, Garatuza-Payan et al. 2001, Jiang & Islam 2001, Jacobs et al. 2004, Patel et al. 2006, Wloczyk 2007, Hoedjes et al. 2008, Galleguillos et al. 2011).

Bastiaanssen et al. (1998a,b) invented the SEBAL-algorithm to account for many error sources by taking the coolest ('wet') and the warmest ('dry') pixel of a scan as calibration basis. This approach may well be the

most popular in counts of applications, derived variants and further developments, e. g. Gómez et al. (2005), Verstraeten et al. (2005), Koloskov et al. (2007), Stisen et al. (2008), Long & Singh (2010), Schuurmans et al. (2011).

Many problems of *ET* estimation from thermal radiances – which also contribute to the challenges of this study – can be explained from a closer look at the relationships between energy and water fluxes. The general energy balance for any surface spot on the Earth reads:

$$R_n + G + S = \lambda ET + H \tag{17}$$

On the left hand side, the energy inputs net radiation R_n, ground heat flux G and heat advection S are summed up. They equal the outgoing fluxes on the right hand side: latent heat by evapotranspiration λET and sensible heat H. Net radiation is principally the driving force for evapotranspiration. The other input terms, G and S, may be neglected for 24 h and *a fortiori* for annual integrations, but both net radiation and Bowen ratio (of sensible to latent heat) have to be determined.

5.2.2.1 *Determining net radiation*

Net radiation is the sum of all radiation components at the ground:

$$R_n = (1 - \alpha) \cdot R_{sg} + R_{la}\downarrow - R_{le}\uparrow \tag{18}$$

In detail, R_n consists of that part of the incoming short-wave global radiation R_{sg} which is not reflected at the surface (therefore α, the land cover dependent albedo), and the long-wave components: surface radiation R_{le} towards the sky (therefore negative) and atmospheric back-radiation R_{la}. While αR_{sg} and R_{le} may be quite directly measured by a remote sensor (only corrected for atmospheric extinction), assumptions or ground measurements have to be made for determining R_{la} and the total global radiation R_{sg}, or R_{la} and α respectively.

The relationship between thermal radiances and actual surface temperature provides additional room for errors, because the Stefan-Boltzmann law $R = \varepsilon \cdot \sigma \cdot T^4$ contains the emission coefficient ε which depends on the radiant material. T denotes the temperature in K and σ is the Stefan-Boltzmann constant of 5·67 W m^{-2} K^{-4}. Both R_{la} and R_{le} can be expressed in terms of specific ε and T values:

$$R_{la} = \varepsilon_a \cdot \sigma \cdot T_a^4 \tag{19}$$

$$R_{le} = \varepsilon_e \cdot \sigma \cdot T_e^4 \tag{20}$$

While ε_e varies only within a small range around 0·95 for natural surfaces (Albertz 1991), the assumption of a single temperature T_a for the atmosphere is a common simplification, and air temperatures can hardly be measured remotely. The SEBAL method mentioned above helps

to circumnavigate the latter problem. For this study, conventionally ground-measured temperature and radiation data are utilized.

Net radiation is routinely derived by SWIM from standard input data containing daily values of global radiation R_{sg}, air temperature T_a, and relative humidity rF. The formulæ in the applied SWIM version generally follow the recommendations of DVWK (1996). Equation 18 is fed with albedo depending on vegetation density and eventual snow coverage:

$$\alpha = \begin{cases} 0{\cdot}23\,(1-\nu) + 0{\cdot}15\,\nu & \text{for } \leq 5\,\text{mm water equivalent} \\ 0{\cdot}6 & \text{for thicker snow cover} \end{cases} \tag{21}$$

$$\nu = \exp[-5 \cdot 10^{-5} \cdot (d_v + 0{\cdot}1)] \tag{22}$$

with d_v being the biomass density in kg ha^{-1} dynamically calculated by the crop and vegetation growth routines. Furthermore, Equations 19 and 20 are merged to a net emittance with the effective emission coefficient ε' and a cloud cover factor ω:

$$R_{la} - R_{le} = \sigma \cdot \varepsilon' \cdot \omega \cdot T_a^4 \tag{23}$$

using the approximations of Brunt (1932) based on vapour pressure e

$$\varepsilon' = 0{\cdot}34 - 0{\cdot}044 \cdot \sqrt{e} \tag{24}$$

which, despite its age, seems to perform better than more recently developed alternatives (cf. Bilbao & Miguel 2007, Choi et al. 2008), and Wright & Jensen (1972) with coefficients by Doorenbos & Pruitt (1977)

$$\omega = 0{\cdot}1 + 0{\cdot}9 \cdot \frac{R_s g}{R_{max}} \tag{25}$$

The vapour pressure e is calculated from T_a and rF according to DVWK (1996), and R_{max} is the theoretically possible clear-sky radiation on the given day at the mean latitude of the model domain.

5.2.2.2 *Determining the Bowen ratio*

Equation 17 shifted about neglecting G and S and divided by $\lambda = \varrho_w \cdot r_v$, which is the energy needed to evaporate one volume unit of water (water density ϱ_w times steam heat r_v), delivers ET, when both R_n and H are known:

$$ET = \frac{1}{\lambda}\,(R_n - H) \tag{26}$$

The calculation of net radiation has been discussed above. The question remains, how much of R_n is transformed into sensible heat and what remains for evapotranspiration, i. e., the Bowen ratio (Bowen 1926a,b, Lewis 1995) has to be determined.

The sensible heat flux H is driven by the vertical temperature gradient $\frac{\partial T}{\partial z}$. In practice, this gradient is represented by the temperature difference $\Delta T = T_s - T_a$ between the soil or plant canopy surface temperature T_s and the 2 m air temperature T_a. The sensible heat flux can then be formulated either via an exchange coefficient C or an aerodynamic resistance for heat r_{ah}:

$$H = \Delta T \cdot c_p C = \Delta T \cdot \frac{\varrho_a c_p}{r_{ah}} \tag{27}$$

In this equation, c_p means the sprecific heat content of the air and ϱ_a its density. Aerodynamic resistance (viz. the exchange coefficient) depends on atmospheric stability, wind velocity u (at a reference height z) and geometric surface characterisics. The latter can be parameterised by zero plane displacement height d and roughness lengths for sensible heat z_{oh} and momentum z_{om}. According to the Monin-Obukhov theory of surface layer similarity (Monin & Obukhov 1954), r_{ah} is then given by

$$r_{ah} = \frac{\left[\ln\left(\frac{z-d}{z_{oh}}\right) - \psi_{sh}\right] \cdot \left[\ln\left(\frac{z-d}{z_{om}}\right) - \psi_{sm}\right]}{k^2 \cdot u(z)} \tag{28}$$

with $k \approx 0{\cdot}4$ being von Kármán's constant, and ψ_{sh} and ψ_{sm} correction terms for the actual stability conditions of the atmosphere (Brutsaert 1982).

Despite the many non-measurable or unknown variables of Equation 28, this is no dead end: the concept is not to parameterize a model by remotely sensed temperatures, but to utilize the data for *additional spatial* calibration. Thus, a global model adjustment to meet the water balance of the entire basin is a neccessary prerequisite.

Using Equations 26 and 27, one can express the basin average of actual evapotranspiration $\overline{ET_a}$ by integrating over the basin area A, regarding R_n, ΔT, and r_{ah} as functions of the co-ordinates x and y:

$$\overline{ET_a} = \frac{1}{\lambda \cdot A}\left(\iint_A R_n(x,y)\,\mathrm{d}A - \varrho_a c_p \iint_A \frac{\Delta T(x,y)}{r_{ah}(x,y)}\,\mathrm{d}A\right) \tag{29}$$

Assuming a well calibrated model, the modelled evapotranspiration height, denoted by ET_{SWIM}, equals the real spatial mean of ET_a, and integrating the spatially varying fluxes could practically be done by summing up the contributions of the n model hydrotopes with areas a_i:

$$\overline{ET_a} = ET_{\mathrm{SWIM}} = \frac{1}{\lambda \cdot A}\left(\sum_{i=1}^{n} R_{n,i} a_i - \varrho_a c_p \sum_{i=1}^{n} \frac{\Delta T_i a_i}{r_{ah,i}}\right) \tag{30}$$

Unfortunately, the aerodynamic resistances $r_{ah,i}$, of which each hydrotope has its own value, are still unknown and change with atmospheric conditions.

The simplest solution would be assuming one common resistance for the entire basin. But from Equation 28, we know the factors which govern r_{ah}: While integrating many observations may approximate an atmospheric mean state which is unlikely to fluctuate on distances below the meteorological meso-γ-scale (i. e. below 200 km), the time-invariant land use pattern will definitely reverberate in the sensible heat flux via its surface structure. Therefore, the general approach taken here is to assume two different effective resistance values: $r_{ah,f}$ for the forested part of the basin and $r_{ah,n}$ for the rest of the domain, because forests differ most distinctively in their effective roughness and displacement heights from the remaining landscape. Elevation effects, including the strongly correlated wind effects, are neglected, and wind speed is not considered by SWIM either. But eventual elevation dependencies can and will be analysed from the results.

A first variant is double usage of Equation 30: for the m forested and the remaining $n - m$ non-forested hydrotopes, relying on the modelled averages of the respective land cover evapotranspiration $ET_{s,f} + ET_{s,n} = ET_{SWIM}$. The resistance values can then be directly calculated as follows:

$$r_{ah,f} = \frac{\varrho_a c_p \sum_{i=1}^{m} \Delta T_i a_i}{\sum_{i=1}^{m} R_{n,i} a_i - \lambda E T_{s,f} \cdot A_f} \tag{31}$$

$$r_{ah,n} = \frac{\varrho_a c_p \sum_{i=m+1}^{n} \Delta T_i a_i}{\sum_{i=m+1}^{n} R_{n,i} a_i - \lambda E T_{s,n} \cdot A_n} \tag{32}$$

A second variant does not presuppose a bias-free evapotranspiration modelling regarding land use, but a number $k > 2$ of gauged sub-basins with different forest shares within the model domain. In this case, the long-term water balance of each sub-basin can be calculated from the measurements, and $r_{ah,f}$ and $r_{ah,n}$ are to be estimated by minimising the error terms ε in the over-determined equation system

$$\begin{aligned}
ET_{a,s1} &= \frac{1}{\lambda \cdot A_{s1}} \left[\sum_{i=j1}^{m1} R_{n,i} a_i - \varrho_a c_p \left(\sum_{i=j1}^{m1} \frac{\delta_f \cdot \Delta T_i a_i}{r_{ah,f}} + \sum_{i=j1}^{m1} \frac{\delta_n \cdot \Delta T_i a_i}{r_{ah,n}} \right) \right] + \varepsilon_1 \\
ET_{a,s2} &= \frac{1}{\lambda \cdot A_{s2}} \left[\sum_{i=j2}^{m2} R_{n,i} a_i - \varrho_a c_p \left(\sum_{i=j2}^{m2} \frac{\delta_f \cdot \Delta T_i a_i}{r_{ah,f}} + \sum_{i=j2}^{m2} \frac{\delta_n \cdot \Delta T_i a_i}{r_{ah,n}} \right) \right] + \varepsilon_2 \\
\vdots &= \qquad\qquad \vdots \qquad\qquad + \vdots \\
ET_{a,sk} &= \frac{1}{\lambda \cdot A_{sk}} \left[\sum_{i=jk}^{mk} R_{n,i} a_i - \varrho_a c_p \left(\sum_{i=jk}^{mk} \frac{\delta_f \cdot \Delta T_i a_i}{r_{ah,f}} + \sum_{i=jk}^{mk} \frac{\delta_n \cdot \Delta T_i a_i}{r_{ah,n}} \right) \right] + \varepsilon_k
\end{aligned} \tag{33}$$

with

$$\delta_f = \begin{cases} 1 & \text{for forested hydrotopes} \\ 0 & \text{for other land use} \end{cases} \tag{34}$$

$$\delta_n = 1 - \delta_f \tag{35}$$

The indices si with $i \in \{1, 2, \cdots, k\}$ refer to the k sub-basins, and the respective $\{ji, ji+1, ji+2, \cdots, mi\}$ indicate the hydrotope numbers within these sub-basins.

5.2.2.3 *From snapshots to annual values*

Hitherto, nothing has been said about the time frame on which Equations 30ff should be applied. Principally, a single day or several years make no difference, provided that *effective* temperature gradients for the entire period can be provided. Effective means that the difference between satellite-derived surface temperature and ground-measured air temperature must always be extrapolated from the snapshot time(s) of the actual measurements to a period average.

Assuming a linear relationship between simultaneously measured temperature gradients on different hydrotopes and their respective evapotranspiration rates, it is possible to calculate their individual evapotranspiration heights for any longer period provided the total ET is known, and relations between the hydrotopes' aerodynamic resistances remain invariant. This works with averages of the ΔT observations for each hydrotope, denoted by overline; the index k refers to the selected hydrotope:

$$ET_{a,k} = ET_{tot} \cdot \frac{A\left(R_{n,k} - \overline{\Delta T_k}\frac{\varrho_a c_p}{r_{ah,k}}\right)}{\sum_{i=1}^{n} a_i\left(R_{n,i} - \overline{\Delta T_i}\frac{\varrho_a c_p}{r_{ah,i}}\right)} \tag{36}$$

It makes hardly any difference whether the measurements were taken at noon or in late afternoon, as long as R_n was positive and dominant compared to G, but note that the resistances r_{ah} have to be fitted accordingly.

5.2.3 *The water balance method*

The classical water balance equation reads:

$$P = ET + Q + \Delta S \tag{37}$$

Evapotranspiration ET should theoretically equal precipitation P minus discharge Q for time scales of several years, because ΔS, the change in water storage of the catchment, gets neglectable compared to the other variables within such a time-span.

Practically, this approach has to grapple with difficulties in measuring catchment precipitation and uncertainties about catchment boundaries; the latter includes unaccounted ground water exchanges with neighbouring areas. The measured discharge may even be influenced by anthropogenic management. But due to lack of better alternatives, the water balance approach is commonly accepted as reference assessment of long-term mean evapotranspiration for river basins.

5.3 RESULTS

The eco-hydrological model SWIM, only globally calibrated on the daily runoff values of the 1990s at the outlet gauge Neu Darchau, was run for the three years 2001–2003. Using the simulated *ET* averages from forested and non-forested hydrotopes, 944 remotely sensed land surface temperature (LST) maps from this period were evaluated. The area-averaged general results of this calculation are summarised in Table 7.

5.3.1 *Application of the remote sensing method*

The LST maps derived from NOAA AVHRR thermal imagery were readily provided by the German DLR Applied Remote Sensing Cluster and could be downloaded via its EOWEB portal (http://www.eoweb.de). These maps cover whole Europe at a resolution of approximately 1·1 km in the map centre. There are several AVHRR products made available this way: two LST maps for each day from daylight and nighttime overpasses, a daily vegetation index (NDVI) map, and composite products for weeks and months. This study utilizes all 944 available daytime LST maps of the years 2001–2003.

Detailed information on these data is given by Tungalagsaikhan & Guenther (2007), including cloud screening procedures and the algorithms applied for computing the LST values from the thermal radiances. The latter had originally been established by Becker & Li (1990) and van de Griend & Owe (1993), and they were proven to be superior to other methods for this part of the world.

The European LST maps were reprojected onto the hydrotope map of the SWIM model, and mean surface temperatures could be calculated for each hydrotope when completely free from cloud cover. Hence, a first problem arises: how to deal with spatio-temporally varying cloud coverage?

Figure 43 demonstrates that the scanning times of the LST maps vary heavily due to satellite orbit characteristics and an intermediate change of the platform. Regarding the ground-measured air temperatures, only three measurements per day were available from the climate stations: minimum, maximum and average temperature. The maximum values, interpolated to sub-basin resolution, had to serve as best estimate for T_a at satellite overpass time.

Here, average temperature gradients had to be determined for the three calender years 2001–2003. One possible approach could be averaging only the seven days having LST maps with less than one per cent cloud cover. But 732 out of the 944 maps show surface temperatures for more than one per cent of the basin – and their information should not be discarded. The solution applied here is to produce a composite map of temperature gradients by averaging all available daily ΔT values

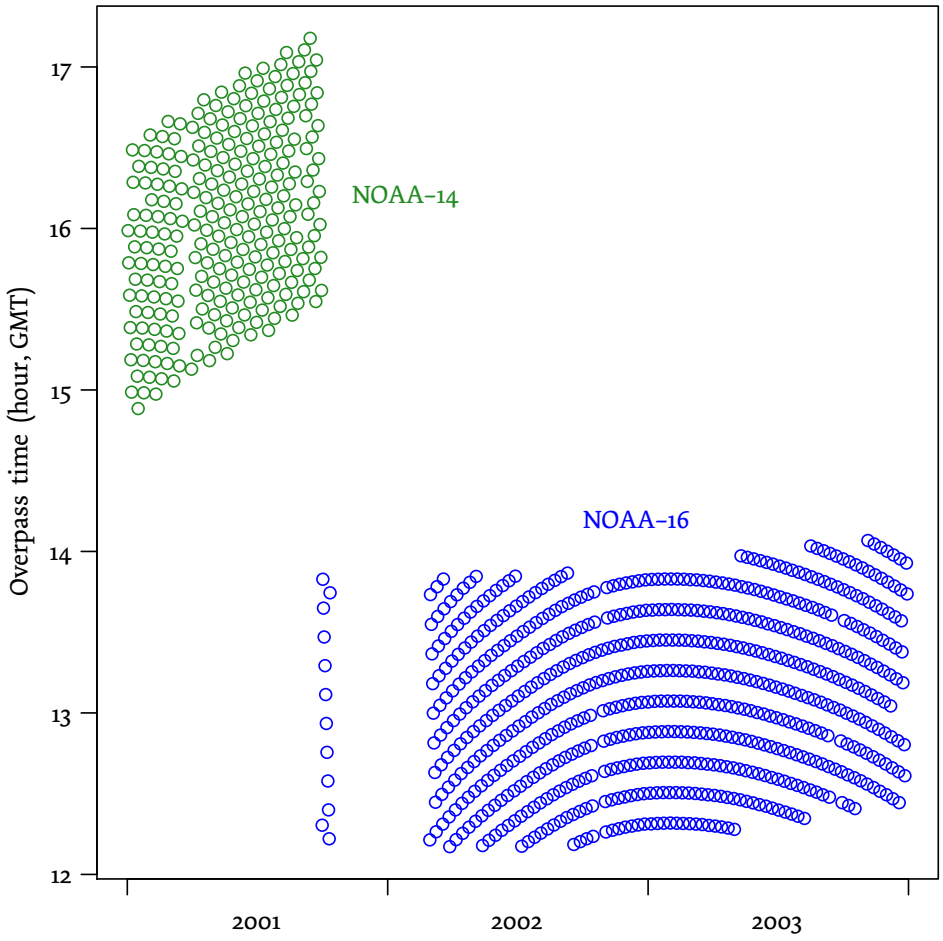

Figure 43: Overpass times of the NOAA AVHRR platforms utilized for the daily LST maps at the centre of the Elbe River basin. Local solar time is about UTC + 50 min. The switch from NOAA-14 to NOAA-16 clearly shifted the bandwidth of scan times from late afternoon towards noon. Calculated from satellite equator crossing data available via URL http://www.noaasis.noaa.gov/NOAASIS/ml/navigation.html (Last accessed in May 2012).

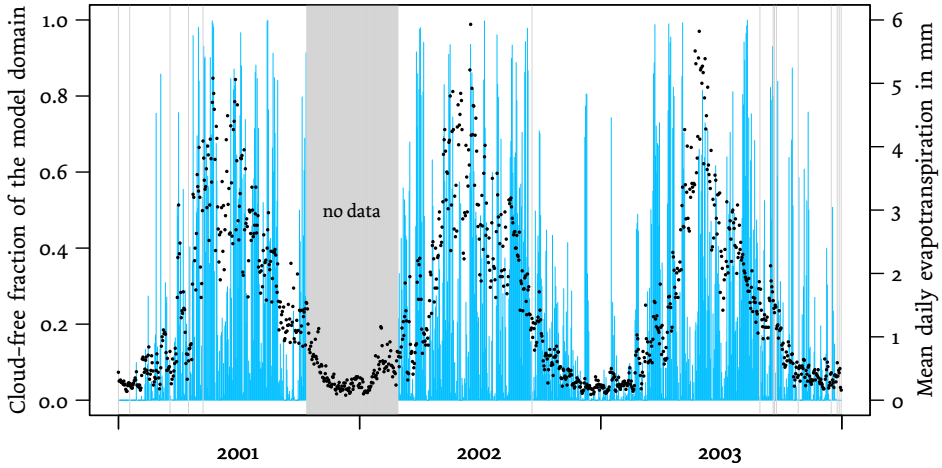

Figure 44: Daily blue-sky fractions (lightblue, left hand y-axis) and average evapotranspiration rates (black dots, right hand y-axis) of the modelled part of the Elbe River basin. Cloud coverage was calculated from the available LST maps (grey colour indicates data gaps), and ET_a values were obtained from the globally pre-calibrated SWIM model.

for each hydrotope and correcting them for cloud cover frequencies as described below.

Figure 44 shows both the blue-sky fractions of the satellite maps and the simulated evapotranspiration for the model domain of SWIM. Luckily, there is a correspondence: especially in wintertime, when the remote sensing information suffers from permanent cloud and snow coverage, or the longer data gap occured, there is only small evapotranspiration. Therefore, no time-dependent weighting scheme to fit LST (and hence ΔT) observation frequencies to evapotranspiration intensities had been applied, and snow cover effects could be neglected.

On the other hand, the spatial pattern of cloudiness shown in Figure 45 had to be considered. Radiation and accordingly heat gradients and evapotranspiration rates are much lower under cloud cover compared to blue sky conditions.

The cloud screening procedure applied by DLR prohibits LST calculations as soon as the respective pixel is *cloud contaminated* (Tungalagsaikhan & Guenther 2007), i. e., is not totally cloud-free. White pixels include all conditions from thin cirrus with hardly dimmed radiation to dense stratus. A 'blue-sky gradient' ΓT was calculated for each hydrotope observation without any white pixels (i. e. for the shares shown in Fig. 45a). The effective temperature gradient ΔT could then be estimated with the average blue-sky fraction of the hydrotope β, shown in Fig. 45b, assuming a mean attenuation factor of $\eta = 0{\cdot}33$ of the cloud layer in white pixels:

$$\Delta T = \beta \cdot \Gamma T + \eta(1 - \beta) \cdot \Gamma T \tag{38}$$

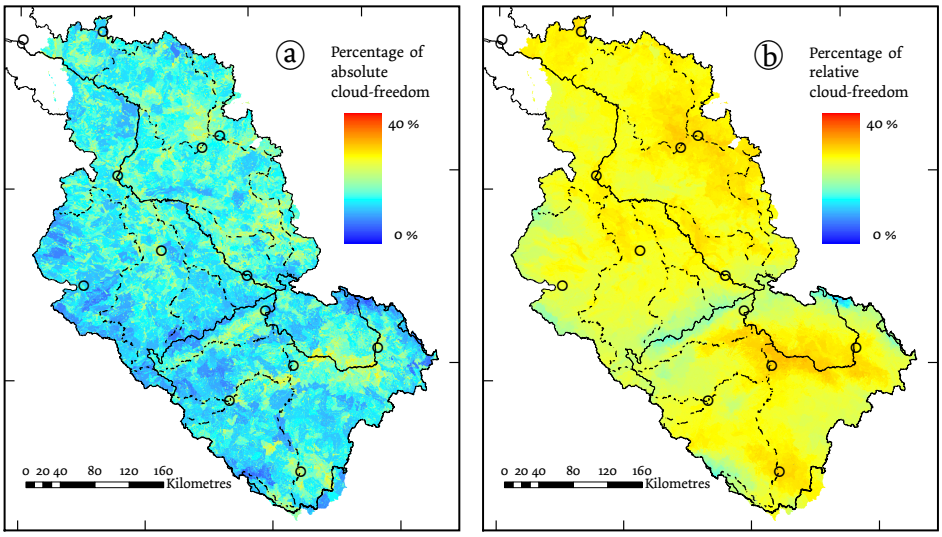

Figure 45: Percentages of cloud-freedom in hydrotopes. (a) Absolute cloud-freedom: hydrotopes are coloured according to the share of scans in which they were entirely cloud-free, i. e., none of their raster cells were cloud-contaminated. (b) Relative cloud-freedom: mean fraction of cloud-free raster cells within the hydrotope, average of all scans. A legend to the orientation features is displayed in Figure 46.

Although the value of η plays an important rôle for the range of these gradients, the resulting *ET* heights are hardly sensitive to it; the relative pattern remains quite stable for different choices of η, and the total evapotranspiration sum is kept to the level obtained from the hydrological model by an appropriate adjustment of the aerodynamic resistances r_{ah}.

The resulting map of average temperature gradients is shown in Figure 46. Mountainous regions, wetlands, or regions with many lakes (near the catchment boundary in the north) are clearly distinguishable by values close to zero. The most extreme gradients were determined for lowland areas in the north of the Czech Republic. This is very probably an artifact due to the sparseness of climate station data in that region.

In 2001 the German part of the Elbe basin experienced an average year regarding radiation and precipiation, 2002 was warm and relatively wet (an extreme flood occurred in August), and in 2003 the vegetation period was exceptionally dry, sunny, and hot (Müller-Westermeier et al. 2002, Müller-Westermeier & Rieke 2003, 2004). This sequence can be confirmed by the *ET* simulations and average temperature gradients; cf. Table 7. The variations in the resistance values can be explained by respective subsequent increases in the numerators of Equations 31 and 32 combined with an increase in the denominators (more R_n, less *ET*) between 2002 and 2003. The resistance values are also sensitive to the adjustment of η: with η = 0·25 instead of 0·33, the time-averaged $r_{ah,f}$ decreases from 99·2 to 87·3 s m^{-1} and $r_{ah,n}$ from 103·6 to 85·4 s m^{-1}.

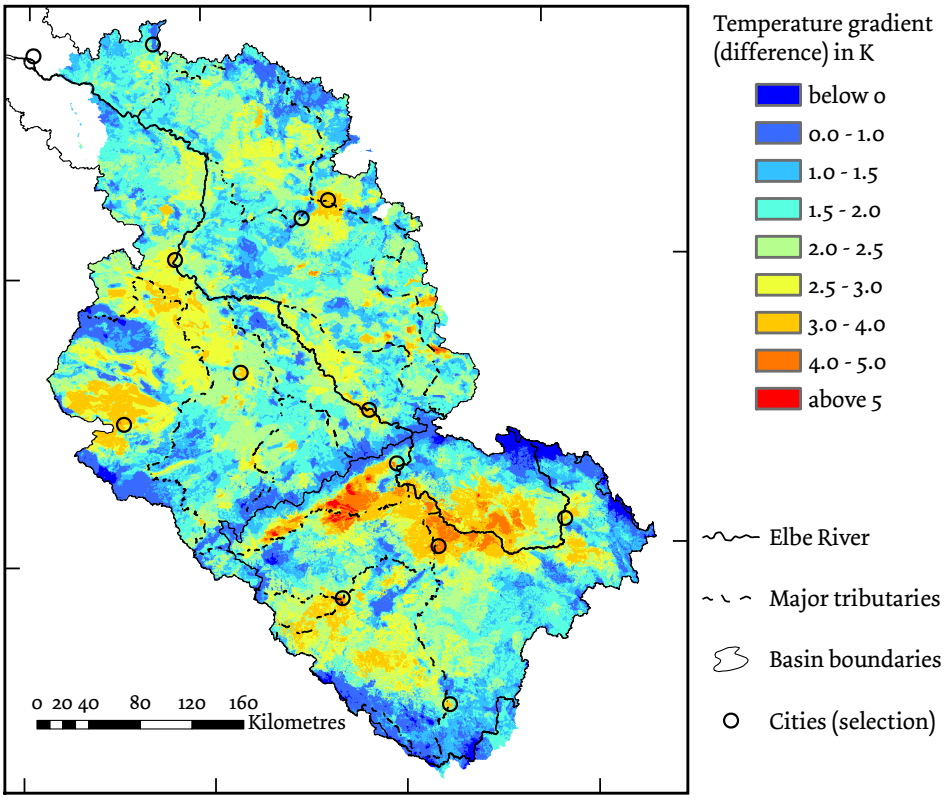

Figure 46: Average temperature gradients: Difference in K between surface and 2 m air temperatures. The originally observed differences between remotely sensed and ground measured temperature data have been corrected for cloud cover frequencies by Equation 38.

Table 7: General results of the evapotranspiration calculation. The total area (134 890 km²) is the modelled part of the Elbe River basin as shown in Figure 47.

		Forested				Non-Forested			
A	km²	42 590				92 300			
		2001	2002	2003	All*	2001	2002	2003	All*
ET	mm a^{-1}	664	693	557	638	503	541	490	511
R_n	MJ m^{-2} a^{-1}	1984	2001	2307	2098	2012	2014	2319	2115
ΔT	K	0·63	1·30	1·86	1·32	1·08	2·13	3·13	2·22
r_{ah}	s m^{-1}	71·0	171·5	79·2	99·2	55·5	124·5	112·5	103·6

*'All' refers to the results for the full data set of the three years 2001–2003.

But in any case, the aerodynamic resistances range in the order of magnitude for vegetated surfaces in temperate climate found by many other authors (e. g. Thom & Oliver 1977, Lindroth 1993, Ramakrishna & Running 1989, Liu et al. 2007).

5.3.2 *Comparison of the three methods' results*[2]

Figure 47 presents the patterns of the three *ET* estimations for the 133 gauged sub-basins in three respective maps, and Figure 48 shows the sub-basin estimations in three scatter plots for the possible pair combinations of the three methods. The first main message is that the variances of both ground corrected and remotely sensed *ET* clearly exceed those of the simulation results from the only globally calibrated hydrological model.

The second insight delivered from Figure 48 is that there is a weak correlation between the model and the remote sensing approach, an even weaker agreement between model and ground based validation, and, finally, practically no relationship between remote sensing and the water balance approach.

In order to shed light into the discrepancy between water balance and remote sensing estimations, we grouped those sub-basins which deviate most from being correlated in the lower right panel of Figure 48 into clusters and highlighted them in a map. The clustering and its geospatial correspondence are shown in Figure 49.

It turns out that all 'deviating' sub-basins are located in the Czech part of the Elbe basin. The cluster of sub-basins marked by red colour which combine low remotely sensed *ET* with medium to high *ET* found by the water balance method concentrate in the lowlands of the northwestern part of the Czech republic, while the opposite combination coloured in blue with high remotely sensed *ET* values was found at sub-basins distributed around the mountainous edge of the Czech area.

Subsetting the data to the 72 German sub-basins clearly increases all correlations as presented in Figure 50. The upper left panel of Figure 50 shows a relatively good agreement between *ET* estimates of the remotely sensed approach and the globally calibrated model simulation. Outliers are dominated by smaller sub-basins which could be expected (cf. the Introduction).

Our second, independent 'ground truth' given by the water balance estimations of evapotranspiration for the sub-basins shows at least little correlation with SWIM and, at least in the German subset, also with the remotely sensed *ET* (compare the lower panels in Figs. 48 and 50)

2 As the original intention of this study was to demonstrate the use of the remote sensing and water balance approaches for spatial calibration of the hydrological model, respective sub-basin *ET* adjustment factors had been calculated and their notional dependencies had been investigated by correlation analyses. These assessments are documented in Appendix B.

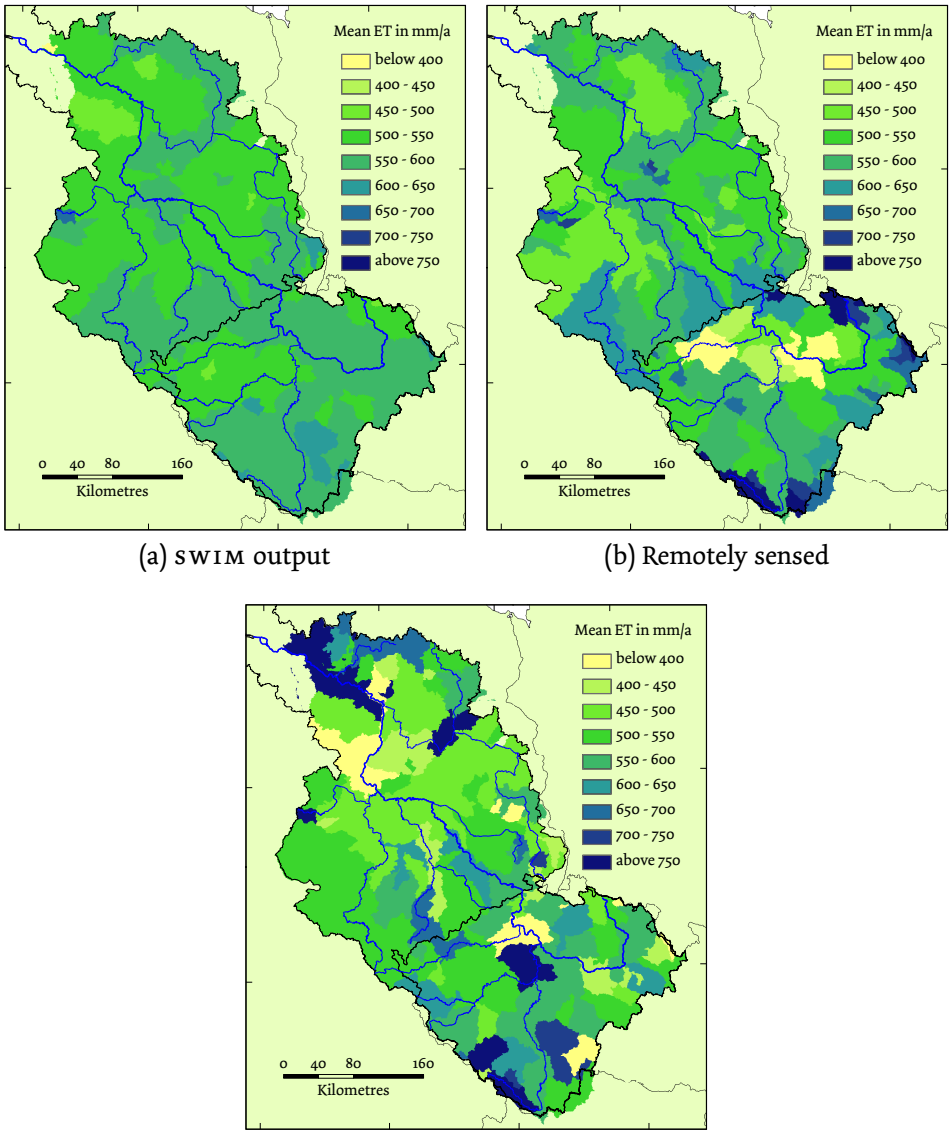

(a) SWIM output (b) Remotely sensed

(c) Result of the water balance method

Figure 47: Three different evapotranspiration patterns from 133 sub-basins in the Elbe River basin: average values for the years 2001–2003.

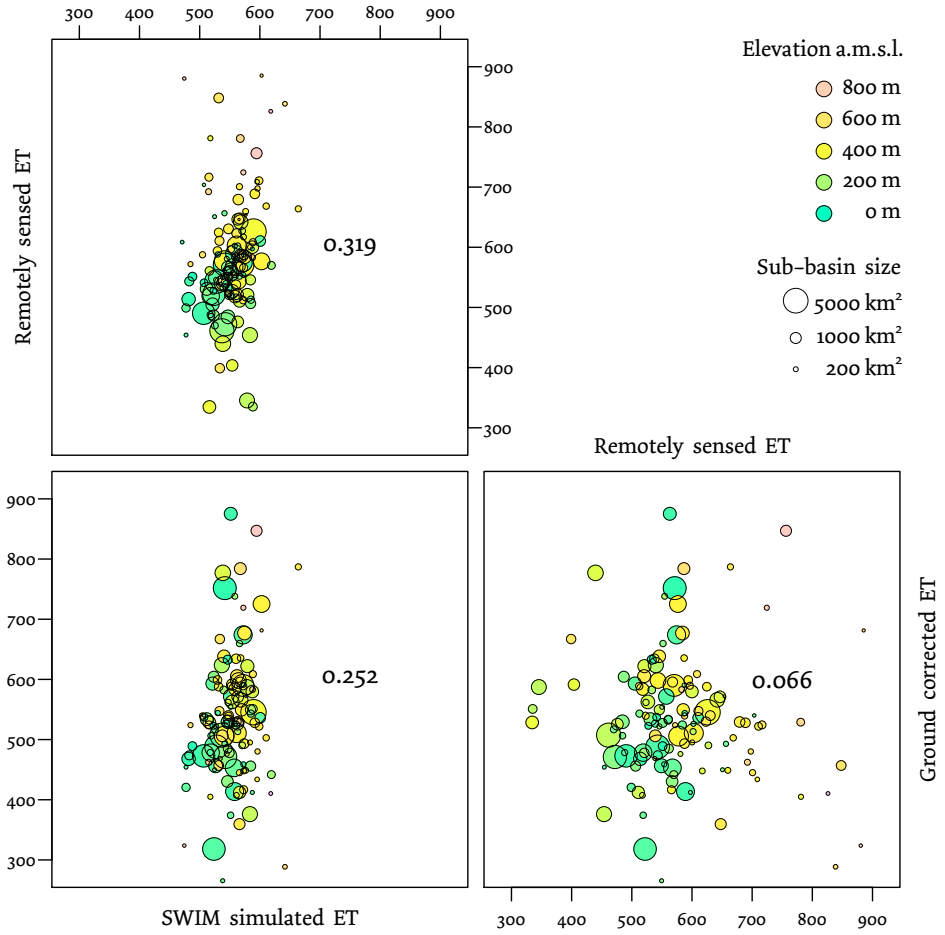

Figure 48: Correlations between remotely sensed, SWIM simulated, and ground corrected evapotranspiration in mm a^{-1}

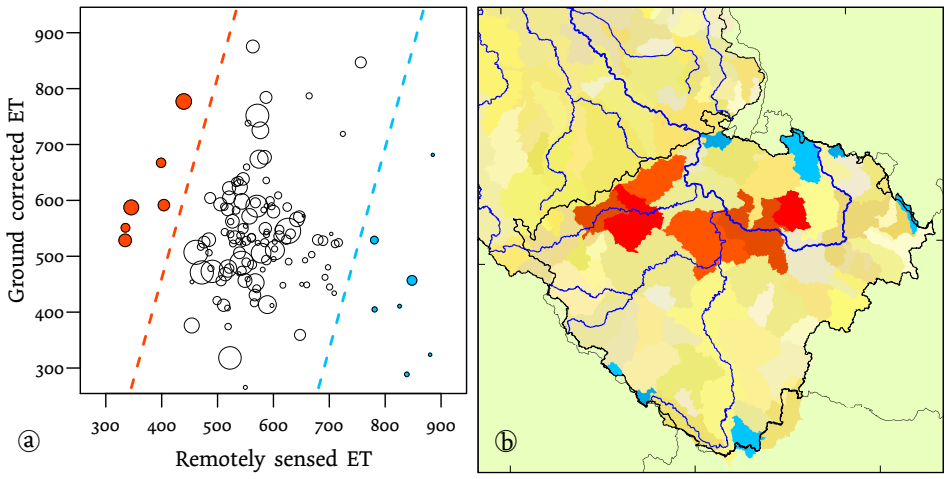

Figure 49: Outlier clusters of sub-basins with strongly deviating remotely sensed and ground corrected *ET*. a) Graphical separation of the clusters from the correlation plot, cf. the lower-right panel of Figure 48. b) Map cut-out with the respective sub-basins highlighted by their cluster colours.

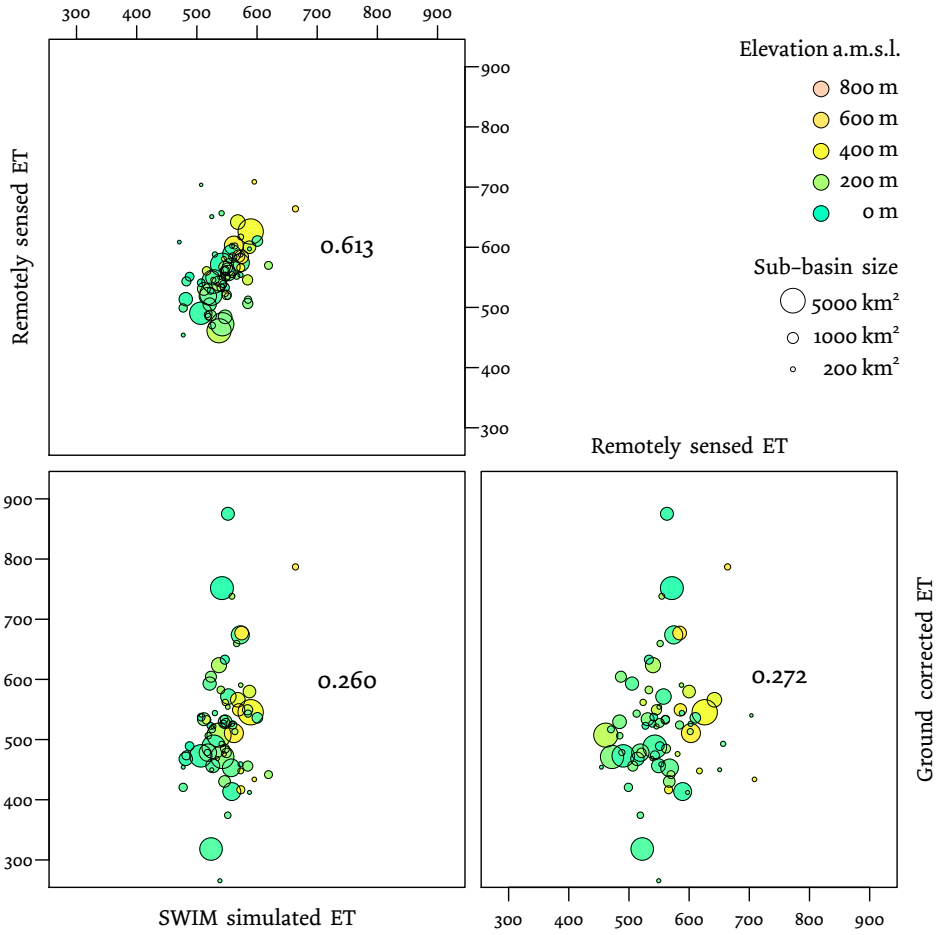

Figure 50: Correlations between remotely sensed, SWIM simulated, and ground corrected evapotranspiration in mm a^{-1} for the 72 sub-basins in the German part of the Elbe River basin

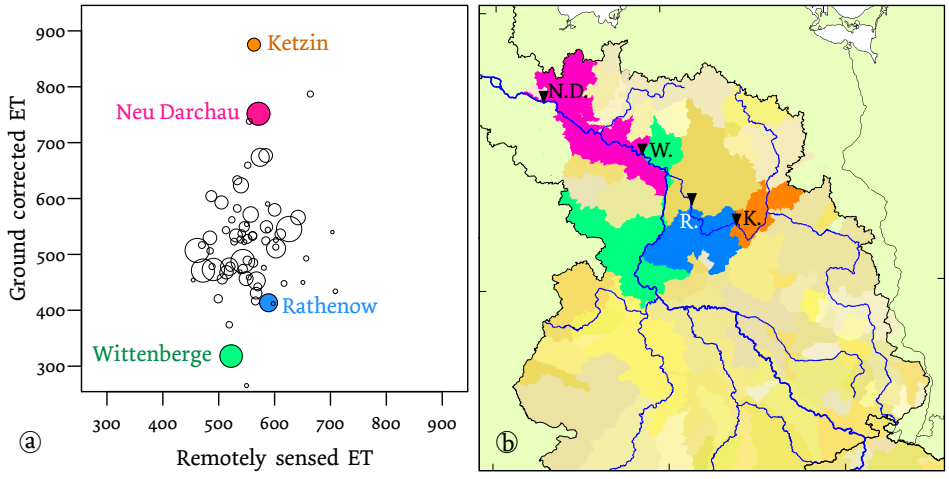

Figure 51: Extreme differences between ground corrected *ET* from neighbouring sub-basins. The sub-basin areas in the dotty plot (a) are named according to their outlet gauges drawn in the map cut-out (b) as black triangles.

While restricting the data basis to the German sub-basins decreased the variance of the remotely sensed *ET* heights, the water balance based estimations still cover a comparably wide range. Again, systematical errors can be identified by mapping the most prominent outliers in the lower right panel of Figure 50, this is done in Figure 51.

It appears that two pairs of subsequent gauge areas at the lower Havel River (Ketzin and Rathenow) and at the Elbe River downstream the Havel (Wittenberge and Neu Darchau) have both been assigned combinations of very low and high *ET* estimates from the water balance method.

5.4 DISCUSSION

5.4.1 *Remote sensing estimations*

The explanation for the heavy noise in the remote sensing estimations for Czech sub-basins is the low density of ground measurements there: The geospatial pattern of the outlier sub-basins in Figure 49 matches that of the most extreme temperature gradients in Figure 46. Taking into account that the spatial density of climate stations of which data were provided was much lower in the Czech part than in the rest of the basin (only 46 out of the 853 stations were located there), it is highly probable that the 2 m air temperature and hence the resulting temperature gradient were systematically biased preventing the remote sensing approach from working properly in this region.

The remaining noise of the remote sensing results in Figure 50 is in the range observed by most recent studies evaluating remotely sensed *ET* by some kind of 'ground truth', be it reference *ET* calculated from lysimeter measurements (Wloczyk 2007, Sánchez et al. 2008), eddy flux or other micrometeorological tower measurements (Verstraeten et al. 2005, Patel et al. 2006, McCabe & Wood 2006, Brunsell et al. 2008, de C. Teixeira et al. 2009), or hydrological model simulations (Boegh et al. 2004, Gao & Long 2008, Galleguillos et al. 2011).

An exception is the study by Immerzeel & Droogers (2008), who calibrated a SWAT application by the remotely sensed evapotranspiration pattern: Their scatter-plot of reference *ET* for 115 model sub-basins simulated without spatial calibration against respective SEBAL results does not show a visible correlation; the numerical value is not given.

5.4.2 *Water balance estimations*

The reason for the outliers in the water balance estimation for subsequent gauges (cf. Fig. 51) are slightly biased discharge measurements causing sweeping oscillating errors.

For example, the inflow from upstream into the area assigned to gauge Wittenberge has a long-term mean of about 695 $m^3 s^{-1}$. Downstream at gauge Neu Darchau the respective value amounts to 760 $m^3 s^{-1}$. At gauge

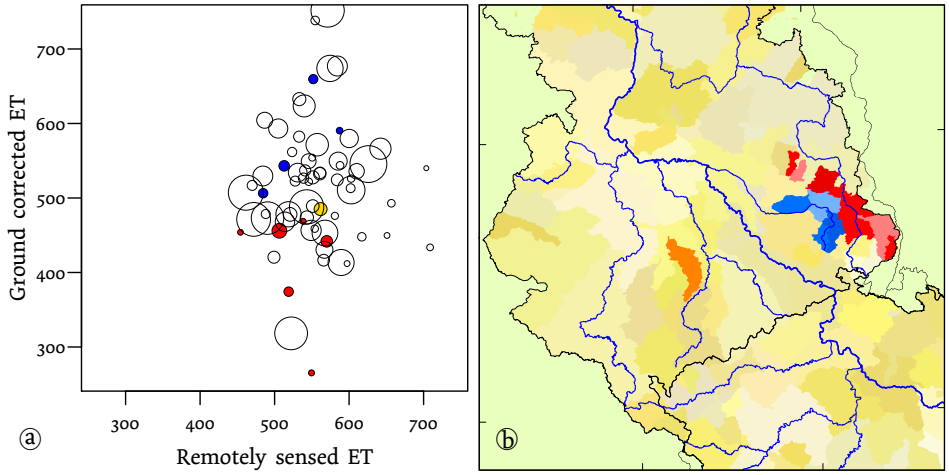

Figure 52: Impacts of open cast mining on ground based *ET* corrections. Red: Sub-basins along the Spree River with maximum ground water pumping in the 1980s. Blue: Schwarze Elster River sub-basins with less pronounced peak before 1970. Yellow/Orange: Pleiße River sub-basin covering an open cast mining area near Leipzig.

Wittenberge, right between these rather equally sized contribution areas, one would expect a mean runoff of about 727·5 $m^3 s^{-1}$. But 737 $m^3 s^{-1}$ is taken as 'correct' measurement there. This is just a deviation of 1·3 % and clearly within gauging uncertainty (cf. Sauer & Meyer 1992, Maniak 2005). But this relatively little shift would mean a discharge of 42 $m^3 s^{-1}$ from the area above Wittenberge and only 23 $m^3 s^{-1}$ from the area below. The climate for both patches does not differ very much, the latter receives even a little more precipitation. Consequently, a rather low evapotranspiration rate is calculated for the area above Wittenberge and a much higher one for the Neu Darchau area. Finally, this leads to the picture shown in Figure 51.

The case for Ketzin and Rathenow is very much the same. In general, measurement errors of subsequent gauges on the same river renders reasonable water balancing impossible when the total runoff is relatively large compared to the discharge from the intermediate area.

Finally, the impacts of another probable error source shall be assessed: the massive anthropogenic ground water extraction from open-cast lignite mining areas that peaked in the 1980s when more than 30 $m^3 s^{-1}$ excess flow were lead into the Spree River Grünewald (2001). In Figure 52, the sub-basins whose discharges were presumably elevated by pumped ground water are coloured according to their river catchment affiliation.

One would expect too low *ET* estimations for open-cast mining affected sub-basins, which would (wrongly) explain their elevated discharge. Figure 52 shows that this holds only true for some sub-basins contributing to the Spree River, drawn in red. For the Pleiße sub-basin (yellow/orange) the plot reveals no visible effect, and the blue-coloured

sub-basins of the Schwarze Elster River catchment seem to be drifted towards *ET* over-estimation.

The Schwarze Elster sub-basins demonstrate the imponderabilities in accounting for open cast mining effects on discharge. While the pumping rates have been thoroughly measured by water meters, natural ground water contributions to streamflow diminished or ceased to a largely unknown extent. Because the ground water pumping into the Schwarze Elster had seen its maximum rates already in the 1960s before most sub-basin gauges went into operation, reduced discharges due to the already generated groundwater deficit are likely to have dominated the calibration periods.

5.4.3 *Eco-hydrological model simulations*

The output of the SWIM simulations are of course also subject to errors. The model water balances of two groups of hydrotopes – forested and non-forested – were taken for adjusting the remote sensing based *ET* values which might have added to the overall noise of the results. It has to be pointed out that the internally computed *LAI* values were left unmodified, although some standard parameterisations for land cover units are questionable for parts of the model domain; e.g. the Ore Mountains. There had been a severe forest dieback in the crest region in the 1980s, but an ideal forest had been modelled.

The breakdown of the socialist economies in Eastern Europe around 1990 had global impacts on evapotranspiration via the phenomena of global dimming and brightening (Wild 2012). This is relevant, because the eco-hydrological model was calibrated on data from before the change (Conradt et al. 2012b, Chapter 2) when global radiation and *ET* were generally lower while the satellite scans were taken under brightening conditions. It remains unclear, to what extent different land uses were affected differently, but individually changing Bowen-ratios might also have contributed to the observed uncertainties.

Finally, it has to be noted that the modelling of lateral water exchanges between sub-basins was limited to stream runoff. Groundwater exchanges affecting plant water availability and thus *ET* were not considered.

5.5 CONCLUSIONS

The comparison of three independent estimations for the spatial evapotranspiration pattern within the Elbe River basin – the semi-distributed model SWIM, the remote sensing approach, and the water balance method – delivered the key finding of this study: The water balance approach does not seem to be more exact than the two other methods. The relatively strong correlation between the modelled and the remotely

sensed estimates tells indeed the opposite, which is meaningful, because the ground based approach is commonly trusted most.

Concerning the recently published climate change impact study for the Elbe River basin (Wechsung et al. 2013) which relies on ground-based spatial calibration (Conradt et al. 2012a,b, 2013a,b, Chapters 2 and 3), the consequence of our findings has to be extra caution when interpreting the results; cf. the assessments of water management options (Kaltofen et al. 2013a,b, Koch et al. 2013a,b) and the related economic consequences (Grossmann et al. 2013).

5.5.1 *Sources of uncertainty*

There are several reasons which have disturbed the validity of the water balance derived evapotranspiration heights, two of them have been shown explicitly. They can be divided up into aleatoric (driven by randomness) and epistemic (caused by lack of knowledge) uncertainties. The following list contains also other likely sources of uncertainty and is not meant to be exhaustive:

A. Aleatoric uncertainties
   1) Biased interpolation of climate data in sparsely instrumented areas
   2) Errors of gauge measurements along major streams affecting intermediate areas

B. Epistemic uncertainties
   3) Unknown groundwater fluxes between adjoining sub-basins
   4) Unknown artificial water transfers between sub-basins
   5) Erroneous or missing provision for the impacts of mining

While we could detect both aleatoric uncertainties listed above, the epistemic examples are natural starting points for further research. Of course, experiences or findings of other studies give some clues for the items in second part of the list.

For example, the assumption of hidden, unaccounted groundwater fluxes is not at all implausible for the lowlands with their dominating sandy sediments. Although significant effects are more likely for small areas, Schaller & Fan (2009) postulated groundwater export or import altering the water balances even for large basins (up to $\approx 50\,000\,\mathrm{km}^2$) in the United States.

For lowland rivers in sub-catchments of the Elbe River basin, Krause & Bronstert (2007) and Krause et al. (2007) investigated and modelled variable interactions between groundwater and surface water. Their findings question directly the credibility of both the SWIM model and the water balance approach for smaller sub-basins in this landscape.

Additionally, many lowland areas of the Elbe River basin are covered with a network of ditches and canals, and their impact is sparsely known.

5.5.2 *Perceptions of reality*

Because differences between remotely sensed hydrological properties and any kind of validation data are so widespread and frequently observed, it is easy to speak of distinct perceptions of reality. Great efforts have been made to merge these differing views into one consistent picture of reality. At present, the most prominent research field is data assimilation (Evensen 2007, Liu & Gupta 2007, Mathieu & O'Neill 2008, Reichle 2008). Practical examples for integrating evapotranspiration patterns retrieved by remote sensing into hydrological modelling give Pan et al. (2008), Qin et al. (2008), Long & Singh (2010), Schuurmans et al. (2011), or Liu et al. (2012), but how about the difference between (merged) perception and reality?

The core concept of data fusion or data assimilation (e. g. by Kalman filtering) – providing best estimates of real values by weighted means of the diverging input data – may lead to biased results, because any weighting is subject to prior assumptions on the error variances of the input data; cf. van Leeuven & Evensen (1996) or McLaughlin (2002) for details about the Bayesian background. The concept may even not be applicable at all when systematic errors override the information content expected from a certain data source. McCabe et al. (2008) quite correspondingly conclude that while achieving hydrological consistency is urgently needed for improving hydrological prediction, there is currently no comprehensive or robust framework for integrating a multitude of observations; simply developing more efficient merging techniques would not be the key issue. Some attempts have at least been made; an example is given by Vrugt et al. (2005) who combined global optimisation and sequential data assimilation in a hybrid framework.

5.5.3 *Recommendations*

Despite these challenges, incorporating additional information by means of remote sensing must be strongly recommended for any distributed modelling project: In any case, it can serve as independent spatial basis of comparison, and only by investigating the differences rather than by interpolating them away, modelling may come closer to reality.

However, our approach of combining remotely sensed with ground measured data for estimating evapotranspiration can only be recommended for areas with high density of meteorological stations. Otherwise, poor performance prevents any meaningful assessment, and an altern-

ative method like SEBAL (Bastiaanssen et al. 1998a,b) should be used instead.

Meteorological and stream gauge measurements will of course remain the bread and butter for driving and calibrating hydrological models. But with the experience of heavily deviating water balances in sub-basins, more care should be taken with respect to probable lateral water fluxes.

If there are only few runoff data from interior stream gauges, a distributed hydrological model can be spatially calibrated on remotely sensed *ET* patterns, but to achieve realistic discharge simulations in space, additional local knowledge, e. g. on groundwater exchange and water management effects, is essential. If there are many data from a lot of interior gauges, a comparison with remotely sensed *ET* patterns should always be used to identify local pecularities and to customise the model respectively.

Finally, this endorses the case made by Beven (2001): The future of hydologic science lies less in the development of new theories and models but in gathering knowledge and understanding about specific areas; it should rather be a "learning about places" (see also Beven 2003, 2007).

ACKNOWLEDGEMENTS We are grateful to Jakob P. Köhler and Stefan Lange for downloading most of the 944 LST map images and to Peter Seifert from DLR for technical assistance in this lengthy process. This work was compiled within the framework of the German GLOWA-Elbe research project (http://www.glowa-elbe.de) funded by the German Ministry for Education and Research (BMBF, http://www.bmbf.de), grant no. 01 LW 0603 A2.

6

DISCUSSION

The four research papers presented in the previous chapters already include individual discussion sections. But there are some interlinking aspects worthwhile to be reconsidered. Thus it is not only due to the faculty's guidelines on cumulative theses (MNFAK 2010) that the 'contribution to the enhancement of the scientific knowledge by the manuscripts at large' („Beitrag zur Erweiterung des wissenschaftlichen Kenntnisstandes ... durch die Manuskripte in ihrer Gesamtheit") shall be discussed here.

If we go back to the questions raised in the Introduction on Page 2, the first one was about the fundamental problem how to deal with the uncertainties in distributed hydrological modelling, and finally a leitmotiv of providing new methods and ideas for better integration of regional environmental characteristics into hydrological modelling was announced. Do the insights from the papers deliver any new ideas about the evident uncertainty problem, especially on the sub-basin level? This is definitively the major issue to wrap up here.

The other introductory questions are more or less answered by the individual contributions:

- Chapter 4: Yes, it is very likely that precipitation is locally influenced by the structure of the landscape. The proposed statistical analysis of principal component residuals – a non-conventional way of using PCA – was shown to be an effective method for trend detection within the noisy signal of daily precipitation measurements.

- Chapter 5: It turned out to be a long and busy road from downloading a pile of land surface temperature maps to obtaining water balance numbers for model sub-basins. There are certainly alternative methodologies for integrating daily satellite scans into modelling, e. g. by continuous data assimilation during the model run, but this assessment finally lead to three independent (and lowly correlated) views on sub-basin water balances which have to be discussed separately with respect to question one.

Regarding the leitmotiv-question about the best way to address the sub-area uncertainties, let's start with an overview of all the evident or probable reasons for local model-reality deviations that could be observed or have at least been supposed:

6.1 KINDS OF ERRORS IN DISTRIBUTED MODELLING

6.1.1 *Error sources observed in the previous chapters*

All the results presented in the previous chapters demonstrate a dazzling array of reasons why runoff simulations for single sub-basins of the Elbe River basin were biased, generally more than the modelled hydrograph at the main outlet. Here is the full list of reasons, roughly ordered by a principle that will be unveiled thereafter:

1. The spatial calibration of sub-basin discharges had several flaws, cf. Section 3.2.3 of Chapter 3 on Page 58, the major one is that reference runoff data covered different time periods whose average values were taken as long-term means, and stationarity was assumed. However, stationarity does not exist in hydrological time series (Hurst effect; cf. e. g. Klemeš 1974).

2. Different aquifer properties within the model domain leading to distinct response functions of the groundwater runoff component were neither covered by the input data nor by the groundwater representation of the model. Poor model performances for the Havel tributary could be enhanced by introducing a two-storage approach (Section Groundwater modelling on Page 31).

3. Inequal spacing of input stations for climate data and the application of simple inverse-distance interpolation lead to errors. In the Discussion of Chapter 3 beginning on Page 69 it is suggested that many high precipitation measurements from the German observation network along the Bavarian Forest biased the respective input for many sub-basins in the Czech republic with sparse station data. How large the errors were that could have been avoided by better interpolation is shown in Section 6.1.1.1 below.

4. Effects of groundwater extractions in mining areas had been considered in principle, but it was impossible to account properly for all these man-made runoff variations; cf. the drastic decline from measurements to the scenario simulation for Havelberg (Havel) in Figure 23, the respective remark in Section 2.3.3 on Page 42, and the list in Section 3.2.3 on Page 58.

5. Lateral water fluxes moving aloof the river system like groundwater exchanges or through artificial canal systems were completely neglected (also in the list on Page 58).

Low quality and resolution of input data is a major cause for small-scale uncertainty. Section 2.4.1 in the Discussion part of Chapter 2 (see Page 46) lists the following three issues:

6. Insufficient spatial density of climate station data in the Czech part of the basin (cf. Figure 25),

7. No adequate wetland representation with respect to small-scale heterogeneity and transition zones (also in the list of Section 3.2.3), and

8. Misfit between idealised land use class and real land cover characteristics. The non-typical forests on the Ore Mountains deliver an obvious example while general errors of the land use and soil parameterisations remain unknown (cf. the second-last paragraph of Section 2.4.1 on Page 48 and the first paragraph of Section 5.4.3 on Page 118).

9. Chapter 4 is entirely devoted to detecting a specific reason for sub-basin deviations – landscape effects (here: local convection triggering) on the atmospherical meso-gamma scale (Orlanski 1975) that cannot be captured by plot-oriented surface hydrotope properties for direct runoff behaviour and evapotranspiration. These effects could only be modelled by coupling a small-scale atmospherical onto the hydrological model as already proposed by Leavesley & Hay (1998) who intended to fill the gaps between station measurements in this way. However, respective approaches are still in their fledgling stages.

The general errors in the land use parameterisations (see Points 6–8 above) gain importance on the local scale, this was named regarding the scenario calculations:

10. Distributed land use changes which rarely affect the discharge behaviour of the entire Elbe River basin may cause strong alterations for certain sub-basins with relatively high shares of change areas (last Paragraph of Chapter 2 on Page 51).

Although it was the declared purpose of the investigation presented in Chapter 5 to reveal model deficiencies in order to improve the spatial representativeness (Section 5.1.3 on Page 96), the only really important discovery was that

11. Discharge data calculated from the difference of two subsequent stream gauges for the reach area between them are affected by high uncertainties (see Figure 51 on Page 115 and the explanation in the Discussion on the following page). This points out that deviations between simulation outputs and observations need neither be caused by modelling errors nor by considerable measurement uncertainties but unwise use of data.

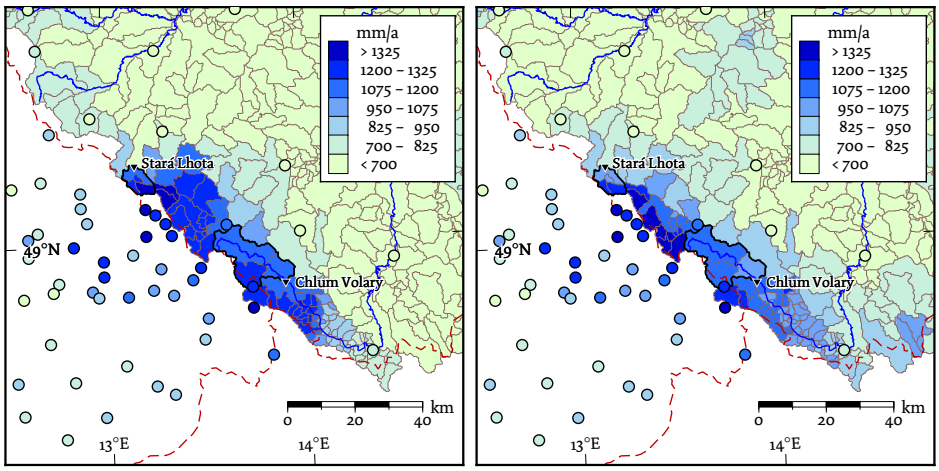

Figure 53: Two different interpolations of precipitation data (annual means of 1951–2003) in the Czech-German boundary region. Left: inverse-distance interpolation. Right: ordinary omni-directional external drift kriging. Elevation dependency has been considered in both cases (underlying trend viz. external drift component).

6.1.1.1 *Best practise makes a difference – Example on point 3*

In order to assess the effect of kriging the precipitation data instead of using inverse-distance interpolation I made an interpolation experiment. I interpolated the mean annual precipitation depths of the recent (1951–2003) measurements from the 853 input stations to the 2278 sub-basins

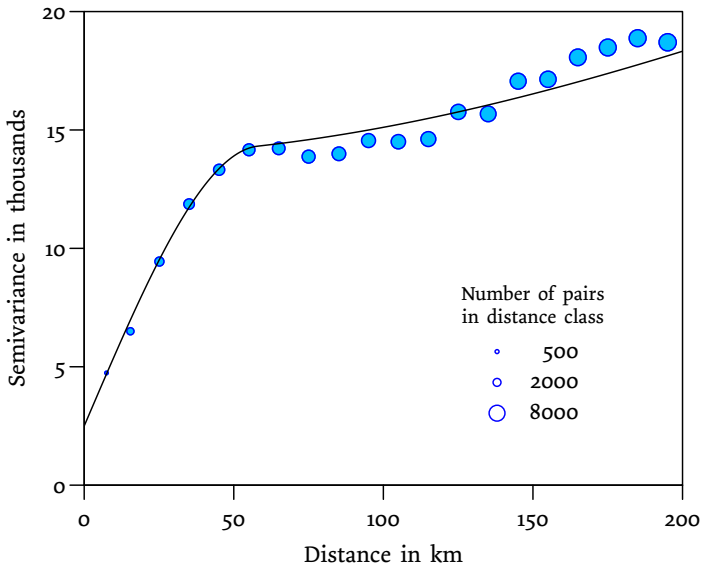

Figure 54: Semivariogram of the annual precipitation averages (station observations). The applied variogram model, drawn as black line, is an eye-fitted additive combination of a spherical and a gaussian term.

twice: one time with the same inverse-distance program that was used to interpolate the daily input weather data for SWIM and another time by kriging. The inverse-distance program was run with the precipitation correction after Richter (1995) switched off, because the kriging software used (the 'gstat' package of R, cf. R Development Core Team 2011) did not have this extra feature.

Figure 53 comprises the resulting maps of the critical Czech-German boundary region drawn in the same way as Figure 32 on Page 70. The left panel shows the result of the inverse-distance interpolation algorithm, the right one the alternative obtained by kriging. Some differences between the inverse-distance results in Figures 32 and 53 are due to individual handling of the single-day interpolations: if the elevation trend remained below 0·4 (as on days with convective storm cells), no such trend was considered. Other differences stem from the Richter-correction which is missing in Fig. 53.

The comparison of the maps confirms the conclusion of Section 3.4 that the inverse-distance method biases many sub-basin outputs at the south-western edge of the model domain towards the high values

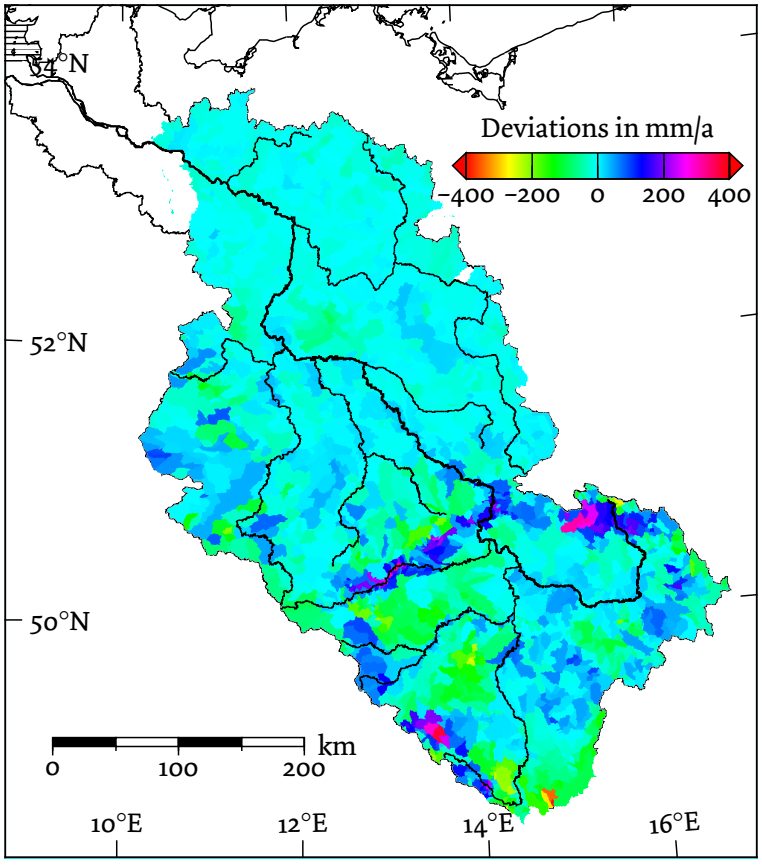

Figure 55: Differences between two precipitation interpolations to sub-basins obtained by inverse-distance weighting and by ordinary kriging of station data.

measured on the German side of the mountain range. Why kriging performs so much better becomes clear from the semivariogram shown in Figure 54: The spatial correlation is practically limited to less than 50 kilometres – even for annual precipitation averages and even if the elevation dependency is considered. (I made some tests with directed variograms, and observed larger differences only in the secondary rise of the semivariance at distances over 100 km. Therefore I chose to stick to a simple omnidirectional variogram model.)

The differences of the maps in Figure 53 are directly striking if one considers that in order to avoid biasing impacts from remote stations to sub-basin outputs the input data used for each sub-basin (centroid) interpolation were limited to the five nearest stations. For kriging, all stations within a radius of 200 km were used.

Finally, a more general idea of how much the kriging approach is superior to inverse-distance interpolation is conveyed by the map of differences for the entire model domain in Figure 55. The most extreme deviations can be found in the Czech part due to the relatively low input station density there. As many differences exceed 100 mm/a, no further explanation is needed about the importance of best practice approaches. However, it shall be added that runoff simulations in small sub-catchments in particular depend on precipitation interpolation (Masih et al. 2011). It's high time to dump the inverse-distance program and consequently use kriging for climate data preprocessing, although this requires automated variogram fitting for all meteorological variables on each single day of the simulation.

6.1.1.2 *Research into the sub-basin scale – Example on point 5*

Groundwater fluxes between sub-basins have been blamed for under- and overestimations of river runoffs, and Schaller & Fan (2009) have been cited as main witnesses in Chapters 3 and 5 that these errors need not be restricted to small catchments. But would it be possible to show a concrete example from within the Elbe River catchment?

I always had the suspicion that a brook descriptively named 'Verlorenwasser' ('Lost water', located south of the city of Brandenburg in the lower Havel River area) would loose a lot of its discharge subterraneously; the runoff was largely over-estimated by the spatially uncalibrated SWIM model.

Looking at the physical map in Figure 56 substantiates the suspicion. The Verlorenwasser catchment is located on a range of hills surrounded by less elevated areas. It is rather sharply bounded by a low terrace in the northeast, in fact the western ending of a much larger structure: the Baruth glacial valley. The gravitational effect could indeed move the groundwater towards the neighbouring sub-basins, especially to the Temnitz catchment.

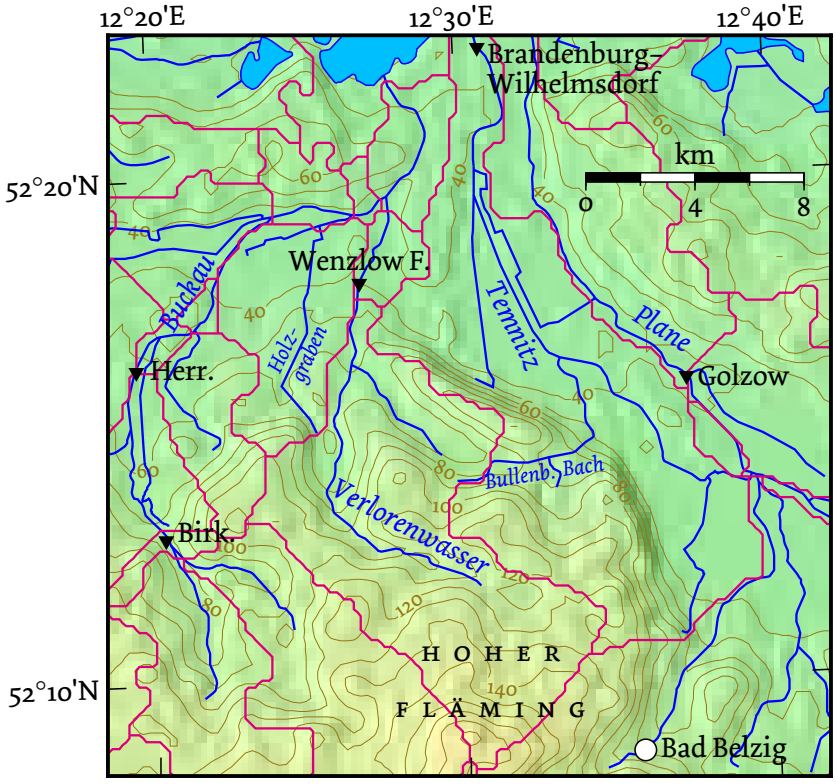

Figure 56: Map of the Verlorenwasser and Temnitz sub-basins. Runoff gauges are marked by black triangles. Abbreviated gauge names read as follows: Herr. = Herrenmühle Forellenanlage (Buckau), Birk. = Birkenreismühle (Buckau), Wenzlow F. = Wenzlow Forellenanlage (Verlorenwasser).

Table 8: Measured long-term discharges in the Verlorenwasser region. The catchment areas have been taken from the hydrological yearbook (DGJ 2007), and long-term discharge means for the years 1980–2009 had been published online by the Ministry of Environment, Health and Consumer Protection of the Federal State of Brandenburg (URL: http://www.mugv.brandenburg.de/lua/gis/abflentw_20110701.zip, last accessed in July 2012).

Gauge, river	A in km²	MQ in m³/s	Mq in mm/a
Birkenreismühle, Buckau	95·0	0·39	130
Herrenmühle F., Buckau	134	0·59	139
Wenzlow F., Verlorenwasser	91·2	0·20	69
Br.-Wilhelmsdorf, Temnitz	153	1·52	314
Golzow, Plane	409	1·52	117

Other cartographic sources add to the evidence: The elevated area is a range of foothills of a larger ridge in the south, a moraine of the Saale glaciation called 'Fläming'. The foothills are in fact a structureless and distorted morainal apron consisting of fluviatile sands (GÜK-BB 1997). These form a porous aquifer with conductivities in the range of 10^{-3}–10^{-4} m/s (HÜK 200 2011).

There are some runoff gauges in the area, and long-term mean discharges of a common time period (1980–2009) could be obtained. This allowed for the comparison of runoff contributions shown in Table 8.

The runoff contribution map of the Hydrological Atlas of Germany, a product of precipitation downscaling and evapotranspiration modelling, shows about two thirds of the square kilometre raster cells on the morainial apron in the category 50–100 mm/a and the one third in 150–200 mm/a. These are surrounded by raster cells which are mainly equally distributed in the categories 0–50 and 100–150 mm/a. In the Temnitz wetland, there is also a patch of cells with negative values (Glugla et al. 2001). Comparing these data to the gauge measurement results, it seems obvious that the Verlorenwasser catchment looses much of its water in favour of the surrounding sub-basins.

But we have to take the groundwater theory with a grain of salt: The Holzgraben northwest of the Verlorenwasser catchment and the upper part of the Bullenberger Bach in the east are man-made ditches reaching into the catchment. They might drag water from the Verlorenwasser to Buckau and Temnitz, too. And there are a lot of connections between Plane and Temnitz – Plane runoff might erroneously be gauged as Temnitz discharge.

However, Pfützner (2005) who applied the distributed modelling system ArcEGMO to develop a detailed river catchment model for the Federal State of Brandenburg, also observed stronger differences between model and reality for smaller catchments and drew practically the same conclusions regarding the important rôle of groundwater in the Havel area – his prime example are the upper Nuthe River (loosing) and the brook Hammerfließ (gaining), both also located on the northern edge of the Fläming and in the Baruth glacial valley, respectively.

Pfützner refined detailed simulations for that region by a coupled groundwater model (GW-ASM), and integrating such capabilities into semi-distributed modelling (cf. Hattermann et al. 2004b) would be a preferrable way to regularly address this issue for larger modelling domains.

6.1.2 *Uncertainty of aleatoric, epistemic, and ontologic uncertainties*

In Section 5.5.1, some uncertainties were subdivided into aleatoric and epistemic ones. This classification of error sources that could either be remediated by more research (epistemic) or have to be accepted as irreducible system noise (aleatoric) was used in engineering (Helton & Burmaster 1996) and brought into geosciences originally for seismic risk assessments. One publication broadly explaining the concept was Senior Seismic Hazard Analysis Comittee (SSHAC): Budnitz et al. (1997), a technical report for U.S. nuclear energy authorities. This report was immediately reviewed by another commission, and the aleatoric–epistemic classification had been severely critisised (Panel on Seismic Hazard Evaluation: Kisslinger et al. 1997): The reviewers refer to passages of the initial report where a belief in only one kind of uncertainty – due to lack of knowledge – is expressed and take up a sceptical stance on the rationale and practical use of this concept.

Nevertheless, the idea of differentiating between epistemic and aleatoric uncertainty made its way into the hydrological literature via flood risk investigations (Apel et al. 2004, Merz & Thieken 2005), and the terminology finally reached the modelling community (Ross et al. 2009, Li & Zhang 2010, Beven et al. 2011).

What is the special value of this separation? Merz & Thieken (2005) give the example of river levee sections of different breaching heights. A section will fail if the river water level exceeds its critical height. Problems in determining these heights exactly would express epistemic uncertainty, and the effective heights are considered to be randomly lower due to material variations representing the aleatoric component.

It makes sense to be aware of two independent uncertainty sources in the above example – if the breaching heights can be determined with low uncertainty, and the levees are all built in the same way from the same material (low uncertainty from the second source), safety measures should concentrate on sections with low breaching heights.

But the epistemic–aleatoric terminology seems to be arbitrary. Isn't the material and inner quality of a levee something that could also be assessed by methods like ground penetrating radar or seismic imaging? Then the effective height uncertainty is as epistemic as the uncertainty of the principal breaching height estimation.

Let us now step through the above list of reasons for uncertainty of discharge modelling results in sub-basins.

Point 1 could have been completely avoided by comparing a different set of years for each sub-basin according to the individual temporal coverage of reference data. This would have required a little more sophisticated coding for the automatical spatial calibration. Taking multi-year averages based on the available data for stable long term means may be common but is bad practise in hydro-engineering.

Regarding the uncertainty category, this is clearly an epistemic case as the required research was just not done: common practise is no excuse for sub-optimal data handling. And it should be noted that getting rid of the resulting chunk of uncertainty would have been rather easy.

Point 2 refers to an obvious structural uncertainty of the model which could be reduced by altering the respective module, so it was also epistemic. No improvement was made regarding the precipitation interpolation error of Point 3, but as the error source could be identified and could have been curtailed – e. g. by kriging instead of inverse distance weighting, see above – this error is epistemic, too.

More efforts like looking for historic water management documentations would also have narrowed down the uncertainties about the groundwater extractions of Point 4 – the statement "it was impossible" was made only with respect to time and/or budget constraints of our work. Given more resources, the assumed lateral water fluxes of Point 5 could also have been investigated area-wide and explicitely considered in the model. The work of Hattermann et al. (2004b) could serve as starting point for the latter.

Now it should be clear which principle governs the order of the list: The higher the number, the harder the research efforts that have to be made to reduce modelling uncertainties. Points 6–8 would require more or better data which are very hard but not totally impossible to obtain: There are in fact more meteorological stations in the Czech Republic than those whose data could be accessed with the given means. Even if there were not, additional measurements could be made at locations in-between, and respective data for the past could be estimated from stochastical relations between the new measurements and synoptic observations of the old network. Finally, the spatial or functional representations of wetlands and land use classes could theoretically also be refined *ad libitum*, e. g. by extensive field mapping campaigns.

The hydrometeorological changes caused by land use alterations would be extremely hard to consider in the modelling, because they are

a non-linear dynamical phenomenon. Point 9 shows that more research, including the methodology, would be needed to expand the knowledge about these effects over larger domains. However, there is even more potential for epistemic uncertainty minimisation within the already acquired data.

Point 10 explains why these and other uncertainties in the spatial representation of hydrologically relevant features cause larger relative modelling errors in small sub-basins than for larger areas. This has nothing to do with the uncertainties as such – which are entirely epistemic –, it is a fundamental problem of scale-dependent error modulation. This is probably the reason behind the 'natural error law of distributed modelling' (cf. Page 1), but it has nothing to do with the epistemic–aleatoric dichotomy.

The last example, Point 11, is similar: The origin of the error – relative uncertainties in discharge observations – is also epistemic (the errors in the runoff gauging could be diminished with some efforts), just the unfavourable idea of using runoff differences between subsequent gauges for estimating local water yields made these (relatively small) errors severely distort the result. Thus it is also a question of good practise how to use error-prone input data, and it seems somehow related to the methodological flaw discussed in the first point.

All these examples show that there are numerous sources of uncertainty, and that it is desireable to clearly differentiate between them. But all these sources turned out to be epistemic. Is there really such a thing as aleatory uncertainty?

Let us review some recent research papers dealing with aleatory and epistemic uncertainties in hydrology. Sun et al. (2012) propose a probabilistic sewer flooding evaluation. Of altogether five uncertainty sources, hyetograph shape, i. e. the intensity variation of a rain event over time, is considered purely aleatoric. Nevertheless, the authors draw from the pool of measured hyetographs in order to generate synthetic rainfall events. This makes sense if the rainfall intensity variations are not only white noise, and their shape patterns could be investigated with respect to the flooding effects. As the hyetograph of a single rain event might even be approximated some minutes in advance by weather radar and help to estimate short-term flooding risks (cf. e. g. Werner & Cranston 2009, Ruzanski & Chandrasekar 2012) the categorisation as aleatoric uncertainty source is highly questionable.

Ross et al. (2009) discriminate between the uncertainty in hydraulic conductivities of aquifer subdomains and the expert-estimated uncertainty of the conductivity measurements. The authors regard measurement uncertainty as epistemic (reducible) and field variability as aleatoric (irreducible). This is somewhat arbitrary: if extensive pumping experiments had been made, the remaining measurement uncertainties would seem rather irreducible, while the uncertainty about the field variability could eventually be further reduced, e. g. by tracer experi-

ments or additional boreholes. Li & Zhang (2010) also worked about uncertainty representation in groundwater modelling, but discuss the specific uncertainties (of conductivity, storage and distribution coefficients) as combinations of both aleatoric and epistemic uncertainties which are not further separated.

"There is no clear-cut boundary between aleatory and epistemic uncertainty", a statement taken from Merz & Thieken (2009), gets to the heart of the problem: As Merz & Thieken explain further, some researcher may model a certain parameter deterministic and minimise epistemic uncertainty by improving her model while another one treats the same parameter probabilistic and accept the actual variations as aleatoric.

6.2 DIMINISHING MARGINAL UNCERTAINTY REDUCTIONS

This gives even more evidence for concluding that the uncertainty level in river basin modelling could be reduced far below the contemporary 'limits of acceptability' (cf. Beven 2006). If we look back on the reasons for modelling errors named in this thesis, practically all of them could be transformed into respective research tasks, and the modelling could be improved by the results of each of these studies.

Abbott & Refsgaard (1996) define the (semi-)distributed hydrological model as the means to do everything that is reasonably possible: as mobilising as much data and testing it with as much knowledge as feasible in order to analyse problems and eventually find solutions concerning the hydrological cycle.

The decisive word here is of course 'reasonably'. According to time and budget limitations, models cannot be improved beyond a certain point. In our Elbe River basin example, substantial improvements were achieved by some straightforward measures (like the automatised spatial evapotranspiration calibration), some more could have been made by relatively compact tasks. Going down the list of reasons for model deviations more and more complex efforts would be required to converge model and reality by comparable amounts.

The behaviour remembers of the economic law of diminishing marginal returns – additional increments of work input yield tendentially diminishing decreases of model output errors. But as a certain effort must be completed in order to lift the model onto a new level of less uncertainty, and as model structures cannot be refined gradually, the relationship between research labour and model fidelity will probably look less like one of the smooth graphs in economy textbooks and more like the stepped pathways shown in Figure 57.

An obvious problem is also illustrated in Figure 57: Usually, any research project in which river basin modelling takes place is limited in budget and time. When a modelling task is set out, it is not clear from the beginning how difficult and time-consuming the first subtask of

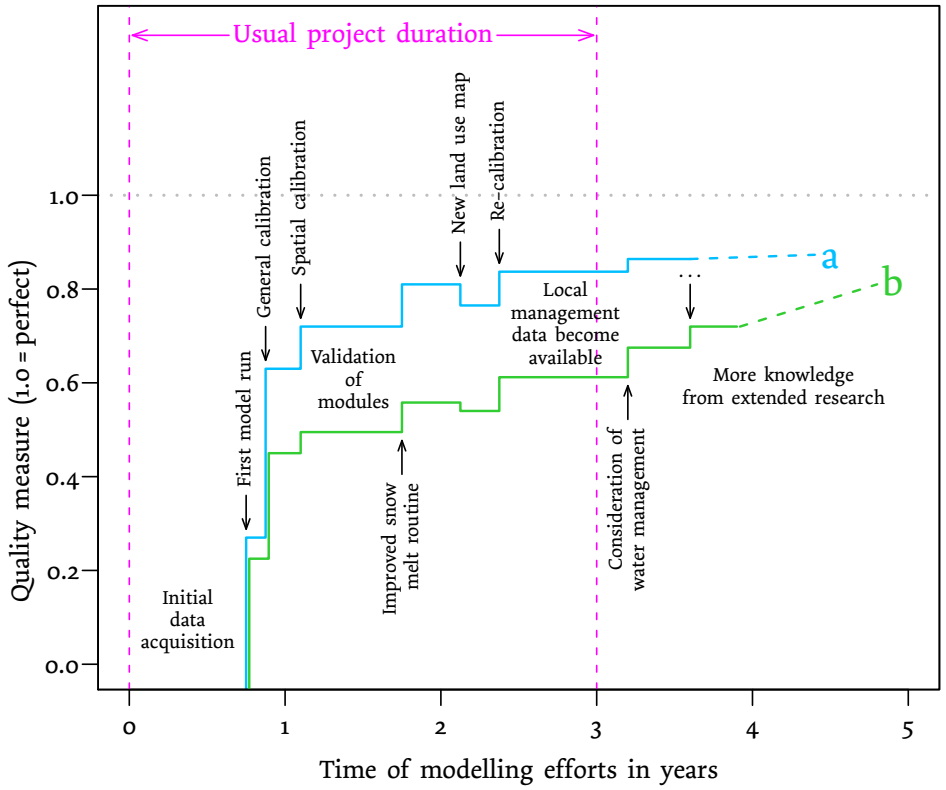

Figure 57: Diminishing marginal uncertainty reductions. The blue path of example case (a) shows the pattern of diminishing modelling progress over time more clearly than the green path of example case (b), but in the long run the latter would also stagnate at some quality level despite more and more efforts.

data acquisition will develop and what kind of uncertainties will have to be mitigated. It might be that the quality of the modelling results develops like the blue graph in Figure 57: after three years of work being rather close to what would have been achievable by double efforts. It might also be that the research project follow the green path and finally come up with results devaluated by a large uncertainty range which could have been narrowed down a lot by some further assessment. The second case can be split up into a variant where the modelling team is aware of the remaining potential for further improving their results and a variant where they think they were on a blue path while they were in fact on a green one.

FINAL REMARKS I do not doubt at all the meaningful applicability of the SWIM modelling of the Elbe River basin as calibrated during the GLOWA-Elbe research project – Abbott & Refsgaard (1996) conclude that the use of a model will nearly always narrow down the range of uncertainty regarding the outcome of some intervention, because it efficiently utilises the available input information. But I am almost sure that our modelling fell short its full potential by far. (Of course, the 'full

potential' equals the theoretical maximum coherence between model and reality that could be achieved by infinite efforts, but it should be possible to come close to that limit even with limited means.)

Some simple but effective measures were simply missed. However, many tasks to improve the model were clear but could not be accomplished anymore. Another observation from the list of reasons for uncertain simulations is that most research is required on the local or sub-basin scale. This confirms Beven (2003) as he concludes "In essence, it would appear that learning about *places*, and taking account of the inherent uncertainty in doing so, will become more important than using particular model structures" (emphasis in the original).

I did not discuss the issue of model complexity so far, but we have seen that it had been increased by implementing a second groundwater storage term (Section 2.2.3.3). Spatial calibration added also to model complexity, because the individual sub-basin parameter sets were originally uniform, thus they represented just one global parameter set.

Of course, a model should be kept as simple as possible, and it is the 'modelling dilemma' that "a simple model cannot be relied upon to make meaningful extrapolative predictions whereas a complex model may have the potential but due to information constraints may be unable to realise it" (Kuczera & Franks 2002). However, I think there is no dilemma as long as more complexity is justified by knowledge about the processes that need this extra complexity to be represented in the model. Hence, the degree of model complexity needs not neccessarily be a "compromise between the desire to keep the model as simple as possible and the need to achieve a prescribed degree of accuracy" (Dooge 1977), but should equal the complexity of process knowledge.

Lack of process knowledge on the sub-basin scale is the real limitation for distributed model fidelity. Large scale modelling projects like GLOWA-Elbe need therefore much more resources to gain reliability compared to modelling studies on a single headwater catchment. Such efforts regularly follow the green path in Figure 57 and should consequently be tendered as long term research projects.

7

SUMMARY

7.1 INTRODUCTION

Within the framework of the German GLOWA-Elbe research project (2000–2010), it had been required to simulate scenarios of quasi-natural water availability for the Elbe River basin in Central Europe. This task was undertaken by SWIM, a spatially semi-distributed eco-hydrological model which had been developed at the Potsdam Instiute for Climate Impact Research.

The special challenge of this modelling was to get realistic results for hundreds of sub-catchments despite degrading model fidelity with decreasing sub-catchment size, a 'natural law' in distributed modelling. Additionally, man-made regional environmental change impacts, e. g. by extensive open-cast mining, handicapped the achievement of the objective.

The motivation for this thesis cristallised into the following questions:

- How can we cope with the uncertainty principle of distributed modelling when distributed outputs of high resolution and quality are required? (The fundamental question of this thesis – more or less addressed by all chapters)
- Do the post-mining landscapes influence the local climate and thus hydrology, in addition to their direct impact? How is it possible to quantify respective effects by standard precipitation measurements of the German Weather Service (DWD)? (Chapter 4)
- How can ready-available, remotely sensed data be utilised for spatially differentiated model calibration? (Chapter 5)

An underlying leitmotiv of all these questions was the intention to provide future research with methods and ideas for a better integration of regional environmental characteristics into hydrological modelling.

The importance of the hydrological modelling for the entire model cluster of the integrative research project GLOWA-Elbe results from many subsequent analyses which used the SWIM results as input. For instance, further water management and in-stream ecological modelling used the simulated quasi-natural discharges, and the water management results were subsequently fed into another model balancing the nutrient loads. An agro-economic sector model also used SWIM outputs finally affecting both land use projections and water use modelling.

The Central-European Elbe River basin covers 148 268 km², of which 134 890 km² are modelled – the northwestern part below the Geesthacht

Weir has been disregarded due to the tidal influence that prohibits regular runoff measurements. Nevertheless, the model domain covers all three major landscapes of the Elbe area: the glacially formed lowlands with sandy substrates and wetlands with peat formations in the north (typically below 200 m a.m.s.l.), the hilly areas with silty and loamy substrates in the middle and the south, and some mountainous regions (typically above 500 m a.m.s.l.), often with thin and stony soil layers. Recent water balance numbers (basin averages) are $P \approx 700$ mm/a and $ET_a \approx 530$ mm/a, hence $Mq \approx 170$ mm/a. The per-capita water availability amounts to 3 m³/d.

The eco-hydology of such a heterogeneous and large area can be efficiently represented by a semi-distributed model. A fully distributed model would mean a rasterised landscape where water fluxes between the cells are numerically discretised from physically based process equations – which is computationally very demanding – while a semi-distributed model is composed of landscape aggregates and does not explicitely calculate the field of lateral fluxes.

Early semi-distributed models were constructed as coupling of several lumped single catchment models. Therefore they have been critisized as 'less physically based' compared to fully distributed models, which would limit their use in scenario simulations, e. g. for estimating land use change effects. This critic seems to be outdated, because the contemporary generation of models, including SWIM, is based on so-called 'hydrotopes', landscape patches characterised by uniform hydrological behaviour. The processes within these hydrotopes are then represented by physically based algorithms, and the sub-basin discharges are not calculated by a questionable parameterisation but aggregated from the individual contributions of the hydrotopes within.

The hydrotope properties for the SWIM setup used here are defined by a combination of five factors – sub-basin affiliation, land use class, soil map unit, wetland property, and temporal discharge inactivation.

The first four are the standard factors of the model; temporal discharge inactivation was introduced in order to represent areas with disturbed runoff formation due to former mining activities. The gradual recession of these areas had been projected and mapped by five-year time steps. The resulting hydrotopes were practically determined by an overlay of five respective maps using GRASS-GIS.

The climate scenario input used in Chapter 2 is appreciated critically: Due to systematic limitations of the STAR model, the climate realisations with increasing temperature trend tend towards drier conditions which are clearly exposed in the runoff projections.

Regarding Chapter 5, the Introduction closes with a view on integrating data from remote sensing into hydrological modelling. According to a bibliometric survey, this has become a 'hot spot' in geosciences: The annual counts of publications about hydrological modelling and remote sensing increased drastically over the last three decades. Currently,

more than 2000 new publications about hydrological modelling and approximately 4000 about remote sensing are added to the Web of Science database each year. These are about triple counts compared to the year 2000. The share of publications *combining* hydrological modelling and remote sensing in all the hydrological modelling publications has also been increased from about 3 % around the year 1990 over approximately 5 % around the year 2000 to 7–8 % nowadays.

The possibilities of using remote sensing data with respect to hydrological modelling range from independent derivation of hydrological system states to data assimilation methods actually driving the models by remotely sensed data. Especially the latter extreme is accompanied by the danger of pseudo-validation of a poor model by biased results from mis-interpreted remote sensing data. Chapter 5 therefore deals with the differences between and the individual values of modelling results, satellite-scan derived, and ground 'truth' data.

7.2 SPATIALLY DIFFERENTIATED DISCHARGE SCENARIOS FOR THE ELBE RIVER BASIN

The first research article (reproduced in Chapter 2) explains the set-up of the SWIM model for the scenario modelling in detail. The scenario period for which quasi-natural sub-basin discharges had to be simulated covers the years 2004–2053. 'Quasi-natural' means that runoff alterations by reservoir operation, flooding of disused mining pits, or artificial water withdrawals should not be included; measured runoff data used for calibration had been revised accordingly beforehand.

The climate scenarios that served as input followed temperature trends of +2·1 and +3·0 K, and four different land use scenarios had been considered. As SWIM works on a daily time-step, climate input data had to be provided on a daily basis. These data, consisting of radiation, air humidity, precipitation, and air temperatures, were interpolated from 853 station locations to 2278 sub-basin centroids. For calibration purposes, station measurements for the years 1951–2003 were treated accordingly.

Spatial input data sources were sub-basin divisions in digital catchment maps of the German Federal Environmental Agency (Umweltbundesamt) and the Czech water management authorities (Povodis), the SRTM elevation data of U.S. NASA, general soil maps of Germany and the Czech Republic, and the European CORINE2000 land use data base.

Some modifications of the model compared to the standard version of SWIM have been made: groundwater drawdown areas caused by mining activities have been considered with zero discharge contribution; their projected shrinkage over time has been modelled in five-year-phases via another map. To maintain consistency with a former study, potential evapotranspiration has been modelled by the so-called Turc-Ivanov approach; it serves as intermediate in calculating actual evapotranspira-

tion ET_a. Two important modifications have been made regarding the groundwater discharge: Groundwater uptake from plants in riparian zones is not taken from the sub-basin groundwater storage but directly subtracted from discharge, and a two-level groundwater storage system has been implemented. Both groundwater modifications led to much better validation results, especially for the Havel River tributary.

Model calibration was performed in two stages: first at basin-scale with one global set of parameters (*ET* correction, soil hydraulic conductivity adjustment, two groundwater and two river routing parameters), then spatially distributed with individual parameter sets (*ET* correction and groundwater α-parameters) for more than 100 gauges covering all parts of the basin. Practically all measured hydrographs had to be revised to exclude direct management effects like reservoir releases to serve as reference data.

Validation results show excellent model fidelity at the main outlet gauge (Nash–Sutcliffe efficiencies up to 0·945), but also a systematic over-estimation of runoff for the decade of the 1990s by 13·5

The scenario results, based on 100 realisations of the STAR climate scenarios, can be interpreted best on the basis of the area-averaged water balance for the years 1961–1990. In these recent decades, there were 701 mm/a precipitation of which 530 mm/a evapotranspirated. Total runoff amounted to 171 mm/a. The scenario with a temperature increase of 2 K showed only slightly less precipitation in its last decade (2044–2053), 691 mm/a, but evapotranspiration (*ET*) increased to 581 mm/a, cutting down the total runoff to 100 mm/a. The other scenario with the stronger temperature trend of 3 K goes even down to 91 mm/a. Both groundwater recharge (contributing more than two thirds to the total runoff) and direct runoff are affected.

These results were rather insensitive to the four different land use scenarios, but this is due to the marginal share of land that changes its disposition between the scenarios. On the local scale, larger percentages of urbanisation or foresting within a (small) sub-basin would cause larger effects, respectively.

The spatial pattern of discharge contributions follows largely the orography. Most discharge comes from the mountainous regions, and these loose most in absolute numbers under scenario conditions; drastic losses can also be observed for wetlands and water surfaces. In the lowland areas, the latter typically show negative contributions due to exceeding *ET*.

The average potential *ET* depths increase much more during the scenario period (from approx. 780 mm/a in 2004 to approx. 900 mm/a in 2053) compared to the actual *ET*, and single realisation years show no correlation between potential and actual *ET*. The first can be explained by the limited water availability, and the second gives evidence why a complex dynamical model is needed to accurately derive actual evapotranspiration.

Lacking limitation of evapotranspiration from riparian zones and wetlands led to single negative runoff outputs under scenario conditions. But the problem became invisible for most cases by aggregating daily to monthly values, and some negative values are of no relevance for runoff threshold exceedances. A threshold of 101 m^3/s at Dresden, a former reference standard for navigability, would on average be exceeded at only 269 days of the year in the last decade of the 2 K scenario, and there would be only 237 days on average under the 3 K scenario.

The closing discussion starts with the problem of decreasing fidelity of model outputs with decreasing size of sub-areas. The low climate station density in the Czech Republic and the rough geometries of the German soil map are considered uncertainty sources. Differences between idealised land use class parameterisations and real land use peculiarities are also taken into account.

Secondly, the systematic discharge over-estimation of the third validation decade (1991–2000) is discussed. Between 20 and 30 m^3/s of this surplus can be ascribed to decreasing mining activities, but the remaining difference could be related to regional re-dimming, re-filling of accumulated groundwater deficits, and the flooding of abandoned open-cast mines. Especially the re-dimming (increasing radiation due to decreasing aerosol contents after 1989) theory is charming, but uncertain radiation measurements give room for speculation. It has to be admitted that the change of runoff dynamics that occured in the Elbe River basin around 1990 has not been fully understood yet.

The scenario results are discussed in comparison with two similar studies formerly made for the German part of the Elbe River basin. The exact water balance numbers are of course different, but the direction and magnitude of expectable changes towards a drier regime are comparable.

Although some effects like the plant fertilisation by increased atmospheric CO_2 content and the combined reduction of plant transpiration are not covered by the modelling, there is much evidence for a change towards drier conditions.

7.3 CALIBRATING PRECIPITATION OR EVAPOTRANSPIRATION?

The title question of Chapter 3 refers to the choice of parameters for the spatial calibration of the Elbe River basin model. The deviations of simulated hydrographs against reference data (measurements adjusted for anthropogenic management effects) for sub-areas of the model domain can be characterised as combinations of general over- or underestimations (global volume error) and seasonal deviations (seasonality error).

Under 'Materials and Methods' several potential error sources for the spatial calibration are listed. These include short reference time series

and missing stationarity, historic discharge data that have long been invalidated in mining areas, coarse generalisation of riparian zones with high *ET* rates, and lateral fluxes between adjoining sub-catchments.

It is obvious that runoff volume errors can easily be reduced by *ET* adjustments – as have been applied for spatial calibration. But this would not be appropriate if a systematic precipitation bias is the error source. Manipulating the groundwater α-parameters might also fit the model output to observed seasonality patterns, but the same holds for parallel adjustments of *ET* and precipitation corrections: *ET* has a strong seasonality in Central Europe, precipitation has not. But which parameters should be finally optimised?

The basic idea of this investigation is tracing the specific signatures of the error source(s) in the simulation errors. During model calibration, this signature transforms into specific optimum parameter combinations. The aim is to evaluate the individual shares of systematic over- or underestimations of precipitation and *ET* for three Czech sub-catchments.

A maximum likelihood-based Markov Chain Monte Carlo (MCMC) approach was used, and the parameter space was defined by three calibration parameters for precipitation, evapotranspiration, and groundwater discharge. Because the methodology needs several thousand model runs, three sub-catchments in the Czech Republic – where model errors were often larger than in the German part of the basin – were extracted from the Elbe model as independent mini-models: Stará Lhota (Úhlava, 81 km²), Žlutice (Střela, 214 km²), and Chlum Volary (Vltava, 347 km²).

The methodology is rooted in a Bayesian framework, although the prior is an equal distribution throughout the whole positive parameter space. Information about the parameter probability distribution is gathered by formulation of an error model and likelihood calculations for subsequent model runs.

We observed the monthly departures between model output and reality for the two years 2002 (including an extreme flood) and 2003 (including a dry summer with an extreme heat wave) and, because the errors seemed rather normally (Gaussian) distributed, chose the normal distribution as error model. Auto-correlation of the monthly values was negligible.

The MCMC approach samples the probability distribution of the calibration parameters as follows: An initial combination of the calibration parameters is defined deliberately. The model is run and a likelihood value is calculated from the errors. Then the MCMC algorithm jumps to another parameter combination; the jump is driven by (pseudo-)random numbers and follows a pre-defined jump distribution. The model is run again, and if the resulting likelihood is higher than with the former parameter combination, the new position in the parameter space is confirmed as new element of the Markov Chain. Otherwise, the new position is taken at a probability equal to the quotient of the likelihoods.

If that fails, the old position is kept. Thousands of successful jumps form a sample of the target distribution.

To minimise the number of steps needed for a satisfactory sample, the jump distributions were chosen of similar variance as the target distributions. Starting in high-density regions of the target distributions avoided so-called burn-in phases. The Markov Chains were computed up to a length of 10 000 elements for each gauge with the exception of Stará Lhota where two such chains were generated and concatenated afterwards.

The samples of the three-dimensional probability distributions are visualised perspectively and via their one- and two-dimensional marginal distributions. The results are interpreted for each gauge separately:

The distribution for Stará Lhota exposes a dominant density maximum at an evapotranspiration correction factor of 0·6 and a precipitation correction factor of 0·9. Concerning that values of 1·0 would be neutral, *ET* correction seems to be preferrable over precipitation correction. This is confirmed by a remakable density of the distribution for a neutral precipitation correction. However, the correlation between these two parameters is high ($r = 0{\cdot}89$).

A bimodal, tubular distribution results for the gauge Žlutice. The preferred combinations of precipitation and *ET* corrections are oriented along a straight line and highly correlated ($r = 0{\cdot}94$). The modi of the two-dimensional marginal distribution show stronger preferences towards a low increase of *ET* (factor values 1·0–1·2) in combination with practically unchanged precipitation. Alternatively, there is also a certain preference towards precipitation factors of about 1·2 combined with *ET* multipliers around 1·45, but a pure evapotranspiration correction seems most reasonable.

Finally, Chlum Volary shows a global density maximum at an *ET* correction factor of 0·75 and an even lower precipitation multiplier of 0·70. This promotes a general over-estimation of the precipitation input in combination with an over-estimation of actual *ET* calculated by SWIM. More evidence for an upward bias in precipitation is given by the tail of the distribution at the neutral *ET* correction; here, the most probable values for precipitation correction are still around 0·8.

To wrap it up, two gauges (Stará Lhota and Žlutice) confirm the preference of evapotranspiration adjustments for spatial calibration, and one (Chlum Volary) should also have got a precipitation correction. Interestingly, the reason for the obviously biased precipitation data of Chlum Volary can be attributed to a problem in the interpolation of station data:

High precipitation measurements of numerous German weather stations along the crest of the Bohemian Forest biased the interpolation results for adjoining parts of the sparsely instrumented Czech Elbe River basin, including the catchment area of Chlum Volary. Apart from this special effect, the analyses confirm that spatial evapotranspiration

calibration instead of precipitation adjustments had been the measure of choice.

7.4 LAKE EFFECTS ON REGIONAL PRECIPITATION

Some landscape patterns may trigger local convection and alter the precipitation pattern on small scales. Such effects have been observed from atmospherical modelling, but evidence based on station measurements was rare except some studies on urbanised areas.

The flooding of disused open-cast lignite mining areas in Lusatia, creating 60 km² of new water surfaces within two decades, provided an excellent opportunity to trace the effects on precipitation over time. The area of investigation is a square of 110 km × 110 km, adjoining the borders of Poland and the Czech Republic. The new water surfaces are clustered around the diagonal from the northwest to the southeast, and there are 25 precipitation stations in the domain whose data are used in this study. Typical values of mean annual precipitation range from 550 mm/a in the northwestern corner to 800 mm/a at the southern edge, correlated with elevation.

In an explanatory analysis, annual precipitation sums of two groups consisting of five rain gauge stations each have been compared. One group is located in the northwest and the other one in the southeast, downwind the emerging lakes. Transforming the first time series onto the level and variance of the other makes it easier to discriminate the deviating development: within the last 10–15 years of the analysis (the overall time frame is 1951–2002), both water surface area and the difference of the smoothed precipitation time series increase simultaneously. The water surfaces enlarged by said 60 km², and the precipitation bias amounts on average to about 20 mm/a. However, the magnitude of precipitation change is clearly below the annual variability; therefore this needs not be a cause–effect relationship but could also be due to a Hurst effect.

The main analysis is a spatial trend analysis on the precipitation measurements of all 25 stations. Because precipitation is highly variable over space and time, a special methodology had been used to separate the local influences on the measurements:

Principal Component Analysis (PCA) has been applied to all station time series. The values of the first principal component time series were taken as regional measure of precipitation. This general intensity measure was then used as independent variable to compute linear regressions with the individual station measurements. The residuals of these fits were taken als station deviations from the common dynamics of all time series – the signals of local changes within the area are thought to be contained here. The linear time-trends of residuals were therefore calculated and their significances checked by non-parametric

tests. The trend estimates were spatially interpolated and mapped. This methodology was also applied to seasonal subsets of the data.

The special value of PCA in this context is that it preserves the dominating common dynamics from different stations much better through the first component than simple averaging would do; deviating patterns from single stations would be mapped to higher order components. In our case, the first principal component explains 71 % of the total variance which gives evidence to the assumption of a common background dynamics throughout the region.

The residuals of any single station time series against their linear regression on the first principal component are heavy-tailed distributions, and no trend can be spotted from their plot. However, respective trends could be calculated; they are further referred to as 'trend anomalies' for not confusing them with the linear trends of raw measurement data. The statistical tests indicated significant trend anomalies at the 95 %-level for nine stations and at the 99·9 %-level for five stations. Apart from one exception, only negative anomalies were found to be significant.

Further research showed that these trend anomalies are largely due to increased convective (thunder-)storm activities during summer. The increasing numbers of such events with anomalies of more than 5 mm/d turned out to be extremely significant.

A contour map of the interpolated anomalies shows a larger area of upward trends with maximal values of more than 2 mm/a along the southern side of the southeastern part of the belt of lakes. A single station located about 20 km west of the map centre (Peickwitz) produced a somehow isolated, strong negative anomaly. The southeastward shift of the area with relatively increasing precipitation compared to the belt of flooded mining holes supports the hypothesis of local evaporation recycling, because the main wind direction at height is northwest.

Seasonal plots of the spatial trends show that the basic pattern of decreases in the northwest and increases in the southeast of the map persists throughout the year, but the polarisation is by far strongest in summer – the season of convective storm events.

Finally, a rough water balance estimation further supports the idea of local water recycling: An area of 2000 km^2 received an average precipitation increase of 1 mm/a while the flooding process changed 3·2 km^2 per year from land to water. This would equal 625 mm/a of additional evaporation from all flooded surfaces, which is just a bit higher than what could be expected from complete recycling. However, an other effect seems more plausible due to the increase in convective storms: The lake pattern triggers local convection, thus increasing precipitation and draining the atmosphere of water transported from remote regions.

The concluding remarks of this chapter are not related to the obvious consequences for small-scale meteorological or spatially distributed

hydrological modelling, because I had not been confronted with the problems of sub-basin model fidelity at the time of writing. Discussed are the implications for landscape planning: new water surfaces are often welcomed, but neither an increase of thunderstorm activity nor extensive evaporation losses are positive effects and have to be considered.

7.5 THREE PERCEPTIONS OF THE EVAPOTRANSPIRATION LANDSCAPE

Chapter 5 starts with a description of the principal problem of comparably large simulation errors for sub-basin discharges in distributed hydrological modelling. Spatial calibration is seen as promising method to overcome these shortcomings by increasing model representativeness in space. An independent mapping of the evapotranspiration (*ET*) pattern through remote sensing (RS) is seen as promising independent data source for this objective.

A glimpse into the literature about RS in hydrological modelling gives some examples of successful applications. There are many examples comparing or assimilating *ET* estimations.

The objective of this study is therefore chosen more generally: not just another spatial calibration but to reveal deficiencies of model and input data. Three evapotranspiration (*ET*) derivations – from the model SWIM, from remotely sensed surface temperatures, and from the gauged water balance in sub-catchments – are to be compared. Finally, the feasibility of the temperature-based approach and its value for model calibration is subject of the research.

The three methods of *ET* estimation are presented in detail. First, the basic concepts and the *ET* calculus of SWIM are described. This is based on the Turc-Ivanov approach using daily mean temperature, net radiation, and relative humidity on cold days. The resulting potential *ET* is input to the computation of actual soil evaporation and plant transpiration which further depend on leaf area index (*LAI*) and soil water availability.

The approach for estimating *ET* on land surface temperatures is based on the energy balance at the Earth surface: The diurnal or annual net radiation R_n equals the sum of latent and sensible heat $\lambda ET + H$. To obtain *ET*, net radiation and the Bowen ratio have to be computed. The former is routinely calculated by SWIM, but the latter depends on the aerodynamic resistance for heat and is harder to determine. Back-calculating from the *ET* area averages – either taken from SWIM for the forested and the non-forested parts of the basin or from water balance calculations in sub-basins with known forest share – seems the best way for approximations.

The classical water balance calculation needs long-term precipitation and runoff measurements for a well-defined catchment area, but

the results may also be biased from measurement uncertainties and groundwater exchanges between neighbouring sub-catchments.

The 134 890 km² of the Elbe River basin simulated by SWIM and the years 2001–2003 were used for comparison. The simulated *ET* averages were 638 mm/a for the 42 590 km² of forested areas and 511 mm/a for the 92 300 km² of non-forested areas. For the RS-based approach, land surface temperature (LST) maps were evaluated. The aerodynamic resistances were found to be in the range of 85–104 s/m; they are in the order of magnitude reported by many other authors.

The practical application of the remote sensing approach depends on the LST maps: They were readily available through a web interface by the German DLR Applied Remote Sensing Cluster and were made from thermal imagery of the NOAA AVHRR satellites. Both daylight and nighttime overpasses yield two maps per day; this study utilises all 944 daytime LST maps of the years 2001–2003.

These maps were reprojected onto the hydrotope map in order to calculate the mean surface temperature for each (completely cloud free) hydrotope. Because there were many days with cloud pixels in many hydrotopes, an effective temperature gradient for each hydrotope was calculated assuming a mean attenuation factor of $\eta = 0{\cdot}33$ of the cloud layer. The resulting *ET* pattern was rather insensitive to the choice of η.

A map of the effective temperature gradients shows values close to zero for mountainous regions, wetlands, or regions with many lakes while the most extreme gradients were determined for lowland areas in the north of the Czech Republic – probably an artifact due to the sparseness of climate station data in that region.

The comparisons of the sub-basin evapotranspiration depths show a smaller variance of the SWIM output compared to the results from the remote sensing approach and those from the ground based water balance method. The latter two are only weakly correlated to the SWIM results (r values of 0·32 and 0·25) and have practically no correlation between themselves.

In order to shed light onto the reasons for the lacking correlation, the sub-basins with the most extreme divergences between the two estimates had been marked in a map: they appeared to be situated entirely in the Czech part of the basin. Sub-basins with low remotely sensed *ET* and medium to high water balance estimations were located in the lower parts of the basin, and the opposite combination was found for sub-basins in the mountaineous regions. The low climate station density in this part of the basin was very likely the cause for the obviously biased results. The remaining noise of the remote sensing results is in the range observed by several recent studies.

Accordingly, the subset of German sub-basins shows higher correlations, especially between remotely sensed and SWIM model results ($r = 0{\cdot}61$). A further analysis of extreme outliers revealed strong deviations for intermediate areas in the course of large rivers with high

discharges due to respectively high absolute gauging errors. The water balance method is not applicable for such cases.

Finally, the effects of extensive groundwater pumping for open-cast lignite mining or flooding of disused mining pits can be blamed for some shifts in the water balance estimations of affected sub-basins. A related problem are probable groundwater exchanges between sub-basins. Therefore, this study concludes that the water balance approach does not seem to be more exact than the other two methods. The concept of 'ground truth' is questionable given the relatively high agreement between remote sensing and model estimations.

The possible error sources are grouped into aleatoric and epistemic uncertainties (a concept critisized in the final Discussion chapter). Data assimilation or fusion frameworks do not really help to minimise the errors, because they just interpolate between different perceptions of reality, hence their results may remain biased.

The final recommendations are that remote sensing information should always be utilised for distributed hydrological modelling, and that research into the reasons for individual deviations – gathering local knowledge – is essential for realistic simulations in space. It is really the "learning about places" (Beven) which is needed more than new theories or models.

7.6 DISCUSSION

The first and primary research question of this thesis is how to deal with the uncertainties in distributed hydrological modelling. Which ideas do the papers that make up Chapters 2–5 provide, especially regarding the sub-basin level?

Other introductory questions have been answered by the individual contributions: Chapter 4 confirmed that precipitation is locally influenced by the landscape; the proposed non-conventional way of using PCA was effective for trend detection within the noisy signal of daily precipiation measurements. And Chapters 5 showed the feasability of the proposed method using remotely sensed LST maps as third alternative for estimating sub-basin *ET*.

Regarding the principal question, eleven different reasons for model–reality runoff deviations on the sub-basin level that have been named in the five preceding chapters are listed. The list contains flaws in the spatial calibration, especially the assumption of stationarity, interpolation errors due to the inverse-distance method applied to inequally spaced input stations, neglected lateral water fluxes, and many more reasons.

The importance of the interpolation method is shown by a comparison of the inverse distance method and kriging applied on the example of annual precipitation depths. The systematic precipitation bias for some sub-basins near the Czech-German boundary, hypothesised in Chapter 3,

could be confirmed, and alerting differences between the interpolation methods exceeding 200 mm/a in both directions are shown in a map.

Another example, the probability for groundwater transfers, is investigated for the brook Verlorenwasser ('Lost Water') at the northern edge of the Fläming moraine ridge. Although no tracer test could be made, analysis of relief and discharge contributions give evidence for groundwater losses into the Temnitz catchment area. Further confirmation can be taken from a modelling study on the Federal State of Brandenburg where practically the same conclusions are drawn for similar catchments, also located between Fläming and the Baruth glacial valley.

The next section deals with the concept of aleatoric, epistemic, and ontologic uncertainties. While epistemic error sources could be remediated by more research, aleatoric errors have to be accepted as irreducible system noise. Some researchers differentiate also ontologic uncertainties from error sources yet unknown.

Stepping through the above list of error sources or reasons for uncertainty in sub-basin discharge modelling, only epistemic uncertainties can be identified. Although the list is ordered in that way that the first points would have been easily addressed (e. g. by using kriging instead of inverse distance interpolation), the higher numbers should also be mitigable by extensive research efforts. The concept of aleatoric uncertainty seems only valid for stochastical models that deal with probabilites, not process representations, and error sources yet unknown (ontologic uncertainties) can possibly be identified by even more research, so they are finally epistemic, too.

The finding that doing more and better research could further increase model fidelity leads to the idea of diminishing marginal uncertainty reductions. In analogy to the economic model of diminishing marginal returns, the progress in hydrologic modelling will decrease with increasing research efforts. But the question is, whether the potential for model enhancements in larger basins can be utilised within the limitations of a typical three years research project and whether the project team are aware of further research needs and model enhancement potentials at the end of the project run time.

Long-term research is indeed needed because large scale projects like GLOWA-Elbe regularly lack process knowledge on the sub-basin scale, and this lack of knowledge is the real limitation for distributed model fidelity.

BIBLIOGRAPHY

Abbott, M. B. & J. C. Refsgaard (1996): Foreword. In: *Distributed Hydrological Modelling*, edited by M. B. Abbott & J. C. Refsgaard, volume 22 of *Water Science and Technology Library*, pages vii–ix. Kluwer Academic Publishers, Dordrecht, The Netherlands. ISBN 0-7923-4042-6. (Cited on pages 134 and 135.)

Abbott, M. B., J. C. Bathurst, J. A. Cunge, P. E. O'Connell & J. Rasmussen (1986a): An introduction to the European Hydrological System – Système Hydrologique Européen, "SHE", 1: History and philosophy of a physically-based, distributed modelling system. *Journal of Hydrology* 87 (1–2): 45–59. doi:10.1016/0022-1694(86)90114-9. (Cited on page 7.)

Abbott, M. B., J. C. Bathurst, J. A. Cunge, P. E. O'Connell & J. Rasmussen (1986b): An introduction to the European Hydrological System – Système Hydrologique Européen, "SHE", 2: Structure of a physically-based, distributed modelling system. *Journal of Hydrology* 87 (1–2): 61–77. doi:10.1016/0022-1694(86)90115-0. (Cited on page 7.)

Ajami, N. K., H. Gupta, T. Wagener & S. Sorooshian (2004): Calibration of a semi-distributed hydrologic model for streamflow estimation along a river system. *Journal of Hydrology* 298 (1–4): 112–135. doi:10.1016/j.jhydrol.2004.03.033. (Cited on page 93.)

Ajami, N. K., Q. Duan & S. Sorooshian (2007): An integrated hydrologic Bayesian multimodel combination framework: Confronting input, parameter, and model structural uncertainty in hydrologic prediction. *Water Resources Research* 43 (1): W01 403. doi:10.1029/2005WR004745. (Cited on page 63.)

Albertz, J. (1991): *Grundlagen der Interpretation von Luft- und Satellitenbildern*. Wissenschaftliche Buchgesellschaft, Darmstadt. ISBN 3-534-07838-1, 204 pages. (Cited on page 102.)

Andersen, J., J. C. Refsgaard & K. H. Jensen (2001): Distributed hydrological modelling of the Senegal River Basin – model construction and validation. *Journal of Hydrology* 247 (3–4): 200–214. doi:10.1016/S0022-1694(01)00384-5. (Cited on pages 28, 54, and 93.)

Andréassian, V., J. Lerat, C. Loumagne, T. Mathevet, C. Michel, L. Oudin & C. Perrin (2007): What is really undermining hydrologic science today? *Hydrological Processes* 21 (20): 2819–2822. doi:10.1002/hyp.6854. (Cited on page 95.)

Andréassian, V., N. Le Moine, C. Perrin, M.-H. Ramos, L. Oudin, T. Mathevet, J. Lerat & L. Berthet (2012): All that glitters is not gold: the case of calibrating hydrological models. *Hydrological Processes* 26 (14): 2206–2210. doi:10.1002/hyp.9264. (Cited on page 95.)

Apel, H., A. H. Thieken, B. Merz & G. Blöschl (2004): Flood risk assessment and associated uncertainty. *Natural Hazards and Earth System Sciences* 4 (2): 295–308. doi:10.5194/nhess-4-295-2004. (Cited on page 131.)

Arnold, J. G., P. M. Allen & G. Bernhardt (1993): A comprehensive surface-groundwater flow model. *Journal of Hydrology* 142 (1–4): 47–69. doi:10.1016/0022-1694(93)90004-S. (Cited on pages 7, 29, 56, and 99.)

Arnold, J. G., R. Srinivasan, R. S. Muttiah & J. R. Williams (1998): Large area hydrologic modeling and assessment Part I: Model development. *Journal of the American Water Resources Association* 34 (1): 73–89. doi:10.1111/j.1752-1688.1998.tb05961.x. (Cited on pages 29, 56, and 99.)

Arnold, J. G., R. Srinivasan, R. S. Muttiah & P. M. Allen (1999): Continental scale simulation of the hydrologic balance. *Journal of the American Water Resources Association* 35 (5): 1037–1051. ISSN 1093-474X. (Cited on page 46.)

Artinyan, E., F. Habets, J. Noilhan, E. Ledoux, D. Dimitrov, E. Martin & P. L. Moigne (2008): Modelling the water budget and the riverflows of the Maritsa basin in Bulgaria. *Hydrology and Earth System Sciences* 12 (1): 21–37. doi:10.5194/hess-12-21-2008. (Cited on pages 28 and 54.)

Atkinson, B. W. (1968): A preliminary examination of the possible effect of London's urban area on the distribution of thunder rainfall 1951–60. *Transactions of the Institute of British Geographers* 44: 97–118. (Cited on page 72.)

ATV-DVWK (2002): *Verdunstung in Bezug zu Landnutzung, Bewuchs und Boden*. DWA-Merkblatt ATV-DVWK-M 504, DWA Deutsche Vereinigung für Wasserwirtschaft, Abwasser und Abfall e.V., Hennef. (Cited on pages 30, 56, and 100.)

Baidya Roy, S. & R. Avissar (2002): Impact of land use / land cover change of regional hydrometeorology in Amazonia. *Journal of Geophysical Research – Atmospheres* 107 (D20): 8037. doi:10.1029/2000JD000266. (Cited on page 71.)

Bastiaanssen, W. G. M., M. Menenti, R. A. Feddes & A. A. M. Holtslag (1998a): A remote sensing surface engergy balance algorithm for land (SEBAL). 1. Formulation. *Journal of Hydrology* 212–213: 198–212. doi:10.1016/S0022-1694(98)00253-4. (Cited on pages 20, 96, 101, and 121.)

Bastiaanssen, W. G. M., H. Pelgrum, J. Wang, Y. Ma, J. F. Moreno, G. J. Roerink & T. van der Wal (1998b): A remote sensing surface engergy balance algorithm for land (SEBAL). 2. Validation. *Journal of Hydrology* 212–213: 213–229. doi:10.1016/S0022-1694(98)00254-6. (Cited on pages 96, 101, and 121.)

Becker, F. & Z. L. Li (1990): Towards a local split method over land surfaces. *International Journal of Remote Sensing* 11 (3): 369–393. doi:10.1080/01431169008955028. (Cited on page 107.)

Bekele, E. G. & J. W. Nicklow (2007): Multi-objective automatic calibration of SWAT using NSGA-II. *Journal of Hydrology* 341 (3–4): 165–176. doi:10.1016/j.jhydrol.2007.05.014. (Cited on pages 28 and 54.)

Bergström, S. & A. Forsman (1973): Development of a conceptual deterministic rainfall-runoff model. *Nordic Hydrology* 4 (3): 147–170. doi:10.2166/nh.1973.012. (Cited on page 7.)

Bergström, S. & L. P. Graham (1998): On the scale problem in hydrological modelling. *Journal of Hydrology* 211 (1–4): 253–265. doi:10.1016/S0022-1694(98)00248-0. (Cited on page 93.)

Berkner, A. (1989): Braunkohlenbergbau, Landschaftsdynamik und territoriale Folgewirkungen in der DDR. *Petermanns Geographische Mitteilungen* 3: 173–190. (Cited on page 74.)

Bernard, M. (1937): Giving areal significance to hydrological research on small areas. In: *Headwaters Control and Use: A Summary of Fundamental Principles and Their Application in the Conservation and Utilization of Waters and Soils Throughout Headwater Areas. Papers presented at the Upstream Engineering Conference, held in Washington, D.C., September 22 and 23, 1936*, pages 50–75. Soil Conservation Service and Forest Service of the United States Department of Agriculture with the cooperation of Rural Electrification Administration, U.S. Government Printing Office, Washington D.C. URL http://babel.hathitrust.org/cgi/pt?id=mdp.39015024264510. Last accessed in October 2012. (Cited on page 7.)

Beven, K. (1989): Changing ideas in hydrology – The case of physically-based models. *Journal of Hydrology* 105 (1–2): 157–172. doi:10.1016/0022-1694(89)90101-7. (Cited on pages 8 and 95.)

Beven, K. (1993): Prophecy, reality and uncertainty in distributed hydrological modelling. *Advances in Water Resources* 16 (1): 41–51. doi:10.1016/0309-1708(93)90028-E. (Cited on page 66.)

Beven, K. (1996): The limits of splitting: Hydrology. *The Science of the Total Environment* 183 (1–2): 89–97. doi:10.1016/0048-9697(95)04964-9. (Cited on pages 95 and 96.)

Beven, K. (2001): How far can we go in distributed hydrological modelling? *Hydrology and Earth System Sciences* 5 (1): 1–12. doi:10.5194/hess-5-1-2001. 2001 EGS Dalton Lecture. (Cited on pages 96 and 121.)

Beven, K. (2006): A manifesto for the equifinality thesis. *Journal of Hydrology* 320 (1–2): 18–36. doi:10.1016/j.jhydrol.2005.07.007. (Cited on pages 66 and 134.)

Beven, K. (2007): Towards integrated environmental models of everywhere: uncertainty, data and modelling as a learning process. *Hydrology and Earth System Sciences* 11 (1): 460–467. doi:10.5194/hess-11-460-2007. (Cited on page 121.)

Beven, K. & A. Binley (1992): The future of distributed models: Model calibration and uncertainty prediction. *Hydrological Processes* 6 (3): 279–298. doi:10.1002/hyp.3360060305. (Cited on pages 55 and 62.)

Beven, K., P. J. Smith & A. Wood (2011): On the colour and spin of epistemic error (and what we might do about it). *Hydrology and Earth System Sciences* 15 (10): 3123–3133. doi:10.5194/hess-15-3123-2011. (Cited on page 131.)

Beven, K. J. (2003): On environmental models of everywhere on the GRID. *Hydrological Processes* 17 (1): 171–174. doi:10.1002/hyp.5090. (Cited on pages 121 and 136.)

Beven, K. J. & M. J. Kirkby (1979): A physically based, variable contributing area model of basin hydrology / un modèle à base physique de zone d'appel variable de l'hydrologie du bassin versant. *Hydrological Sciences Bulletin* 24 (1): 43–69. doi:10.1080/02626667909491834. (Cited on pages 7 and 55.)

Biemelt, D. (2001): *Bestimmung der Grundwasserneubildung auf Offenlandbereichen der Lausitzer Bergbaufolgelandschaft*. Ph.D. thesis, BTU Cottbus, Fakultät Umweltwissenschaften und Verfahrenstechnik. (Cited on page 91.)

Bilbao, J. & A. H. D. Miguel (2007): Estimation of daylight downward longwave atmospheric irradiance under clear-sky and all-sky conditions. *Journal of Applied Meteorology and Climatology* 46 (6): 878–889. doi:10.1175/JAM2503.1. (Cited on page 103.)

Blazejczak, J., M. Gornig & E. Schulz (2013): Szenarien zur Demografie und Ökonomie in der Elbe-Region. In: *Die Elbe und ihr Einzugsgebiet im globalen Wandel*, edited by F. Wechsung, V. Hartje, S. Kaden, M. Venohr, B. Hansjürgens & P. Gräfe, chapter 2.5. Weißensee Verlag, Berlin. In press. (Cited on page 38.)

Blobel, V. & E. Lohrmann (1989): *Statistische und numerische Methoden der Datenanalyse*. Teubner, Stuttgart. ISBN 3-519-03243-0, 358 pages. (Cited on page 34.)

Blöschl, G. (2001): Scaling in hydrology. *Hydrological Processes* 15 (4): 709–711. doi:10.1002/hyp.432. (Cited on page 95.)

Boegh, E., M. Thorsen, M. B. Butts, S. Hansen, J. S. Christiansen, P. Abrahamsen, C. B. Hasager, N. O. Jensen, P. van der Keur, J. C. Refsgaard, K. Schelde, H. Soegaard & A. Thomsen (2004): Incorporating remote sensing data in physically based distributed agro-hydrological modelling. *Journal of Hydrology* 287 (1–4): 279–299. doi:10.1016/j.jhydrol.2003.10.018. (Cited on pages 96 and 116.)

Bosilovich, M. & S. Schubert (2002): Water vapor tracers as diagnostics of the regional hydrologic cycle. *Journal of Hydrometeorology* 3 (2): 149–165. doi:10.1175/1525-7541(2002)003<0149:WVTADO>2.0.CO;2. (Cited on page 73.)

Bossard, M., J. Feranec & J. Otahel (2000): *Corine land cover technical guide – Addendum 2000*. Technical Report 40, European Environmental Agency, Copenhagen, Denmark. URL http://www.eea.europa.eu/publications/tech40add/at_download/file. Last accessed in October 2012. (Cited on pages 11, 29, 57, and 74.)

Bowen, I. S. (1926a): *The ratio of heat losses by conduction and evaporation from any water surface*. Ph.D. thesis, California Institute of Technology, Pasadena, CA. 12 pp. (Cited on page 103.)

Bowen, I. S. (1926b): The ratio of heat losses by conduction and evaporation from any water surface. *Physical Review* 27 (6): 779–787. doi:10.1103/PhysRev.27.779. (Cited on page 103.)

Brocca, L., T. Moramarco, F. Melone, W. Wagner, S. Hasenauer & S. Hahn (2012): Assimilation of surface- and root-zone ASCAT soil moisture products into rainfall-runoff modeling. *IEEE Transactions on Geoscience and Remote Sensing* 50 (7, Part 1): 2542–2555. doi:10.1109/TGRS.2011.2177468. (Cited on page 21.)

Bronstert, A., J. Carrera, P. Kabat & S. Lütkemeier (editors) (2005): *Coupled Models for the Hydrological Cycle – Integrating Atmosphere, Biosphere, and Pedosphere*. Springer, Berlin, Heidelberg, New York. ISBN 978-3-540-22371-9, XX + 346 pages. (Cited on page 92.)

Bronstert, A., A. Bardossy, C. Bismuth, H. Buiteveld, M. Disse, H. Engel, U. Fritsch, Y. Hundecha, R. Lammersen, D. Niehoff & N. Ritter (2007): Multi-scale modelling of land-use change and river training aspects on floods in the rhine basin. *River Research and Applications* 23 (10): 1102–1125. doi:10.1002/rra.1036. Erratum: *River Research and Applications* 24 (3) 353, doi:10.1002/rra.1074. (Cited on page 95.)

Brunsell, N. A., J. M. Ham & C. E. Owensby (2008): Assessing the multi-resolution information content of remotely sensed variables and elevation for evapotranspiration in a tall-grass prairie environment. *Remote Sensing of Environment* 112 (6): 2977–2987. doi:10.1016/j.rse.2008.02.002. (Cited on page 116.)

Brunt, D. (1932): Notes on radiation in the atmosphere. I. *Quarterly Journal of the Royal Meteorological Society* 58 (247): 389–418. doi:10.1002/qj.49705824704. (Cited on page 103.)

Brutsaert, W. (1982): *Evaporation into the atmosphere – Theory, History, and Applications*. Kluver Academic Publishers, Dordrecht. ISBN 9027712476, 316 pages. (Cited on page 104.)

Bultot, F. & G. L. Dupriez (1976): Conceptual hydrological model for an average-sized catchment area, II. Estimate of parameters, validity of model, applications. *Journal of Hydrology* 29 (3–4): 273–292. doi:10.1016/0022-1694(76)90041-X. (Cited on page 55.)

Burian, S. J. & J. M. Shepherd (2005): Effect of urbanization on the diurnal rainfall pattern in Houston. *Hydrological Processes* 19: 1089–1103. doi:10.1002/hyp.5647. (Cited on page 72.)

Büttner, G., J. Feranec & G. Jaffrain (2002): *Corine land cover update 2000*. Technical Report 89, European Environmental Agency, Copenhagen. URL http://edz.bib.uni-mannheim.de/daten/edz-bn/eua/02/techrep89.pdf. Last accessed in October 2012. (Cited on page 74.)

de C. Teixeira, A. H., W. G. M. Bastiaanssen, M. D. Ahmad & M. G. Bos (2009): Reviewing SEBAL input parameters for assessing evapotranspiration and water productivity for the Low-Middle São Francisco River basin, Brazil – Part A: Calibration and validation. *Agricultural and Forest Meteorology* 149 (3–4): 462–476. doi:10.1016/j.agrformet.2008.09.016. (Cited on page 116.)

Cao, W. Z., W. B. Bowden, T. Davie & A. Fenemor (2006): Multi-variable and multi-site calibration and validation of SWAT in a large mountainous catchment with high spatial variability. *Hydrological Processes* 20 (5): 1057–1073. doi:10.1002/hyp.5933. (Cited on pages 28 and 54.)

CEC (1995): *Corine Land Cover*. Technical report, Commission of the European Communities, Luxemburg. URL http://www.eea.europa.eu/publications/COR0-landcover/at_download/file. Last accessed in October 2012. (Cited on pages 11, 29, and 57.)

Changnon, S. A., Jr (1980): Evidence of urban and lake influences on precipitation in the Chicago area (US). *Journal of Applied Meteorology* 19 (10): 1137–1159. doi:10.1175/1520-0450(1980)019<1137:EOUALI>2.0.CO;2. (Cited on page 72.)

Changnon, S. A., Jr & F. A. Huff (1986): The urban-related nocturnal rainfall anomaly at St. Louis. *Journal of Applied Meteorology* 25 (12): 1985–1995. doi:10.1175/1520-0450(1986)025<1985:TURNRA>2.0.CO;2. (Cited on page 72.)

Cheng, S. J. (2011): The best relationship between lumped hydrograph parameters and urbanized factors. *Natural Hazards* 56 (3): 853–867. doi:10.1007/s11069-010-9596-4. (Cited on page 51.)

Choi, M., J. M. Jacobs & W. P. Kustas (2008): Assessment of clear and cloudy sky parameterizations for daily downwelling longwave radiation over different land surfaces in Florida, USA. *Geophysical Research Letters* 35 (20): L20 402. doi:10.1029/2008GL035731. (Cited on page 103.)

Clark, D., C. Taylor & A. Thorpe (2004): Feedback between the land surface and rainfall at convective length scales. *Journal of Hydrometeorology* 5 (4): 625–639. doi:10.1175/1525-7541(2004)005<0625:FBTLSA>2.0.CO;2. (Cited on page 71.)

Cole, C. A., C. P. Cirmo, D. H. Wardrop, R. P. Brooks & J. Peterson-Smith (2008): Transferability of an HGM wetland classification scheme to a longitudinal gradient of the central Appalachian Mountains: Initial hydrological results. *Wetlands* 28 (2): 439–449. ISSN 0277-5212. (Cited on page 34.)

Conradt, T., Z. W. Kundzewicz, F. Hattermann & F. Wechsung (2007): Measured effects of new lake surfaces on regional precipitation. *Hydrological Sciences Journal* 52 (5): 936–955. doi:10.1623/hysj.52.5.936. (Cited on page 99.)

Conradt, T., F. F. Hattermann, H. Koch & F. Wechsung (2012a): Precipitation or evapotranspiration? Bayesian analysis of potential error sources in the simulation of sub-basin discharges in the Czech Elbe River basin. *Regional Environmental Change* 12 (3): 649–661. doi:10.1007/s10113-012-0280-y. (Cited on pages 28, 46, 95, and 119.)

Conradt, T., H. Koch, F. F. Hattermann & F. Wechsung (2012b): Spatially differentiated management-revised discharge scenarios for an integrated analysis of multi-realisation climate and land use scenarios for the Elbe River basin. *Regional Environmental Change* 12 (3): 633–648. doi:10.1007/s10113-012-0279-4. (Cited on pages 54, 56, 57, 94, 95, 118, and 119.)

Conradt, T., H. Koch, F. F. Hattermann & F. Wechsung (2013a): Szenariosimulationen des Wasserabflusses. In: *Die Elbe und ihr Einzugsgebiet im globalen Wandel*, edited by F. Wechsung, V. Hartje, S. Kaden, M. Venohr, B. Hansjürgens & P. Gräfe, chapter 2.3. Weißensee Verlag, Berlin. In press. (Cited on pages 54, 94, and 119.)

Conradt, T., H. Koch, F. F. Hattermann & F. Wechsung (2013b): Validierung von Lokalkorrekturen der Verdunstung bei den Szenariosimulationen des Wasserabflusses. In: *Die Elbe und ihr Einzugsgebiet im globalen Wandel*, edited by F. Wechsung, V. Hartje, S. Kaden, M. Venohr, B. Hansjürgens & P. Gräfe, chapter 2.4. Weißensee Verlag, Berlin. In press. (Cited on pages 46 and 119.)

Conradt, T., F. Wechsung & A. Bronstert (2013c): Three perceptions of reality – Comparing spatial patterns of evapotranspiration from a distributed hydrological model, remotely sensed surface temperatures, and sub-basin water balances. *Hydrology and Environmental System Sciences* (Chapter 5, submitted).

Cooley, H. S., W. J. Riley, M. S. Torn & Y. He (2005): Impact of agricultural practice on regional climate in a coupled land surface mesoscale model. *Journal of Geophysical Research – Atmospheres* 110 (D03113): 10 pp. doi:10.1029/2004JD005160. (Cited on page 71.)

Cowles, M. K. & B. P. Carlin (1996): Markov chain Monte Carlo convergence diagnostics: a comparative review. *Journal of the American Statistical Association* 91 (434): 883–904. URL http://www.jstor.org/stable/2291683. (Cited on page 63.)

Cramer, W., F. Wechsung & P. Gräfe (2005): GLOWA-Elbe II – Project I: Project integration and coordination. In: GLOWA – *Global change in the Hydrological Cycle: Status Report 2005*, pages 70–73. PT-DLR Environmental Research and Technology – Project management organization on behalf of the Federal Ministry of Education and Research, Bonn. URL http://www.glowa-elbe.de/pdf/glowa-statusreport_en.pdf. Last accessed in March 2012. (Cited on page 2.)

Das, T., A. Bárdossy, E. Zehe & Y. He (2008): Comparison of conceptual model performance using different representations of spatial variability. *Journal of Hydrology* 356 (1–2): 106–118. doi:10.1016/j.jhydrol.2007.11.017. (Cited on page 93.)

Day, P. (1926): Precipitation in the drainage area of the Great Lakes, 1875–1924. *Monthly Weather Review* 54 (3): 85–106. (Cited on page 72.)

DeMarchi, C., F. Xing, T. Croley, C. He & Y. Wang (2011): Application of a distributed large basin runoff model to Lake Erie: Model calibration and analysis of parameter spatial variation. *Journal of Hydrologic Engineering* 16 (3): 193–202. doi:10.1061/(ASCE)HE.1943-5584.0000304. (Cited on page 95.)

DGJ (1995a): volume 1990 (1.11.1989–31.12.1990) of *Deutsches Gewässerkundliches Jahrbuch – Elbegebiet, Teil I: Von der Grenze der CR bis zur*

Havelmündung. Landesamt für Umweltschutz Sachsen Anhalt, Halle/Saale. (Cited on pages 58 and 191.)

DGJ (1995b): volume 1990 (1.11.1989–31.12.1990) of *Deutsches Gewässerkundliches Jahrbuch – Elbegebiet, Teil II: Havel mit deutschem Odergebiet*. Landesumweltamt Brandenburg, Potsdam. (Cited on pages 58 and 191.)

DGJ (1995c): volume 1990 (1.11.1989–31.12.1990) of *Deutsches Gewässerkundliches Jahrbuch – Elbegebiet, Teil III: Untere Elbe*. Freie und Hansestadt Hamburg, Wirtschaftsbehörde Strom- und Hafenbau. (Cited on pages 58 and 191.)

DGJ (2007): volume 1998 (1.11.1997–31.12.1998) of *Deutsches Gewässerkundliches Jahrbuch – Elbegebiet, Teil II: Havel mit deutschem Odergebiet*. Landesumweltamt Brandenburg, Potsdam. (Cited on page 130.)

Dietrich, O., S. Schweigert & J. Steidl (2008): Impact of climate change on the water balance of fen wetlands in the Elbe Lowland. In: *After wise use – the future of peatlands*, edited by C. Farrell & J. Feehan, volume 1 of *Proceedings of the 13th international peat congress, Tullamore, Ireland, 8–13 June 2008*, pages 32–35. International Peat Society, Jyväskylä, Finland. ISBN 0-9514890-4-6. (Cited on page 26.)

Dietrich, O., J. Steidl & D. Pavlik (2012): The impact of global change on the water balance of large wetlands in the Elbe Lowland. *Regional Environmental Change* 12 (4): 701–713. doi:10.1007/s10113-012-0286-5. (Cited on page 26.)

Dietrich, O., D. Pavlik, S. Schweigert & J. Steidl (2013): Wasserhaushalt großer Feuchtgebiete im Elbe-Tiefland. In: *Die Elbe und ihr Einzugsgebiet im globalen Wandel*, edited by F. Wechsung, V. Hartje, S. Kaden, M. Venohr, B. Hansjürgens & P. Gräfe, chapter 3.3. Weißensee Verlag, Berlin. In press. (Cited on page 26.)

van Dijk, A. I. J. M. & L. J. Renzullo (2011): Water resource monitoring systems and the role of satellite observations. *Hydrology and Earth System Sciences* 15 (1): 39–55. doi:10.5194/hess-15-39-2011. (Cited on page 96.)

Dixon, P. G. & T. L. Mote (2003): Patterns and causes of Atlanta's urban heat island-initiated precipitation. *Journal of Applied Meteorology* 42 (9): 1273–1284. doi:10.1175/1520-0450(2003)042<1273:PACOAU>2.0.CO;2. (Cited on page 72.)

Doherty, J. (2004): *PEST Model-Independent Parameter Estimation*. User manual, Watermark Numerical Computing. URL http://www.pesthomepage.org/getfiles.php?file=pestman.pdf. Last accessed in February 2012. (Cited on page 34.)

Dooge, C. I., James (1977): Problems and methods of rainfall-runoff modelling. In: *Mathematical Models for Surface Water Hydrology*, edited by T. A. Ciriani, U. Maione & J. R. Wallis, pages 71–108. John Wiley & Sons, London, New York, Sydney, and Toronto. ISBN 0-471-99400-6. Proceedings of the Workshop held at the IBM Scientific Center, Pisa, Italy (December 9–12, 1974). (Cited on page 136.)

Doorenbos, J. & W. O. Pruitt (1977): *Guidelines for predicting crop water requirements*. Number 24 in FAO irrigation and drainage papers. Food and Agriculture Organisation of the United Nations, Rome, revised edition. ISBN 9251002797, 144 pages. (Cited on page 103.)

Drogue, G., C. Wagner, N. Mahr, L. Hoffmann & L. Pfister (2006): Topography and recent winter rainfall regime change in temperate Western European areas: A case study in the Rhine-Meuse basin. *International Journal of Climatology* 26 (6): 785–796. doi:10.1002/joc.1285. (Cited on page 72.)

DVWK (1996): *Ermittlung der Verdunstung von Land- und Wasserflächen*. DWA-Merkblatt DVWK-M 238, DWA Deutsche Vereinigung für Wasserwirtschaft, Abwasser und Abfall e.V., Hennef. (Cited on pages 30, 56, 100, and 103.)

Ebel, B. A. & K. Loague (2006): Physics-based hydrologic-response simulation: Seeing through the fog of equifinality. *Hydrological Processes* 20 (13): 2887–2900. doi:10.1002/hyp.6388. (Cited on page 66.)

El-Nasr, A. A., J. G. Arnold, J. Feyen & J. Berlamont (2005): Modelling the hydrology of a catchment using a distributed and a semi-distributed model. *Hydrological Processes* 19 (3): 573–587. doi:10.1002/hyp.5610. (Cited on page 8.)

Eltahir, E. A. B. & R. L. Bras (1996): Precipitation recycling. *Reviews of Geophysics* 34 (3): 367–378. doi:10.1029/96RG01927. (Cited on page 73.)

Engeland, K. & L. Gottschalk (2002): Bayesian estimation of parameters in a regional hydrological model. *Hydrology and Earth System Sciences* 6 (5): 883–898. doi:10.5194/hess-6-883-2002. (Cited on page 62.)

Engeland, K., C.-Y. Xu & L. Gottschalk (2005): Assessing uncertainties in a conceptual water balance model using Bayesian methodology / Estimation bayésienne des incertitudes au sein d'une modélisation conceptuelle de bilan hydrologique. *Hydrological Sciences Journal* 50 (1): 45–63. doi:10.1623/hysj.50.1.45.56334. (Cited on page 62.)

Evensen, G. (2007): *Data Assimilation – The Ensemble Kalman Filter*. Springer, Heidelberg. ISBN 978-3-540-38300-0, XXII + 280 pages. (Cited on page 120.)

Farr, T., P. Rosen, E. Caro, R. Crippen, R. Duren, S. Hensley, M. Kobrick, M. Paller, E. Rodriguez, L. Roth, D. Seal, S. Shaffer, J. Shimada, J. Umland, M. Werner, M. Oskin, D. Burbank & D. Alsdorf (2007): The shuttle radar topography mission. *Reviews of Geophysics* 45 (2): RG2004. doi:10.1029/2005RG000183. (Cited on pages 10 and 29.)

Fatichi, S., V. Y. Ivanov & E. Caporali (2012): A mechanistic ecohydrological model to investigate complex interactions in cold and warm water-controlled environments: 2. Spatiotemporal analyses. *Journal of Advances in Modeling Earth Systems* 4 (M05003): 22 pp. doi:10.1029/2011MS000087. (Cited on page 20.)

Faulhaber, P. & B. Willamowski (2002): Schifffahrtsbedingungen der Elbe – Ein Überblick über die Bezugswasserstände für Ausbau und Unterhaltung. In: *Die Elbe – neue Horizonte des Flussgebietsmanagements*, edited by W. Geller, P. Punčochář, H. Guhr, j. von Tümpling, W., J. Medek, J. Smrťak, H. Feldmann & O. Uhlmann, pages S287–S290. 10. Magdeburger Gewässerschutzseminar, Teubner, Stuttgart. ISBN 3-519-00420-8. (Cited on page 46.)

Fauville, A. (2002): *Isotopengeochemische Untersuchungen zum Stoffhaushalt geogen schwefelsaurer Bergbaurestseen des Lausitzer Braunkohlenreviers unter besonderer Berücksichtigung geochemisch gesteuerter Sanierungsverfahren*. Ph.D. thesis, Fakultät für Geowissenschaften, Ruhr-Universität Bochum. URL http://e-docs.geo-leo.de/bitstream/handle/11858/00-1735-0000-0001-321E-5/Fauville2001.pdf. Last accessed in October 2012. (Cited on page 91.)

Fedra, K. (1983): *Environmental modeling under uncertainty: Monte Carlo simulation*. IIASA Research Report RR-83-028, International Institute for Applied System Analysis, Laxenburg, Austria. (Cited on page 55.)

Fernandez, W., R. M. Vogel & A. Sankarasubramanian (2000): Regional calibration of a watershed model. *Hydrological Sciences Journal* 45 (5): 689–707. doi:10.1080/02626660009492371. (Cited on pages 28 and 54.)

Feyen, L., M. Kalas & J. A. Vrugt (2008): Semi-distributed parameter optimization and uncertainty assessment for large-scale streamflow simulation using global optimization. *Hydrological Sciences Journal* 53 (2): 293–308. doi:10.1623/hysj.53.2.293. (Cited on page 93.)

FGG Elbe (2005): *Zusammenfassender Bericht der Flussgebietsgemeinschaft Elbe über die Analysen nach Artikel 5 der Richtlinie 2000/60/EG (A-Bericht)*. Technical report, Flussgebietsgemeinschaft Elbe, Magdeburg. (Cited on pages 97 and 99.)

Finger, D., F. Pellicciotti, M. Konz, S. Rimkus & P. Burlando (2011): The value of glacier mass balance, satellite snow cover images, and hourly discharge for improving the performance of a physically based

distributed hydrological model. *Water Resources Research* 47 (W07519): 14 pp. doi:10.1029/2010WR009824. (Cited on page 95.)

Finke, W. & B. Bjarsch (1996): Methoden zur Bereinigung von Abflußmeßreihen um die Einflüsse der Wassernutzungen. *Deutsche Gewässerkundliche Mitteilungen* 40 (5): 194–203. (Cited on page 26.)

Flores, A. N., R. L. Bras & D. Entekhabi (2012): Hydrologic data assimilation with a hillslope-scale-resolving model and L band radar observations: Synthetic experiments with the ensemble Kalman filter. *Water Resources Research* 48 (W08509): 19 pp. doi:10.1029/2011WR011500. (Cited on page 21.)

Freeze, R. A. & R. L. Harlan (1969): Blueprint for a physically-based digitally-simulated hydrologic response model. *Journal of Hydrology* 9 (3): 237–258. doi:10.1016/0022-1694(69)90020-1. (Cited on page 7.)

Galleguillos, M., F. Jacob, L. Prévot, A. French & P. Lagacherie (2011): Comparison of two temperature differencing methods to estimate daily evapotranspiration over a Mediterranean vineyard watershed from ASTER data. *Remote Sensing of Environment* 115 (6): 1326–1340. doi:10.1016/j.rse.2011.01.013. (Cited on pages 101 and 116.)

Gao, Y. & D. Long (2008): Intercomparison of remote sensing-based models for estimation of evapotranspiration and accuracy assessment based on SWAT. *Hydrological Processes* 22 (25): 4850–48 869. doi:10.1002/hyp.7104. (Cited on page 116.)

Garatuza-Payan, J., R. T. Pinker, W. J. Shuttleworth & C. J. Watts (2001): Solar radiation and evapotranspiration in northern Mexico estimated from remotely sensed measurements of cloudiness. *Hydrological Sciences Journal* 46 (3): 465–478. doi:10.1080/02626660109492839. (Cited on page 101.)

Gassman, P. W., M. R. Reyes, C. H. Green & J. G. Arnold (2007): The soil and water assessment tool: Historical development, applications, and future research directions. *Transactions of the ASABE* 50 (4): 1211–1250. ISSN 0001-2351. (Cited on pages 29, 56, and 99.)

Gedney, N., P. M. Cox, R. A. Betts, O. Boucher, C. Huntingford & P. A. Stott (2006): Detection of a direct carbon dioxide effect in continental river runoff records. *Nature* 439: 835–838. doi:10.1038/nature04504. (Cited on page 50.)

Gerstengarbe, F.-W. & P. C. Werner (2005): Simulationsergebnisse des regionalen Klimamodells STAR. In: *Auswirkungen des globalen Wandels auf Wasser, Umwelt und Gesellschaft im Elbegebiet*, edited by F. Wechsung, A. Becker & P. Gräfe, volume 6 of *Konzepte für die nachhaltige Entwicklung einer Flusslandschaft*, chapter II-1.3, pages 110–118. Weißensee Verlag, Berlin. ISBN 978-3-89998-062-2. (Cited on pages 18, 26, and 92.)

Gerstengarbe, F.-W., P. C. Werner, B. Orlowsky & M. Wodinski (2013): Regionale Klimaszenarien. In: *Die Elbe und ihr Einzugsgebiet im globalen Wandel*, edited by F. Wechsung, V. Hartje, S. Kaden, M. Venohr, B. Hansjürgens & P. Gräfe, chapter 2.2. Weißensee Verlag, Berlin. In press. (Cited on pages 18, 37, 39, and 49.)

Gerten, D., S. Schaphoff, U. Haberlandt, W. Lucht & S. Sitch (2004): Terrestrial vegetation and water balance – hydrological evaluation of a dynamic global vegetation model. *Journal of Hydrology* 286 (1–4): 249–270. doi:10.1016/j.jhydrol.2003.09.029. (Cited on page 46.)

Githui, F., B. Selle & T. Thayalakumaran (2012): Recharge estimation using remotely sensed evapotranspiration in an irrigated catchment in southeast Australia. *Hydrological Processes* 26 (9): 1379–1389. doi:10.1002/hyp.8274. (Cited on pages 96 and 99.)

Glenn, E. P., T. M. Doody, J. P. Guerschman, A. R. Huete, E. A. King, T. R. McVicar, A. I. J. M. Van Dijk, T. G. Van Niel, M. Yebra & Y. Zhang (2011): Actual evapotranspiration estimation by ground and remote sensing methods: the Australian experience. *Hydrological Processes* 25 (26): 4103–4116. doi:10.1002/hyp.8391. (Cited on page 96.)

Glugla, G. & B. König (1989): VERMO – Ein Modell für die Berechnung des Jahresganges der Evaporation, Versickerung und Grundwasserneubildung. In: *Tagungsbericht 275*, pages 85–91. Akademie der Landwirtschaftswissenschaften der DDR, Berlin. (Cited on pages 30 and 56.)

Glugla, G., P. Jankiewicz, C. Rachimow, K. Richter, G. Fürtig, P. Krahe, W. Neubert & A. Klämt (2001): Mittlere jährliche Abflusshöhe. In: *Hydrologischer Atlas von Deutschland*, map 3.5. Bundesministerium für Umwelt, Naturschutz und Reaktorsicherheit (Federal Ministry for the Environment, Nature Conservation and Nuclear Safety, BMU), Berlin and Bonn. URL https://geoportal.bafg.de/portal/Start.do. Map includes description in both German and English, accessed online in July 2012. (Cited on page 130.)

Gong, D.-Y. & C.-H. Ho (2002): Shift in the summer rainfall over the Yangtze River valley in the late 1970s. *Geophysical Research Letters* 29 (10): 1436 (78-1–78-4). doi:10.1029/2001GL014523. (Cited on page 72.)

Grayson, R. B., I. D. Moore & T. A. McMahon (1992): Physically based hydrologic modeling: 2. Is the concept realistic? *Water Resources Research* 28 (10): 2659–2666. doi:10.1029/92WR01259. (Cited on page 95.)

van de Griend, A. A. & M. Owe (1993): On the relationship between thermal emissivity and the normalised difference vegetation index for natural surfaces. *International Journal of Remote Sensing* 14 (6): 1119–1131. doi:10.1080/01431169308904400. (Cited on page 107.)

Grossmann, M., H. Koch, N. Lienhoop, S. Vögele, K. Mutafoğlu, J. Möhring, O. Dietrich & M. Kaltofen (2013): Economic risks associated with low flows in the Elbe River Basin (Germany): an integrated economic-hydrologic approach to assess vulnerability to climate change. *Regional Environmental Change* Submitted. (Cited on pages 3 and 119.)

Grünewald, U. (2001): Water resources management in river catchments influenced by lignite mining. *Ecological Engineering* 17 (2–3): 143–152. doi:10.1016/S0925-8574(00)99154-3. (Cited on pages 1, 14, 26, 28, 33, 48, 99, and 117.)

Grünewald, U. (2003): Die »hydrologische Problematik« von Tagebauseen: Wassermenge, Wasserqualität und zukünftige Nutzung. *Petermanns Geographische Mitteilungen* 147: 14–21. (Cited on page 28.)

Gupta, S. K. & S. I. Solomon (1977a): Distributed numerical model for estimating runoff and sediment discharge of ungaged rivers 1. The information system. *Water Resources Research* 13 (3): 613–618. doi:10.1029/WR013i003p00613. (Cited on page 7.)

Gupta, S. K. & S. I. Solomon (1977b): Distributed numerical model for estimating runoff and sediment discharge of ungaged rivers 3. Comparison with other simple techniques. *Water Resources Research* 13 (3): 631–636. doi:10.1029/WR013i003p00631. (Cited on page 7.)

GWP-INBO (2009): *A Handbook for Integrated Water Resources Management in Basins*. Global Water Partnership (GWP) and International Network of Basin Organizations (INBO), Stockholm and Paris. URL http://www.gwptoolbox.org/images/stories/Docs/gwp_inbo%20handbook%20for%20iwrm%20in%20basins_eng.pdf. Last accessed in March 2012. (Cited on page 3.)

GWP-TAC (2000): *Integrated Water Resources Management*. TAC Background Papers 4, Global Water Partnership, Technical Advisory Committee (TAC), Stockholm. URL http://www.gwptoolbox.org/images/stories/gwplibrary/background/tac_4_english.pdf. Last accessed in March 2012. (Cited on page 3.)

Gómez, M., A. Olioso, J. A. Sobrino & F. Jacob (2005): Retrieval of evapotranspiration over the Alpilles/ReSeDA experimental site using airborne POLDER sensor and a thermal camera. *Remote Sensing of Environment* 96 (3–4): 399–408. doi:10.1016/j.rse.2005.03.006. (Cited on page 102.)

GÜK-BB (1997): *Geologische Übersichtskarte des Landes Brandenburg 1 : 300 000*. Landesamt für Geowissenschaften und Rohstoffe Brandenburg and Landesvermessungsamt Brandenburg, Potsdam, 1st edition. (Cited on page 130.)

Güntner, A. (2002): *Large-scale hydrological modelling in the semi-arid north-east of Brazil*. Ph.D. thesis, Universität Potsdam. URL http://www.pik-potsdam.de/research/publications/pikreports/.files/pr77.pdf. Also published as PIK Report 77 at Potsdam Institute for Climate Impact Research; last accessed in October 2012. (Cited on pages 28, 54, and 93.)

Habeck, A., V. Krysanova & F. Hattermann (2005): Integrated analysis of water quality in a mesoscale lowland basin. *Advances in Geosciences* 5: 13–17. doi:10.5194/adgeo-5-13-2005. (Cited on page 29.)

Halfon, E. & R. J. Maguire (1983): Distribution and transformation of fenitrothion sprayed on a pond: Modeling under uncertainty. In: *Uncertainty and forecasting of water quality*, edited by M. B. Beck & G. van Straten, pages 117–128. Springer, New York. ISBN 3540124195. (Cited on page 55.)

Hartje, V., T. Ansmann, J. Blazejczak, H. Gömann, M. Gornig, M. Grossmann, T. Hillenbrand, J. Hoymann, P. Kreins, P. Markewitz, K. Mutafoğlu, A. Richmann, C. Sartorius, E. Schulz, S. Vögele & R. Walz (2013): Regionalisierung globaler sozioökonomischer wandelprozesse für die wasserwirtschaft. In: *Die Elbe und ihr Einzugsgebiet im globalen Wandel*, edited by F. Wechsung, V. Hartje, S. Kaden, M. Venohr, B. Hansjürgens & P. Gräfe, chapter 2.1. Weißensee Verlag, Berlin. In press. (Cited on page 38.)

Hartwich, R., J. Behrens, W. Eckelmann, G. Haase, A. Richter, G. Roeschmann & R. Schmidt (1995): *Bodenübersichtskarte der Bundesrepublik Deutschland 1 : 1 000 000 (BÜK 1000)*. Karte mit Erläuterungen, Textlegende und Leitprofilen, Bundesanstalt für Geowissenschaften und Rohstoffe, Hannover. (Cited on pages 11, 29, 48, and 56.)

Hastings, W. K. (1970): Monte-Carlo sampling methods using Markov chains and their applications. *Biometrika* 57 (1): 97–109. doi:10.1093/biomet/57.1.97. (Cited on page 64.)

Hattermann, F., V. Krysanova & A. Habeck (2004a): Integrating wetlands and riparian zones in regional hydrological modeling. In: *Complexity and Integrated Resources Management – 2nd Biennal Meeting of the International Environmental Modelling and Software Society (iEMSs)*, pages 920–926. (Cited on page 29.)

Hattermann, F., V. Krysanova, F. Wechsung & M. Wattenbach (2004b): Integrating groundwater dynamics in regional hydrological modelling. *Environmental Modelling & Software* 19 (11): 1039–1051. doi:10.1016/j.envsoft.2003.11.007. (Cited on pages 131 and 132.)

Hattermann, F. F. (2005): *Integrated Modelling of Global Change Impacts in the German Elbe River basin*. Ph.D. thesis, Universität Potsdam. URL http://opus.kobv.de/ubp/volltexte/2005/605/pdf/

hattermann2.pdf. Last accessed in October 2012. (Cited on pages 29 and 92.)

Hattermann, F. F., V. Krysanova, J. Post, F.-W. Gerstengarbe, P. C. Werner & F. Wechsung (2005a): Assessing uncertainty of water availability in a Central European river basin (Elbe) under climate change. In: *Integrated modelling of global change impacts in the German Elbe River basin*, edited by F. F. Hattermann, pages 119–149. PhD Thesis, Universität Potsdam. URL http://opus.kobv.de/ubp/volltexte/2005/605/pdf/hattermann2.pdf. Last accessed in October 2012. (Cited on page 50.)

Hattermann, F. F., V. Krysanova & F. Wechsung (2005b): Folgen von Klimawandel und Landnutzungsänderungen für den Landschaftswasserhaushalt und die landwirtschaftlichen Erträge im Gebiet der deutschen Elbe. In: *Auswirkungen des globalen Wandels auf Wasser, Umwelt und Gesellschaft im Elbegebiet*, edited by F. Wechsung, A. Becker & P. Gräfe, volume 6 of *Konzepte für die nachhaltige Entwicklung einer Flusslandschaft*, chapter II-2.2.2, pages 151–164. Weißensee Verlag, Berlin. ISBN 978-3-89998-062-2. (Cited on pages 26, 30, 31, 42, and 50.)

Hattermann, F. F., M. Wattenbach, V. Krysanova & F. Wechsung (2005c): Runoff simulations on the macroscale with the ecohydrological model SWIM in the Elbe catchment – validation and uncertainty analysis. *Hydrological Processes* 19 (3): 693–714. doi:10.1002/hyp.5625. (Cited on pages 28, 29, and 56.)

Hattermann, F. F., V. Krysanova, A. Habeck & A. Bronstert (2006): Integrating wetlands and riparian zones in river basin modelling. *Ecological Modelling* 199 (4): 379–392. doi:10.1016/j.ecolmodel.2005.06.012. (Cited on pages 29 and 31.)

Helton, J. C. & D. E. Burmaster (1996): Guest editorial: Treatment of aleatory and epistemic uncertainty in performance assessments for complex systems. *Reliability Engineering & System Safety* 54 (2–3): 91–94. doi:10.1016/S0951-8320(96)00066-X. Editorial to a Special Issue (pages 91–262) containing 13 scientific articles about uncertainties in risk assessment. (Cited on page 131.)

Heuvelmans, G., B. Muys & J. Feyen (2004): Analysis of the spatial variation in the parameters of the SWAT model with application in Flanders, Northern Belgium. *Hydrology and Earth System Sciences* 8 (5): 931–939. doi:10.5194/hess-8-931-2004. (Cited on page 34.)

Hjelmfelt, A. T., Jr. & C. R. Amerman (1980): The mathematical basin model of Merrill Bernard. In: *The Influence of Man on the Hydrological Regime with Special Reference to Representative and Experimental Basins – Proceedings of the Helsinki Symposium, 23–26 June 1980*, number 130 in IAHS Publications ('Red Books' series), pages 343–349. International

Association of Hydrological Sciences, Adlard & Son Ltd, Bartholomew Press, Dorking, Surrey, UK. (Cited on page 7.)

Hoedjes, J. C. B., A. Chehbouni, F. Jacob, J. Ezzahar & G. Boulet (2008): Delivering daily evapotranspiration from remotely sensed instantaneous evaporative fraction over olive orchard in semi-arid Morocco. *Journal of Hydrology* 354 (1–4): 53–64. doi:10.1016/j.jhydrol.2008.02.016. (Cited on page 101.)

Hofmann, H., K. Knöller & D. Lessmann (2008): Mining lakes as groundwater-dominated hydrological systems: assessment of the water balance of Mining Lake Plessa 117 (Lusatia, Germany) using stable isotopes. *Hydrological Processes* 22 (23): 4620–4627. doi:10.1002/hyp.7071. (Cited on page 91.)

Hornberger, G. M. & R. C. Spear (1981): An approach to the preliminary analysis of environmental systems. *Journal of Environmental Management* 12 (1): 7–18. (Cited on page 55.)

Hotelling, H. (1933): Analysis of a complex of statistical variables into principal components. *Journal of Educational Psychology* 24 (6): 417–441. doi:10.1037/h0071325. (Cited on page 80.)

Hoymann, J. (2010a): Spatial allocation of future residential land use in the Elbe River Basin. *Environment and Planning B: Planning and Design* 37 (5): 911–928. doi:10.1068/b36009. (Cited on pages 38 and 51.)

Hoymann, J. (2010b): *Modelling future residential development – a scenario analysis for the Elbe River Basin*. Ph.D. thesis, Technical University of Berlin. (Cited on pages 28, 38, and 51.)

Hoymann, J. (2011): Accelerating urban sprawl in depopulating regions: a scenario analysis for the Elbe River Basin. *Regional Environmental Change* 11 (1): 73–86. doi:10.1007/s10113-010-0120-x. (Cited on pages 38 and 51.)

Hoymann, J., J. Dekkers & E. Koomen (2013): Szenarien zur Siedlungsflächenentwicklung. In: *Die Elbe und ihr Einzugsgebiet im globalen Wandel*, edited by F. Wechsung, V. Hartje, S. Kaden, M. Venohr, B. Hansjürgens & P. Gräfe, chapter 2.6. Weißensee Verlag, Berlin. In press. (Cited on pages 28, 38, and 51.)

Hsu, K. L., J. L. Li & S. Sorooshian (2012): To improve model soil moisture estimation in arid/semi-arid region using in situ and remote sensing information. *Paddy and Water Environment* 10 (3): 165–173. doi:10.1007/s10333-011-0308-9. (Cited on page 21.)

Huff, F. A. & S. A. Changnon (1973): Precipitation modification of major urban areas. *Bulletin of the American Meteorological Society* 54 (12): 1220–1232. doi:10.1175/1520-0477(1973)054<1220:PMBMUA>2.0.CO;2. (Cited on page 72.)

Hurst, H. E. (1951): Long-term storage capacity of reservoirs. *Transactions of the American Society of Civil Engineers* 116: 770–799. (Cited on page 58.)

Hurst, H. E. (1957): Suggested statistical model of some time series which occur in nature. *Nature* 180 (4584): 494. doi:10.1038/180494a0. (Cited on page 58.)

HÜK 200 (2011): *Hydrogeologische Übersichtskarte von Deutschland 1 : 200 000 (HÜK 200), Oberer Grundwasserleiter*. Bundesanstalt für Geowissenschaften und Rohstoffe, Hannover. URL http://geoviewer.bgr.de. Sheet CC3934 Magdeburg, revision of 2011. Accessed online in July 2012. (Cited on page 130.)

ICPER (2005): *Internationale Flussgebietseinheit Elbe – Merkmale der Flussgebietseinheit, Überprüfung der Umweltauswirkungen menschlicher Tätigkeiten und wirtschaftliche Analyse der Wassernutzung*. Report to the European Commission in accordance with the Water Framework Directive (2005 report for the international district of the Elbe River basin), International Commission for the Protection of the Elbe River Basin, Dresden. URL http://www.ikse-mkol.org/uploads/media/Bericht2005_A_Dt_22022005.pdf. Last accessed in February 2012; German language version, also published in Czech. (Cited on page 26.)

IfWW (1958): N-A-U-*Karte über das Gebiet der Deutschen Demokratischen Republik 1 : 200 000. Niederschlagshöhen und -gleichen, Abflußhöhen und -gleichen, Unterschiedswerte und -gleichen, Abflüsse und Abflußspenden 1921–1940*. Institut für Wasserwirtschaft, Berlin. (Cited on page 58.)

Iman, R. L., J. C. Helton & J. E. Campbell (1981): An approach to sensitivity analysis of computer models – 1 Introduction, input variable selection and prelimimary variable assessment. *Journal of Quality Technology* 13 (3): 174–183. ISSN 0022-4065. (Cited on page 34.)

Immerzeel, W. W. & P. Droogers (2008): Calibration of a distributed hydrological model based on satellite evapotranspiration. *Journal of Hydrology* 349 (3–4): 411–424. doi:10.1016/j.jhydrol.2007.11.017. (Cited on pages 96, 99, and 116.)

Ivanov, N. N. (1954): Об определении величины испаряемости (Estimation of the amount of evaporation). *Известия Всесоюзного Географического Общества (Proceedings of the All-Union Geographic Society)* 86 (2): 189–195. In Russian. (Cited on page 100.)

Ivanov, V. Y., E. R. Vivoni, R. L. Bras & D. Entekhabi (2004): Preserving high-resolution surface and rainfall data in operational-scale basin hydrology: a fully distributed physically-based approach. *Journal of Hydrology* 298 (1–4): 80–111. doi:10.1016/j.jhydrol.2004.03.041. (Cited on page 93.)

Jacobs, J. M., M. C. Anderson, L. C. Friess & G. R. Diak (2004): Solar radiation, longwave radiation and emergent wetland evapotranspiration estimates from satellite data in Florida, USA / Estimations à partir de données satellitales du rayonnement solaire, du rayonnement de grande longueur d'onde et de l'évapotranspiration d'une zone humide de Floride (EUA). *Hydrological Sciences Journal* 49 (3): 461–476. doi:10.1623/hysj.49.3.461.54352. (Cited on page 101.)

Jaurequi, E. & E. Romales (1996): Urban effects on convective precipitation in Mexico City. *Atmospheric Environment* 30 (20): 3383–3389. doi:10.1016/1352-2310(96)00041-6. (Cited on page 72.)

Jensen, K. H. & A. Mantoglou (1992): Future of distributed modelling. *Hydrological Processes* 6 (3): 255–264. doi:10.1002/hyp.3360060303. (Cited on page 7.)

Jhorar, R. K., A. A. M. F. R. Smit, W. G. M. Bastiaanssen & C. W. J. Roest (2011): Calibration of a distributed irrigation water management model using remotely sensed evapotranspiration rates and groundwater heads. *Irrigation and Drainage* 60 (1): 57–69. doi:10.1002/ird.541. (Cited on page 96.)

Jiang, L. & S. Islam (2001): Estimation of surface evaporation map over Southern Great Plains using remote sensing data. *Water Resources Research* 37 (2): 329–340. doi:10.1029/2000WR900255. (Cited on page 101.)

Jolliffe, I. T. (2002): *Principal Component Analysis*. Springer, New York, Berlin, and Heidelberg, 2nd edition. ISBN 0-387-95442-2, viii + 487 pages. (Cited on page 80.)

Kaden, S., M. Kaltofen, R. Timmermann, T. Lüllwitz & M. Roers (2010): Die Elbe-Expert-Toolbox – ein Entscheidungshilfesystem für das integrale wasserwirtschaftliche, (öko-)hydrologische und sozioökonomische Management eines Flusseinzugsgebietes. In: *Angewandte Geoinformatik 2010 – Beiträge zum 22. AGIT-Symposium Salzburg*, edited by J. Strobl, T. Blaschke & G. Griesebner, pages 290–299. Wichmann / VDE Verlag, Berlin. ISBN 978-3-87907-495-2. URL http://www.vde-verlag.de/proceedings-de/537495038.html. (Cited on page 3.)

Kaltofen, M., M. Hentschel, S. Kaden, O. Dietrich & H. Koch (2013a): Wasserverfügbarkeit im deutschen Elbegebiet. In: *Die Elbe und ihr Einzugsgebiet im globalen Wandel*, edited by F. Wechsung, V. Hartje, S. Kaden, M. Venohr, B. Hansjürgens & P. Gräfe, chapter 3.1. Weißensee Verlag, Berlin. In press. (Cited on pages 26, 42, 46, and 119.)

Kaltofen, M., M. Hentschel, S. Kaden, O. Dietrich & H. Koch (2013b): Modelling of water availability in the Elbe River basin and impacts of

global change in the German part. *Regional Environmental Change* In preparation. (Cited on page 119.)

Kavetski, D., S. W. Franks & G. Kuczera (2003): Confronting input uncertainty in environmental modelling. In: *Calibration of watershed models*, edited by Q. Duan, H. V. Gupta, S. Sorooshian, A. N. Rousseau & R. Turcotte, Water Science and Application, chapter 3.1, pages 49–68. American Geophysical Union, Washington D.C. ISBN 0-87590-355-X. doi:10.1029/WS006p0049. (Cited on page 63.)

Kavetski, D., G. Kuczera & S. W. Franks (2006a): Bayesian analysis of input uncertainty in hydrological modeling: 1. Theory. *Water Resources Research* 42 (3): W03 407. doi:10.1029/2005WR004368. (Cited on page 62.)

Kavetski, D., G. Kuczera & S. W. Franks (2006b): Bayesian analysis of input uncertainty in hydrological modeling: 2. Application. *Water Resources Research* 42 (3): W03 408. doi:10.1029/2005WR004376. (Cited on page 62.)

Khakbaz, B., B. Imam, K. Hsu & S. Sorooshian (2012): From lumped to distributed via semi-distributed: Calibration strategies for semi-distributed hydrologic models. *Journal of Hydrology* 418–419: 61–77. doi:10.1016/j.jhydrol.2009.02.021. (Cited on page 95.)

Kitanidis, P. K. & R. L. Bras (1979): Collinearity and stability in the estimation of rainfall-runoff model parameters. *Journal of Hydrology* 42 (1–2): 91–108. doi:10.1016/0022-1694(79)90008-8. (Cited on page 55.)

Kite, G. W. & P. Droogers (2000): Comparing evapotranspiration estimates from satellites, hydrological models and field data. *Journal of Hydrology* 229 (1–2): 3–18. doi:10.1016/S0022-1694(99)00195-X. (Cited on page 101.)

Kite, G. W. & A. Pietroniro (1996): Remote sensing applications in hydrological modelling. *Hydrological Sciences Journal* 41 (4): 563–591. doi:10.1080/02626669609491526. (Cited on page 96.)

Klemeš, V. (1974): The Hurst phenomenon: a puzzle? *Water Resources Research* 10 (4): 675–688. doi:10.1029/WR010i004p00675. (Cited on pages 58 and 124.)

Klemeš, V. (1982): Empirical and causal models in hydrology. In: *Scientific Basis of Water Resource Management*, edited by A. o. M. Geophysics Study Committee, Geophysics Research Board & N. R. C. Phys. Science, Studies in geophysics, pages 95–104. National Academy Press, Washington, D.C. (Cited on page 95.)

Klemeš, V. (1983): Conceptualization and scale in hydrology. *Journal of Hydrology* 65 (1–3): 1–23. doi:10.1016/0022-1694(83)90208-1. (Cited on page 96.)

Klemeš, V. (1986): Dilettantism in hydrology: Transition or destiny? *Water Resources Research* 22 (9S): 177S–188S. doi:10.1029/WR022i09Sp0177S. (Cited on page 95.)

Klemeš, V. (1988): A hydrological perspective. *Journal of Hydrology* 100 (1–3): 3–28. doi:10.1016/0022-1694(88)90179-5. (Cited on page 96.)

Koch, H. (2005): *Wasserbewirtschaftungsstrategien in vom Bergbau überprägten Einzugsgebieten im Kontext des globalen Wandels und deren integrierte Bewertung*. Ph.D. thesis, BTU Cottbus. Aktuelle Reihe 1/2005. (Cited on page 28.)

Koch, H., F. Wechsung & U. Grünewald (2010): Analyse jüngerer Niedrigwasserabflüsse im tschechischen Elbeeinzugsgebiet. *Hydrologie und Wasserbewirtschaftung* 54 (3): 169–178. URL http://www.hywa-online.de/hefte/2010/HyWaH32010.pdf. Last accessed in October 2012. (Cited on page 36.)

Koch, H., M. Kaltofen, S. Kaden & U. Grünewald (2013a): Wasserverfügbarkeit im tschechischen Elbegebiet. In: *Die Elbe und ihr Einzugsgebiet im globalen Wandel*, edited by F. Wechsung, V. Hartje, S. Kaden, M. Venohr, B. Hansjürgens & P. Gräfe, chapter 3.2. Weißensee Verlag, Berlin. In press. (Cited on pages 26, 42, 46, and 119.)

Koch, H., M. Kaltofen, S. Kaden & U. Grünewald (2013b): Effects of global change on water availability in the Czech Elbe region. *Regional Environmental Change* In preparation. (Cited on pages 26, 46, and 119.)

Koloskov, G., K. Mukhamejanov & T. W. Tanton (2007): Monin–Obukhov length as a cornerstone of the SEBAL calculations of evapotranspiration. *Journal of Hydrology* 335 (1–2): 170–179. doi:10.1016/j.jhydrol.2006.11.010. (Cited on page 102.)

Koutsoyiannis, D. (2005): Uncertainty, entropy, scaling and hydrological stochastics. 2. Time depencence of hydrological processes and time scaling / Incertitude, entropie, effet d'échelle et propriétés stochastiques hydrologiques. 2. Dépendance temporelle des processus hydrologiques et échelle temporelle. *Hydrological Sciences Journal* 50 (3): 405–426. doi:10.1623/hysj.50.3.405.65028. (Cited on page 79.)

Krause, S. & A. Bronstert (2007): The impact of groundwater–surface water interactions on the water balance of a mesoscale lowland river catchment in northeastern Germany. *Hydrological Processes* 21 (2): 169–184. doi:10.1002/hyp.6182. (Cited on pages 99 and 119.)

Krause, S., A. Bronstert & E. Zehe (2007): Groundwater–surface water interactions in a North German lowland floodplain – Implications for the river discharge dynamics and riparian water balance. *Journal of Hydrology* 347 (3–4): 404–417. doi:10.1016/j.jhydrol.2007.09.028. (Cited on page 119.)

Krysanova, V., D.-I. Müller-Wohlfeil & A. Becker (1998): Development and test of a spatially distributed hydrological/water quality model for mesoscale watersheds. *Ecological Modelling* 106 (2–3): 261–289. doi:10.1016/S0304-3800(97)00204-4. (Cited on pages 7, 28, 29, 53, 56, and 99.)

Krysanova, V., A. Bronstert & D.-I. Müller-Wohlfeil (1999): Modelling river discharge for large drainage basins: from lumped to distributed approach. *Hydrological Sciences Journal* 44 (2): 313–331. doi:10.1080/02626669909492224. (Cited on page 99.)

Krysanova, V., F. Wechsung, J. Arnold, R. Srinivasan & J. Williams (2000): SWIM *(Soil and Water Integrated Model) User Manual*. PIK Report 69, Potsdam Institute for Climate Impact Research, Potsdam, Germany. URL http://www.pik-potsdam.de/research/publications/pikreports/.files/pr69.pdf. Last accessed in October 2012. (Cited on pages 7, 28, 29, 54, 56, and 99.)

Krysanova, V., F. Hattermann & A. Habeck (2005): Expected changes in water resources availability and water quality with respect to climate change in the Elbe River basin (Germany). *Nordic Hydrology* 36 (4–5): 321–333. ISSN 0029-1277. (Cited on page 26.)

Kuczera, G. & S. W. Franks (2002): Testing hydrologic models: Fortification or falsification? In: *Mathematical Models of Large Watershed Hydrology*, edited by V. P. Singh & D. K. Frevert, chapter 5, pages 141–186. Water Resources Publications, Highland Ranch, Colorado, USA. ISBN 1-887201-34-3. (Cited on page 136.)

Leavesley, G. & L. Hay (1998): The use of coupled atmospheric and hydrological models for water-resources management in headwater basins. In: *Hydrology, Water Resources, and Ecology in Headwaters – Proceedings of the Headwater'98 conference held in Meran/Merano, Italy, from 20 to 23 April 1998*, edited by K. Kovar, U. Tappeiner, N. E. Peters & R. G. Craig, number 248 in IAHS Publications ('Red Books' series), pages 259–265. IAHS Press, Wallingford, Oxfordshire, UK. ISBN 1-901502-45-7. ISSN 0144-7815. (Cited on page 125.)

Leavesley, G. H., R. W. Lichty, B. M. Troutman & L. G. Saindon (1983): *Precipitation-Runoff Modeling System: User's Manual*. Water-Resources Investigations Report 83-4238, United States Department of the Interior – Geological Survey (USGS), Denver, CO. URL http:

//pubs.usgs.gov/wri/1983/4238/report.pdf. Last accessed in September 2012. (Cited on page 7.)

Lee, H., N. R. McIntyre, H. S. Wheater & A. R. Young (2006): Predicting runoff in ungauged UK catchments. *Proceedings of the Institute for Civil Engineering in Water Management* 159 (2): 129–138. ISSN 1741-7589. (Cited on page 34.)

van Leeuven, P. J. & G. Evensen (1996): Data assimilation and inverse methods in terms of a probabilistic formulation. *Monthly Weather Review* 124 (12): 2898–2913. doi:10.1175/1520-0493(1996)124<2898:DAAIMI>2.0.CO;2. (Cited on page 120.)

Lei, X. H., Y. Tian, W. H. Liao, W. Bai, Y. W. Jia, Y. Z. Jiang & H. Wang (2012): Development of an AutoWEP distributed hydrological model and its application to the upstream catchment of the Miyun Reservoir. *Computers & Geosciences* 44: 203–213. doi:10.1016/j.cageo.2011.10.016. (Cited on page 20.)

Lewis, J. M. (1995): The story behind the Bowen ratio. *Bulletin of the American Meteorological Society* 76 (12): 2433–2443. doi:10.1175/1520-0477(1995)076<2433:TSBTBR>2.0.CO;2. (Cited on page 103.)

Li, H. & K. J. Zhang (2010): Development of a fuzzy-stochastic nonlinear model to incorporate aleatoric and epistemic uncertainty. *Journal of Contaminant Hydrology* 111 (1–4): 1–12. doi:10.1016/j.jconhyd.2009.10.004. (Cited on pages 131 and 134.)

Lindroth, A. (1993): Aerodynamic and canopy resistance of short-rotation forest in relation to leaf area index and climate. *Boundary-Layer Meteorology* 66 (3): 265–279. doi:10.1007/BF00705478. (Cited on page 112.)

Lindström, G., B. Johansson, M. Persson, M. Gardelin & S. Bergström (1997): Development and test of the distributed HBV-96 hydrological model. *Journal of Hydrology* 201 (1–4): 272–288. doi:10.1016/S0022-1694(97)00041-3. (Cited on page 7.)

Liu, S., L. Lu, D. Mao & L. Jia (2007): Evaluating parameterizations of aerodynamic resistance to heat transfer using field measurements. *Hydrology and Earth System Sciences* 11 (2): 769–783. doi:10.5194/hess-11-769-2007. (Cited on page 112.)

Liu, T., P. Willems, X. W. Feng, Q. Li, Y. Huang, A. M. Bao, X. Chen, F. Veroustraete & Q. H. Dong (2012): On the usefulness of remote sensing input data for spatially distributed hydrological modelling: case of the Tarim River basin in China. *Hydrological Processes* 26 (3): 335–344. doi:10.1002/hyp.8129. (Cited on pages 95 and 120.)

Liu, Y. & H. V. Gupta (2007): Uncertainty in hydrologic modeling: Toward an integrated data assimilation framework. *Water Resources Research* 43 (7): W07 401. doi:10.1029/2006WR005756. (Cited on page 120.)

Liu, Y., P. Soonthornnonda, J. Li & E. R. Christensen (2011): Stormwater runoff characterized by GIS determined source areas and runoff volumes. *Environmental Management* 47 (2): 201–217. doi:10.1007/s00267-010-9591-2. (Cited on page 51.)

Long, D. & V. P. Singh (2010): Integration of the GG model with SEBAL to produce time series of evapotranspiration of high spatial resolution at watershed scales. *Journal of Geophysical Research* 115 (D21128): 22 pp. doi:10.1029/2010JD014092. (Cited on pages 102 and 120.)

de Luís, M., J. Raventós, J. González-Hidalgo, J. Sánchez & J. Cortina (2000): Spatial analysis of rainfall trends in the region of Valencia (east Spain). *International Journal of Climatology* 20 (12): 1451–1469. doi:10.1002/1097-0088(200010)20:12<1451::AID-JOC547>3.0.CO;2-0. (Cited on page 72.)

Maidment, D. R. (editor) (1993): *Handbook of Hydrology*. McGraw-Hill, New York, 1st edition. ISBN 978-0070397323, 1424 pages. (Cited on pages 29 and 56.)

Mandelbrot, B. B. & J. R. Wallis (1968): Noah, Joseph, and operational hydrology. *Water Resources Research* 4 (5): 909–918. doi:10.1029/WR004i005p00909. (Cited on page 58.)

Mandelbrot, B. B. & J. R. Wallis (1969): Some long-run properties of geophysical records. *Water Resources Research* 5 (2): 321–340. doi:10.1029/WR005i002p00321. (Cited on page 58.)

Maniak, U. (2005): *Hydrologie und Wasserwirtschaft – Eine Einführung für Ingenieure*. Springer, Heidelberg, 5th edition. ISBN 3540200916, 666 pages. (Cited on page 117.)

Mantovan, P. & E. Todini (2006): Hydrological forecasting uncertainty assessment: Incoherence of the GLUE methodology. *Journal of Hydrology* 330 (1–2): 368–381. doi:10.1016/j.jhydrol.2006.04.046. (Cited on page 62.)

Marković, D. & M. Koch (2005): Wavelet and scaling analysis of monthly precipitation extremes in Germany in the 20th century: Interannual to interdecadal oscillations and the North Atlantic Oscillation influence. *Water Resources Research* 41 (9): W09 420. doi:10.1029/2004WR003843. (Cited on page 79.)

Marshall, C., R. Pielke Sr., L. Steyaert & D. Willard (2004): The impact of anthropogenic land-cover change on the Florida Peninsula Sea Breezes and warm season sensible weather. *Monthly Weather Review* 132 (1): 28–52. doi:10.1175/1520-0493(2004)132<0028:TIOALC>2.0.CO;2. (Cited on page 71.)

Masih, I., S. Maskey, S. Uhlenbrook & V. Smakhtin (2011): Assessing the impact of areal precipitation input on streamflow simulations using the SWAT model. *Journal of the American Water Resources Association* 47 (1): 179–195. doi:10.1111/j.1752-1688.2010.00502.x. (Cited on page 128.)

Mathieu, P.-P. & A. O'Neill (2008): Data assimilation: From photon counts to Earth System forecasts. *Remote Sensing of Environment* 112 (4): 1258–1267. doi:10.1016/j.rse.2007.02.040. (Cited on page 120.)

Matsumoto, M. & T. Nishimura (1998): Mersenne twister: a 623-dimensionally equidistributed uniform pseudo-random number generator. *ACM Transactions on Modeling and Computer Simulation (TOMACS)* 8 (1): 3–30. doi:10.1145/272991.272995. (Cited on page 64.)

McCabe, M. F. & E. F. Wood (2006): Scale influences on the remote estimation of evapotranspiration using multiple satellite sensors. *Remote Sensing of Environment* 105 (4): 271–285. doi:10.1016/j.rse.2006.07.006. (Cited on page 116.)

McCabe, M. F., E. F. Wood, R. Wójcik, M. Pan, J. Sheffield, H. Gao & H. Su (2008): Hydrological consistency using multi-sensor remote sensing data for water and energy cycle studies. *Remote Sensing of Environment* 112 (2): 430–444. doi:10.1016/j.rse.2007.03.027. (Cited on page 120.)

McKay, M. D., R. J. Beckman & W. J. Conover (1979): A comparison of three methods for selecting values of input variables in the analysis of output from a computer code. *Technometrics* 21 (2): 239–245. doi:10.1080/00401706.1979.10489755. (Cited on page 34.)

McLaughlin (1995): Recent developments in hydrologic data assimilation. *Reviews of Geophysics* 33 (Supplement Part 2): 977–984. doi:10.1029/95RG00740. (Cited on page 21.)

McLaughlin (2002): An integrated approach to hydrologic data assimilation: interpolation, smoothing, and filtering. *Advances in Water Resources* 25 (8–12): 1275–1286. doi:10.1016/S0309-1708(02)00055-6. (Cited on page 120.)

Merz, B. & A. H. Thieken (2005): Separating natural and epistemic uncertainty in flood frequency analysis. *Journal of Hydrology* 309 (1–4): 114–132. doi:10.1016/j.jhydrol.2004.11.015. (Cited on page 131.)

Merz, B. & A. H. Thieken (2009): Flood risk curves and uncertainty bounds. *Natural Hazards* 51 (3): 437–458. doi:10.1007/s11069-009-9452-6. (Cited on page 134.)

Merz, R., J. Parajka & G. Blöschl (2009): Scale effects in conceptual hydrological modeling. *Water Resources Research* 45 (9): W09 405. doi:10.1029/2009WR007872. (Cited on page 93.)

Metropolis, N., A. W. Rosenbluth, M. N. Rosenbluth, A. H. Teller & E. Teller (1953): Equation of state calculations by fast computing machines. *The Journal of Chemical Physics* 21 (6): 1087–1092. doi:10.1063/1.1699114. (Cited on page 64.)

Miller, N. L., J. Jin & C.-F. Tsang (2005): Local climate sensitivity of the Three Gorges Dam. *Geophysical Research Letters* 32 (L16704): 4 pp. doi:10.1029/2005GL022821. (Cited on page 73.)

MNFAK (2010): *Richtlinien für die Anfertigung einer kumulativen Dissertation*. Mathematisch-Naturwissenschaftliche Fakultät der Universität Potsdam. URL http://www.uni-potsdam.de/fileadmin/projects/mnfakul/assets/Promotion/KumDissertation.pdf. Revision of February 2010. Last accessed in October 2012. (Cited on page 123.)

Mo, X., F. Pappenberger, K. Beven, S. Liu, A. de Roo & Z. Lin (2006): Parameter conditioning and prediction uncertainties of the LISFLOOD-WB distributed hydrological model / Conditionnement de paramétrage et incertitudes de prévision du modèle hydrologique distribué LISFLOOD-WB. *Hydrological Sciences Journal* 51 (1): 45–65. doi:10.1623/hysj.51.1.45. (Cited on page 93.)

Mohaupt-Jahr, B., M. Keil & R. Kiefl (editors) (2004): *Corine Land Cover 2000 in Germany and Europe and its use for environmental applications*. Federal Ministry for the Environment, Nature Conservation and Nuclear Safety (BMU), Bonn, Germany, Federal Environmental Agency (UBA), Berlin and German Aerospace Center (DLR), Oberpfaffenhofen, Workshop Proceedings, Berlin, 20–21 January 2004. URL http://www.umweltdaten.de/publikationen/fpdf-l/2698.pdf. Last accessed in October 2012. (Cited on page 74.)

Monin, A. S. & A. M. Obukhov (1954): Основные закономерности турбулентного перемешивания в приземном слое атмосферы (Basic laws of turbulent mixing in the ground layer of the atmosphere). *Труды Геофизического института Академии наук СССР (Transactions of the Geophysical Institute of the Academy of Sciences of the USSR)* 24 (151): 163–187. In Russian. (Cited on page 104.)

Moorcroft, P. R. (2003): Recent advances in ecosystem-atmosphere interactions: An ecological perspective. *Proceedings of the Royal*

Society of London – Series B: Biological Sciences 270 (1521): 1215–1227. doi:10.1098/rspb.2002.2251. (Cited on page 71.)

Moran, M. S., W. P. Kustas, A. Vidal, D. I. Stannard, J. H. Blanford & W. D. Nichols (1994): Use of ground-based remotely sensed data for surface energy balance evaluation of a semiarid rangeland. *Water Resources Research* 30 (5): 1339–1349. doi:10.1029/93WR03064. (Cited on page 101.)

Moussa, R., N. Chahinian & C. Bocquillon (2007): Distributed hydrological modelling of a Mediterranean mountainous catchment – Model construction and multi-site validation. *Journal of Hydrology* 337 (1–2): 35–51. doi:10.1016/j.jhydrol.2007.01.028. Erratum: *Journal of Hydrology* 345 (3–4): 254, doi:10.1016/j.jhydrol.2007.08.012. (Cited on pages 28, 54, and 93.)

Mölders, N. (1998): Landscape changes over a region in east Germany and their impact upon the processes of its atmospheric water-cycle. *Meteorology and Atmospheric Physics* 68 (1–2): 79–98. doi:10.1007/BF01025386. (Cited on pages 73 and 91.)

Mölders, N. (1999a): *Einfache und akkumulierte Landnutzungsänderungen und ihre Auswirkung auf Evapotranspiration, Wolken- und Niederschlagsbildung*. Mitteilungen 15, Institut für Meteorologie, Leipzig. Habilitation. (Cited on pages 73, 88, and 91.)

Mölders, N. (1999b): On the atmospheric response to urbanization and open-pit mining under various geostrophic wind conditions. *Meteorology and Atmospheric Physics* 71 (3–4): 205–228. doi:10.1007/s007030050056. (Cited on page 73.)

Mölders, N. (1999c): On the effect of different flooding stages of the Oder and different land use types on the distributions of evapotranspiration, cloudiness and rainfall in the Brandenburg-Polish border area. *Contributions to Atmospheric Physics* 72 (1): 1–24. ISSN 0303-4186. (Cited on page 73.)

Mölders, N. & A. Raabe (1997): Testing the effect of a two-way-coupling of a meteorological and a hydrologic model on the predicted local weather. *Atmospheric Research* 45 (2): 81–107. doi:10.1016/S0169-8095(97)00035-5. (Cited on page 73.)

Mölders, N. & W. Rühaak (2002): On the impact of explicitly predicted runoff on the simulated atmospheric response to small-scale land-use changes – an integrated modeling approach. *Atmospheric Research* 63 (1–2): 3–38. doi:10.1016/S0169-8095(02)00002-9. (Cited on page 73.)

Müller-Westermeier, G. & W. Rieke (2003): Die Witterung in Deutschland. In: *Klimastatusbericht 2002*, pages 79–87. Deutscher Wetterdienst, Offenbach. ISBN 3-88148-388-8. (Cited on page 110.)

Müller-Westermeier, G. & W. Rieke (2004): Die Witterung in Deutschland. In: *Klimastatusbericht 2003*, pages 71–78. Deutscher Wetterdienst, Offenbach. ISBN 3-88148-394-2. (Cited on page 110.)

Müller-Westermeier, G., G. Czeplak & A. Kreis (2002): Die Witterung in Deutschland. In: *Klimastatusbericht 2001*, pages 125–130. Deutscher Wetterdienst, Offenbach. ISBN 3-88148-380-2. (Cited on page 110.)

Nagler, P. (2011): The role of remote sensing observations and models in hydrology: the science of evapotranspiration. *Hydrological Processes* 25 (26): 3977–3978. doi:10.1002/hyp.8436. Preface to Special Issue. (Cited on page 96.)

Nakicenovic, N., J. Alcamo, G. Davis, B. de Vries, J. Fenhann, S. Gaffin, K. Gregory, A. Grübler, T. Y. Jung, T. Kram, E. Lebre La Rovere, L. Michaelis, S. Mori, T. Morita, W. Pepper, H. Pitcher, L. Price, K. Riahi, A. Roehrl, H.-H. Rogner, A. Sankovski, M. Schlesinger, P. Shukla, S. Smith, R. Swart, S. van Rooijen, N. Victor & Z. Dadi (2000): *Special report on emissions scenarios: a special report of Working Group III of the Intergovernmental Panel on Climate Change*. Ed. by Nakicenovic, N. and R. Swart. Cambridge University Press, Cambridge. ISBN 978-0521804936, 570 pages. URL http://www.ipcc.ch/ipccreports/sres/emission/index.php?idp=0. Last accessed in February 2012. (Cited on page 38.)

Nash, J. E. & J. V. Sutcliffe (1970): River flow forecasting through conceptual models Part I – A discussion of principles. *Journal of Hydrology* 10 (3): 282–290. doi:10.1016/0022-1694(70)90255-6. (Cited on page 31.)

Notebaert, B., G. Verstraeten, P. Ward, H. Renssen & A. V. Rompaey (2011): Modeling the sensitivity of sediment and water runoff dynamics to Holocene climate and land use changes at the catchment scale. *Geomorphology* 126 (1–2): 18–31. doi:10.1016/j.geomorph.2010.08.016. (Cited on page 51.)

Němeček, J. & J. Kozák (2003): Approaches to the solution of a soil map of the Czech republic at the scale 1 : 200,000 using SOTER methodology. *Plant, Soil and Environment* 49 (7): 291–297. ISSN 1214-1178. (Cited on page 29.)

Oesterle, H. (2001): Reconstruction of daily global radiation for past years for use in agricultural models. *Physics and Chemistry of the Earth, Part B: Hydrology, Oceans and Atmosphere* 26 (3): 253–256. doi:10.1016/S1464-1909(00)00248-3. (Cited on page 57.)

Orlanski, I. (1975): A rational subdivision of scales for atmospheric processes. *Bulletin of the American Meteorological Society* 56 (5): 527–530. ISSN 0003-0007. (Cited on page 125.)

Orlowsky, B. (2007): *Setzkasten Vergangenheit – ein kombinatorischer Ansatz für regionale Klimasimulationen*. Ph.D. thesis, Universität Hamburg. (Cited on pages 18 and 36.)

Österle, H., F.-W. Gerstengarbe & P. C. Werner (2006): Ein neuer meteorologischer Datensatz für Deutschland, 1951–2003. In: *Beiträge zur 7. Deutschen Klimatagung 'Klimatrends: Vergangenheit und Zukunft'*. Meteorologisches Institut, Ludwig-Maximilians-Universität München, 9.–11. Oktober 2006. (Cited on page 57.)

Pan, M., E. F. Wood, R. Wójcik & M. F. McCabe (2008): Estimation of regional terrestrial water cycle using multi-sensor remote sensing observations and data assimilation. *Remote Sensing of Environment* 112 (4): 1282–1294. doi:10.1016/j.rse.2007.02.039. (Cited on page 120.)

Panel on Seismic Hazard Evaluation: Kisslinger, C., K. Aki, W. J. Arabasz, D. K. Benson, J. E. Ebel, T. C. Hanks, J. S. Langer, N. C. Rasmussen, L. Reiter & D. Veneziano (1997): *Review of Recommendations for Probabilistic Seismic Hazard Analysis: Guidance on Uncertainty and Use of Experts*. Review report, National Research Council (NRC), National Academy of Sciences (NAS), Washington, DC. National Academy Press. Also published as Appendix to Senior Seismic Hazard Analysis Comittee (SSHAC): Budnitz et al. (1997). (Cited on page 131.)

Patel, N. R., D. Rakhesh & A. J. Mohammed (2006): Mapping of regional evapotranspiration in wheat using Terra/MODIS satellite data / Cartographie de l'évapotranspiration régionale du blé grâce à des données satellitales Terra/MODIS. *Hydrological Sciences Journal* 51 (2): 325–335. doi:10.1623/hysj.51.2.325. (Cited on pages 101 and 116.)

Pearson, K. (1901): On lines and planes of closest fit to systems of points in space. *The London, Edinburgh and Dublin Philosophical Magazine and Journal of Sciences – Series 6* 2 (11): 559–572. doi:10.1080/14786440109462720. (Cited on page 80.)

Pechlivanidis, I. G., N. R. McIntyre & H. S. Wheater (2010): Calibration of the semi-distributed PDM rainfall–runoff model in the Upper Lee catchment, UK. *Journal of Hydrology* 386 (1–4): 198–209. doi:10.1016/j.jhydrol.2010.03.022. (Cited on page 93.)

Pfützner, B. (1997): Ermittlung hydrologischer Grundlagen für den wiederentstehenden Salzigen See in Sachsen-Anhalt. In: *Tagungsband zum Symposium 'Modellierung in der Hydrologie'*. TU Dresden, 22.–24. September 1997. (Cited on page 91.)

Pfützner, B. (2005): Bewirtschaftungsmöglichkeiten im Einzugsgebiet der Havel – Endbericht Teilprojekt 4 „Erstellung eines komplexen Flussgebietsmodells für die Havel". Research report, published by Büro für Angewandte Hydrologie (BAH) with collaboration of P. Hesse,

Berlin, iii + 113 pages. URL http://www.havelmanagement.net/Havel-ger/Publikationen/Endberichte/Endbericht_TP4.pdf. Last accessed in September 2012. (Cited on page 131.)

Pickup, G. (1977): Testing the efficiency of algorithms and strategies for automatic calibration of rainfall-runoff models / Essais de l'efficacité des algorithms et des stratégies pour l'étalonnage des modèles pluie-écoulement. *Hydrological Sciences Bulletin* 22 (2): 257–274. doi:10.1080/02626667709491716. (Cited on page 55.)

Pielke, R. A. (2001): Influence of the spatial distribution of vegetation and soils on the prediction on cumulus convective rainfall. *Reviews of Geophysics* 39 (2): 151–177. doi:10.1029/1999RG000072. (Cited on page 71.)

Pitman, A. & G. Narisma (2005): The role of land surface processes in regional climate change: A case study of future land cover change over south western Australia. *Meteorology and Atmospheric Physics* 89 (1–4): 235–249. doi:10.1007/s00703-005-0131-1. (Cited on page 71.)

Pitman, A., G. Narisma, R. Pielke Sr. & N. Holbrook (2004): Impact of land cover change on the climate of southwest Western Australia. *Journal of Geophysical Research – Atmospheres* 109 (D18109): 12 pp. doi:10.1029/2003JD004347. (Cited on page 71.)

Pokhrel, P. & H. V. Gupta (2010): On the use of spatial regularization strategies to improve calibration of distributed watershed models. *Water Resources Research* 46 (W01505): 17 pp. doi:10.1029/2009WR008066. (Cited on page 93.)

Pokhrel, P. & H. V. Gupta (2011): On the ability to infer spatial catchment variability using streamflow hydrographs. *Water Resources Research* 47 (W08534): 13 pp. doi:10.1029/2010WR009873. (Cited on page 95.)

Post, J., T. Conradt, F. Suckow, V. Krysanova, F. Wechsung & F. F. Hattermann (2008): Integrated assessment of cropland soil carbon sensitivity to recent and future climate in the Elbe River basin / Evaluation intégrée de la sensibilité du carbone des sols agricoles au climat récent et futur dans le bassin de l'Elbe. *Hydrological Sciences Journal* 53 (5): 1043–1058. doi:10.1623/hysj.53.5.1043. (Cited on pages 29 and 56.)

Qin, C., Y. Jia, Z. B. Su, Z. Zhou, Y. Qiu & S. Suhui (2008): Integrating remote sensing information into a distributed hydrological model for improving water budget predictions in large-scale basins through data assimilation. *Remote Sensing of Environment* 8 (7): 4441–4465. doi:10.3390/s8074441. (Cited on page 120.)

Quiel, K., A. Becker, V. Kirchesch, A. Schöl & H. Fischer (2011): Influence of global change on phytoplankton and nutrient cycling in the Elbe

River. *Regional Environmental Change* 11 (2): 405–421. doi:10.1007/s10113-010-0152-2. (Cited on pages 3 and 26.)

Quiel, K., A. Schöl, V. Kirchesch, A. Becker & H. Fischer (2013): Phytoplankton und Nährstoffumsatz im Elbestrom. In: *Die Elbe und ihr Einzugsgebiet im globalen Wandel*, edited by F. Wechsung, V. Hartje, S. Kaden, M. Venohr, B. Hansjürgens & P. Gräfe, chapter 4.2. Weißensee Verlag, Berlin. In press. (Cited on page 26.)

R Development Core Team (2011): *R: A Language and Environment for Statistical Computing*. R Foundation for Statistical Computing, Vienna, Austria. URL http://www.R-project.org. Last accessed in October 2012. ISBN 3-900051-07-0. (Cited on pages 64 and 127.)

Ramakrishna, R. N. & S. W. Running (1989): Estimation of regional surface resistance to evapotranspiration from NDVI and thermal-IR AVHRR data. *Journal of Applied Meteorology* 28 (4): 276–284. doi:10.1175/1520-0450(1989)028<0276:EORSRT>2.0.CO;2. (Cited on page 112.)

Reed, S., V. Koren, M. Smith, Z. Zhang, F. Moreda, D.-J. Seo & DMIP Participants (2004): Overall distributed model intercomparison project results. *Journal of Hydrology* 298 (1–4): 27–60. doi:10.1016/j.jhydrol.2004.03.031. (Cited on pages 28, 54, and 94.)

Refsgaard, J. C. (1996): Model and data requirements for simulation of runoff and land surface processes in relation to global circulation models. In: *Land Surface Processes in Hydrology: Trials and Tribulations of Modeling and Measuring – Proceedings of the NATO advanced workshop Global Environmental Change*, edited by S. Sorooshian, H. Gupta & J. Rodda, number 46 in NATO ASI Subseries I, pages 423–445. Springer, Berlin, New York, Heidelberg. ISBN 978-3540617679. (Cited on page 8.)

Refsgaard, J. C., B. Storm & T. Clausen (2010): Système Hydrologique Europeén (SHE): review and perspectives after 30 years development in distributed physically-based hydrological modelling. *Hydrology Research* 41 (5): 355–377. doi:10.2166/nh.2010.009. (Cited on pages 7 and 9.)

Reichel, F. & W. Uhlmann (1995): *Wasserbeschaffenheit in Tagebaurestseen: Bergbaubedingte Wasserbeschaffenheit in Tagebaurestseen – Analyse, Bewertung und Prognose – Untersuchungen im Lausitzer Braunkohlenrevier*. Studien und Tagungsberichte 6, Landesumweltamt Brandenburg, Potsdam. (Cited on page 91.)

Reichle, R. H. (2008): Data assimilation methods in the Earth sciences. *Advances in Water Resources* 31 (11): 1411–1418. doi:10.1016/j.advwatres.2008.01.001. (Cited on pages 21 and 120.)

Richter, D. (1984): *Verdunstung*, volume 6 of *Klimadaten der Deutschen Demokratischen Republik – Ein Handbuch für die Praxis – Reihe B*. Meteorologischer Dienst der Deutschen Demokratischen Republik, Potsdam. (Cited on page 100.)

Richter, D. (1995): *Ergebnisse methodischer Untersuchungen zur Korrektur des systematischen Meßfehlers des Hellmann-Niederschlagsmessers*. Technical report, Deutscher Wetterdienst (German Weather Service, DWD), Offenbach. (Cited on pages 30 and 127.)

Rieland, M. (2004): Das BMBF-Programm GLOWA: Instrumente für ein vorausschauendes Management großer Flusseinzugsgebiete. *Hydrologie und Wasserbewirtschaftung* 48 (2): 83–84. (Cited on pages 1 and 2.)

Ritchie, J. T. (1972): A model for predicting evaporation from a row crop with incomplete cover. *Water Resources Research* 8 (5): 1204–1213. doi:10.1029/WR008i005p01204. (Cited on pages 30 and 100.)

Ross, J. L., M. M. Ozbek & G. F. Pinder (2009): Aleatoric and epistemic uncertainty in groundwater flow and transport simulation. *Water Resources Research* 45 (12): W00B15. doi:10.1029/2007WR006799. (Cited on pages 131 and 133.)

Ruzanski, E. & V. Chandrasekar (2012): An investigation of the short-term predictability of precipitation using high-resolution composite radar observations. *Journal for Applied Meteorology and Climatology* 51 (5): 912–925. doi:10.1175/JAMC-D-11-069.1. (Cited on page 133.)

Santhi, C., N. Kannan, J. G. Arnold & M. Di Luzio (2008): Spatial calibration and temporal validation of flow for regional scale hydrologic modeling. *Journal of the American Water Resources Association* 44 (4): 829–846. doi:10.1111/j.1752-1688.2008.00207.x. (Cited on pages 58 and 95.)

Sauer, V. B. & R. W. Meyer (1992): *Determination of error in individual discharge measurements*. Open-File Report 92-144, U.S. Geological Survey. URL http://pubs.usgs.gov/of/1992/ofr92-144/. (Cited on page 117.)

Schaller, M. F. & Y. Fan (2009): River basins as groundwater exporters and importers: Implications for water cycle and climate modeling. *Journal of Geophysical Research – Atmospheres* 114 (D04103): 21 pp. doi:10.1029/2008JD010636. (Cited on pages 58, 119, and 128.)

Schultz, G. A. (1987): Parameter determination and input estimation in rainfall-runoff modelling based on remote sensing techniques. In: *Water for the Future: Hydrology in Perspective (Proceedings of the International Symposium on Water for the Future held in Rome, April 1987)*, edited

by J. C. Rodda & N. C. Matalas, number 164 in IAHS Publications ('Red Books' series), pages 425–438. IAHS Press, Wallingford, U.K. ISBN 0-947571-06-X. (Cited on page 96.)

Schultz, G. A. (1988): Remote sensing in hydrology. *Journal of Hydrology* 100 (1–3): 239–265. doi:10.1016/0022-1694(88)90187-4. (Cited on pages 21 and 96.)

Schultz, G. A. (1993): Hydrological modeling based on remote sensing information. *Advances in Space Research* 13 (5): 149–166. doi:10.1016/0273-1177(93)90540-R. (Cited on page 21.)

Schuurmans, J. M., F. C. van Geer & M. F. P. Bierkens (2011): Remotely sensed latent heat fluxes for model error diagnosis: a case study. *Hydrology and Earth System Sciences* 15 (3): 759–769. doi:10.5194/hess-15-759-2011. (Cited on pages 95, 96, 102, and 120.)

Schönlau, J. & A. van der Veen (editors) (2005): *GLOWA – Globaler Wandel des Wasserkreislaufes / GLOWA – Global Change and the Hydrological Cycle*. Federal Ministry for Education and Research (Bundesministerium für Bildung und Forschung, BMBF), Bonn, Berlin, 43 pages. URL http://www.bmbf.de/pub/glowa_dt-eng.pdf. Text both in German and in English. Online version last accessed in August 2011. (Cited on page 2.)

Scott, R. & F. Huff (1996): Impacts of the Great Lakes on regional climate conditions. *Journal of Great Lakes Research* 22 (4): 845–863. doi:10.1016/S0380-1330(96)71006-7. (Cited on page 72.)

Seibert, J., S. Uhlenbrook, C. Leibundgut & S. Halldin (2000): Multiscale calibration and validation of a conceptual rainfall-runoff model. *Physics and Chemistry of the Earth, Part B: Hydrology, Oceans and Atmosphere* 25 (1): 59–64. doi:10.1016/S1464-1909(99)00121-5. (Cited on page 95.)

Sen, O., B. Wang & Y. Wang (2004): Impacts of re-greening the desertified lands in northwestern China: Implications from a regional climate model experiment. *Journal of the Meteorological Society of Japan* 82 (6): 1679–1693. doi:10.2151/jmsj.82.1679. (Cited on page 71.)

Senatsverwaltung (1992): *Gewässerkundlicher Jahresbericht für Berlin und Umland*. Abflußjahr 1991 (November 1990 bis Oktober 1991), Senatsverwaltung für Stadtentwicklung und Umweltschutz, Berlin. (Cited on page 58.)

Senior Seismic Hazard Analysis Comittee (SSHAC): Budnitz, R. J., G. Apostolakis, D. M. Boore, L. S. Cluff, K. J. Coppersmith, C. A. Cornell & P. A. Morris (1997): *Recommendations for Probabilistic Seismic Hazard Analysis: Guidance on Uncertainty and Use of Experts – Main Report*. Technical Report NUREG/CR-6372, Volume 1, Lawrence Livermore

National Laboratory, Livermore, CA. URL http://www.nrc.gov/reading-rm/doc-collections/nuregs/contract/cr6372/. Prepared for the U.S. Nuclear Regulatory Commission, the U.S. Department of Energy, and the Electric Power Research Institute; last accessed in October 2012. (Cited on pages 131 and 179.)

Shepherd, J. M., H. Pierce & A. J. Negri (2002): Rainfall modification by major urban areas: Observations from spaceborne rain radar on the TRMM satellite. *Journal of Applied Meteorology* 41 (7): 689–701. doi:10.1175/1520-0450(2002)041<0689:RMBMUA>2.0.CO;2. (Cited on page 72.)

Shi, J. C., Y. Du, J. Y. Du, L. M. Jiang, L. N. Chai, K. B. Mao, P. Xu, W. J. Ni, C. Xiong, Q. Liu, C. Z. Liu, P. Guo, Q. Cui, Y. Q. Li, J. Chen, A. Q. Wang, H. J. Luo & Y. H. Wang (2012): Progresses on microwave remote sensing of land surface parameters. *Science China – Earth Sciences* 55 (7): 1052–1078. doi:10.1007/s11430-012-4444-x. (Cited on page 20.)

Simon, M., V. Bekele, B. Kulasová, C. Maul, R. Oppermann & P. Řehák (2005): *Die Elbe und ihr Einzugsgebiet – Ein geografisch-hydrologischer und wasserwirtschaftlicher Überblick*. International Commission on the Protection of the Elbe River, Magdeburg, 258 pages. URL http://www.ikse-mkol.org/index.php?id=208. Last accessed in February 2012. (Cited on page 26.)

Singh, U. K., L. Ren & S. Kang (2010): Simulation of soil water in space and time using an agro-hydrological model and remote sensing techniques. *Agricultural Water Management* 97 (8): 1210–1220. doi:10.1016/j.agwat.2010.03.002. (Cited on page 96.)

Sivakumar, B. (2008): Undermining the science or undermining nature? *Hydrological Processes* 22 (6): 893–897. doi:10.1002/hyp.7004. (Cited on page 95.)

Smith, M. B., V. Koren, S. Reed, Z. Zhang, Y. Zhang, F. Moreda, Z. Cui, N. Mizukami, E. A. Anderson & B. A. Cosgrove (2012a): The distributed model intercomparison project – Phase 2: Motivation and design of the Oklahoma experiments. *Journal of Hydrology* 418–419: 3–16. doi:10.1016/j.jhydrol.2011.08.055. (Cited on page 94.)

Smith, M. B., V. Koren, Z. Zhang, Y. Zhang, S. M. Reed, Z. Cui, F. Moreda, B. A. Cosgrove, N. Mizukami, E. A. Anderson & DMIP 2 Participants (2012b): Results of the DMIP 2 oklahoma experiments. *Journal of Hydrology* 418–419: 17–48. doi:10.1016/j.jhydrol.2011.08.056. (Cited on page 94.)

Snelder, T. H., N. Lamouroux, J. R. Leathwick, H. Pella, E. Sauquet & U. Shankar (2009): Predictive mapping of the natural flow

regimes of France. *Journal of Hydrology* 371 (1–2): 57–67. doi:10.1016/j.jhydrol.2009.04.11. (Cited on page 34.)

Solomon, S. I. & S. K. Gupta (1977): Distributed numerical model for estimating runoff and sediment discharge of ungaged rivers 2. Model development. *Water Resources Research* 13 (3): 619–629. doi:10.1029/WR013i003p00619. (Cited on page 7.)

Spear, R. C. & G. M. Hornberger (1980): Eutrophication in Peel Inlet – II. Identification of critical uncertainties via generalized sensitivity analysis. *Water Research* 14 (1): 43–49. doi:10.1016/0043-1354(80)90040-8. (Cited on page 55.)

Srinivasan, R., T. S. Ramanarayanan, J. G. Arnold & S. T. Bednarz (1998): Large area hydrologic modeling and assessment Part II: Model application. *Journal of the American Water Resources Association* 34 (1): 91–101. doi:10.1111/j.1752-1688.1998.tb05962.x. (Cited on page 99.)

Stedinger, J. R., R. M. Vogel, S. U. Lee & R. Batchelder (2008): Appraisal of the generalized likelihood uncertainty estimation (GLUE) method. *Water Resources Research* 44 [printed 45 (12)]: W00B06. doi:10.1029/2008WR006822. (Cited on page 62.)

Stidd, C. (1975): Irrigation increases rainfall? *Science* 188 (4185): 279–280. doi:10.1126/science.188.4185.279. (Cited on page 72.)

Stisen, S., I. Sandholt, A. Norgaard, R. Fensholt & K. H. Jensen (2008): Combining the triangle method with thermal inertia to estimate regional evapotranspiration – Applied to MSG-SEVIRI data in the Senegal River basin. *Remote Sensing of Environment* 112 (3): 1242–1255. doi:10.1016/j.rse.2007.08.013. (Cited on page 102.)

Stisen, S., M. F. McCabe, J. C. Refsgaard, S. Lerer & M. B. Butts (2011): Model parameter analysis using remotely sensed pattern information in a multi-constraint framework. *Journal of Hydrology* 409 (1–2): 337–349. doi:10.1016/j.jhydrol.2011.08.030. (Cited on page 95.)

Sun, S., G. Fu, S. Djordjević & S.-T. Khu (2012): Separating aleatory and epistemic uncertainties: Probabilistic sewer flooding evaluation using probability box. *Journal of Hydrology* 420–421: 360–372. doi:10.1016/j.jhydrol.2011.12.027. (Cited on page 133.)

Sánchez, J. M., G. Scavone, V. Caselles, E. Valor, V. A. Copertino & V. Telesca (2008): Monitoring daily evapotranspiration at a regional scale from Landsat-TM and ETM+ data: Application to the Basilicata region. *Journal of Hydrology* 351 (1–2): 58–70. doi:10.1016/j.jhydrol.2007.11.041. (Cited on page 116.)

Thom, A. S. & H. R. Oliver (1977): On Penman's equation for estimating regional evaporation. *Quarterly Journal of the Royal Meteorological Society* 103 (436): 345–357. doi:10.1002/qj.49710343610. (Cited on page 112.)

Tomášek, M. (2003): *Půdy České republiky (The Soils of the Czech Republic)*. Česká geologická služba (Czech Geological Survey), Prague. ISBN 80-7075-607-1, 67 pages. In Czech. (Cited on page 29.)

Tungalagsaikhan, P. & K. P. Guenther (2007): NOAA AVHRR derived land surface temperature maps (LST) – Source, image characteristics, and processing. *Online publication* URL http://eoweb.dlr.de/short_guide/D-LST.html. Last accessed in September 2012. (Cited on pages 107 and 109.)

Turc, L. (1961): Évaluation des besoins en eau d'irrigation, évaporation potentielle. *Annales agronomiques* 12 (1): 13–49. In French. (Cited on page 100.)

Venohr, M., D. Opitz & H. Behrendt † (2013): Nährstoffeinträge und -frachten im Elbegebiet. In: *Die Elbe und ihr Einzugsgebiet im globalen Wandel*, edited by F. Wechsung, V. Hartje, S. Kaden, M. Venohr, B. Hansjürgens & P. Gräfe, chapter 4.1. Weißensee Verlag, Berlin. In press. (Cited on page 26.)

Verstraeten, W. W., F. Veroustraete & J. Feyen (2005): Estimating evapotranspiration of European forests from NOAA-imagery at satellite overpass time: Towards an operational processing chain for integrated optical and thermal sendor data products. *Remote Sensing of Environment* 96 (2): 256–276. doi:10.1016/j.rse.2005.03.004. (Cited on pages 102 and 116.)

Vinukollu, R. K., J. Sheffield, E. F. Wood, M. G. Bosilovich & D. Mocko (2012): Multimodel analysis of energy and water fluxes: Intercomparison between operational analyses, a land surface model, and remote sensing. *Journal of Hydrometeorology* 13 (1): 3–26. doi:10.1175/2011JHM1372.1. (Cited on page 96.)

Voß, A. (2007): *Untersuchung und Modellierung der Stickstoff- und Phosphorumsatz- und Transportprozesse in mesoskaligen Einzugsgebieten des Tieflandes am Beispiel von Nuthe, Hammerfließ und Stepenitz*. Ph.D. thesis, Universität Potsdam. URL http://opus.kobv.de/ubp/volltexte/2007/1548/pdf/voss_diss.pdf. Last accessed in October 2012. (Cited on page 29.)

Vrugt, J. A., H. V. Gupta, W. Bouten & S. Sorooshian (2003): A Shuffled Complex Evolution Metropolis algorithm for optimization and uncertainty assessment of hydrologic model parameters. *Water Resources Research* 39 (8): 1201. doi:10.1029/2002WR001642. (Cited on page 62.)

Vrugt, J. A., C. G. H. Diks, H. V. Gupta, W. Bouten & J. M. Verstraten (2005): Improved treatment of uncertainty in hydrologic modeling: Combining the strengths of global optimization and data assimilation. *Water Resources Research* 41 (1): W01 017. doi:10.1029/2004WR003059. (Cited on page 120.)

Wechsung, F. (2005): Herausforderungen des globalen Wandels für die Elbe-Region. In: *Auswirkungen des globalen Wandels auf Wasser, Umwelt und Gesellschaft im Elbegebiet*, edited by F. Wechsung, A. Becker & P. Gräfe, volume 6 of *Konzepte für die nachhaltige Entwicklung einer Flusslandschaft*, chapter I-1, pages 3–57. Weißensee Verlag, Berlin. ISBN 978-3-89998-062-2. (Cited on page 92.)

Wechsung, F., A. Hanspach, F. Hattermann, P. C. Werner & F.-W. Gerstengarbe (2006): *Klima und anthropogene Wirkungen auf den Niedrigwasserabfluss der mittleren Elbe: Konsequenzen für Unterhaltungsziele und Ausbaunutzen*. Contract study, Potsdam-Institute for Climate Impact Research. URL http://glowa-elbe.de/pdf/publications/elbe_nw_1p31.pdf. Last accessed November 2011. (Cited on page 50.)

Wechsung, F., H. Koch & P. Gräfe (editors) (2011): *Elbe-Atlas des globalen Wandels*. Weißensee Verlag, Berlin. ISBN 978-3-89998-200-8, 102 pages. (Cited on page 4.)

Wechsung, F., V. Hartje, S. Kaden, M. Venohr, B. Hansjürgens & P. Gräfe (editors) (2013): *Die Elbe und ihr Einzugsgebiet im globalen Wandel*. Weißensee Verlag, Berlin. In press. (Cited on page 119.)

Wendling, U. & H.-G. Schellin (1986): Neue Ergebnisse zur Berechnung der potentiellen Evapotranspiration. *Zeitschrift für Meteorologie* 36 (3): 214–217. ISSN 0084-5361. (Cited on page 100.)

Wendling, U., P. Fuchs & G. Müller-Westermeier (2000): Mittlere jährliche potentielle Verdunstungshöhe als Gras-Referenzverdunstung. In: *Hydrologischer Atlas für Deutschland*, map 2.12. Bundesministerium für Umwelt, Naturschutz und Reaktorsicherheit (Federal Ministry for the Environment, Nature Conservation and Nuclear Safety, BMU), Bonn and Berlin. Map includes description in both German and English; unchanged in the 3rd edition (2003). (Cited on page 91.)

Werner, M. & M. Cranston (2009): Understanding the value of radar rainfall nowcasts in flood forecasting and warning in flashy catchments. *Meteorological Applications* 16 (1): 41–55. doi:10.1002/met.125. (Cited on page 133.)

Werner, P. & F.-W. Gerstengarbe (1997): Proposal for the development of climate scenarios. *Climate Research* 8 (3): 171–182. doi:10.3354/cr0008171. (Cited on pages 18 and 36.)

Werner, P. C. (2007): Personal communication. Potsdam-Institute for Climate Impact Research. (Cited on page 48.)

Wild, M. (2012): Enlightening global dimming and brightening. *Bulletin of the American Meteorological Society* 93 (1): 27–37. doi:10.1175/BAMS-D-11-00074.1. (Cited on page 118.)

Wild, M., H. Gilgen, A. Roesch, A. Ohmura, C. N. Long, E. G. Dutton, F. Forgan, A. Kallis, V. Russak & A. Tsvetkov (2005): From dimming to brightening: decadal changes in solar radiation at Earth's surface. *Science* 308 (5273): 847–850. doi:10.1126/science.1103215. (Cited on page 48.)

Williams, J. R. & R. W. Hann (1978): *Optimal operation of large agricultural watersheds with water quality constraints*. Technical Report 96, Texas Water Resources Institute, Texas A&M University, College Station, TX. (Cited on page 101.)

Williams, J. R., A. D. Nicks & J. G. Arnold (1985): Simulator for water resources in rural basins. *Journal of Hydraulic Engineering* 111 (6): 970–986. doi:10.1061/(ASCE)0733-9429(1985)111:6(970). (Cited on page 7.)

Wilson, J. (1977): Effect of Lake Ontario on precipitation. *Monthly Weather Review* 105 (2): 207–214. doi:10.1175/1520-0493(1977)105<0207:EOLOOP>2.0.CO;2. (Cited on page 72.)

Wloczyk, C. (2007): *Entwicklung und Validierung einer Methodik zur Ermittlung der realen Evapotranspiration anhand von Fernerkundungsdaten in Mecklenburg-Vorpommern*. Ph.D. thesis, Universität Rostock, Agrar- und Umweltwissenschaftliche Fakultät. ISBN 978-3-86009-010-7. (Cited on pages 20, 101, and 116.)

Woolhiser, D. A. (1996): Search for physically based runoff model – a hydrologic El Dorado? *Journal of Hydraulic Engineering* 122 (3): 122–129. doi:10.1061/(ASCE)0733-9429(1996)122:3(122). (Cited on page 9.)

Wright, J. L. & M. E. Jensen (1972): Peak water requirements of crops in southern Idaho. *Journal of the Irrigation and Drainage Division, Proceedings of the American Society of Civil Engineers* 98 (IR2): 193–201. ISSN 0044-7978. (Cited on page 103.)

Xie, H., L. Longuevergne, C. Ringler & B. R. Scanlon (2012): Calibration and evaluation of a semi-distributed watershed model of Sub-Saharan Africa using GRACE data. *Hydrology and Earth System Sciences* 16 (9): 3083–3099. doi:10.5194/hess-16-3083-2012. (Cited on page 95.)

Yamanaka, T., J. Shimada & K. Miyaoka (2002): Footprint analysis using event-based isotope data for identifying source area of precipitated water. *Journal of Geophysical Research – Atmospheres* 107 (4624): 7 pp. doi:10.1029/2001JD001187. (Cited on page 73.)

Yang, D., S. Herath & K. Musiake (2000): Comparison of different distributed hydrological models for characterization of catchment spatial variability. *Hydrological Processes* 14 (3): 403–416. doi:10.1002/(SICI)1099-1085(20000228)14:3<403::AID-HYP945>3.0.CO;2-3. (Cited on page 8.)

Yang, J., P. Reichert & K. C. Abbaspour (2007): Bayesian uncertainty analysis in distributed hydrologic modeling: A case study in the Thur River basin (Switzerland). *Water Resources Research* 43 (10): W10 401. doi:10.1029/2006WR005497. (Cited on page 62.)

Yang, Y. T., S. H. Shang & L. Jiang (2012): Remote sensing temporal and spatial patterns of evapotranspiration and the responses to water management in a large irrigation district of North China. *Agricultural and Forest Meteorology* 164: 112–122. doi:10.1016/j.agrformet.2012.05.011. (Cited on page 20.)

Zhang, X., R. Srinivasan & M. Van Liew (2008): Multi-site calibration of the SWAT model for hydrologic modeling. *Transactions of the ASABE* 51 (6): 2039–2049. ISSN 0001-2351. (Cited on page 95.)

Zhang, X., R. Srinivasan & M. Van Liew (2010): On the use of multi-algorithm, genetically adaptive multi-objective method for multi-site calibration of the SWAT model. *Hydrological Processes* 24 (8): 955–969. doi:10.1002/hyp.7528. (Cited on page 95.)

A

APPENDIX: DISCHARGE DATA

In the following tables, the data sources for the mean discharges *(MQ)* are abbreviated as follows:

ČHMÚ	Czech Hydrometeorological Institute, Prague
GRDC	Global Runoff Data Centre, Koblenz
DGJ I–III	Deutsches Gewässerkundliches Jahrbuch, Elbegebiet, Teil I, Teil II, or Teil III (DGJ 1995a,b,c)
PIK	Potsdam Institute for Climate Impact research, Potsdam
e	Estimation based on the gauge data in the line above, which are marked with a downarrow (↓) in the ID column.

Table 9: Calibration gauges: Upper Labe above Vltava

ID	Gauge, River	Period	MQ m^3s^{-1}	Data source	A km^2	Upstream gauges
100	Les Království, Labe	1961–1990	8·66	ČHMÚ	532	—
101	Horní Maršov, Úpa	1961–1990	2·52	ČHMÚ	82	—
109	Jaroměř, Labe	1961–1990	17·12	ČHMÚ	1834	100, 101
↓	Krčín, Metuje	1966–1990	5·30	ČHMÚ	498	
110	Metuje confluence into Labe	1966–1990	5·90	e	608	—
111	Pastviny–Nekoř, Divoká O.	1961–1990	3·69	ČHMÚ	182	—
112	Kostelec nad Orlici, Div. O.	1961–1990	8·36	ČHMÚ	489	111
113	Čermná nad Orlici, Ticha O.	1961–1990	7·88	ČHMÚ	691	—
114	Tyniste nad Orlici, Orlice	1961–1990	20·17	ČHMÚ	1554	112, 113
115	Dašice, Loučná	1961–1990	3·60	ČHMÚ	624	—
116	Padrty (Seč), Chrudimka	1961–1987	2·27	ČHMÚ	225	—
117	Úhřetice, Novohradka	1961–1990	2·79	ČHMÚ	460	—
118	Nemošice, Chrudimka	1961–1990	6·37	ČHMÚ	857	116, 117
119	Přelouč, Labe	1970–1990	60·16	ČHMÚ	6435	109, 110, 114, 115, 118
120	Pařížov, Doubrava	1961–1990	1·76	ČHMÚ	201	—
121	Sány, Cidlina	1961–1990	5·67	ČHMÚ	1153	—
129	Nymburk, Labe	1961–1990	76·50	ČHMÚ	9724	119, 120, 121
130	Vestec, Mrlina	1961–1990	1·96	ČHMÚ	459	—
131	Železný Brod, Jizera	1961–1990	17·27	ČHMÚ	792	—
132	Tuřice, Jizera	1961–1990	26·45	GRDC	2158	131
↓	Brandýs nad Labem	1961–1990	106·97	ČHMÚ	13 109	
139	Labe above Vltava confluence	1961–1990	109·50	e	13 714	129, 130, 132

Table 10: Calibration gauges: Vltava

Vltava above Berounka						
ID	Gauge, River	Period	MQ m^3s^{-1}	Data source	A km^2	Upstream gauges
200	Vyšší Brod, Vltava	1961–1990	12·93	ČHMÚ	998	—
201	Římov, Malše	1961–1990	3·87	ČHMÚ	494	—
202	Roudné, Malše	1961–1990	6·96	ČHMÚ	963	201
210	Pilař, Lužnice	1961–1990	5·75	ČHMÚ	942	—
211	Hamr, Nežárka	1961–1990	12·49	ČHMÚ	982	—
212	Bechyně, Lužnice	1961–1990	22·57	ČHMÚ	4055	210, 211
213	Modrava, Vydra	1961–1990	3·33	ČHMÚ	90	—
214	Katovice, Otava	1961–1990	14·13	ČHMÚ	1133	213
215	Husinec, Blanice	1961–1990	2·04	ČHMÚ	212	—
216	Písek, Otava	1961–1990	23·58	ČHMÚ	2914	214, 215
217	Dolní Ostrovec, Lomnice	1961–1990	1·73	ČHMÚ	390	—
220	Chlístov, Sázava	1961–1990	5·37	ČHMÚ	795	—
221	Zruč, Sázava	1961–1990	9·51	ČHMÚ	1421	220
222	Želiv, Želivka	1961–1990	2·48	ČHMÚ	431	—
224	Radonice, Blanice	1961–1990	2·57	ČHMÚ	539	—
↓	Nespeky, Sázava	1961–1990	21·41	ČHMÚ	4038	
225	Sázava confl. into Vltava	1961–1990	22·90	e	4349	221, 222, 224
239	Vrané, Vltava	1961–1990	105·53	ČHMÚ	17 785	200, 202, 212, 216, 217, 225
Berounka and Vltava below						
ID	Gauge, River	Period	MQ m^3s^{-1}	Data source	A km^2	Upstream gauges
240	Trpísty, Úterský Potok	1961–1990	1·25	ČHMÚ	297	—
241	Hracholusky, Mže	1963–1990	8·70	ČHMÚ	1609	240
242	České Údolí, Radbuza	1976–1990	6·34	ČHMÚ	1263	—
243	Stará Lhota, Úhlava	1970–1990	1·57	ČHMÚ	81	—
244	Štěnovice, Úhlava	1961–1990	6·27	ČHMÚ	893	243
245	Plzeň Koterov, Úslava	1961–1990	3·94	ČHMÚ	734	—
246	Žlutice, Střela	1969–1990	1·16	ČHMÚ	214	—
247	Nová Huť, Klabava	1961–1990	2·05	ČHMÚ	359	—
248	Beroun, Berounka	1961–1990	37·78	ČHMÚ	8285	241, 242, 244, 245, 246, 247
299	Vraňany, Vltava	1982–1990	133·56	ČHMÚ	28 057	239, 248

Table 11: Calibration gauges: Labe below Vltava

ID	Gauge, River	Period	MQ m^3s^{-1}	Data source	A km^2	Upstream gauges
Ohře						
300	Skalka, Ohře	1964–1990	6·93	ČHMÚ	689	—
301	Jesenice, Odrava	1972–1990	2·92	ČHMÚ	412	—
302	Horka, Libocký potok	1963–1990	0·60	ČHMÚ	70	—
303	Svatava, Svatava	1964–1990	3·89	ČHMÚ	294	—
304	Březová, Teplá	1961–1990	2·71	ČHMÚ	294	—
309	Karlovy Vary-Drahovice, Ohře	1961–1990	27·65	ČHMÚ	2861	300, 301, 302, 303, 304
310	Stranná, Ohře	1961–1990	33·28	ČHMÚ	3598	309
311	Louny, Ohře	1961–1990	37·84	ČHMÚ	4962	310
Labe from Vltava to Czech-German boundary						
ID	Gauge, River	Period	MQ m^3s^{-1}	Data source	A km^2	Upstream gauges
319	Ústí nad Labem	1961–1990	300·22	ČHMÚ	48 541	139, 299, 311
320	Trmice, Bílina	1961–1990	7·25	ČHMÚ	932	—
330	Stráž, Ploučnice	1961–1990	1·10	ČHMÚ	121	—
331	Benešov, Ploučnice	1961–1990	9·46	ČHMÚ	1156	330
339	Děčín, Labe	1961–1990	318·66	GRDC	51 104	319, 320, 331
340	Hřensko, Kamenice	1962–1990	2·70	ČHMÚ	215	—

Table 12: Calibration gauges: Elbe above Havel

ID	Gauge, River	Period	MQ m^3s^{-1}	Data source	A km^2	Upstream gauges
Elbe from Czech-German boundary						
349	Dresden, Elbe	1961–1990	334·85	PIK	53 096	339, 340
350	Merzdorf, Döllnitz	1979–1990	1·02	PIK	211	—
359	Torgau, Elbe	1961–1990	340·28	PIK	55 211	349, 350
Schwarze Elster						
ID	Gauge, River	Period	MQ m^3s^{-1}	Data source	A km^2	Upstream gauges
370	Trado + Trado 2, Schw. Elster	1964–1990	0·94	DGJ I	166	—
371	Zescha, Hoyw. Schwarzwasser	1966–1990	1·08	DGJ I	180	—
372	Neuwiese, Schwarze Elster	1966–1990	3·06	PIK	669	370, 371
373	Lauchhammer, Schw. Elster	1974–1990	6·92	DGJ I	1513	372
375	Plessa, Hammergraben	1976–1990	1·86	DGJ I	213	—
382	Großdittmannsdorf, Gr. Röder	1979–1990	2·51	PIK	300	—
384	Bad Liebenwerda, Schw. Elster	1971–1990	16·60	DGJ I	3184	382
↓	Schadewitz, Kleine Elster	1971–1990	2·15	DGJ I	637	
386	Kleine Elster confl. into S. E.	1971–1990	2·35	e	717	—
389	Löben, Schwarze Elster	1974–1990	21·70	DGJ I	4327	384, 386
Elbe from Schwarze Elster to Havel						
ID	Gauge, River	Period	MQ m^3s^{-1}	Data source	A km^2	Upstream gauges
399	Wittenberg, Elbe	1961–1990	373·37	PIK	61 879	359, 389
	for Mulde and Saale, see Table 13					
489	Nutha, Nuthe	1972–1990	1·63	DGJ I	509	—
499	Barby, Elbe	1961–1990	577·88	PIK	94 060	439, 469, 489

Table 13: Calibration gauges: Mulde and Saale

ID	Gauge, River	Period	MQ m^3s^{-1}	Data source	A km^2	Upstream gauges
Mulde						
410	Göritzhain, Chemnitz	1976–1990	7·64	DGJ I	532	—
419	Wechselburg, Zwickauer M.	1980–1990	20·52	PIK	2107	410
430	Erlln, Freiberger Mulde	1961–1990	35·70	DGJ I	2983	—
439	Bad Düben, Mulde	1961–1990	64·70	DGJ I	6171	419, 430
Saale above Weiße Elster						
440	Hachelbich, Wipper	1962–1990	3·27	DGJ I	524	—
441	Bennungen, Helme	1980–1990	8·36	PIK	902	—
442	Laucha, Unstrut	1980–1990	34·23	PIK	6218	440, 441
449	Naumburg Grochlitz, Saale	1980–1990	76·53	PIK	11 449	442
Weiße Elster						
450	Greiz, Weiße Elster	1980–1990	10·28	PIK	1255	—
452	Zeitz, Weiße Elster	1980–1990	16·19	PIK	2504	450
453	Gößnitz, Pleiße	1981–1990	1·68	PIK	293	—
454	Regis-Serbitz, Pleiße	1964–1990	3·49	DGJ I	769	453
↓	Böhlen, Pleiße	1979–1990	8·20	PIK	1359	
455	Pleiße confl. into Weiße E.	1979-1990	8·80	e	1474	454
459	Oberthau, Weiße Elster	1973–1990	26·30	DGJ I	4939	452, 455
Bode and Lower Saale						
460	Wendefurth, Bode	1968–1990	3·54	DGJ I	309	—
461	Meisdorf, Selke	1980–1990	1·66	PIK	184	—
462	Wegeleben, Bode	1980–1990	8·75	PIK	1215	460, 461
468	Hadmersleben, Bode	1980–1990	14·51	PIK	2758	462
469	Calbe Grizehne, Saale	1961–1990	126·14	PIK	23 719	449, 459, 468

Table 14: Calibration gauges: Upper Havel and Spree

ID	Gauge, River	Period	*MQ* m^3s^{-1}	Data source	*A* km^2	Upstream gauges
Havel above Spree						
501	Ravensbrück, Hegensteinfließ	1974–1990	1·14	PIK	180	—
502	Bredereiche Schl. OP, Havel	1986–1990	6·79	DGJ II	1129	501
509	Borgsdorf, Havel	1976–1990	14·32	PIK	3114	502
Spree						
520	Bautzen Weite Bleiche, Spree	1979–1990	3·30	PIK	276	—
521	Gröditz, Löbauer Wasser	1979–1990	1·66	PIK	195	—
522	Lieske, Spree	1979–1990	5·27	PIK	775	520, 521
524	Särichen, Weißer Schöps	1963–1990	0·83	DGJ II	135	—
526	Boxberg, Schwarzer Schöps	1979–1990	6·12	PIK	639	—
529	Bräsinchen, Spree	1971–1990	19·20	DGJ II	2187	522, 524, 526
531	Müschen, Greifenh. Fließ	1971–1990	3·00	DGJ II	337	—
533	Boblitz, Dobra	1971–1990†	1·51	DGJ II	158	—
534	Ragow, Wudritz	1971–1990‡	0·68	DGJ II	94	—
535	Treppendorf, Berste	1967–1990	1·51	PIK	346	—
539	Lübben Zusammenfluß, Spree	1961–1990	28·49	PIK	4492	529, 531, 533, 534, 535
541	Märkisch Buchholz, Dahme	1976–1990	1·58	PIK	550	—
550	Grünheide, Löcknitz	1978–1990	0·88	DGJ II	170	—
559	Sophienwerder, Spree*	1981–1990	54·20	DGJ II	10 309	539, 541, 550

*including Kleinmachnow Schleuse OP, Teltowkanal (205 km^2)
†without missing year 1986
‡without missing years 1984 and 1987

Table 15: Calibration gauges: Havel below Spree

ID	Gauge, River	Period	MQ m^3s^{-1}	Data source	A km^2	Upstream gauges
560	Woltersdorf, Hammerfließ	1968–1990	1·18	DGJ II	208	—
561	Babelsberg, Nuthe	1961–1990	9·17	PIK	1787	560
569	Ketzin, Havel	1965–1990	77·01	PIK	16 173	559, 561
572	Trebitz UP, Plane	1963–1990*	0·82	DGJ II	224	—
573	Golzow, Plane	1971–1990	1·36	DGJ II	422	572
574	Brandenbg.-Wilh'dorf, Temnitz	1963–1990	1·60	DGJ II	153	—
575	Wenzlow F., Verlorenwasser	1976–1990	0·24	DGJ II	91	—
577	Herrenmühle For'anl., Buckau	1980–1990	0·64	DGJ II	135	—
589	Rathenow Hauptschl. UP, Hav.	1961–1990	93·45	PIK	19 288	569, 573, 574, 575, 577
590	Rheinsberg Wehr OP, Rhin	1977–1990	1·42	DGJ II	139	—
591	Alt Ruppin Schleuse OP, Rhin	1980–1990	3·24	PIK	516	590
599	Havelberg-Stadt, Havel	1981–1990	113·30	PIK	24 297	589, 591

*without missing years 1969–1971

Table 16: Calibration gauges: Elbe below Havel to Weir Geesthacht

ID	Gauge, River	Period	MQ m^3s^{-1}	Data source	A km^2	Upstream gauges
620	Wolfshagen, Stepenitz	1977–1990	3·70	PIK	575	—
649	Wittenberge, Elbe	1961–1990	736·79	PIK	123 532	499, 599, 620
650	Dobbrun, Biese	1971–1990*	5·43	DGJ III	1597	—
660	Gadow, Löcknitz	1961–1990	2·43	PIK	468	—
670	Malliß OP, Müritz-Elde Wstr.	1970–1990	11·00	DGJ III	2920	—
680	Salzwedel, Jeetzel	1971–1990	3·22	DGJ III	676	—
681	Lüchow, Jeetzel	1967–1990	6·54	DGJ III	1300	680
692	Laave, Rögnitz	1961–1990	2·73	DGJ III	390	—
693	Garlitz, Sude	1961–1990	4·59	PIK	735	—
696	Witzeetze, Linau	1971–1990	0·37	DGJ III	106	—
699	Neu Darchau, Elbe	1961–1990†	760·32	PIK	131 950	649, 660 670, 681

*without missing years 1982–1984
†without missing years 1971–1980

B

APPENDIX: CORRELATION ANALYSES OF ADJUSTMENT FACTORS

The original intention of the research presented in Chapter 5 had been the demonstration of spatial calibration of the distributed hydrological model by adjustment factors for sub-basin evapotranspiration (*ET*). Such factors had been calculated from the *ET* depths derived from remote sensing as well as from the water balance estimations. This Appendix presents some correlation analyses around these factors which did not fit into the submitted manuscript.

For remote sensing, the factors were obtained as follows: Averaging the 'remotely sensed' hydrotope $ET_{a,k}$ from Equation 36 to the gauged sub-basins, and dividing these $ET_{a,j}$ by the spatially uncalibrated SWIM averages $ET_{\text{SWIM},j}$ delivers evapotranspiration adjustment factors $c_{\text{RS:SWIM},j}$:

$$ET_{a,j} = \sum_{k=i_j}^{i_{j+1}-1} \frac{a_k \cdot ET_{a,k}}{a_j} \tag{39}$$

$$c_{\text{RS:SWIM},j} = \frac{ET_{a,j}}{ET_{\text{SWIM},j}} \tag{40}$$

In the following, the $c_{\text{RS:SWIM},j}$ shall be addressed as 'remotely sensed factors'.

Ideally, the 'ground based' *ET* corrections from long-term gauge measurements of the sub-basins should not deviate from their remotely sensed counterparts. As the original idea was to propose the remote sensing approach as alternative for spatial calibration, the remotely sensed adjustments shall be treated as predictive variable for the 'ground truth' of the ground based adjustments. Accordingly, Figure 58 shows the latter on the *y*-axis and – no dependency.

As mentioned in Section 5.2.2.2, correct average evapotranspiration calculations of the forested and the non-forested part of the basin have been assumed. Any misparameterisation of a land use class would bias the relationships between the two land use groups. But a systematic bias should leave its footprint in the correlation between forest shares and evapotranspiration adjustments. Accordingly, a two-dimensional regression including both remotely sensed adjustments plus forest share should be able to reproduce the ground based corrections if there were any systematic correlations. A hidden relationship would also lead to a higher coefficient of determination R^2 than the sum of the R^2 values of the single regression models.

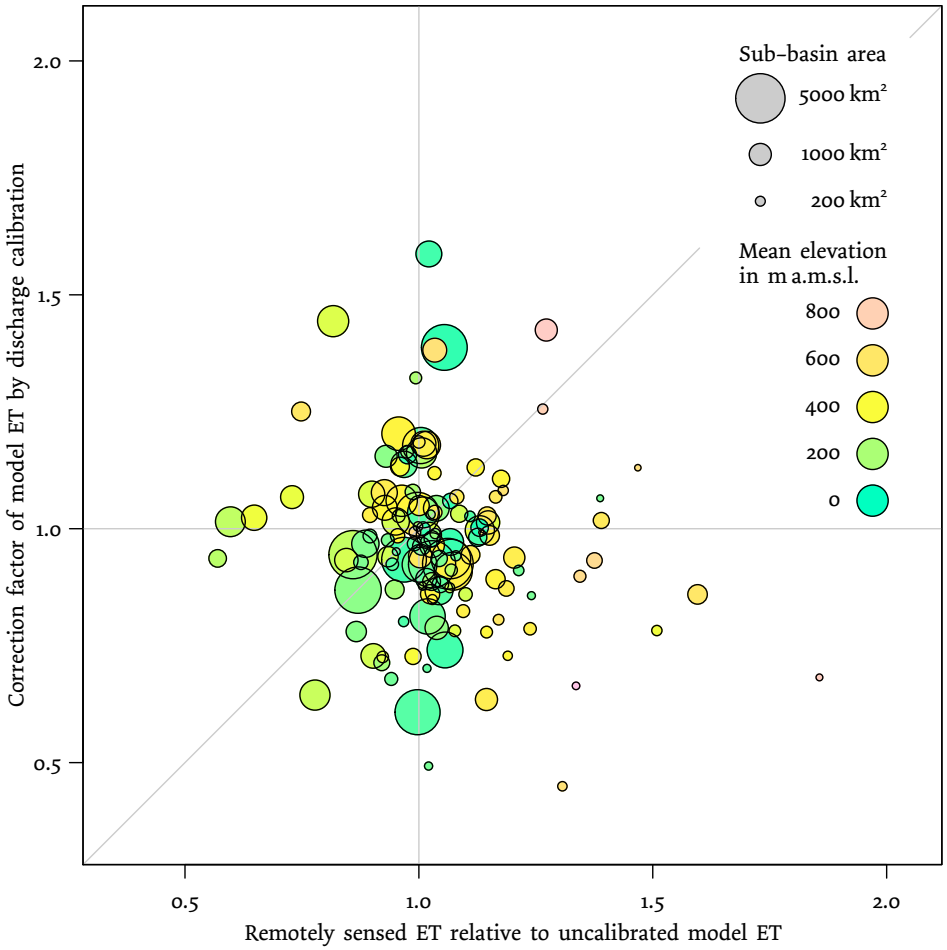

Figure 58: Comparison of remote sensing to ground based evapotranspiration adjustment factors for all 133 gauged sub-basins. The area-weighted numerical correlation coefficient equals –0·021, which means that there is practically no correlation.

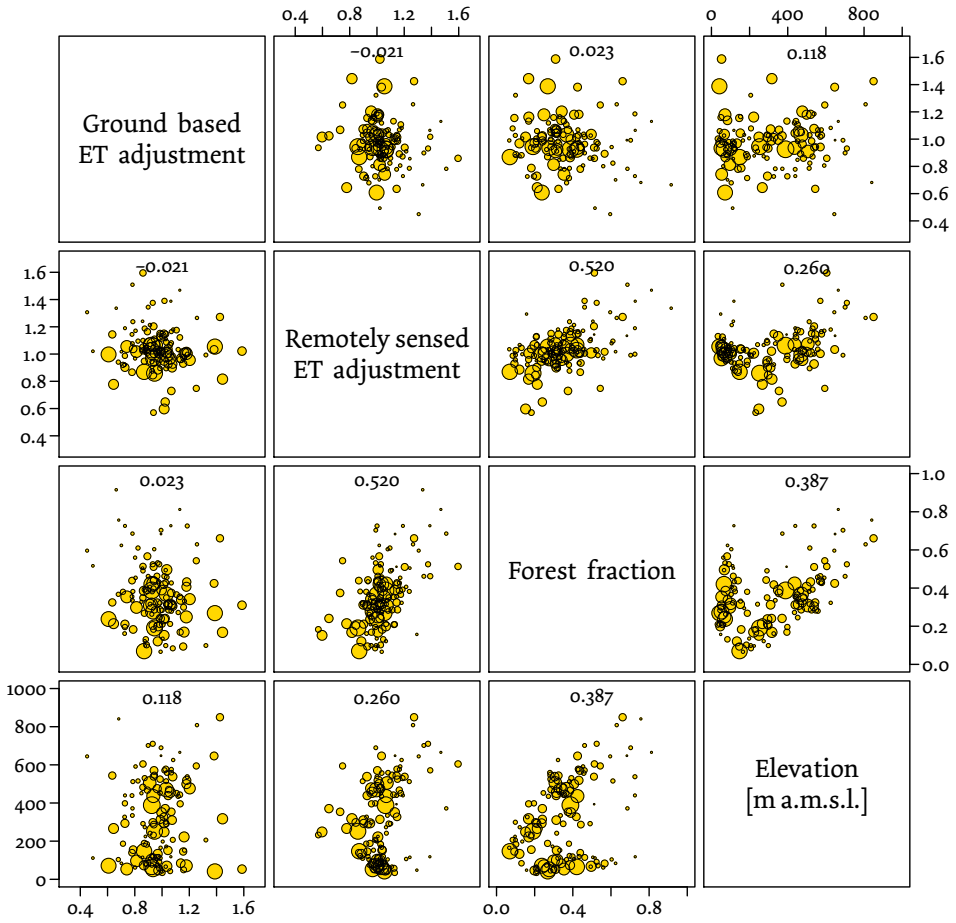

Figure 59: Correlation matrix plot for adjustments, forest share, and elevation. The labels written in the boxes on the main diagonal refer to the *x*-axis of the respective column panel and the *y*-axis of the respective row panel. Thus, the whole plot is symmetrical. The numbers in the plot boxes are the numerical correlation values; area-weighting of the data is considered.

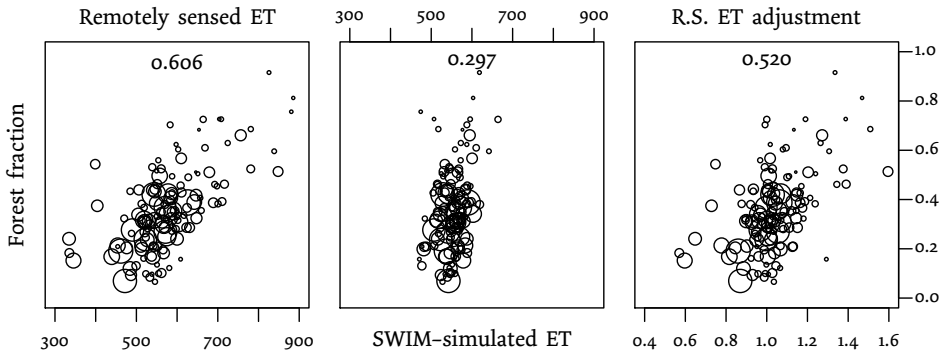

Figure 60: Dependencies of remotely sensed and SWIM simulated evapotranspiration in mm a^{-1} on forest share (left and middle panel). The right panel shows the resulting *ET* adjustments.

Figure 59 shows the relationships between all relevant variables. For any simple linear regression, the coefficient of determination R^2 equals the square-root of the numerical correlation between the variables. Fitting a linear model of the form $y = ax + b$ for the ground based on the remotely sensed *ET* adjustments would therefore explain only $-0{\cdot}021^2 = 0{\cdot}044\,\%$ of the variance of y (and disregard the negative correlation which factually devalues the concept of 'variance explanation' in this case).

Evaluating elevation effects delivers comparable results. Although there is a slight response of the ground based adjustments to the mean elevation of the respective sub-basins ($R^2 = 1{\cdot}4\,\%$, which is still far from being statistically significant at the 95 %-level), the combination of elevation and remotely sensed adjustments as independent variables ($y = ax_1 + bx_2 + c$) increases R^2 only by 0·3 %.

The linear regression of ground based adjustments on forest share yields an equally small coefficient of determination, and taking both forest share and remotely sensed adjustments into the set of predictors increases R^2 only marginally to 0·2 %. Plainly said, there is no relationship. Thus, we could not detect a model bias between forested and non-forested hydrotopes which could explain the complete independence between remotely sensed and ground based evapotranspiration adjustments.

Of course, the relatively strong correlation between forest share and remotely sensed adjustments (higest value in Fig. 59) could theoretically be caused by biased SWIM simulations: The remotely sensed factors are calibrated on simulated average *ET* heights of the forested and the non-forested part of the basin. But taking into account the evidence from the missing correlation between ground based factors and forest shares, the explanation seems to be more complex. Figure 60 shows forest fraction dependencies of both underlying *ET* calculations besides their resulting factor plot: SWIM shows relatively little variance in *ET*, while the remote sensing estimations are well correlated with forest share.

Both remote sensing estimations and forest share are either strongly dependent on elevation or show a distinct dependency structure (cf. the lower right panels of Figure 59) which could have caused the apparent inconsistency.

Including the full set of elevation, forest fraction and remotely sensed adjustments as predictors ($y = ax_1+bx_2+cx_3+d$) gives practically no further increase at all which again argues against any hidden dependency.

DECLARATION / ERKLÄRUNG

Hereby I declare that this work has not been submitted to any other university or higher education institute, that it is solely my own work – except for the shares of the co-authors in the journal articles as clarified in detail on Pages 23 and 24 –, and that all aids and sources used have been listed.

Hiermit erkläre ich, daß diese Arbeit an keiner anderen Hochschule eingereicht wurde und daß sie – abgesehen von den auf den Seiten 23 und 24 im einzelnen erläuterten Anteilen der Koautoren der Zeitschriftenbeiträge – von mir selbständig und ausschließlich mit den angegebenen Mitteln angefertigt wurde.

Potsdam, 8. Januar 2013

Tobias Conradt

[Hand-written signature only in submitted print copies]